

# Structures, dipoles and dynamics of large molecules in their excited singlet states

## Inaugural-Dissertation

zur Erlangung des Doktorgrades  
der Mathematisch-Naturwissenschaftlichen Fakultät  
der Heinrich-Heine-Universität Düsseldorf

vorgelegt von

**Michael Schneider**

aus Freiburg im Breisgau

Düsseldorf, 16. April 2019

aus dem Institut für Physikalische Chemie I  
der Heinrich-Heine-Universität Düsseldorf

Gedruckt mit der Genehmigung der  
Mathematisch-Naturwissenschaftlichen Fakultät der  
Heinrich-Heine-Universität Düsseldorf

Referent: Prof. Dr. Michael Schmitt  
Korreferent: Prof. Dr. Rainer Weinkauff

Tag der mündlichen Prüfung: 24. Mai 2019

# Contents

<b>Eigenständigkeitserklärung</b>	<b>V</b>
<b>Danksagung</b>	<b>VII</b>
<b>Übersicht</b>	<b>IX</b>
<b>Abstract</b>	<b>XI</b>
<b>1. Introduction</b>	<b>1</b>
1.1. Dimethoxybenzenes . . . . .	2
1.2. 3-Cyanoindole . . . . .	4
<b>2. Theoretical Background</b>	<b>7</b>
2.1. Principles of rotational spectroscopy . . . . .	7
2.1.1. Symmetric Rotor . . . . .	11
2.1.2. Asymmetric Rotor . . . . .	12
2.1.3. Stark Effect . . . . .	14
2.2. Characterization of Excited States . . . . .	16
<b>3. Experimental Setup</b>	<b>21</b>
3.1. The Laser System . . . . .	22
3.1.1. The Pump Laser . . . . .	22
3.1.2. The Ring Dye Laser . . . . .	23
3.1.3. The Frequency Doubler . . . . .	25
3.1.4. The Determination of the Relative Frequency . . . . .	25
3.1.5. The Determination of the Absolute Frequency . . . . .	27
3.2. The Molecular Beam Apparatus . . . . .	27
3.2.1. The Molecular Beam . . . . .	27
3.2.2. The Vacuum Apparatus . . . . .	29

<b>4. Spectrum Evaluation via Evolutionary Algorithms</b>	<b>35</b>
<b>5. Publication on Rotamers of 1,3-Dimethoxybenzene</b>	<b>39</b>
Rotationally Resolved Electronic Spectroscopy of the Rotamers of 1,3-Dimethoxybenzene . . . . .	39
5.1. Abstract . . . . .	39
5.2. Introduction . . . . .	40
5.3. Experimental section . . . . .	42
5.3.1. Experimental procedures . . . . .	42
5.3.2. Quantum chemical calculations . . . . .	43
5.3.3. Fits of the rovibronic spectra using evolutionary algorithms . . . . .	43
5.4. Results . . . . .	44
5.4.1. Computational Results . . . . .	44
5.4.2. Experimental results . . . . .	47
5.4.3. Conformational assignment . . . . .	49
5.5. Discussion . . . . .	52
5.6. Conclusion . . . . .	56
5.7. Acknowledgements . . . . .	57
5.8. Publication . . . . .	58
<b>6. Publication on Dipole Moments of Rotamers of Dimethoxybenzenes</b>	<b>59</b>
Excited state dipole moments and transition dipole orientations of different ro- tamers of 1,2-, 1,3, and 1,4-dimethoxybenzene . . . . .	59
6.1. Abstract . . . . .	59
6.2. Introduction . . . . .	60
6.3. Computational Methods . . . . .	62
6.3.1. Quantum chemical calculations . . . . .	62
6.3.2. Fits of the rovibronic spectra using evolutionary algorithms . . . . .	62
6.4. Experimental Methods . . . . .	62
6.5. Results . . . . .	63
6.5.1. Computational Results . . . . .	63
6.5.2. Experimental Results . . . . .	68
6.6. Discussion . . . . .	79
6.6.1. Permanent Dipole Moments . . . . .	79
6.6.2. Transition Dipole Moments . . . . .	83
6.7. Conclusions . . . . .	86

6.8. Acknowledgements . . . . .	88
6.9. Publication . . . . .	88
<b>7. Publication on 3-Cyanoindole and its Water Complex</b>	<b>91</b>
Rotationally Resolved Electronic Spectroscopy of 3-Cyanoindole and the 3-Cyanoindole-water complex . . . . .	91
7.1. Abstract . . . . .	91
7.2. Introduction . . . . .	92
7.3. Experimental section . . . . .	94
7.3.1. Experimental procedures . . . . .	94
7.3.2. Quantum chemical calculations . . . . .	95
7.3.3. Fits of the rovibronic spectra using evolutionary algorithms . . . . .	95
7.4. Results . . . . .	96
7.4.1. Computational Results . . . . .	96
7.4.2. Experimental results . . . . .	102
7.5. Discussion . . . . .	106
7.5.1. 3-Cyanoindole . . . . .	106
7.5.2. 3-Cyanoindole-water . . . . .	115
7.6. Conclusions . . . . .	118
7.7. Acknowledgements . . . . .	119
7.8. Publication . . . . .	119
<b>8. Summary</b>	<b>121</b>
<b>9. List of Publications and Conference Contributions</b>	<b>123</b>
<b>Bibliography</b>	<b>125</b>
<b>A. Online Supporting Material</b>	<b>143</b>
A.1. Supplementary to Chapter 5 . . . . .	143
A.2. Supplementary to Chapter 6 . . . . .	153
A.3. Supplementary to Chapter 7 . . . . .	158



# Eigenständigkeitserklärung

Ich versichere an Eides Statt, dass die Dissertation von mir selbständig und ohne unzulässige fremde Hilfe unter Beachtung der "Grundsätze zur Sicherung guter wissenschaftlicher Praxis" an der Heinrich-Heine-Universität Düsseldorf erstellt worden ist.

Düsseldorf, 16. April 2019

---

Ort, Datum

---

Michael Schneider



# Danksagung

Endlich! Nach über einem Jahrzehnt (mit Unterbrechung) an der Uni Düsseldorf stehe ich am Ende meiner Doktorarbeit. Daher möchte ich mich abschließend herzlichst bei einigen Leuten bedanken:

- Allen voran möchte ich mich bei meinem Doktorvater Michael Schmitt für die Aufnahme in den Arbeitskreis, der Betreuung meiner Promotion, der Möglichkeit in Mexico zu forschen sowie für die vielen anregenden und fachlichen Diskussionen bedanken.
- Prof. Dr. Rainer Weinkauff für die Bereitschaft sich als Zweitgutachter zur Verfügung zu stellen.
- Josy und Martin Wilke für die gute Zusammenarbeit während meiner Masterzeit.
- Frau Hebestreit, welche mich fast während meiner gesamten Promotion begleitete. Erst als Bachelorandin, dann als Masterandin und schließlich als Kollegin. Ohne dich wären die ganzen kleinen Unfälle im Labor nur halb so lustig gewesen. Schön, dass wir immer was zu lachen hatten!
- Dr. Leonardo Álvarez Valtierra und seinem Team für die freundliche Aufnahme während meines Aufenthalts in Mexico. Muchas gracias dafür!
- Leo Meerts für die Hilfe rund um die genetischen Algorithmen.
- Natürlich dem gesamten Arbeitskreis für die vielen Kaffeerunden, Grillfeste und sonstigen Ablenkungen.
- Andrea Lotzwick für die netten Gespräche und ausdauernde Hilfe bei Verwaltungsangelegenheiten.
- Klaus Kelbert beim unermüdlichen Kampf gegen Heizung und Hochspannung.
- Dieter Marx für die Diskussionen rund um exotische Reiseziele. Die Gespräche mit dir waren immer eine angenehme Abwechslung vom Laboralltag.
- Bei meiner Familie für die Unterstützung!



# Übersicht

Mittels hochaufgelöster Fluoreszenzspektroskopie können verschiedene Molekülparameter isolierter Moleküle untersucht werden, welche zur Bestimmung der geometrischen Struktur, sowie der elektronischen Natur des elektronischen Grund- und ersten angeregten Zustands dienen. Dafür wurden im Rahmen dieser Arbeit die verschiedenen Rotamere von 1,2-, 1,3- und 1,4-Dimethoxybenzol sowie 4-Cyanoindol und dessen Wassercluster untersucht.

Ein Teil dieser Arbeit beschäftigte sich mit der Untersuchung des Konformerenraums von 1,3-Dimethoxybenzol. Dabei wurden die intensivsten Schwingungsbanden von 1,3-Dimethoxybenzol rotationsaufgelöst untersucht und anhand der Rotationskonstanten den verschiedenen Rotameren zugeordnet. Es wurde eines der drei möglichen planaren Rotameren nicht gefunden und die vermutete Ursprungsbande eines Rotamers stellte sich als eine Schwingungsbande eines anderen Rotamers heraus. Das nicht gefundene Rotamer hat die Struktur bei der beide Methoxygruppen parallel nach oben zeigen. Weitere Untersuchungen anhand von quantenchemischen Rechnungen zeigten, dass das Rotamer aufgrund seiner nicht planaren Geometrie im elektronisch angeregten Zustand und eines daraus folgenden niedrigen Franck-Condon-Faktors eine zu geringe Intensität hat, um untersucht zu werden. Eine ähnliche Beobachtung wurde bereits bei der Untersuchung des Konformerenraums von 1,3-Methoxyphenol gemacht. Die Ergebnisse hierzu sind in Kapitel 5 detailliert aufgeführt.

In Kapitel 6, welches sich mit den Dipolmomenten der drei Konstitutionsisomere von Dimethoxybenzol beschäftigt, wurden die Dipolmomente mittels Vektoraddition hergeleitet und mit den experimentellen Ergebnissen verglichen. Dabei zeigte sich, dass die Vektoraddition gut für den elektronischen Grundzustand funktioniert. Für den ersten elektronisch angeregten Zustand funktioniert diese Methode nur für asymmetrische und nicht für symmetrische Moleküle. Dieses Verhalten konnte auf eine Mischung der Zustände für asymmetrische Moleküle zurückgeführt werden.

Weiter wurde 3-Cyanoindol und das 3-Cyanoindol Wassercluster analysiert. Anhand der Rotationskonstanten konnte das beobachtete Wassercluster eindeutig als die Struktur,

bei der das Wassermolekül über Wasserstoffbrückenbindung an das NH des Indolgerüsts gebunden ist, identifiziert werden. Die Analyse der elektronischen Natur des ersten angeregten Zustands zeigte, sowohl für 3-Cyanoindol als auch für das Wassercluster, einen  $L_b$ -Charakter. Somit findet eine Absenkung des  $L_a$  Zustands unter den  $L_b$  Zustand nicht statt, wie es beispielsweise bei 4-Cyanoindol zu beobachten ist. Die Untersuchung der Fluoreszenzlebenszeiten zeigte weiter eine abfallende Lebensdauer vom Monomer zum Wassercluster und eine äußerst kurze in wässriger Lösung. Dem steht eine Verlängerung der Fluoreszenzlebensdauer bei Deuterierung der NH Position gegenüber.

# Abstract

Using rotationally resolved fluorescence spectroscopy it is possible to obtain several molecular parameters of the electronic ground and first excited state and use them for structural assignment or for the determination of the electronic nature of these states. The focus of this doctoral thesis is on investigations on several rotamers of 1,2-, 1,3- and 1,4-dimethoxybenzene as well as on 3-cyanoindole and its water cluster.

One chapter deals with investigations of the conformational landscape of 1,3-dimethoxybenzene. The most intensive vibrational bands of 1,3-dimethoxybenzene were recorded with rotational resolution and assigned via rotational constants to the different rotamers. One of the three possible planar rotamers was not found and the assumed origin band of this rotamer turned out as a vibrational band of another rotamer. The not observed rotamer has the structure where both methoxy groups are pointing at each other. Further investigations via quantum chemical calculations have shown a non-planar geometry of this rotamer in the first excited state and a resulting small Franck-Condon factor. The results were presented in chapter 5 in detail.

Chapter 6 focuses on the dipole and transition dipole moments of the rotamers of 1,2-, 1,3- and 1,4-dimethoxybenzene. The permanent dipole moments were derived via vectorial addition of the fragment dipole moments and compared to the experimental dipole moment. This method works well for the electronic ground state. For the first excited state this method works only for asymmetrical, but not for symmetrical molecules. This behavior was traced back to a state mixing of the excited states for asymmetrical molecules. Further investigations were analyzing 3-cyanoindole and its water cluster. Via rotational constants the observed water cluster was identified as the structure where the water moiety is connected via a hydrogen bond to the NH of the indole frame. The analysis of the electronic nature of the first excited state showed  $L_b$  character for both, the monomer and the cluster. A lowering of the  $L_a$  state and thereby a change in the order of the  $L_a$  and  $L_b$ , as observed for 4-cyanoindole does not occur. Finally, 3-cyanoindole shows a decreasing fluorescence lifetime from monomer to the 1:1 cluster and to solution. However, the deuteration of the

NH position of 3-cyanoindole results in a decrease of the fluorescence lifetime.

# 1 | Introduction

Spectroscopy is an important technique for analyzing structures, excited states and molecular properties in chemistry. It is based on the interaction between electromagnetic radiation and matter like ions, atoms, molecules, fragments or clusters. Depending on the wavelength of the electromagnetic radiation, several compositions of matter can interact with radiation and many spectroscopic methods to investigate various properties of matter exist. In molecular spectroscopy the focus lies on the interaction of vibrational, rotational and/or electronic states with radiation. This allows to study a variety of molecular properties. Since this doctoral thesis deals with *high resolution laser induced fluorescence spectroscopy* (**HRLIF**), this method will be specified hereafter in detail.

In HRLIF spectroscopy the electronic excitation takes place in a molecular beam. With the help of this technique it is possible to investigate molecules, not only isolated and without interaction of their environment, but also single stable rotamers. Inside the molecular beam all molecules exist in low vibrational levels of the electronic ground state. For the excitation a narrow-band UV laser light is used. This laser light has enough energy to excite the molecules into the first electronic state and due to its narrow-band character it is possible to excite specific rotational levels. The molecules emit fluorescence light which contains a lot of molecular information. The evaluation of the fluorescence spectrum, by means of evolutionary algorithms, provides the values of all molecular parameters. Namely, the rotational constants for the ground and first electronic state, the orientation of the transition dipole moment, the electronic origin and the fluorescence lifetime. Stark experiments additionally accesses the determination of the permanent dipole moments for the ground and first electronic state. With these information, in combination with high level *ab initio* calculations, it is possible to obtain knowledge about structures, the electronic nature and the behavior upon excitation of molecules. Further theoretical and experimental background of this experimental technique is explained in the Chapters 2 and 3, respectively.

A considerable attention of HRLIF spectroscopy is about investigations on substituted in-

doles and bisubstituted benzenes. The current level of knowledge about these molecules, their derivatives and the molecules investigated in this thesis is given in the following subchapters.

## 1.1. Dimethoxybenzenes

A broad range of molecules is provided by disubstituted benzenes. Well-known representatives are dihydroxybenzene, methoxyphenol and dimethoxybenzene, which are derived from anisole and phenol, respectively. These molecules have two hydroxy groups, a hydroxy and a methoxy group or two methoxy groups attached to the benzene ring. Due to the six positions of the benzene ring, the groups can be attached at the 1,2-, 1,3- and 1,4-position of the ring. Therefore, three constitutional isomers exist for every disubstituted benzene. Since the methoxy and hydroxy group are free to rotate along their bond to the benzene ring, there exist several planar isomers, called rotamers. The planar rotamers of the three constitutional isomers of dimethoxybenzene are presented in Figure 1.1.

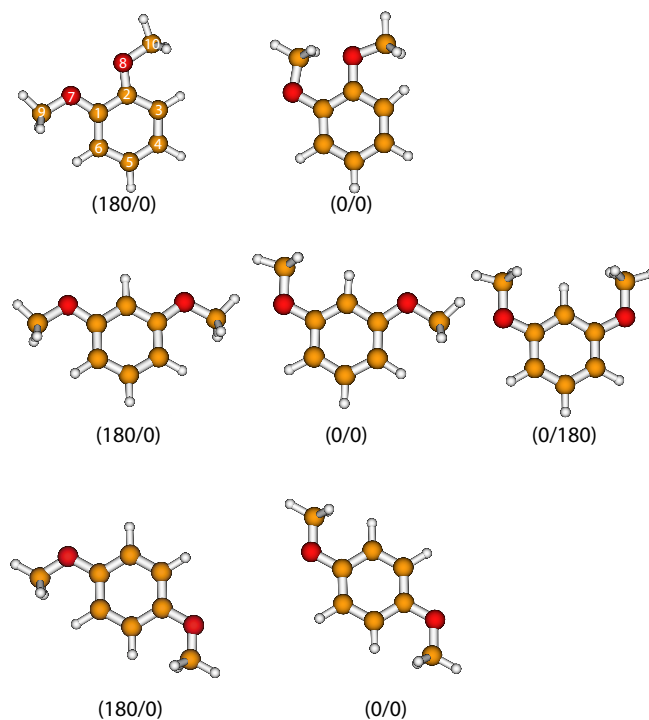


**Figure 1.1.:** Structures of the possible planar rotamers of 1,2-, 1,3- and 1,4-dimethoxybenzene. The value in brackets refers to the dihedral angle for the nomenclature.

The label in brackets refers to the dihedral angle of the first two substituent atoms in respect to the carbon atoms of the ring, starting from lowest atom number. For the (180/0) rotamer of 1,2-dimethoxybenzene these angles are formed by the atoms C9, O7, C1 and C2 for the first ( $\cong 180^\circ$ ) and C2, C3, O8 and C10 for the second ( $\cong 0^\circ$ ) dihedral angle.

It is possible to transfer one rotamer into another by rotating the functional groups and overcoming an intermediate barrier. The molecular beam method allows the investigation of these stable rotamers in a supersonic jet and determine their structures and energies for excitation.

Derivatives of disubstituted benzenes have been studied previously[1, 2]. These studies have shown that for the meta-position of dihydroxybenzene and methoxyphenol not all possible planar rotamers have been found in molecular beam experiments. The missing rotamer for 1,3-dihydroxybenzene and 1,3-methoxyphenol was the rotamer where both substituents show up in the same direction (according to the (0/180) isomer in the second line of Figure 1.1). The absence of this rotamer was explained by its non-planarity in the first excited state, which results in a small Franck-Condon factor upon excitation. However, Breen *et al.*[3] found via R2PI (resonant two-photon ionization) spectroscopy three vibronic bands for 1,3-dimethoxybenzene and assigned them to the origins of the three possible planar rotamers of 1,3-dimethoxybenzene (middle line of Figure 1.1). Therefore, the conformational landscape will be investigated for 1,3-dimethoxybenzene by rotational resolved spectroscopy for further structural studies. The results are presented in Chapter 5.

Rotational resolved investigations on 1,2-, 1,3- and 1,4-dimethoxybenzene rotamers further plays an interesting role due to the positive mesomeric effect (+M) and its influence to their electronic properties depending on the positions and orientations of the methoxy groups. By performing Stark experiments the permanent dipole moment of molecules for the electronic ground and first excited state can be determined. Comparison with experimental permanent dipole moments and dipole moments derived from vectorial addition of their fragment dipole moments have shown ambivalent results, since the success depends on the nature and position of the fragment. These studies were performed on the disubstituted benzene aminobenzonitrile (ABN). The results showed that this rule works for 3ABN in the ground, but for 2ABN only in the excited state. Reasons were given by an off-axis mixing in the excited state and a non-planarity of the component parts in the ground state[4, 5]. Wilke *et al.*[6] investigated the prediction of dipole moments via vector addition of fragment dipole moments on several substituted indoles. For 5-methoxyindole they

found that the rule fails in the excited state due to the electron density flow from the substituent into the chromophore, caused by the +M effect of the methoxy group. Therefore, the permanent dipole moments of the different constitutional isomers of dimethoxybenzenes and their transition dipole moment orientations will be investigated via rotationally resolved Stark spectroscopy, in combination with *ab initio* calculations, in order to be able to make more general statements as well about the influence of the methoxy-group position and orientation as the application of the vectorial addition model to these rotamers.

## 1.2. 3-Cyanoindole

Indole is the frame and main component of many biomolecules in nature as amino acids or neurotransmitters. For indole and its derivatives two energetically close  $\pi\pi^*$  states exist with different photophysical properties and fluorescence behaviors. These  $\pi\pi^*$  states are named  $^1L_a$  and  $^1L_b$  state in the nomenclature of Platt[7]. There are several properties to determine and distinguish the first two excited states as an  $^1L_a$  or as an  $^1L_b$  state. The indications thereof are explained in Chapter 2.2 in detail. One parameter to distinguish these states are their different permanent dipole moments. For example, in indole the  $^1L_a$  state has a dipole moment of 5.69 D in contrast to 2.17 D for the  $^1L_b$  state[8]. For indole in the gas phase the  $^1L_b$  state energetically lower than the  $^1L_a$  state. Several studies showed that it is possible to change the energetic order of these two states by adding different substituents to the chromophore or through cluster formations. Korter *et al.* [9] investigated the indole water cluster in the gas phase, using high resolution spectroscopy in combination with *ab initio* calculations. They showed the  $^1L_b$  character of the first excited state of the water cluster. Its electronic origin was shifted by  $132\text{ cm}^{-1}$  to the red, compared to the indole monomer. This most stable water cluster was forming a trans-linear  $\text{NH}\cdots\text{O}$  hydrogen bond. Further, they showed that the water moiety changes its position and orientation by absorbing a photon. Other studies were focusing on substituent effects. The attachment of a cyano group to the chromophore changes the electronic properties of the molecule. 5-cyanoindole was studied by Wilke *et al.* [6]. They were able to show the influence of the cyano group to the order of the  $^1L_a$  and  $^1L_b$  state. The lowest excited singlet state was determined as an  $^1L_a$  state.[6, 10] Reasons, why the  $^1L_a$  is energetically lower than the  $^1L_b$  state, are explained by the negative mesomeric (-M) and inductive (-I) effect of the cyano group, moving electron density from the chromophore to the substituent.

Therefore, it is of great interest to study 3-cyanoindole and its water cluster via high

resolution spectroscopy. The cyano group attached to the pyrrole ring of the indole frame might have great influence on photophysical properties, the most stable 1:1 water cluster structure and/or on fluorescence lifetimes.



## 2 | Theoretical Background

### 2.1. Principles of rotational spectroscopy

For the interpretation and simulation of rovibronic spectra it is necessary to solve the time-independent Schrödinger equation (Equation 2.1). The solution allows to calculate the eigenvalues of the molecular energy levels and thereby the transition energies of a transition between two states as well as the wave functions with the resulting transition intensities of two states, which is given by the transition dipole moment (Equation 2.2).

$$\hat{H}\Psi_m = E\Psi_m \quad (2.1)$$

$$M(\Psi_m \leftarrow \Psi_n) = \langle \Psi_n^* | \hat{O} | \Psi_m \rangle \quad (2.2)$$

(With:  $\hat{H}$  as Hamiltonian,  $E_m$  as eigenvalue of an energy level,  $\Psi$  as wave function,  $\hat{O}$  as dipole operator)

The operators  $\hat{H}$  and  $\hat{O}$  have to be determined to describe and calculate the positions and intensities of rotational spectra. To describe rotational spectra, the Hamiltonian can be derived from the rigid rotator model in classical mechanics. This model uses the simplification that no centrifugal distortion occurs. The moment of inertia of a rigid rotor is defined in Equation 2.3, containing the masses of the nuclei  $m_i$  and their distance  $r_i$  to a perpendicular axis  $\alpha$ :

$$I_\alpha = \sum_{i=1}^n m_i r_{i\alpha}^2 \quad (2.3)$$

In classical mechanics the kinetic energy of a rigid rotor is a function of the moment of

inertia and of the vector of the angular velocity  $\vec{\omega}$ . Its energy is calculated via Equation 2.4:

$$T_{Rot} = \frac{1}{2} \vec{\omega}^T I \vec{\omega} \quad (2.4)$$

Molecules, seen as rigid rotors have, as rigid bodies in general, three orthogonal main inertial axes ( $a$ ,  $b$  and  $c$ ) with their origin in the center of mass. This means, that for every molecule three moments of inertia exist ( $I_a$ ,  $I_b$  and  $I_c$ ) along these inertial axes. By definition the axes were chosen to be the  $I_a$  with the smallest and  $I_c$  with the highest moment of inertia ( $I_a \leq I_b \leq I_c$ ). By the ratio of the moments of inertia to each other, molecules are classified into different types of rotors, shown in Table 2.1.[11, 12]

**Table 2.1.:** Definition of different types of rotors

Type of rotor	Definition	Example
linear	$I_a = 0, I_b = I_c$	H <sub>2</sub>
spheric	$I_a = I_b = I_c$	SF <sub>6</sub>
prolate symmetrical	$I_a < I_b = I_c$	CH <sub>3</sub> Br
oblate symmetrical	$I_a = I_b < I_c$	C <sub>6</sub> H <sub>6</sub>
aymmetric	$I_a < 0, I_b < I_c$	H <sub>2</sub> O

$I$  from Equation 2.4 is expressed trough a tensor. This tensor results from the masses  $m_i$  of a  $n$  atomic molecule and the cartesian coordinate system with its origin in the center of mass.

$$\tilde{I} = \begin{pmatrix} I_{xx} & I_{xy} & I_{xz} \\ I_{yx} & I_{yy} & I_{yz} \\ I_{zx} & I_{zy} & I_{zz} \end{pmatrix} \quad (2.5)$$

$$\begin{aligned} I_{xx} &= \sum_{i=1}^n m_i (y_i^2 + z_i^2) & I_{xy} &= I_{yz} = - \sum_{i=1}^n m_i x_i y_i \\ I_{yy} &= \sum_{i=1}^n m_i (x_i^2 + z_i^2) & I_{yz} &= I_{zy} = - \sum_{i=1}^n m_i y_i z_i \\ I_{zz} &= \sum_{i=1}^n m_i (x_i^2 + y_i^2) & I_{zx} &= I_{xz} = - \sum_{i=1}^n m_i z_i x_i \end{aligned} \quad (2.6)$$

The diagonal elements of this tensor (Equations 2.5 and 2.6) are the moments of inertia

and the off-diagonal elements are the products of inertia. The similarity transformation, shown in Equation 2.7, the axes of the molecule coordinate system is rotated onto the main inertial axes of the molecule.

$$\mathbf{U}^{-1} \begin{pmatrix} I_{xx} & I_{xy} & I_{xz} \\ I_{yx} & I_{yy} & I_{yz} \\ I_{zx} & I_{zy} & I_{zz} \end{pmatrix} \mathbf{U} = \begin{pmatrix} I_a & 0 & 0 \\ 0 & I_b & 0 \\ 0 & 0 & I_c \end{pmatrix} \quad (2.7)$$

This transformation diagonalizes the tensor of inertia and the diagonal elements are the moments of inertia  $I_a$ ,  $I_b$  and  $I_c$ , whereby Equation 2.4 results in Equation 2.8.

$$T_{Rot} = \frac{1}{2}I_a\omega_a^2 + \frac{1}{2}I_b\omega_b^2 + \frac{1}{2}I_c\omega_c^2 \quad (2.8)$$

The Hamiltonian is determined via the quantum mechanical correspondence principle. Consequently, the moments of inertia are replaced by the angular momentums, according to the corresponding axis, and the angular momentums were transformed into the angular momentum operator  $\hat{J}$  ( $J_\alpha = I_\alpha\omega_\alpha$ ).

$$\hat{H}_{Rot} = \frac{\hat{J}_a^2}{2I_a} + \frac{\hat{J}_b^2}{2I_b} + \frac{\hat{J}_c^2}{2I_c} \quad (2.9)$$

In molecular spectroscopy it is usual to express the energy between two transition levels in frequency. Thus, rotational constants (Equation 2.10) were implemented and Equation 2.9 results in Equation 2.11:

$$A \equiv \frac{h^2}{8\pi^2 I_a} \geq B \equiv \frac{h^2}{8\pi^2 I_b} \geq C \equiv \frac{h^2}{8\pi^2 I_c} \quad (2.10)$$

$$\hat{H}_{Rot} = \frac{4\pi^2}{h} (A\hat{J}_a^2 + B\hat{J}_b^2 + C\hat{J}_c^2) \quad (2.11)$$

The exact rotation of a molecule (or body in general) in space has to be described via two coordinate systems. A molecule-fixed coordinate system and a space-fixed coordinate system. The molecule-fixed system has its origin in the center of mass, while the space-fixed system is chosen that its origin coincides with the origin of the molecule fixed system. The spaced-fixed coordinate system can be converted into the molecule-fixed system to

obtain the principle axis system. In the principal axes system are the axes of the coordinate system in agreement with the main inertial axis of the molecule. The transformation takes place by rotating the coordinate system around three Eulerian angles. First, the molecule-fixed system  $(x, y, z)$  is turned anticlockwise around the  $z$ -axis by the angle  $\phi$  along and a new coordinate system with the axes  $x', y'$  and  $z'$  is created (a). Then, an anti-clockwise rotation around the  $x'$  axis by the angle  $\theta$  creates the  $x', y''$  and  $z'$  coordinate system (b). Finally, the rotation along the  $z'$  axis by the angle  $\chi$  creates the space-fixed coordinate system  $X, Y, Z$  (c). This process is shown in Figure 2.1.[11, 26]

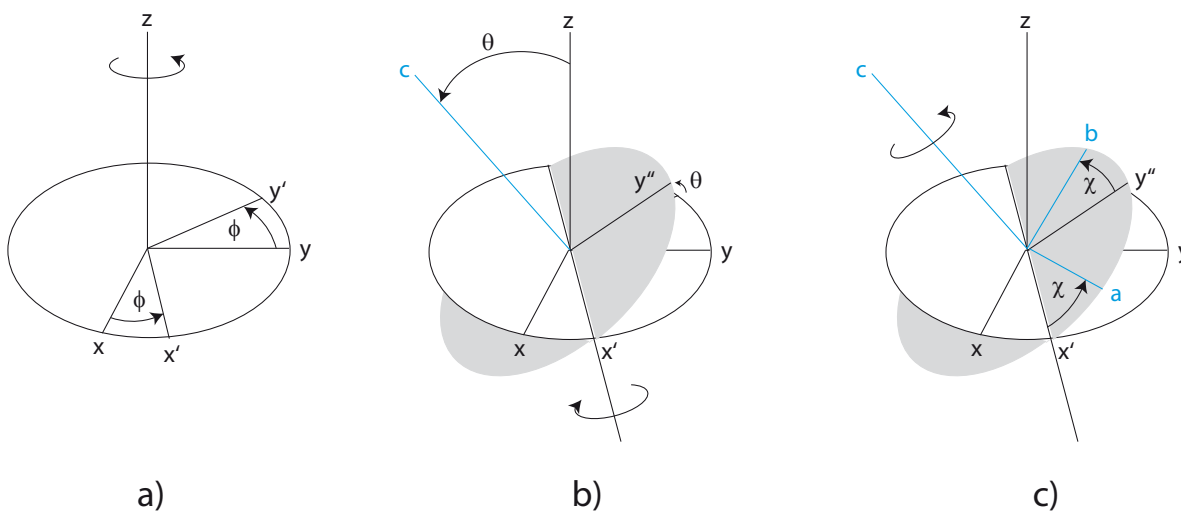


**Figure 2.1.:** Rotations at the transformation from the coordinate system into the principal axis system via three Eulerian angles.[13]

The commutator rules for the angular momentum operators of the molecule- and space-fixed coordinate system are given in Equation 2.12. The equations show that different components of the angular momentum operator in a coordinate system do not commute, but components of different coordinate systems do commute and every component of  $\hat{J}$  commutes with the square of the angular momentum  $\hat{J}^2$ . Since, the Hamiltonian changes with the square of the angular momentum operator  $\hat{J}^2$ , a quantization of the rotation results, which leads to the quantum number  $J$ . Further, the commutator of the Hamiltonian with the projection of the angular momentum of a space-fixed axis  $\hat{J}_z$  leads to a further quantum number  $M$ . In the case of two equal moments of inertial (as for linear, symmetrical and spherical rotors) the Hamiltonian commutes with the projection onto the molecular axis. This projection can be described by a the quantum number  $K$ . [11, 14]

$$\begin{aligned}
 [\hat{\mathbf{J}}^2, \hat{\mathbf{J}}_i] &= 0 & i = X, Y, Z \\
 [\hat{\mathbf{J}}^2, \hat{\mathbf{J}}_\alpha] &= 0 & \alpha = x, y, z \\
 [\hat{\mathbf{J}}_\alpha, \hat{\mathbf{J}}_i] &= 0 \\
 [\hat{\mathbf{J}}_i, \hat{\mathbf{J}}_j] &= ie_{ijk}\hbar\hat{\mathbf{J}}_k \\
 [\hat{\mathbf{J}}_\alpha, \hat{\mathbf{J}}_\beta] &= -ie_{\alpha\beta\gamma}\hbar\hat{\mathbf{J}}_\gamma \\
 [\hat{\mathbf{H}}_{rot}, \hat{\mathbf{J}}^2] &= 0 \\
 [\hat{\mathbf{H}}_{rot}, \hat{\mathbf{J}}_z] &= 0 \\
 [\hat{\mathbf{H}}_{rot}, \hat{\mathbf{J}}_c] &= i\hbar \left( \frac{1}{2I_a} - \frac{1}{2I_b} \right) (\hat{\mathbf{J}}_a\hat{\mathbf{J}}_b - \hat{\mathbf{J}}_b\hat{\mathbf{J}}_a)
 \end{aligned} \tag{2.12}$$

cyclic permutation	$e_{ijk} = e_{kij} = e_{jki}$
anticyclic permutation	$e_{kji} = e_{jik} = e_{ikj}$
all other permutationen	0

### 2.1.1. Symmetric Rotor

For the symmetric rotor with its two equal moments of inertia Equation 2.11 can be simplified. Depending if the two higher ( $I_c = I_b$ ) or the smaller ( $I_a = I_b$ ) moments of inertia are equal, the symmetric rotor is distinguished between a prolate ( $I_c = I_b$ ) and a oblate top, respectively. The solution of the Hamiltonian and therefore the solution of the rotational energy is:

$$\hat{H}_{Rot} = B\hat{\mathbf{J}}^2 + (A - B)\hat{J}_a^2 \tag{2.13}$$

$$E(J, K) = BJ(J + 1) + (A - B)K^2 \tag{2.14}$$

for the prolate and:

$$\hat{H}_{Rot} = B\hat{\mathbf{J}}^2 + (C - B)\hat{J}_a^2 \tag{2.15}$$

$$E(J, K) = BJ(J + 1) + (C - B)K^2 \quad (2.16)$$

for the oblate rotor, with the quantum numbers  $J = 0, 1, 2, \dots$  and  $K = 0, \pm 1, \dots, \pm J$ . The sign of  $K$  has no influence to the energy due to its quadratic character in Equation 2.16.  $K$  is two-fold degenerated for  $K \neq 0$  due to the different directions of rotation. For every rotational level exist  $(J+1)$   $K$ -levels. Further, selection rules allow only transitions where  $\Delta J = \pm 1$  and  $\Delta K = 0$  is fulfilled.[12, 15]

### 2.1.2. Asymmetric Rotor

As most molecules, the molecules investigated in this thesis, are asymmetrical rotors. Asymmetrical rotors have three different moments of inertia and the Hamiltonian cannot be simplified and is expressed in Equation 2.17:

$$\hat{H} = \frac{\hat{J}_a^2}{2I_a} + \frac{\hat{J}_b^2}{2I_b} + \frac{\hat{J}_c^2}{2I_c} \quad (2.17)$$

However, the asymmetric rotor can be seen as an intermediate between a prolate and a oblate top, transformed by deformation. Nevertheless, the description of the energy levels by the quantum number  $K$  fails and two pseudo quantum numbers  $K_a$  and  $K_c$  have to be implemented. These two pseudo quantum numbers describe a complete prolate and oblate rotor, respectively (Figure 2.2). To characterize if asymmetric rotors have more prolate or oblate character Ray's asymmetry parameter  $\kappa$  is used[12]:

$$\kappa = \frac{2B - A - C}{A - C} \quad (2.18)$$

The value of  $\kappa$  presents a completely prolate character for -1 and a complete oblate character for +1. For complete asymmetric rotors  $\kappa$  is 0. Another expression to describe the pseudo quantum numbers  $K_a$  and  $K_c$  is made by  $\tau$ .  $\tau$  is the difference of the two pseudo quantum numbers and has values from  $-J$  to  $+J$ [12]:

$$\tau = K_a - K_c \quad (2.19)$$

The formula of the Hamiltonian can not be reduced on the expressions  $J$  and  $J^2$  and the formula still contains the expressions  $J_x^2$ ,  $J_y^2$  and  $J_z^2$  referring to the space-fixed coordinates.[12, 15]

$$\hat{H}_{asym} = \frac{1}{2}(A + C)J(J + 1) + \frac{1}{2}(A - C) [J_x^2 - J_y^2 + \kappa J_z^2] \quad (2.20)$$

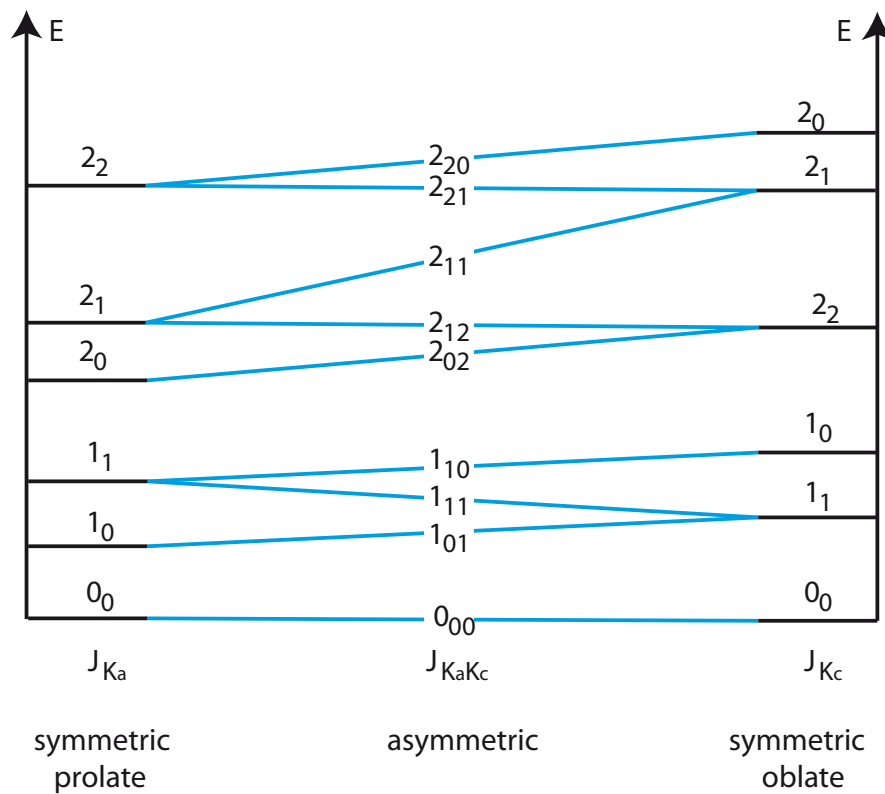


**Figure 2.2.:** Relationship of the energy levels of an asymmetrical rotor in respect to the transformation from prolate to oblate.[15, 16]

Due to the conservation of angular momentum only  $\Delta J = 0, \pm 1$  transitions are allowed upon excitation. Depending of the change of the angular momentum the transitions are named P-branch ( $\Delta J = -1$ ), Q-branch ( $\Delta J = 0$ ) or R-branch ( $\Delta J = +1$ ). A prerequisite for rotational transitions is a permanent dipole moment of the molecule. For asymmetric molecules the dipole moment has components along all three main inertial axes which results in the selection rules shown in Table 2.2.[12]

### 2.1.3. Stark Effect

The Stark effect describes the impact of an electric field ( $\epsilon$ ) on the rotational levels of a molecule and is used to determine its permanent dipole moments. Through this impact on rotational levels the Hamiltonian for the rotational energy from Equation 2.11 has to be extended with a perturbation operator  $\widehat{H}'$ :

$$\widehat{H}_{Stark} = \widehat{H}_{Rot} + \widehat{H}' \quad (2.21)$$

with:

$$\widehat{H}' = \epsilon \widehat{H}_\epsilon^{(1)} + \epsilon^2 \widehat{H}_\epsilon^{(2)} \quad (2.22)$$

The Stark effect Hamiltonian  $\widehat{H}_\epsilon$  is derived from the interaction energy between an electric dipole  $\mu$  moment and an electric field  $\epsilon$  in classical mechanics ( $E = -\mu\epsilon$ ). To transfer this to the energy of rotational levels, the electric field  $\epsilon$  has to be seen in a space-fixed electric field along the  $Z$  axis and constant in magnitude,  $\mu$  has to be seen as the electric dipole moment of the molecule in the molecule fixed-coordinate system, referring onto the principal inertial axes  $x, y, z$  and  $\Phi_{Zg}$  as the direction cosinus of the  $x, y, z$  axes in respect to the space-fixed  $Z$  axis:[17, 18]

$$\widehat{H}_\epsilon = -\epsilon \sum_{g=x,y,z} \mu_g \Phi_{Zg} \quad (2.23)$$

Therefore, the total energy of the rotational levels is a sum of the unperturbed energy and the Stark effect energy of the first and second order (Equation 2.24).

$$E_S = E^0 + E^1 + E^2 \quad (2.24)$$

**Table 2.2.:** Selection rules for an asymmetric rotor

	Dipole component	$\Delta K_a$	$\Delta K_c$
a-type	$\mu_a \neq 0$	0, $\pm 2, \pm 4, \dots$	$\pm 1, \pm 3, \pm 5, \dots$
b-type	$\mu_b \neq 0$	$\pm 1, \pm 3, \pm 5, \dots$	$\pm 1, \pm 3, \pm 5, \dots$
c-type	$\mu_c \neq 0$	$\pm 1, \pm 3, \pm 5, \dots$	0, $\pm 2, \pm 4, \dots$

For a symmetric rotor with a dipole component only along the c-axis, the Stark effect Hamiltonian can be simplified. For example, if a molecule possesses a dipole moment component only along the c axis, this dipole moment component equates to the total dipole moment of the molecule and simplification of the Hamiltonian results:

$$\widehat{H}_\epsilon = -\epsilon\mu\Phi_{Zz} \quad (2.25)$$

and the energy of the Stark effect results in:

$$E_\epsilon^{(1)} = -\frac{\mu\epsilon KM_J}{J(J+1)} \quad (2.26)$$

for the first order and:

$$E_\epsilon^{(2)} = \frac{\mu^2\epsilon^2}{2hB} \left[ \frac{(J^2 - K^2)(J^2 - M^2)}{J^3(2J+1)(2J-1)} - \frac{[(J+1)^2 - K^2][(J+1)^2 - M^2]}{(J+1)^3(2J+1)(2J+3)} \right] \quad (2.27)$$

for the second order. Equations 2.26 and 2.27 are showing that for  $K = 0$  exists no first-order Stark effect and only the Stark effect second order occurs. Further, for the first-order Stark effect the  $M_J$  degeneracy is lifted and splits into  $(2J+1)$  rotational levels. This is in contrast to the second-order Stark effect, where the degeneracy is partly lifted by  $M_J^2$  squared, what results in only  $(J+1)$  rotational levels.[17, 18]

For asymmetrical molecules the  $K$  degeneracy is lifted and thereby only the Stark effect second order occurs. The energy of a state  $J, \tau, M_J$  is a function of all dipole components along the inertial axes as well as all other states  $J', \tau'$  which are in interaction with this state.[17, 18]

$$E_{\epsilon,\gamma}^{(2)} = \mu_\gamma^2 \epsilon^2 \sum_{J',\tau'} \frac{\langle J, \tau, M_J | \Phi_{Z\tau} | J', \tau', M'_J \rangle^2}{E_{J\tau}^0 - E_{J'\tau'}^0} \quad (2.28)$$

$$\begin{aligned}
 E_{\epsilon,\gamma}^{(2)} = & \mu_\gamma^2 \epsilon^2 \left[ \frac{J^2 - M_J^2}{4J^2(4J^2 - 1)} \sum_{\tau'} \frac{\langle J, \tau | \Phi_{Z\tau} | J - 1, \tau' \rangle^2}{E_{J\tau}^0 - E_{J-1\tau'}^0} \right. \\
 & + \frac{M_J^2}{4J^2(J+1)^2} \sum_{\tau'} \frac{\langle J, \tau | \Phi_{Z\tau} | J, \tau' \rangle^2}{E_{J\tau}^0 - E_{J\tau'}^0} \\
 & \left. + \frac{(J+1)^2 - M_J^2}{4(J+1)^2(2J+1)(2J+3)} \sum_{\tau'} \frac{\langle J, \tau | \Phi_{Z\tau} | J+1, \tau' \rangle^2}{E_{J\tau}^0 - E_{J+y\tau'}^0} \right] \quad (2.29)
 \end{aligned}$$

Equation 2.28 shows the quadratic character of  $M_J^2$ . Consequently, the degeneracy of  $M$  is lifted and for  $M$  exist  $(J+1)$  sublevels. Except for  $M = 0$  are all two-fold degenerated. The dipole moment components have to be calculated for all main inertial axes. By summing up these dipole moments, the square of the total dipole moment of the molecule is received. Due to its quadratic character no information about its direction can be given.

$$\mu = \sqrt{\mu_a^2 + \mu_b^2 + \mu_c^2} \quad (2.30)$$

Figure 2.3 shows the band splittings for several  $J'' = 1$  to  $J' = 2$  transitions of a R-branch of an asymmetric rotor. Selection rules allow only  $\Delta M = 0, \pm 1$  transitions, depending on the polarization of the excitation light to the direction of the electric field. For a parallel orientation of the excitation light and the electric field  $\pi$  transitions with  $\Delta M = 0$ , while for a perpendicular orientation  $\sigma$  transitions with  $\Delta M = \pm 1$  are allowed.[17, 18]

## 2.2. Characterization of Excited States

For indole and its derivatives two energetically close  $\pi\pi^*$  states with different photophysical properties and fluorescence behaviors exist. Platt investigated these two lowest excited singlet states on cata-condensed hydrocarbons and labeled them as  ${}^1L_a$  and  ${}^1L_b$ , depending if the electron density is located at the atoms (a) or bonds (b).[7] Weber[19] transferred this nomenclature to indoles. Since the different dipole moments of the  ${}^1L_a$  (5.69 D) and  ${}^1L_b$  (2.17 D)[8] state in indole, their energetic order can be manipulated via different solvents. For example, the  ${}^1L_a$  state with its high dipole moment is stabilized in polar solvents and therefore the first excited state is an  ${}^1L_a$  state.[20] Naturally, for measurements in the gas phase this manipulation does not work. However, it is possible to manipulate the order of these states by adding either substituents with different inductive and mesomeric effects or attaching single solvent molecules to the chromophore.

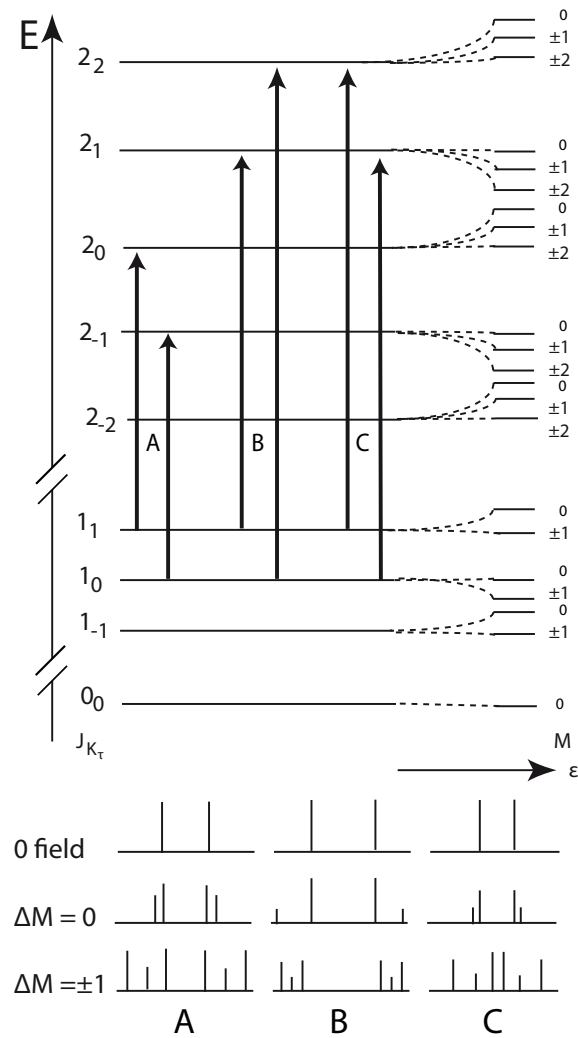


**Figure 2.3.:** Band splittings of the R-branch lines of an asymmetric rotor when an electric field is applied. According to:  $J'' = 1$  to  $J' = 2$  transitions,  $\mu_a = 1D$ ,  $E = 10000$  V and  $A = 2.0$ ,  $B = 1.05$ ,  $A = 1.0cm^{-1}$ . The strengths of the splitting is in dependence of the square of  $\epsilon$ . [18]

The electronic nature of several substituted indoles in the gas phase have already been studied and the nature of their first excited state was determined.[2, 21] Four criteria were used to distinguish between the  ${}^1L_a$  or  ${}^1L_b$  state for indoles, which were specified hereafter:

- The orientation of the transition dipole moment  $\theta$
- The magnitude of the permanent dipole moments
- The involved frontier orbitals upon excitation
- The changing of the bond lengths upon excitation

The orientations of the angles of the transition dipole moment of the  ${}^1L_a$  and  ${}^1L_b$  state of indole are shown in Figure 2.4. Trough measurements only the angle of  $\theta$  can be determined, but not the sign in respect to the main inertial axis  $a''$ . Therefore the sign has to be determined via measurements of further isotopologues and the resulting change of theta, caused by the rotation of the main inertial system or via quantum chemical calculations.

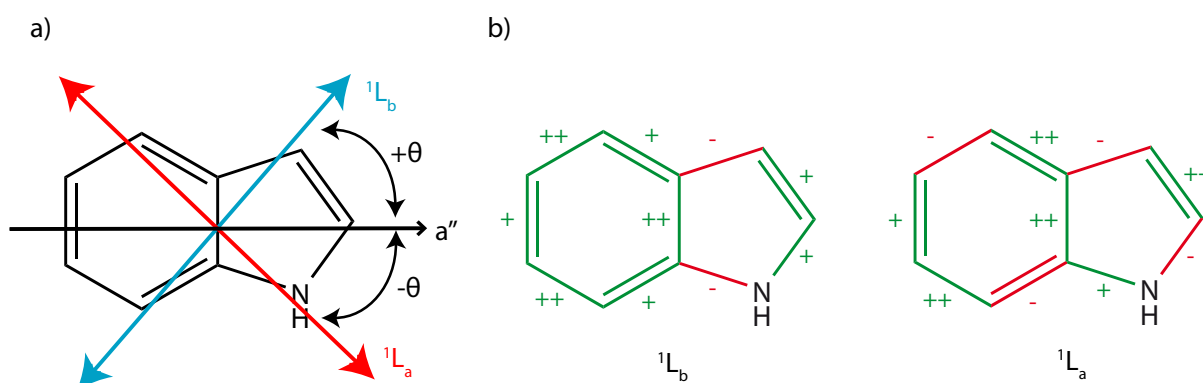


**Figure 2.4.:** Distinction of the  ${}^1L_a$  and  ${}^1L_b$  state in indole. a) Different orientations of the transition dipole moment of the two states. b) Changing of the bond lengths upon excitation of the two states.[15]

As mentioned above, the  ${}^1L_a$  state has a much higher permanent dipole than the  ${}^1L_b$  state and has to be considered for the assignment as well. A high permanent dipole moment of the first excited singlet state leads to an  ${}^1L_a$  character and a small dipole moment to an  ${}^1L_b$  character. The change of the bond lengths upon excitation is shown in Figure 2.4. For an  ${}^1L_a$  state the bond lengths increase and decrease alternating over the whole molecule, while for the  ${}^1L_b$  state mainly the benzene ring is expanded. Finally, a look on the frontier orbitals can give a hint to the assignment of the states. For excitation into the  ${}^1L_a$  are

mostly HOMO  $\rightarrow$  LUMO (more than 80 %) transitions involved, in contrast to the  $^1L_b$  state where the excitation is a combination of a over 70 % HOMO-1  $\rightarrow$  LUMO and a over 20 % HOMO  $\rightarrow$  LUMO+2 transition. All values refer to indole and were transferred to its derivatives for the assignment of excited states. The classification of Platt's nomenclature describing the nodal planes either bisecting the bonds or through the atoms is transferred by Heilbronner and Murrell to substituted benzenes, having a  $C_2$  symmetry axis [22]. In this classification the indices  $a$  and  $b$  are describing the symmetry in respect to the  $C_2$  symmetry axis. An orientation of the transition dipole moment along this axis leads to an  $^1L_a$ , while an orientation perpendicular to this axis leads to an  $^1L_b$  state.

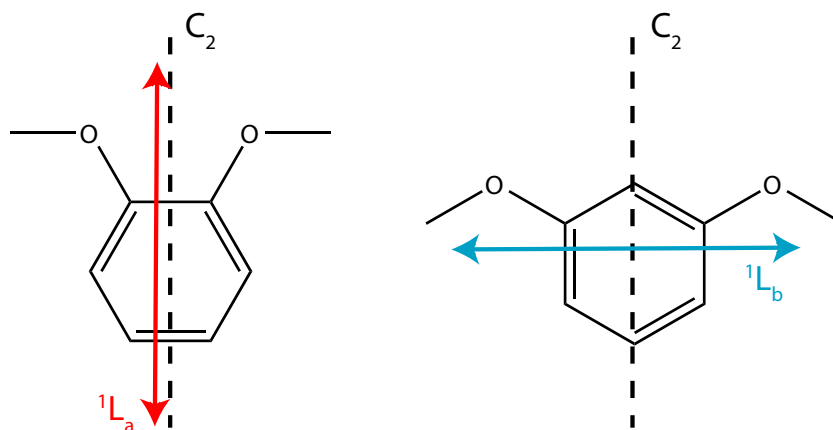


**Figure 2.5.:** Orientation of the transition dipole moment for an  $^1L_a$  and an  $^1L_b$  state along the  $C_2$  symmetry axis on the example on 1,2-dimethoxybenzene and 1,3-dimethoxybenzene, respectively.

Further, the excitation into the corresponding state leads to a benzenoid distortion of the ring in an  $^1L_a$  and a quinone-like distortion for an  $^1L_b$  state, respectively. These distortions can be derived from the changing of the rotational constants between the ground and first excited state. For a benzenoid distortion the differences of all rotational constants  $\Delta A$ ,  $\Delta B$  and  $\Delta C$  will decrease more or less equal, but for a quinone-like distortion  $\Delta A$  will much bigger while there will be almost no differences between the  $B$  and  $C$  constants.[23]



### 3 | Experimental Setup

A special experimental setup is necessary to record rotationally resolved fluorescence spectra. First, a narrow-band variable frequency UV light source is required to stimulate the molecules to fluorescence and second, a molecular beam is needed to obtain isolated molecules.

The laser system where the UV light is created consists of a dye-laser driven by a pump laser, a reference cell for frequency stabilization, a unit for frequency-doubling (second harmonic generation) and additionally a iodine cell and a Fabry-Pérot interferometer for absolute and relative frequency determination (Figure 3.1).

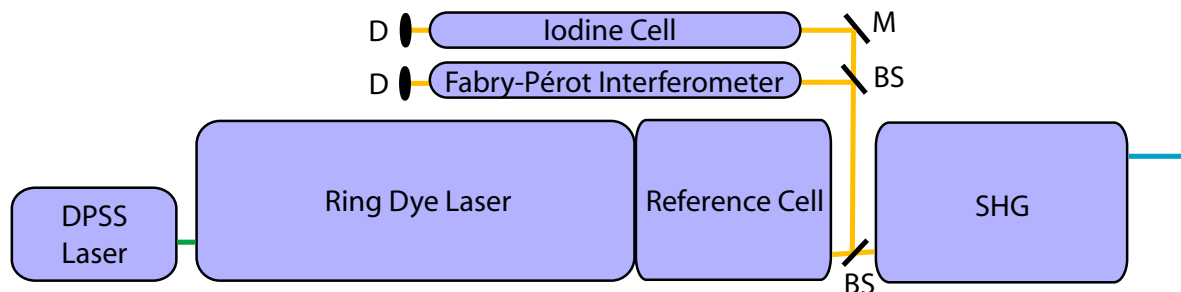


**Figure 3.1.:** Setup of the laser system. Abbreviations: DPSS = diode pumped solid state laser, D = detector, M = mirror, BS = beam splitter, SHG = second harmonic generation.

The molecular beam is created in a special molecular beam apparatus. In this apparatus the molecules were also stimulated to fluorescence and the fluorescence light is detected onto the photomultiplier (Figure 3.8). To protect the laser system from vacuum pump vibrations of the molecular beam apparatus, the two parts are spatially separated and the UV laser light is lead via mirrors to the molecular beam apparatus.

The following chapters will give a closer look on both parts and their components.

### 3.1. The Laser System

#### 3.1.1. The Pump Laser

In this work the Newport Spectra Physics *Millennia eV*, 15 W diode pumped solid state laser is used to drive the dye laser. This laser emits light at a wavelength of 532 nm and can be operated at a power up to 15 W.

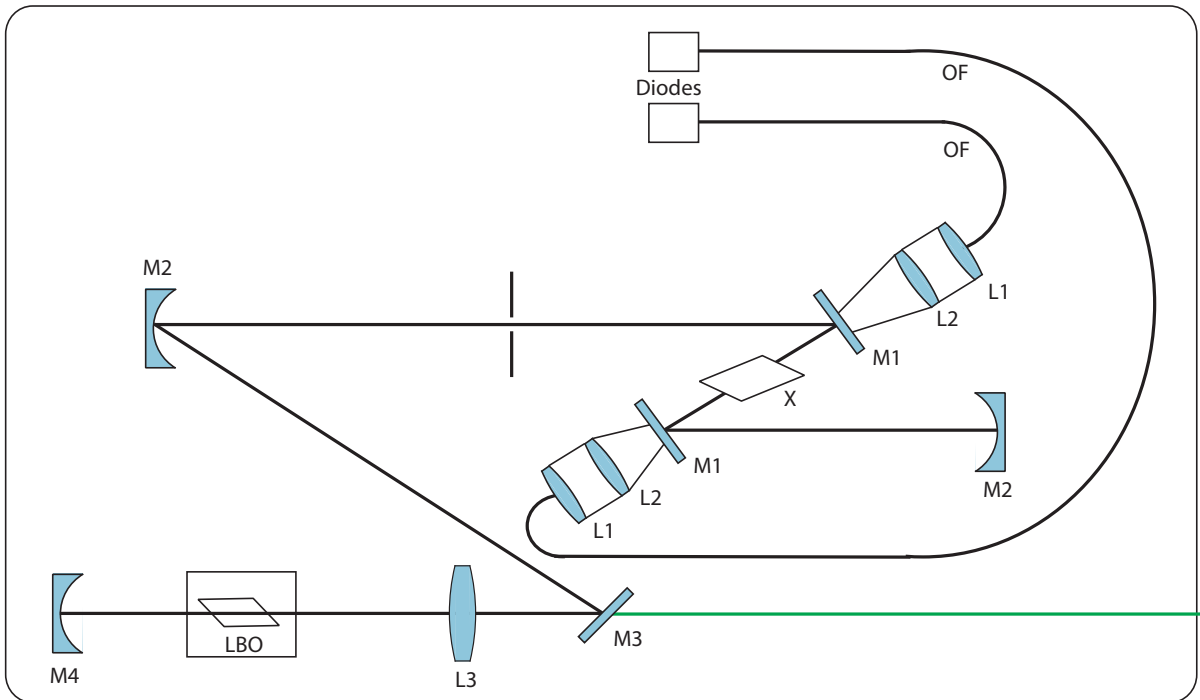


**Figure 3.2.:** Setup of the pump laser Spectra Physics Millennia eV [13, 24]. Abbreviations: OF = optical fiber, L = lens, X = yttrium-vanadate crystal, M = mirror, LBO = lithium triborate crystal.

To emit light at this wavelength, light of two diodes with a wavelength of 809 nm is lead via optical fibers (OF) and focused via lenses (L1, L2) on a Neodymium-doped Yttrium vanadate crystal (X)  $Nd : YVO_4$ . The crystal absorbs the light and emits light at a wavelength of 1064 nm, which is enhanced in a resonator formed by the mirrors M1. These mirrors are highly reflective at 1064 nm and highly transmissive at 809 nm. After this, light of 1064 nm wavelength is directed by mirrors M2 to a nonlinear Lithium triborate crystal for second harmonic generation. Finally, light with a wavelength of 532 nm leaves the laser through the output coupler (M3) and enters the dye laser. (Figure 3.2) [13, 24]

### 3.1.2. The Ring Dye Laser

In this work the ring dye laser *Matisse DS* from Sirah Lasertechnik GmbH is used. The schematic structure of this laser is shown in Figure 3.3.

Inside the dye laser hits the incoming laser beam a laminar dye jet, which circulates with a pressure of 20 bar. Thus, the dye molecules were excited from the electronic ground state  $S_0$  into vibrational excited states of the first electronic state  $S_1$ . By relaxation to the vibrational ground state  $v = 0$  of the  $S_1$  state, the electrons were able to relax under the emission of light to vibrational excited states of the electronic ground state. The high pressure of the dye jet is necessary to prevent high triplet concentration. High triplet concentrations would inhibit the fluorescence.

The dye laser can be used with several in ethylene glycol solved dyes. The different dyes emit light in different ranges. Due to the interaction of the dye molecules with the solvent a broad range of the emitted light is created. For investigations in this work, Rhodamine 110 and Rhodamine 6G were used as dyes. These dyes emit light from 545 nm to 585 nm and 560 nm to 615 nm, respectively.[25]

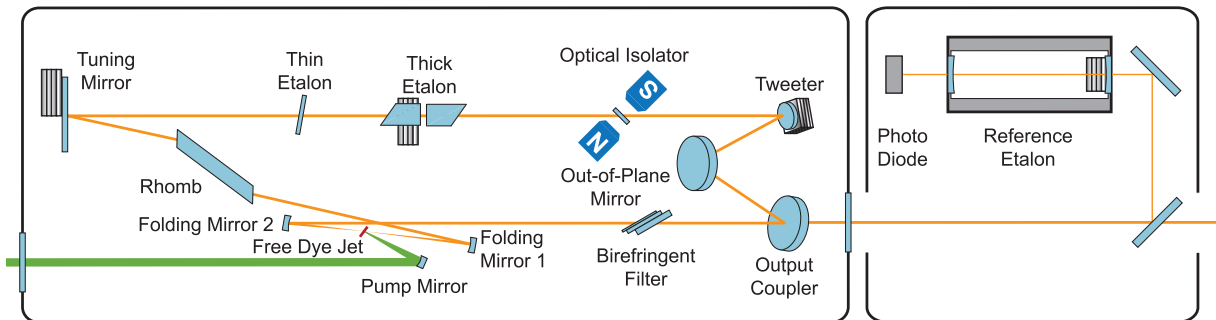


**Figure 3.3.:** Setup of the dye laser *Matisse DS* and its reference cell.[25, 26]

The fluorescence light from the dye jet propagates via the two folding mirrors FM 1 and FM 2 into the resonator and light amplification by stimulated emission occurs. Inside of the cavity the light can propagate in both directions, however only the anticlockwise circulation is desired and selected by means of an optical diode utilize the Faraday effect and an out-of-plane mirror. Via three wavelength selective elements, arranged in decreasing bandwidth, it is possible to select one frequency of the broad emission of the dye. The first filter is a birefringent filter and selects roughly a passband. This filter contains three birefringent quartz plates (Lyot filter) which are related in 1 : 3 : 15 thickness. The plates are orientated in Brewster's angle and create a passband of around  $2 \text{ cm}^{-1}$ .

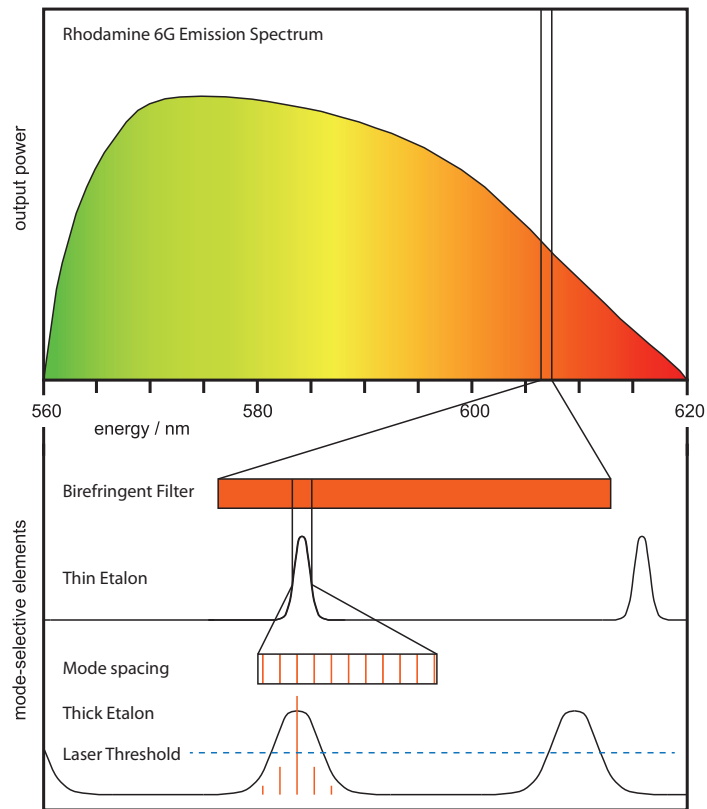


**Figure 3.4.:** Emission spektrum of Rhodamine 6G in ethylene glycol and the free spectral range of the optical elements to create a narrow-band frequency.[27]

The next wavelength selective element is a Fabry-Pérot etalon, called *thin etalon*. The *thin etalon* is constructed with two semi-reflector mirrors having a fix distance to each other. The last wavelength selective element, the *thick etalon*, contains two prism, of those one is mounted on a tunable piezoelectric motor. Via these three wavelength selective elements it is possible to run the laser with a linewidth of 250 kHz (Figure3.4).[25, 27]

To scan the laser, the tuning mirror on a piezoelectric motor is moved and the optical wavelength of the cavity is changed. The scan process takes place over a range of 1 - 2  $\text{cm}^{-1}$ . To run the laser stable on one frequency a reference cell is needed. For this, a small part of the light is coupled into an external reference cell, containing a reference etalon. In this cell a reference signal is detected and with the fast moving tweeter inside of the ring dye laser it is possible to compensate smallest interferences, caused by vibrations or fluctuations in the dye jet.[13, 25, 27]

### 3.1.3. The Frequency Doubler

For the excitation into the first electronic singlet state UV light is needed. Therefore, the main part of the laser light out of the dye laser is coupled in an external cavity for second harmonic generation. The frequency doubling unit *WaveTrain* of Newport Spectra-Physics is used in this experimental setup. (Figure 3.5).

Frequency doubling requires the equality of the phase velocity of the incoming wave and the harmonic wave. This is achieved by a nonlinear optical media, using a  $\beta$ -barium borate crystal, which is unique for its birefringent character and its small absorption in the frequency range of the fundamental wave. Depending on the operated wavelength, the crystal has to be tilted for phase matching adjustment.[13, 16, 25, 28, 29]

Inside the frequency doubling unit the incoming laser beam passes a lens (L1) and a tube for phase modulation. The phase modulator is connected with an optical fiber (OF) to a fiber coupler (FC) and a weak signal for frequency stabilization is added to the fundamental. Then, the laser beam enters the resonator after passing two mirrors (BM1 and BM2), a lens (L2), a beam shifter (BS) and a brewster window. The resonator contains two for the fundamental wave highly reflecting mirrors (M1 and M2), a  $\beta$ -barium borate crystal (X) and a prism (P) mounted on a piezoelectric motor. The resonator is constructed based on the delta concept. After passing the crystal, the frequency doubling occurs and the UV light is able to leave the resonator through a wavelength selective mirror (M2) and passes a brewster window and a cylindrical lens. To leave the laser, the beam is lead via two bending mirrors (BM3 and BM4) and a prism expander (PE) out of the doubling unit. Two detectors, one for the fundamental (FD) and one for the harmonic wave (HD) measure the intensity to support and improve the adjustment. Finally, the laser beam is lead via mirrors into the molecular beam apparatus.

### 3.1.4. The Determination of the Relative Frequency

Due to fluctuations of the scan velocity of the tuning mirror, distortions in the recorded spectrum can occur. To eliminate these distortions, a small part of the output beam of the dye laser is coupled into a Fabry-Pérot interferometer. The transmission is detected and a spectrum is recorded simultaneously to the experimental fluorescence spectrum (Figure 3.1). The interferometer consists of a 499 nm long ZERODUR<sup>®</sup> tube, located in vacuum, with a convex-concave coupling mirror and a concave-planar output mirror. The radius of curvature inside is 501 mm and the surface is highly reflective between 540 nm to 620 nm. The interferometer transmits only certain wavelengths and the free spectral

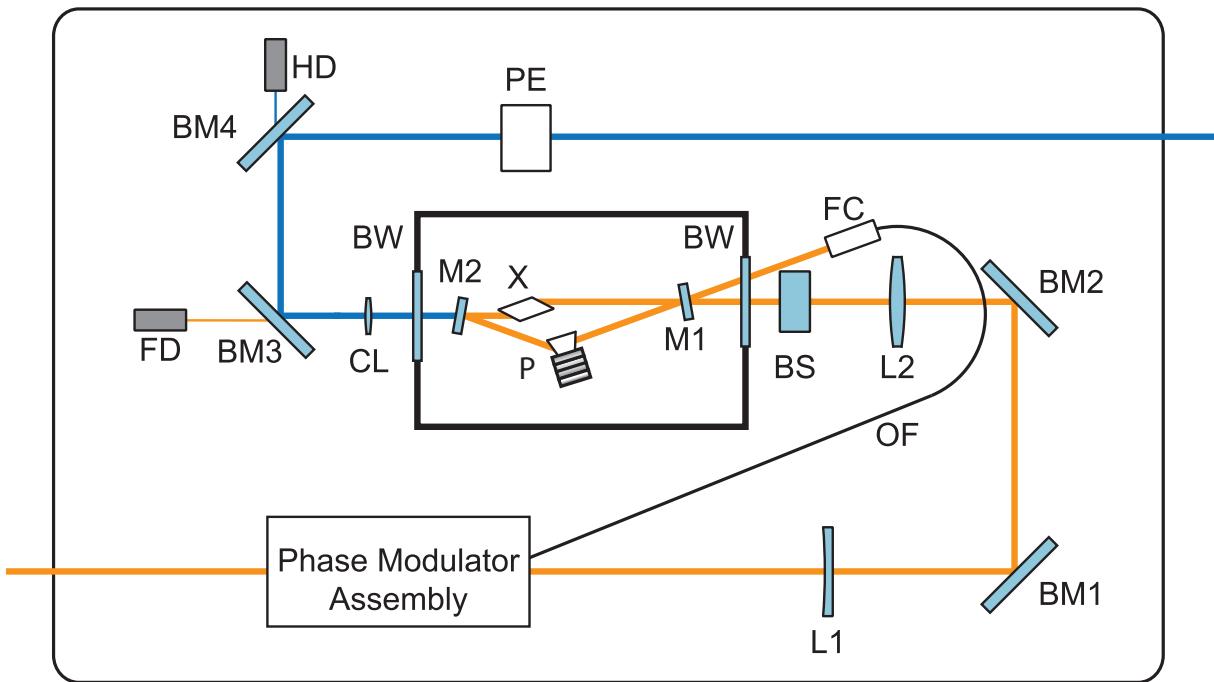


**Figure 3.5.:** Setup of the frequency doubling[26]. Abbreviations: L = lens, BM = bending mirrors, BS = beam shifter, BW = brewster window, M = mirror, X =  $\beta$ -barium borate crystal (BBO), P = prism, OF = optical fiber, FC = fiber coupler, CL = cylindrical lens, FD = detector (Fundamental), HD = detector (Harmonic), PE = prism expander.

range was determined to 149.9434(56) MHz [30]. With the transmission spectrum and the knowledge of the free spectral range it is possible to linearize the fluorescence spectrum.

### 3.1.5. The Determination of the Absolute Frequency

To determine the absolute frequency a iodine cell is applied. The iodine cell is a 50 cm long evacuated and with little iodine crumbs filled glass tube. For frequency determination a small part of the laser light is coupled into the tube and a iodine absorption spectrum is recorded parallel to the fluorescence spectrum. (Figure 3.1) By comparison of the absorption spectrum with tabulated bands in a iodine atlas[31], it is possible to determine the frequency with an accuracy of  $0.1 \text{ cm}^{-1}$ .

## 3.2. The Molecular Beam Apparatus

### 3.2.1. The Molecular Beam

The excitation and fluorescence emission of the investigated molecules takes place in a molecular beam. To create a molecular beam the molecules were transferred into the gas phase and expanded through a nozzle into the vacuum. Depending on the nature of the expansion, two kinds of beams were distinguished: *Effusive expansion* and *supersonic jet*. *Supersonic jets* were further classified into uncollimated beams (*free jet*) and collimated beams (*molecular beam*). For laser spectroscopic investigations molecular beams have several advantages[11]:

- The molecules exist isolated in the beam. Therefore, the molecular parameters can be determined without interaction with the environment.
- Due to the fast expansion and the resulting adiabatic cooling process low kinetic energy of translation, low rotational and low vibrational temperatures were achieved and the population distribution is limited on low rotational and vibrational levels. Thereby, there are no band overlaps and it is also possible to resolve the rotational structure of big molecules.
- In the molecular beam it is possible to investigate weakly bound clusters as dimers, molecule-water clusters or molecule-noble gas clusters. Under normal conditions these clusters are not stable.

To create a molecular beam in this setup, the sample is converted into the gas phase and expanded out of a reservoir through a nozzle into a chamber with lower pressure. The nature of the expansion depends on the relation of the pressure inside of the reservoir

( $p_0$ ), the pressure inside of the vacuum chamber ( $p_1$ ) and of the heat capacity ratio ( $\gamma$ ). If Equation 3.1 is fulfilled, supersonic expansion occurs.

$$\frac{p_0}{p_b} = \left( \frac{\gamma + 1}{2} \right)^{\frac{\gamma}{\gamma-1}} \quad (3.1)$$

At the beginning the statistical average velocity of the molecules is zero. Due to the lower pressure inside of the vacuum chamber, compared to the reservoir, the gas expands through the nozzle into the chamber. For supersonic expansion, the average mean free path is smaller than the diameter of the nozzle ( $D$ ). This results in many collisions between the molecules and kinetic energy of translation is given from fast to slow molecules. Through this process the assimilation of the relative speeds happens and undirected kinetic energy is converted into directed kinetic energy of translation. By this process the Maxwell–Boltzmann distribution (Equation 3.2) is narrowed and shifted to higher velocities[11, 26, 32]. (Figure 3.6)

$$\frac{dN}{d\nu} = \nu^3 \exp\left(-\frac{m\nu^2}{2kT}\right) \quad (3.2)$$

(Abbreviations:  $N$  = number of particles,  $\nu$  = particle velocity,  $m$  = particle masses,  $k$  = Boltzmann’s constant,  $T$  = gas temperature)

The adiabatic expansion and the collisions between the molecules results in a high occupation of low vibrational and rotational level of the electronic ground state. This effect can be enhanced by adding a carrier gas to the molecules during the expansion. The additional collisions between the carrier gas and the molecules results in that more kinetic energy of translation is emitted and extreme low temperatures ( $T \leq 1$  Kelvin) were achieved. By adding a carrier gas to the molecular beam, the beam is termed *seeded beam*. After leaving out the nozzle the expanding gas passes a skimmer. The skimmer has the shape of a hollow cone with an aperture of 1 mm on top. The skimmer is also the entry to the next vacuum chamber. The small opening conduces to cut out the central area of the expansion. The rounded sidewalls of the skimmer helps to derive the other molecules. After passing the skimmer, a collimated directed molecular beam with a low Doppler broadening is received.[33] Another function of the skimmer is to maintain the molecular beam. At the nozzle the sample leaks out with a Mach number of 1 (corresponds to the speed of sound). The Mach number is defined by the flow velocity and the local speed

of sound, which further depends on the temperature. Therefore, the cooling at adiabatic expansion leads to a reduce of the local speed of sound, what results in an increasing Mach number.

$$M = \frac{v}{a} \quad (3.3)$$

with

$$a = \sqrt{\frac{\gamma RT}{m}} \quad (3.4)$$

(Abbreviations:  $M$  = Mach number,  $v$  = flow velocity,  $a$  = local speed of sound,  $\gamma$  = heat capacity ratio,  $R$  = gas constant,  $T$  = temperature,  $m$  = molar mass)

This is only valid for the area between the aperture of the nozzle and the Mach disc shock. At the Mach disc shock the flow velocity is slower than the speed of sound and the molecular beam collapses. By putting the skimmer in front of the Mach disc shock, it is possible to prevent the collapse of the molecular beam. The distance  $X$  between the aperture of the nozzle to the Mach disc shock can be calculated via Equation 3.5, to determine the position of the skimmer.[34]

$$X = 0,67D\sqrt{\frac{p_0}{p_1}} \quad (3.5)$$

The described processes are shown in Figure 3.6 in detail.

### 3.2.2. The Vacuum Apparatus

The vacuum apparatus (Figure 3.8) consists of three lineary connected vacuum chambers. The chambers, which are connected by skimmers, have a decreasing pressure and were termed expansion (VK1), buffer (VK2) and measurement chamber (VK3). The first skimmer aperture (S1) has a diameter of 1 mm, the second (S2) of 3 mm. All chambers were connected to a prevacuum, created with three rotary vane pumps (*TRIVAC*) in combination with roots (*RUVAC*). These pumps work permanently, while the additional high vacuum pumps were activated only for measurements. The high vacuum pumps were an oil diffusion pump (Leybold *DI 8000*) in the first and a turbomolecular pump (Leybold *TURBOVAC*) in the second and third vacuum chamber. In the last chamber a cold trap

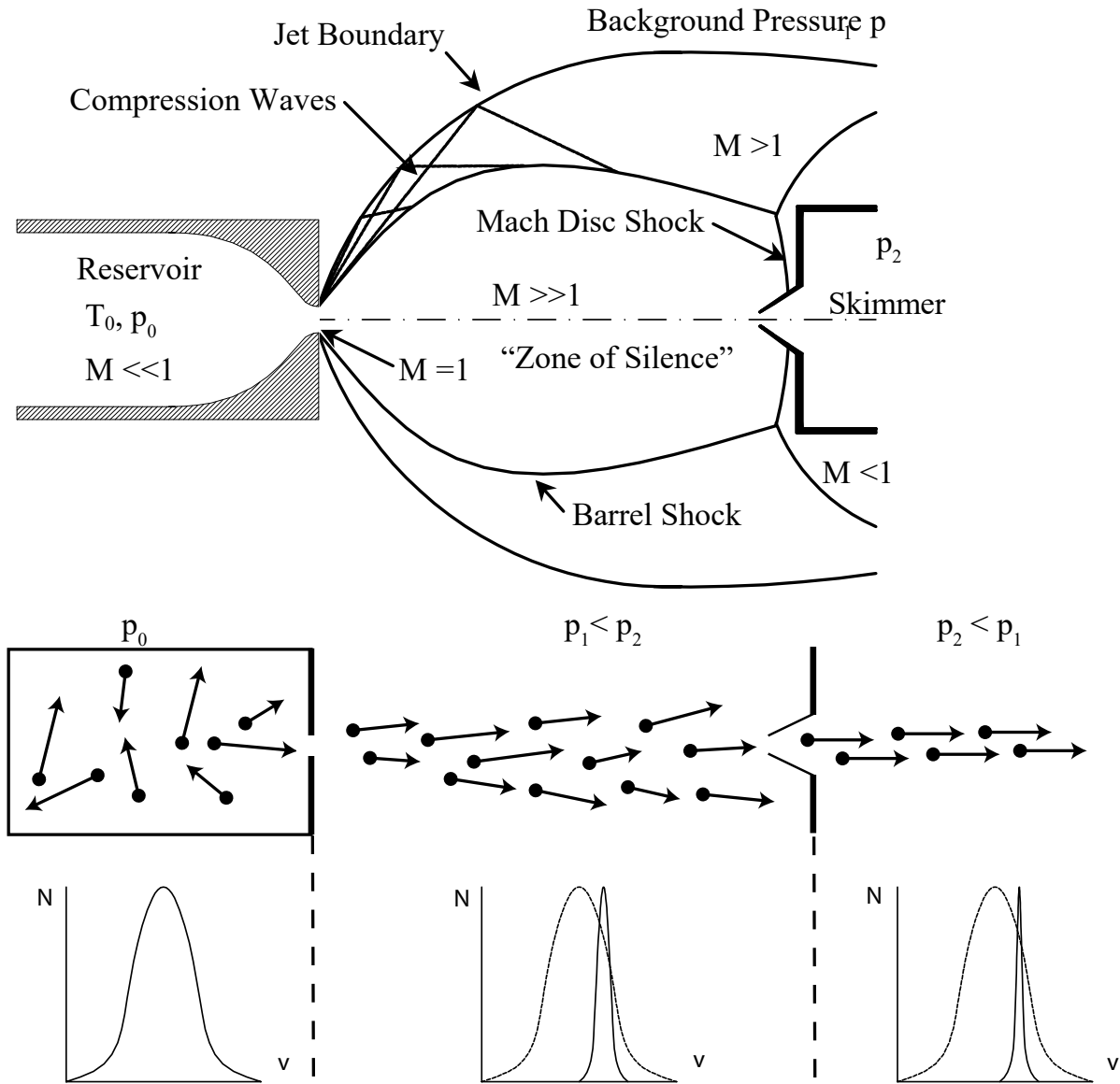


**Figure 3.6.:** Sketch of a supersonic expansion, the different zones and directions of the molecules as well as the velocity distribution by passing the nozzle and the skimmer.[35] Abbreviations:  $M$  = Mach number,  $T$  = temperature,  $p$  = pressure,  $N$  = number of particles,  $v$  = velocity

(baffle) is additionally placed. With this setup a decreasing pressure of  $10^{-5}$  bar in the first chamber up to a pressure of  $10^{-7}$  bar in the last chamber is achieved. At the end of the last chamber a quadrupole (QP) is located and connected to the prevacuum and a turbomolecular pump (TP3). The quadrupole is used to align the molecular beam for perfectly passing the skimmers. At the beginning of measurements, the flexible tube to the reservoir is vented with noble gas (argon) and the sample is poured in. The reservoir and the nozzle can be heated via heating sleeves (Mickenhagen) up to  $250^{\circ}\text{C}$  to transfer the sample into the gas phase for the expansion. In the third vacuum chamber (VK3) the UV laser beam and the molecular beam hit each other in right angle. The resulting fluorescence light is detected via imaging optics onto the photomultiplier (PM) and the spectrum is recorded on the computer. Figure 3.7 shows a closer look on the path of the molecular beam. For Stark measurements two nickel grids exist above and below the position, where the laser beam and the molecular beam cross. The round nickel grids have diameter of 50 mm and a stitch density of 28 wires per centimeter, which allows 95% transmission of the fluorescence light. A voltage up to 10000 V can be applied on the grids (5000 V on each). The distance of the grids is 2.349(5) cm, which results in an electric field up to 4200 V/cm.[15] To determine the applied voltage precisely, a voltagemeter (Vitrek *4700 Precision HV Meter*) is used.[15, 36]

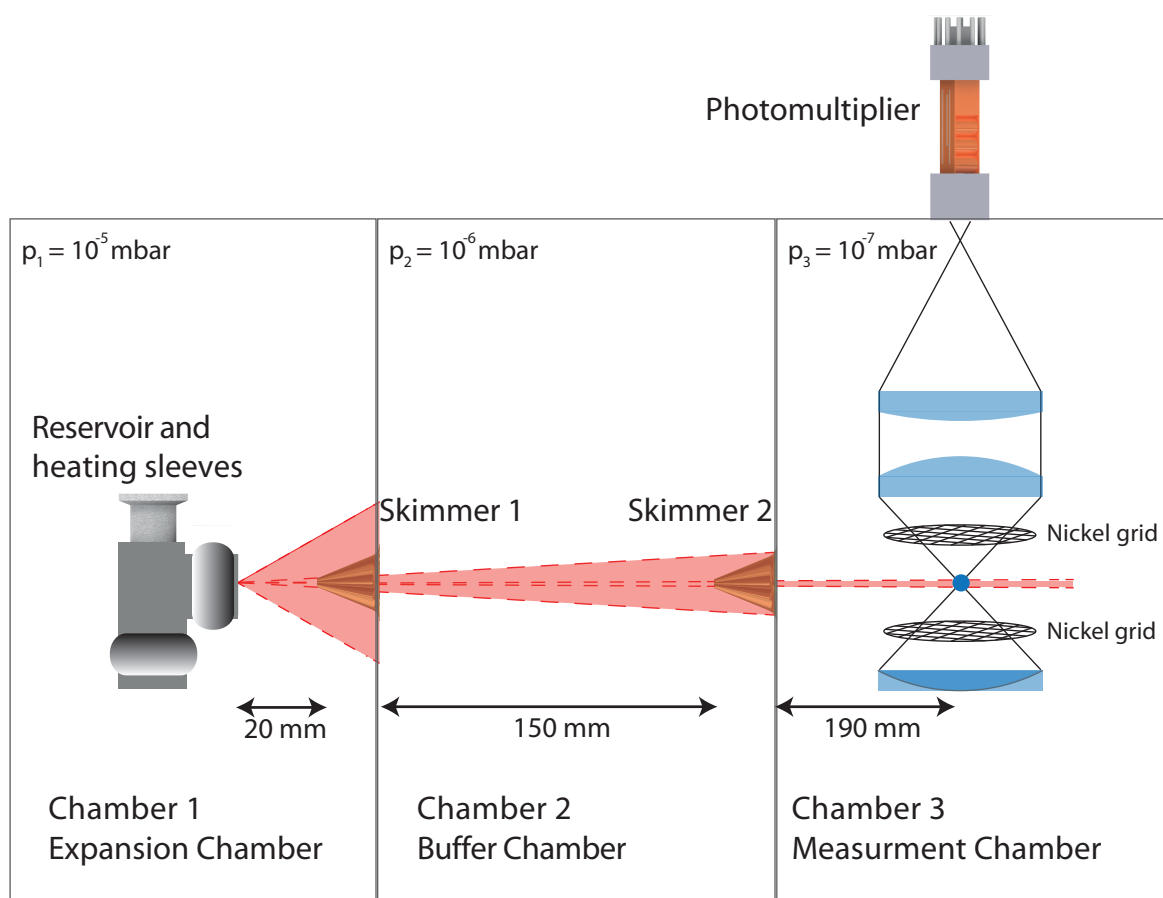
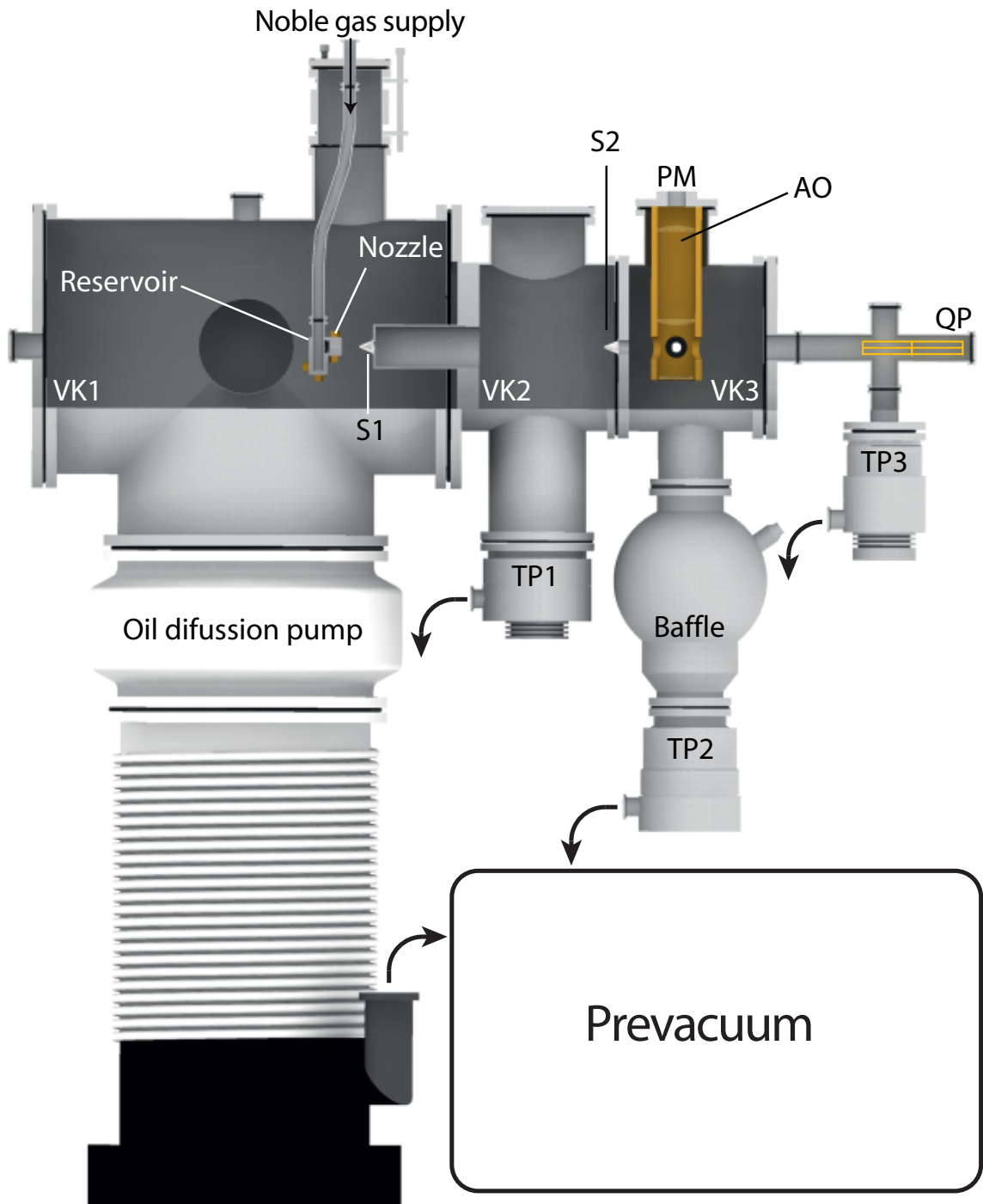


Figure 3.7.: Path of the molecular beam trough the chambers.[15, 26].



**Figure 3.8.:** Schematic setup of the molecular beam apparatus. Abbreviations: VK = vacuum chamber, S = skimmer, TP = turbomolecular pump, AO = imaging optic, PM = photomultiplier, QP = quadrupol.[26]



## 4 | Spectrum Evaluation via Evolutionary Algorithms

The rovibronic fluorescence spectra are evaluated via evolutionary algorithms. These algorithms are inspired by evolutionary processes in the nature and are a powerful tool to solve complex optimization problems. The prerequisite for using these algorithms on evaluation of rotationally resolved spectra, is the existence and knowledge of a suitable Hamiltonian. The Hamiltonian describes the positions and intensities of the spectral bands and therefore several parameters are needed to fit the spectrum (see Chapter 2.1). These parameters are the rotational constants in the electronic ground and first excited state ( $A''$ ,  $B''$  and  $C''$  and  $A'$ ,  $B'$  and  $C'$ , respectively), the angle of the transition dipole moment  $\theta$  relative to the main inertial axis  $a''$  and  $\phi$  relative to  $c''$ , respectively, the relative position of the electronic origin  $\nu_0$ , the Lorentzian width and the temperature parameters  $T_1$  and  $T_2$  and their weighting factor  $\omega$ . The temperature parameters can be lead back to the two-temperature model. This model is used to determine the population of the corresponding energy level (Equation 4.1).

$$n_i = e^{\frac{E_i}{kT_1}} + \omega e^{\frac{E_i}{kT_2}} \quad (4.1)$$

(Abbreviations:  $n_i$ : Population of the Rotational Level  $i$ ,  $E_i$ : Energy of the Level  $i$ ,  $k$ : Boltzmann Constant,  $T_1$ : Temperature 1,  $T_2$ : Temperature 2,  $\omega$ : Weighting Factor)

For Stark experiments and therefore for the fitting process three dipole moment parameters  $\mu''_a$ ,  $\mu''_b$ ,  $\mu''_c$  for the electronic ground state and  $\mu'_a$ ,  $\mu'_b$ ,  $\mu'_c$  for the first excited state are needed. Additionally, the Hamiltonian for zero field spectra does not work anymore for Stark experiments and a different Hamiltonian has to be implemented for the correct description of the positions and line intensities of the spectrum.

To start the fitting process, a set of start values as well as the upper and lower limit of the parameters range is defined and grouped to form several individuals. Every individual

is a possible solution and corresponds to a simulated spectrum. The quality of the fit of the simulated spectra to the experimental spectrum is monitored and described by a cost function (Equation 4.2). The cost function compares the integrals of the simulated and experimental spectrum and will be zero for perfect agreement.

$$C = \sum_{i=1}^N \left( \frac{p_i^{exp}}{W^{exp}} - \frac{p_i^{calc}}{W^{calc}} \right)^2 \quad (4.2)$$

(Abbreviations: C = cost function, N = number of spectrum points ,  $p_i = i^{th}$  spectrum point , W = integral of the spectrum)

If the cost function reaches a sufficient agreement, the fitting process will be stopped and is accomplished. Otherwise, the worst individuals will be dismissed and individuals with good agreement parameters according to the experimental spectrum will be selected and their information will be combined via a crossover process for reproduction. Finally, the evaluation of the fitness will start again over the cycle, until a good cost function and thus a good agreement of the simulated and experimental spectrum is reached. In general a sufficient agreement is reached after 400 - 600 cycles. (Figure 4.1)[37, 38]

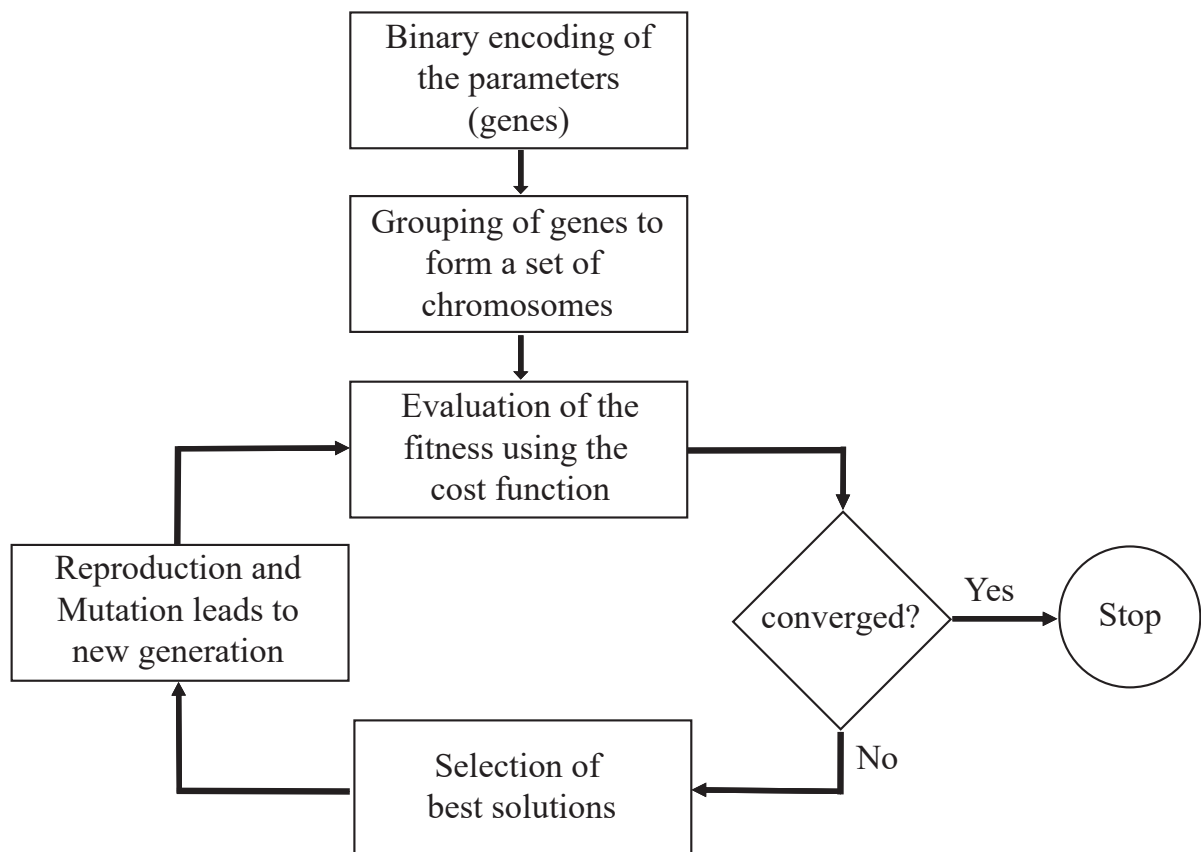


**Figure 4.1.:** Sketch of the genetic algorithm process.[39]



# 5 | Publication on Rotamers of 1,3-Dimethoxybenzene

## Rotationally Resolved Electronic Spectroscopy of the Rotamers of 1,3-Dimethoxybenzene

Michael Schneider,<sup>a</sup> Martin Wilke,<sup>a</sup> Marie-Luise Hebestreit,<sup>a</sup> José Arturo Ruiz-Santoyo,<sup>b</sup> Leonardo Álvarez-Valtierra,<sup>b</sup> John T. Yi,<sup>c</sup> W. Leo Meerts,<sup>d</sup> David W. Pratt,<sup>e</sup> and Michael Schmitt<sup>b 1</sup>

<sup>a)</sup> *Heinrich-Heine-Universität, Institut für Physikalische Chemie I,  
D-40225 Düsseldorf, Germany.*

<sup>b)</sup> *Universidad de Guanajuato-Campus León,  
División de Ciencias e Ingenierías, León, Guanajuato 37150, México.*

<sup>c)</sup> *Winston-Salem State University,  
Department of Chemistry, Winston-Salem, North Carolina 27110, USA*

<sup>d)</sup> *Radboud University, Institute for Molecules and Materials  
Felix Laboratory, Nijmegen, 6525 ED, The Netherlands*

<sup>e)</sup> *University of Vermont,  
Department of Chemistry, Burlington, Vermont 05405, USA*

### 5.1. Abstract

Conformational assignments in molecular beam experiments are often based on relative energies, although there are many other relevant parameters, such as conformer-

---

<sup>1</sup>E-mail: mschmitt@uni-duesseldorf.de

dependent oscillator strengths, Franck-Condon factors, quantum yields and vibronic couplings. In the present contribution, we investigate the conformational landscape of 1,3-dimethoxybenzene using a combination of rotationally resolved electronic spectroscopy and high level *ab initio* calculations. The electronic origin of one of the three possible planar rotamers (rotamer (0,180) with both substituents pointing at each other) has not been found. Based on the calculated potential energy surface of 1,3-dimethoxybenzene in the electronic ground and lowest excited state, we show that this can be explained by a distorted non-planar geometry of rotamer (0,180) in the  $S_1$  state.

## 5.2. Introduction

The investigation of equilibria between conformers or rotamers, which are separated by intermediate barriers ( $\approx 5$ -10 kJ/mol) and/or have small absolute energy differences ( $< 1$  kJ/mol) compared to the thermal energy  $kT$  per mol at room temperature ( $\approx 2.48$  kJ/mol at 25 °C), has only been made possible by the development of molecular beam techniques.[40, 41] The stabilization of selected low energy conformers at the resulting low temperatures in molecular beams, along with the simplification of the spectra due to population of few quantum states at these temperatures, aids in the assignment of observed spectral features to particular molecular species. On the other hand, however, the cooling in molecular beams is far from thermodynamic equilibrium, and different degrees of freedom cool down at individual rates. Mostly, a delicate balance between several factors determines the number and type of conformers observed in a molecular beam, including the energy differences of the conformers, barrier heights, the final temperature in the molecular beam, and the ratio of vibrational to conformational cooling. [42–46]

Here, we focus on the rotamer distribution in three hydroxy and/or methoxybenzenes; 1,3-dihydroxybenzene, 1-hydroxy-3-methoxybenzene, and 1,3-dimethoxybenzene (see Figure 5.1; two dihedral angles<sup>2</sup>, defining the orientations of the substituents with respect to the chromophore distinguish the different rotamers of each constitutional isomer). 1,3-dihydroxybenzene (resorcinol) has been the topic of several experimental and computational studies. [47–52] Using rotationally resolved laser induced fluorescence spectroscopy, two rotamers could be identified in the molecular beam spectra as (180,180) / (0,0) and (180,0). [53] Wilke *et al.*[54] examined the rotamers of 1-hydroxy-3-methoxybenzene and

---

<sup>2</sup>Two dihedral angles, which define the orientation of the substituents with respect to the chromophore are selected. Two carbon atom of the chromophore and both heavy atoms of the individual substituents are needed. The first angle starts at the lowest unsubstituted carbon atom in the benzene ring C(2) and the second one at C(4), so that both angles are formed by C(2)C(1)O(7)C(9) and C(4)C(5)O(8)C(10). For systems with two identical substituents, rotamer (180,180) and (0,0) are equivalent.

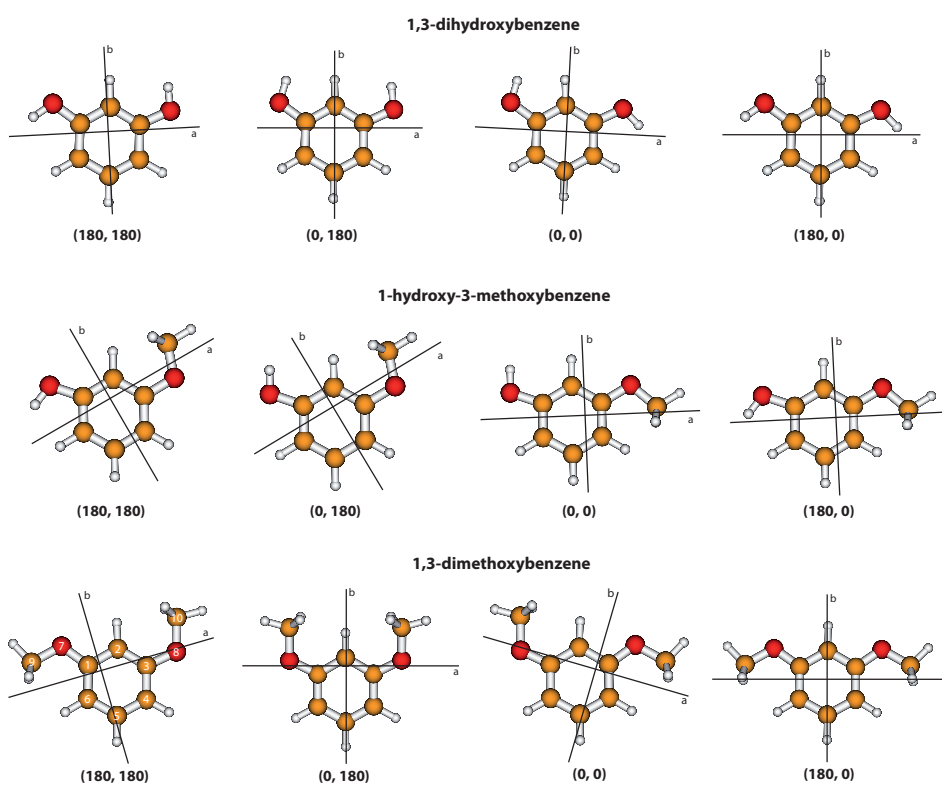


**Figure 5.1.:** Structures of the low energy rotamers of 1,3-dihydroxybenzene, 1-hydroxy-3-methoxybenzene, and 1,3-dimethoxybenzene with their main inertial axes. The nomenclature for the rotamers uses the dihedral angles of the hydroxy and methoxy groups, respectively. For details see text.

found three different rotamers, namely (180, 180), (180, 0) and (0, 0). Breen *et al.*[55] assigned three vibronic bands in the resonant two-photon ionization (R2PI) molecular beam spectrum of 1,3-dimethoxybenzene at 36 101.5, 36 163.9, and 36 256.9  $\text{cm}^{-1}$  to the electronic origins of three different rotamers. Yang *et al.*[56] performed two-color resonant two-photon mass-analyzed threshold ionization spectroscopy to investigate selected rotamers of 1,3-dimethoxybenzene in their cationic states. They found three different ionization potentials for the three lowest-energy bands in the R2PI spectrum of 1,3-dimethoxybenzene from ref.[55] and also concluded the existence of three different rotamers.

Surprisingly, rotamer (0, 180) has not been observed in molecular beam experiments of 1,3-dihydroxybenzene and 1-hydroxy-3-methoxybenzene, while all structures have been assigned in the case of 1,3-dimethoxybenzene.[55, 56] In the present contribution, we use a combination of rotationally resolved electronic spectroscopy and high-level quantum mechanical calculations to investigate the conformational landscape of 1,3-dimethoxybenzene and compare it to that of 1,3-dihydroxybenzene and 1-hydroxy-3-methoxybenzene. In contrast to the results of Breen [55] and Yang [56], only two of the three conformers could be found and identified. Several reasons for the absence of the missing conformers are discussed.

## 5.3. Experimental section

### 5.3.1. Experimental procedures

1,3-Dimethoxybenzene ( $\geq 98\%$ ) was purchased from Sigma-Aldrich and used without further purification. To record rotationally resolved electronic spectra, the sample was heated to  $60^\circ\text{C}$  and co-expanded with 550 mbar of argon into the vacuum through a 200  $\mu\text{m}$  nozzle. After the expansion, a molecular beam was formed using two skimmers (1 mm and 3 mm) linearly aligned inside a differentially pumped vacuum system consisting of three vacuum chambers. The molecular beam was crossed at right angles with the laser beam 360 mm downstream of the nozzle. To create the excitation beam, 10 W of the 532 nm line of a diode pumped solid state laser (Spectra-Physics Millennia eV) pumped a single frequency ring dye laser (Sirah Matisse DS) operated with Rhodamine 110. The output of the dye laser was frequency doubled in an external folded ring cavity (Spectra Physics Wavetrain) with a resulting power of about 5 mW during the experiments. The spectral bandwidth in the UV is 800 kHz. The fluorescence light of the samples was collected perpendicular to the plane defined by laser and molecular beam by an imaging optics setup consisting of a concave mirror and two plano-convex lenses onto the photocathode

of a UV enhanced photomultiplier tube (Thorn EMI 9863QB). The signal output was then discriminated and digitized by a photon counter and transmitted to a PC for data recording and processing. The relative frequency was determined using a *quasi* confocal Fabry-Perot interferometer. The absolute frequency was obtained by comparing the recorded spectrum to the tabulated lines in the iodine absorption spectrum.[31] A detailed description of the experimental setup for rotationally resolved laser induced fluorescence spectroscopy has been given previously. [57, 58]

### 5.3.2. Quantum chemical calculations

Structure optimizations were performed employing Dunning’s correlation-consistent polarized valence triple zeta (cc-pVTZ) basis set from the TURBOMOLE library. [59, 60] The equilibrium geometries of the electronic ground and the lowest excited singlet states were optimized using the approximate coupled cluster singles and doubles model (CC2) employing the resolution-of-the-identity approximation (RI).[61–63] Vibrational frequencies and zero-point corrections to the adiabatic excitation energies were obtained from numerical second derivatives using the NumForce script. [64] A natural-bond-orbital (NBO) analysis [65] was performed at the optimized geometries by using the wavefunctions from the CC2 calculations as implemented in the TURBOMOLE package. [66]

Calculations of the potential energy surface (PES) were performed using the Scan keyword in GAUSSIAN 09 package at DFT/B3LYP/cc-pVTZ level of theory. [67] It was built by scanning the two dihedral torsional angles in steps of 5° from 0° to 360°.

### 5.3.3. Fits of the rovibronic spectra using evolutionary algorithms

Evolutionary algorithms allow us to make a quick and successful automatic assignment of the rotationally resolved spectra, even for large molecules and dense spectra. [68–71] Beside a correct Hamiltonian to describe the spectrum and reliable intensities inside the spectrum, an appropriate search method is needed. Evolutionary strategies are a powerful tool to handle complex multiparameter optimizations and find the global optimum. For the analysis of the presented high-resolution spectra, we used the covariance matrix adaptation evolution strategy (CMA-ES), which is described in detail elsewhere. [72, 73] In this variant of global optimizers mutations are adapted via a CMA mechanism to find the global minimum, even on rugged search landscapes that are additionally complicated due to noise, local minima and/or sharp bends.

## 5.4. Results

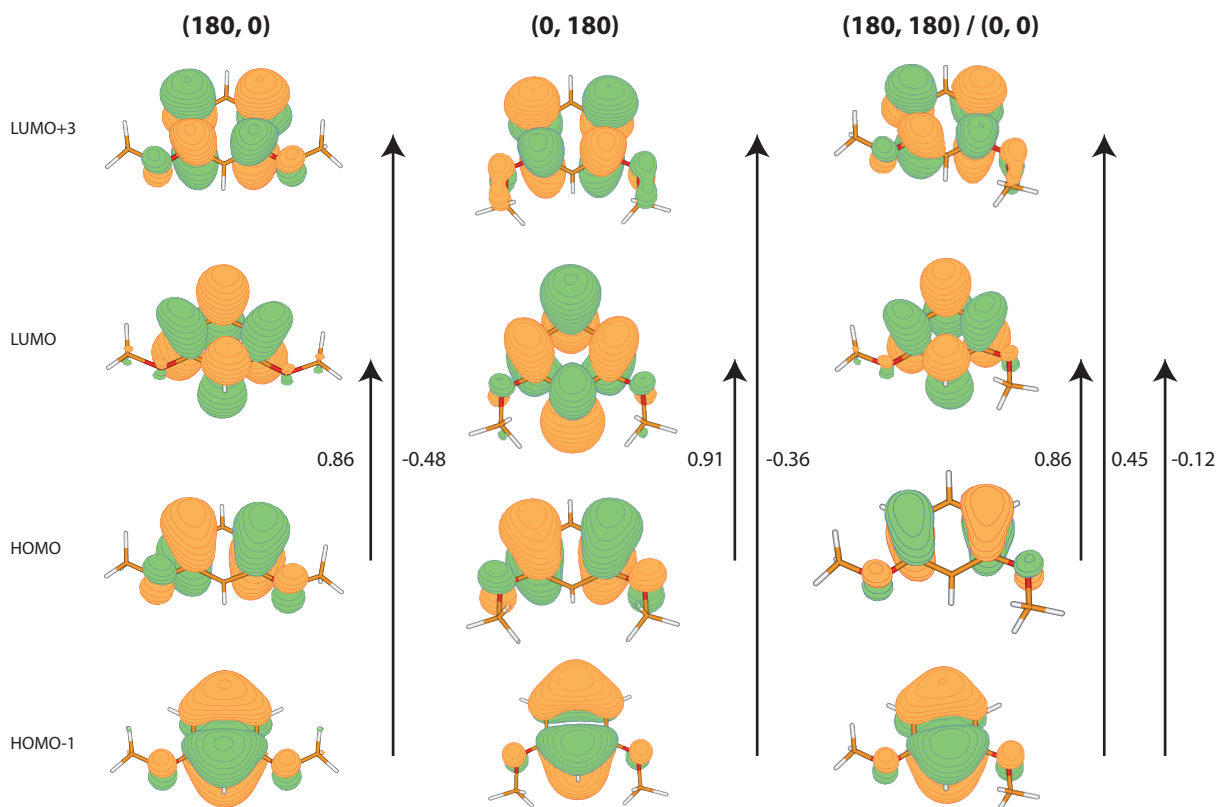
### 5.4.1. Computational Results

Table 7.1 summarizes the molecular properties of three low energy rotamers of 1,3-dimethoxybenzene at the CC2/cc-pVTZ level of theory. These are the rotational constants in the ground ( $A''$ ,  $B''$ ,  $C''$ ) and lowest electronically excited ( $A'$ ,  $B'$ ,  $C'$ ) states, their changes upon excitation ( $\Delta A$ ,  $\Delta B$ ,  $\Delta C$ ) and the inertial defects of the respective states ( $\Delta I$ ). Apart from structural parameters, also electronic information such as the orientation of the transition dipole moment (TDM) vector and the adiabatic excitation energy  $\nu_0$  are compiled in Table 7.1.

**Table 5.1.:** Molecular properties of the three possible rotamers of 1,3-dimethoxybenzene at CC2/cc-pVTZ level of theory. For details see text.

	$(180, 180) / (0, 0)$	$(180, 0)$	$(0, 180)$
$A'' / \text{MHz}$	2539	3486	1892
$B'' / \text{MHz}$	893	771	1108
$C'' / \text{MHz}$	666	636	705
$\Delta I'' / \text{u}\text{\AA}^2$	-6.40	-6.40	-6.41
$A' / \text{MHz}$	2482	3358	1863
$B' / \text{MHz}$	880	763	1091
$C' / \text{MHz}$	655	626	695
$\Delta I' / \text{u}\text{\AA}^2$	-6.42	-6.42	-7.44
$\Delta A / \text{MHz}$	-57	-128	-29
$\Delta B / \text{MHz}$	-13	-8	-17
$\Delta C / \text{MHz}$	-11	-10	-10
$\theta / ^\circ$	6	0	0
$\nu_0 / \text{cm}^{-1}$	36 809	36 986	36 455

The TDM-orientation is given by the angle  $\theta$  of the TDM-vector with the principal inertial  $a$ -axis. As can be seen from Table 7.1, the TDM-vectors of rotamer (180,0) and (0,180) are aligned perfectly along the  $a$ -axis, while that of rotamer (180,180) / (0,0) is rotated by less than  $10^\circ$  towards the  $b$ -axis. Since the TDM depends on the charge redistribution upon electronic excitation, its orientation can be inferred from the molecular orbitals and the coefficients of the respective excitations that are shown in Figure 5.2. For all three possible rotamers, the lowest electronically excited state is dominated by a LUMO  $\leftarrow$  HOMO excitation with smaller contributions of a LUMO+3  $\leftarrow$  HOMO-1 transition and LUMO  $\leftarrow$  HOMO-1 for rotamer (180,180) / (0,0). From Figure 5.2, it becomes clear that the electron density upon excitation is transferred along the inertial  $a$ -axis which leads



**Figure 5.2.:** Frontier orbitals of the different rotamers of 1,3-dimethoxybenzene and the coefficients of the respective excitations according to CC2/cc-pVTZ calculations.

to an angle  $\theta$  of  $0^\circ$  for the highly symmetric rotamers (180,0) and (0,180) with its point group  $C_{2v}$ .

The CC2-calculated relative energies of the possible rotamers, the barriers separating the different rotamers and the adiabatic excitation energies from the ground to lowest electronically excited singlet state are shown in Figure 5.3.

The rotamers (180,180) and (0,0) are equivalent and therefore have the same energy, which is the lowest in the electronic ground state of all possible rotamers of 1,3-dimethoxybenzene. Rotating one of the methyl groups by  $\pm 180^\circ$  leads to a destabilization of  $226\text{ cm}^{-1}$  for rotamer (0,180) and  $188\text{ cm}^{-1}$  for rotamer (180,0). In the lowest electronically excited state, rotamer (0,180) is the more stable one and (180,0) the less, with an energy gap of around  $500\text{ cm}^{-1}$ . Given these facts, the excitation energies are expected to increase in the order  $(0,180) < (180,180) / (0,0) < (180,0)$ .

The barriers separating the minima in the ground state were calculated by varying the dihedral angles of the substituent with the chromophore in steps of  $10^\circ$ . Thus, the transition states belong to structures with one of the substituent perpendicular to the

chromophore, as it is the case for 2-methoxyphenol [74] and 3-methoxyphenol [54]. The resulting barriers are around  $1400\text{ cm}^{-1}$  above the global minimum of rotamer (180, 180) / (0, 0) and in general agreement with the results from Yang *et al.* [56]

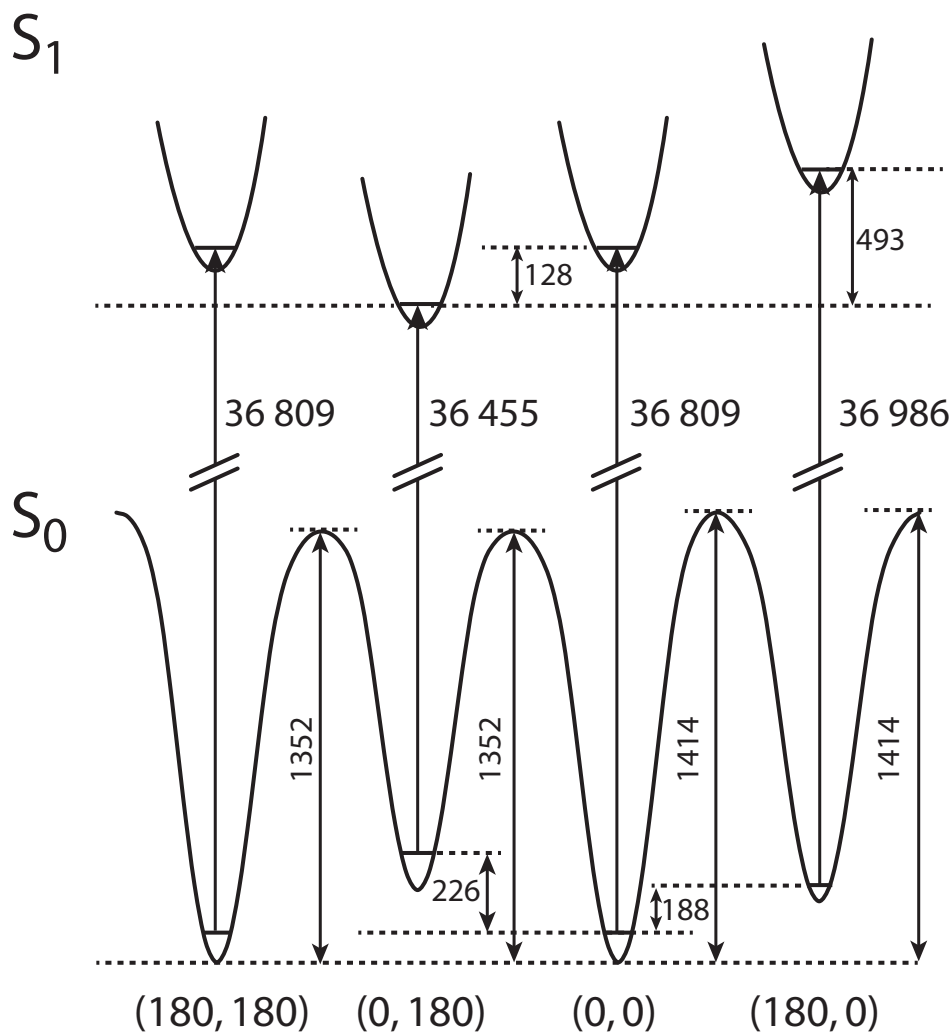


**Figure 5.3.:** Relative energies of the possible rotamers of 1,3-dimethoxybenzene according to CC2/cc-pVTZ calculations. All energies are given in  $\text{cm}^{-1}$ .

Rotating both substituents simultaneously leads to saddle points in the same energy range as the transition states for the one-dimensional rotation. This is shown in the two-dimensional potential energy surface shown in Figure 5.4. The minima and transition states are located at lines that are parallel to the individual coordinates of each of the rotations. Three different paths, which connect the equivalent minima (180, 180) and (0, 0), are possible. A one-dimensional rotation of one methoxy group along dihedral angle 1 in Figure 5.4 leading to rotamer (0, 180) is followed by a one-dimensional rotation of the other methoxy group along dihedral angle 2. Interchanging the order of rotation results in

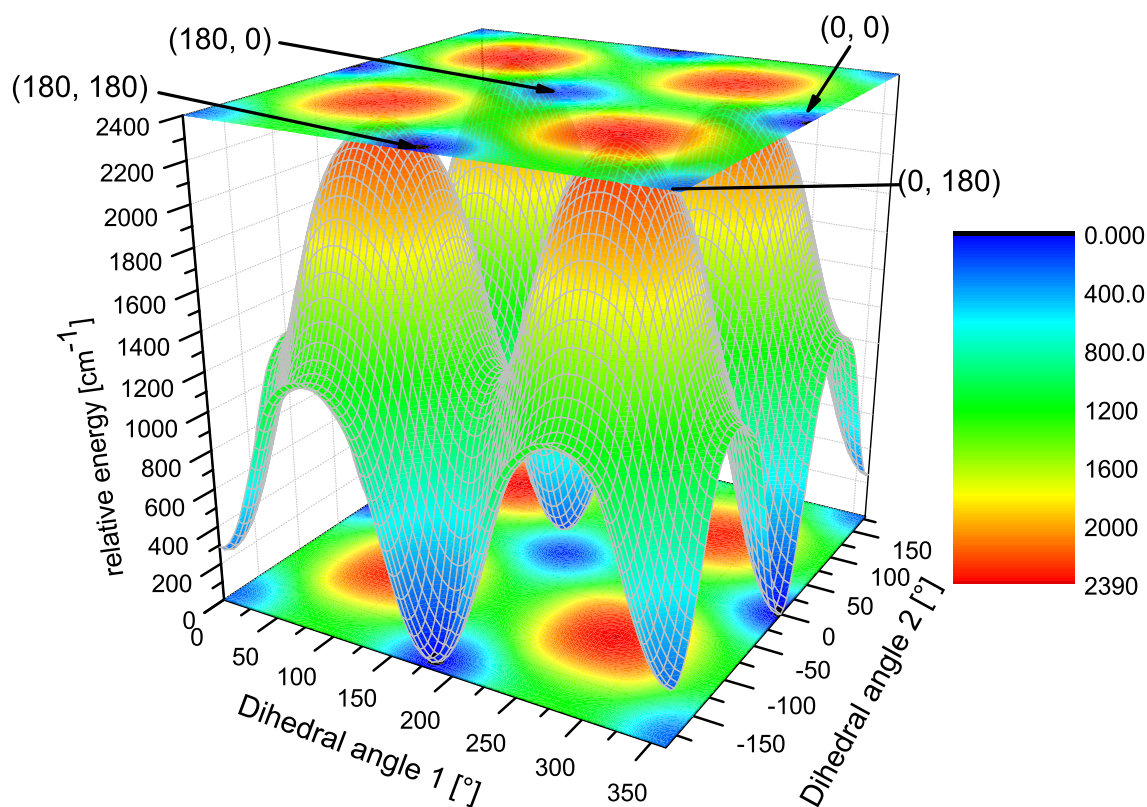


**Figure 5.4.:** Two-dimensional potential energy surface of 1,3-dimethoxybenzene in the ground state created by varying the dihedral angles of the substituents with the aromatic plane in steps of  $5^\circ$  at DFT/B3LYP/cc-pVTZ level of theory.

a path with the (180,0) rotamer as intermediate. Both paths follow saddle points, which are about  $1400\text{ cm}^{-1}$  above the minimum structures. The direct (concerted) transition from (180,180) to (0,0) has the highest barrier of the three different paths with a value greater than  $2300\text{ cm}^{-1}$ . Thus, the motions can be treated in a one-dimensional manner; no cooperative effects of the rotations of both substituents are expected.

### 5.4.2. Experimental results

Figure A.3 shows the rotationally resolved spectrum of the electronic origin of the lowest energy band in the resonant two-photon ionization (R2PI) spectrum recorded by Yang *et al.*[56], denoted as the *A* band. The spectrum of the second lowest energy band, denoted as the *B* band, is shown in Figure A.4. Both experimental spectra are accompanied by a simulation using the best parameters from a CMA-ES fit, given in Table 5.2. These include the rotational constants in the electronic ground ( $A''$ ,  $B''$ ,  $C''$ ) and first electronically

excited ( $A'$ ,  $B'$ ,  $C'$ ) states, the respective inertial defects ( $\Delta I$ ), the angle of the TDM vector with the inertial  $a$ -axis ( $\theta$ ), the excited state lifetime ( $\tau$ ) and the origin frequency ( $\nu_0$ ).

**Table 5.2.:** Molecular parameters obtained from a CMA-ES fit of the rovibronic spectra of three transition bands of 1,3-dimethoxybenzene. This includes the ground and excited state rotational constants. Double-primed constants belong to the ground state and single-primed to the excited state. The angle of the transition dipole moment with the main inertial axis  $a$  is given by  $\theta$  and the adiabatic excitation energy by  $\nu_0$ .

	$A$ band	$B$ band	$C$ band
$A''$ / MHz	2533.44(45)	3461.98(360)	2533.17(60)
$B''$ / MHz	887.52(2)	768.20(4)	887.41(12)
$C''$ / MHz	663.11(2)	634.01(4)	663.04(7)
$\Delta I''$ / $\text{u}\text{\AA}^2$	-6.78	-6.74	-6.79
$A'$ / MHz	2477.65(45)	3338.30(360)	2483.22(61)
$B'$ / MHz	875.60(3)	760.63(4)	873.59(13)
$C'$ / MHz	652.93(3)	624.86(4)	653.61(8)
$\Delta I'$ / $\text{u}\text{\AA}^2$	-7.14	-7.03	-8.8
$\Delta A$ / MHz	-55.80(1)	-123.68(1)	-49.96(4)
$\Delta B$ / MHz	-11.93(1)	-7.57(1)	-13.82(2)
$\Delta C$ / MHz	-10.18(1)	-9.15(1)	-9.44(2)
$\theta$ / $^\circ$	$\pm 14.5(1)$	$0.0^3$	$\pm 12(2)$
$\tau$ / ns	12.1(1)	17.0(1)	4.1(5)
$\nu_0$ / $\text{cm}^{-1}$	36117.61(2)	36185.72(1)	36268.75(10)

The electronic origins of both rotamers show a small deviation of less than one wavenumber compared to their low resolution values. [56] The  $A$  band is dominated by  $a$ -type transitions with less than 10% of  $b$ -type contributions. Hence, the TDM vector is almost parallel to the inertial  $a$ -axis and makes an angle of approximately  $15^\circ$  with it. For reasons of symmetry, which will be discussed in the next section, the  $\theta$  angle of the  $B$  band was set to zero. The fit of the line shapes to Voigt profiles using a Gaussian (Doppler) contribution of 18 MHz yielded Lorentzian contributions of  $13.11 \pm 0.1$  MHz for the  $A$  band and  $9.35 \pm 0.1$  MHz for the  $B$  band. These line widths are equivalent to excited lifetimes of  $12.1 \pm 0.1$  ns for the  $A$  and  $17.0 \pm 0.2$  ns for the  $B$  band.

The  $C$  band, which was assigned by Yang *et al.*[56] to the origin of another rotamer, has a considerably smaller intensity than the  $A$  and  $B$  bands. The rovibronic spectrum of the  $C$  band is shown in Figure S1 of the online supporting material. The fit of this band resulted in the same rotational constants as for the electronic ground state of the  $A$  band and slightly different rotational constants for the excited state. Thus, it is obvious that the  $C$  band is not the origin of another rotamer, as assumed by Yang *et al.*[56] and

Breen *et al.*[55] They assigned the  $C$  band to the missing  $(0, 180)$  rotamer. According to the present analysis, it can safely be assigned to a vibronic band, which is built on the  $A$  origin. The resulting molecular parameters are shown in Table 5.2.

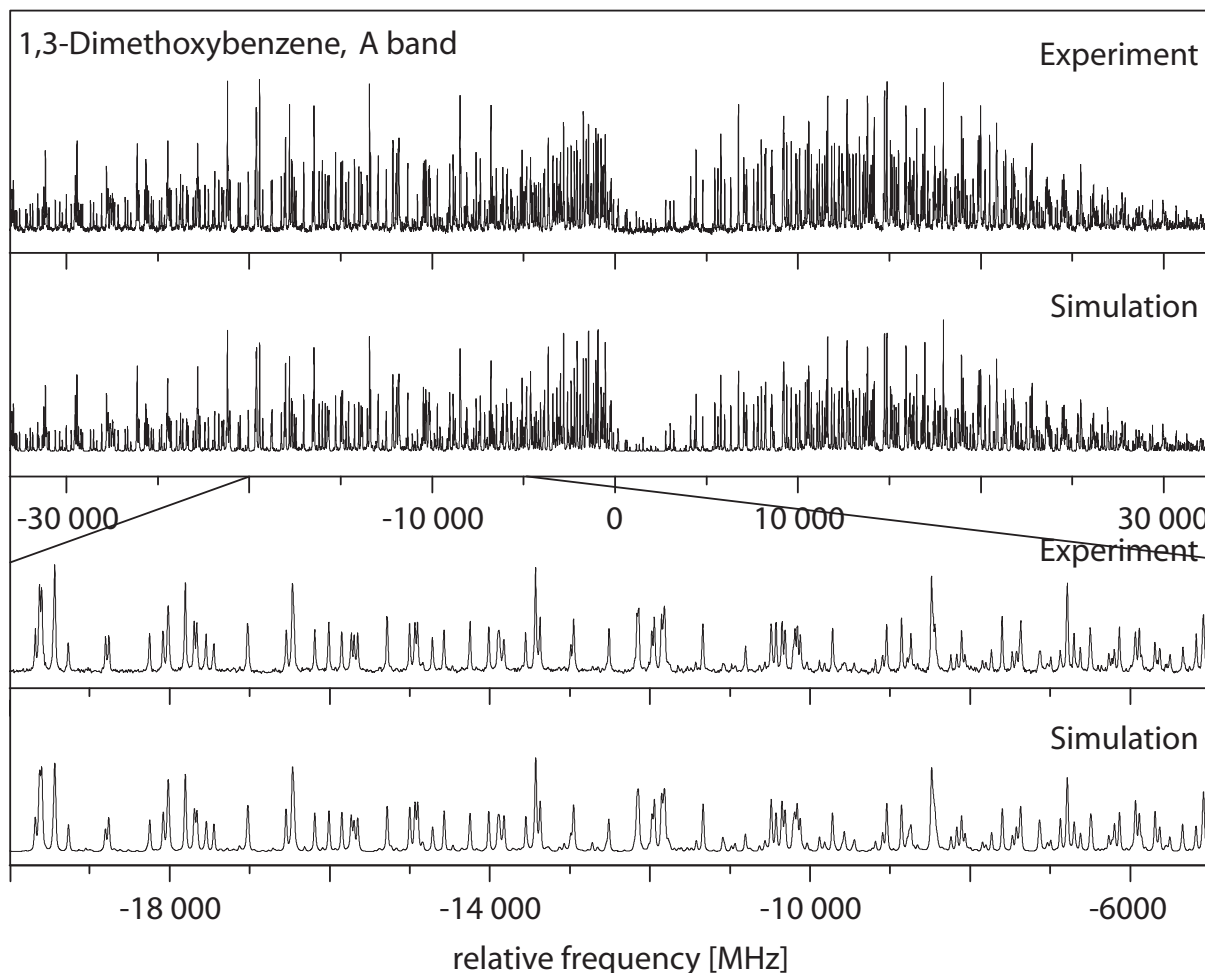


**Figure 5.5.:** Rotationally resolved spectrum of the electronic origin of the  $A$  band of 1,3-dimethoxybenzene, along with a simulation using the best CMA-ES fit parameters, given in Table 5.2. A modified version of this Figure with the residues of the fit is available in the ESI

### 5.4.3. Conformational assignment

While the vibrational frequencies of different rotamers are often quite similar, rotational constants or inertial moments are extremely sensitive to conformational changes. As a consequence of this, even the slightest geometry changes can lead to dramatically different sets of rotational constants, especially if heavy atoms are involved. This can be seen

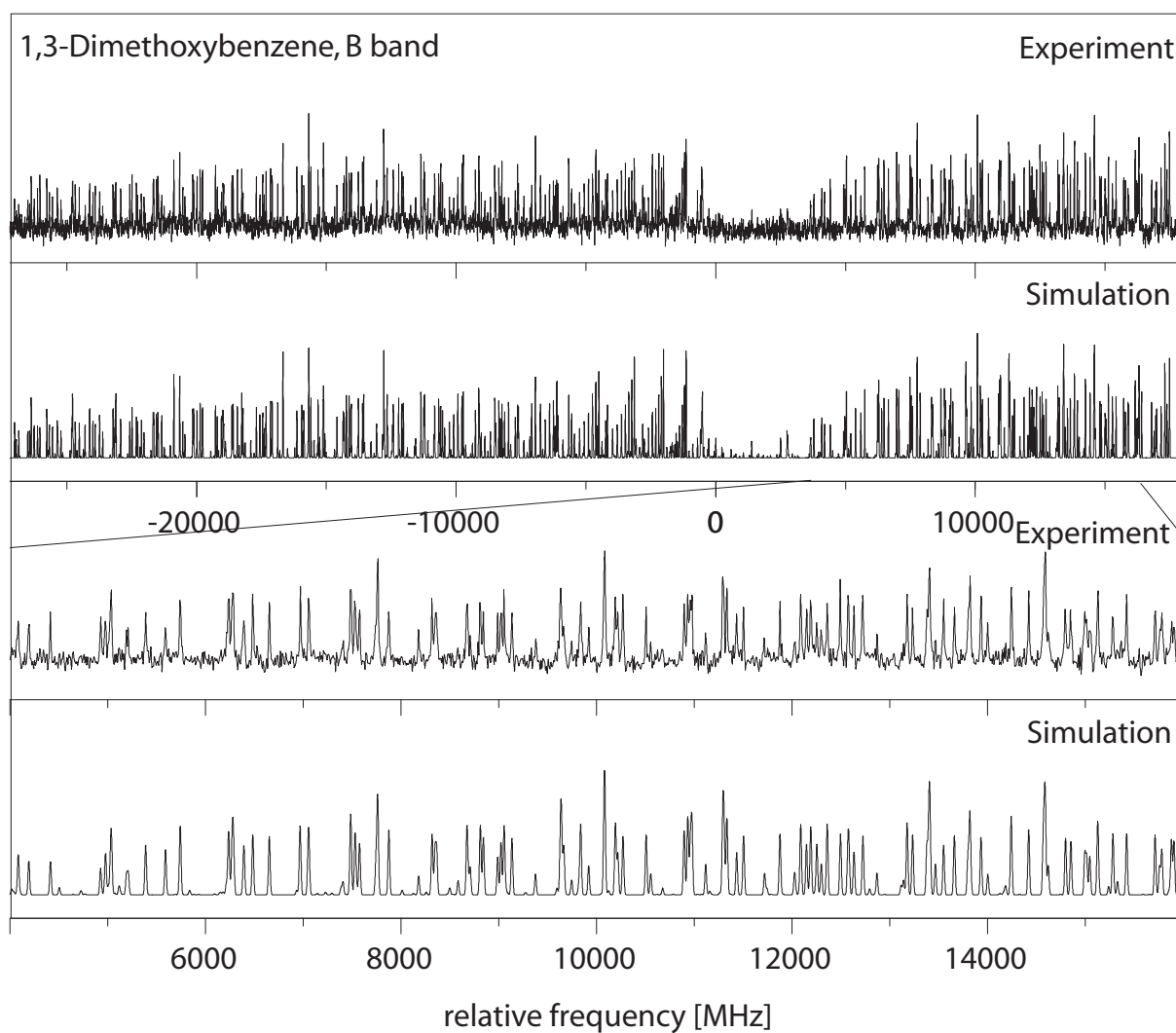


**Figure 5.6.:** Rotationally resolved spectrum of the electronic origin of the *B* band of 1,3-dimethoxybenzene, along with a simulation using the best CMA-ES fit parameters, given in Table 5.2. A modified version of this Figure with the residues of the fit is available in the ESI

from the calculated and experimental rotational constants of the different rotamers of 1,3-dimethoxybenzene in Table 7.1 and 5.2. Going from rotamer (0, 180) to (180, 180) / (0, 0), which is accompanied by a single rotation of a methyl group about  $120^\circ$ , leads to a change of around 700 MHz in the  $A''$  and 200 MHz in the  $B''$  constant. These changes are one third of the absolute values! Similar values are observed for a second rotation of the other methyl group, ending in rotamer (180, 0). Since all rotamers are planar (at least in the electronic ground state) and the inertial  $c$ -axis is perpendicular to the aromatic plane, the rotational constant  $C$  remains almost unaffected by the geometry changes. However, each rotamer shows a characteristic set of rotational constants, which makes it possible to assign the observed bands to the respective structures.

Comparing the rotational constants of the experimental  $A$  and  $B$  band from Table 5.2 with the calculated values of all possible rotamers in Table 7.1, it becomes obvious that the  $A$  band belongs to rotamer (180, 180) / (0, 0) and the  $B$  band to rotamer (180, 0), which is in agreement with the assignment made by Yang *et al.* [56] A direct comparison between the *ab initio* and experimental rotational constants is problematic, since the experimental constants are vibrationally averaged, while *ab initio* constants are equilibrium constants. In first approximation, vibrational averaging between rotamers of the same molecule is similar. Thus, the vibrational averaging effect cancels out in the difference of the rotational constants of different rotamers. The experimental  $A$  and  $B$  band have a difference of -931.56 MHz (-863.67 MHz) in the  $A''$  ( $A'$ ), +119.31 MHz (+114.96 MHz) in the  $B''$  ( $B'$ ) and +29.11 MHz (+28.68 MHz) in the  $C''$  ( $C'$ ) rotational constant. This fits well with the deviations of the rotational constants of the (180,180/ 0,0) and the (180,0) rotamer, which are -947 MHz (-876 MHz) for  $A''$  ( $A'$ ), +122 MHz (+117 MHz) for  $B''$  ( $B'$ ) and +30 MHz (+29 MHz) for  $C''$  ( $C'$ ). This enables us to assign the  $A$  band to rotamer (180,180/ 0,0) and the  $B$  band to rotamer (180,0).

A further confirmation of this assignment comes from the comparison of the calculated and experimental adiabatic excitation energies. The electronic origin of the  $A$  band shows a redshift of  $68\text{ cm}^{-1}$  compared to that of the  $B$  band. The combination of rotamers (180, 180) / (0, 0) and (180, 0) exhibit a calculated red shift of  $177\text{ cm}^{-1}$  while the electronic origin of rotamer (0, 180) is redshifted by more than  $300\text{ cm}^{-1}$ .

## 5.5. Discussion

The first question that we address is the planarity of the rotamers observed for 1,3-dimethoxybenzene in both electronic states. The inertial defect<sup>4</sup> of the planar singly methoxy substituted benzene (anisole) in the ground state has been determined to  $-3.409 \text{ u}\text{\AA}^2$  using microwave spectroscopy[75] and to  $-3.584 \text{ u}\text{\AA}^2$  in the lowest excited singlet state by rotationally resolved laser induced fluorescence spectroscopy.[76] The experimentally determined inertial defect for the *A* rotamer (180, 180) / (0, 0) is  $-6.78 \text{ u}\text{\AA}^2$  for the electronic ground state and  $-7.14 \text{ u}\text{\AA}^2$  for the electronically excited state. For the *B* rotamer (180, 0),  $-6.74$  and  $-7.03 \text{ u}\text{\AA}^2$  are found. These values are slightly less than twice the inertial defect of anisole in its respective states. The larger inertial defect in the excited state points to an increased contribution of out-of-plane vibrations, as in the case of anisole. From the point of view of the inertial defects, both rotamers have a planar heavy atom structure.

Changing the methoxy group to a hydroxy group results in a planar structure with an inertial defect of  $-0.031$  and  $-0.18 \text{ u}\text{\AA}^2$  in the lowest two singlet states of phenol. [77] The same holds true for the two experimentally observed rotamers of 1,3-dihydroxybenzene (180, 180) / (0, 0) and (180, 0), with inertial defects close to zero in both states. [50, 53]

For the mixed molecule 1-hydroxy-3-methoxybenzene, the three experimentally observed rotamers (180, 180), (0, 0) and (180, 0) possess equally planar heavy atom structures in both states. This can be inferred from their inertial defects of  $-3.50$ ,  $3.46$ , and  $3.47 \text{ u}\text{\AA}^2$  in the electronic ground and  $-3.80$ ,  $-3.75$  and  $-3.73 \text{ u}\text{\AA}^2$  in the lowest electronically excited state. [54]

**Table 5.3.:** Summary of different excitation energies of the 1,3-dimethoxybenzene rotamers at CC2/cc-pVTZ level of theory. All energies are given in  $\text{cm}^{-1}$ .

	(180, 180) / (0, 0)	(180, 0)	(0, 180)
$\Delta E_{adiabatic}$ incl. ZPE	36 809	36 986	36 455
$\Delta E_{adiabatic}$ excl. ZPE	38 334	38 428	37 837
$\Delta E_{vertical}$ @ opt. $S_0$ geometry	39 807	39 728	39 476
$\Delta E_{vertical}$ @ opt. $S_1$ geometry	36 784	37 059	34 546

However, for the fourth possible rotamer of 1-hydroxy-3-methoxybenzene (0, 180), theory predicts a non-planar structure in the lowest electronically excited state, which is the reason for its absence in molecular beam studies due to a vanishingly small Franck-

<sup>4</sup>The inertial defect is defined as  $I_c - I_a - I_b$ , where the  $I_g$  are the moments of inertia with respect to the main inertial axes  $g$  of the molecule.

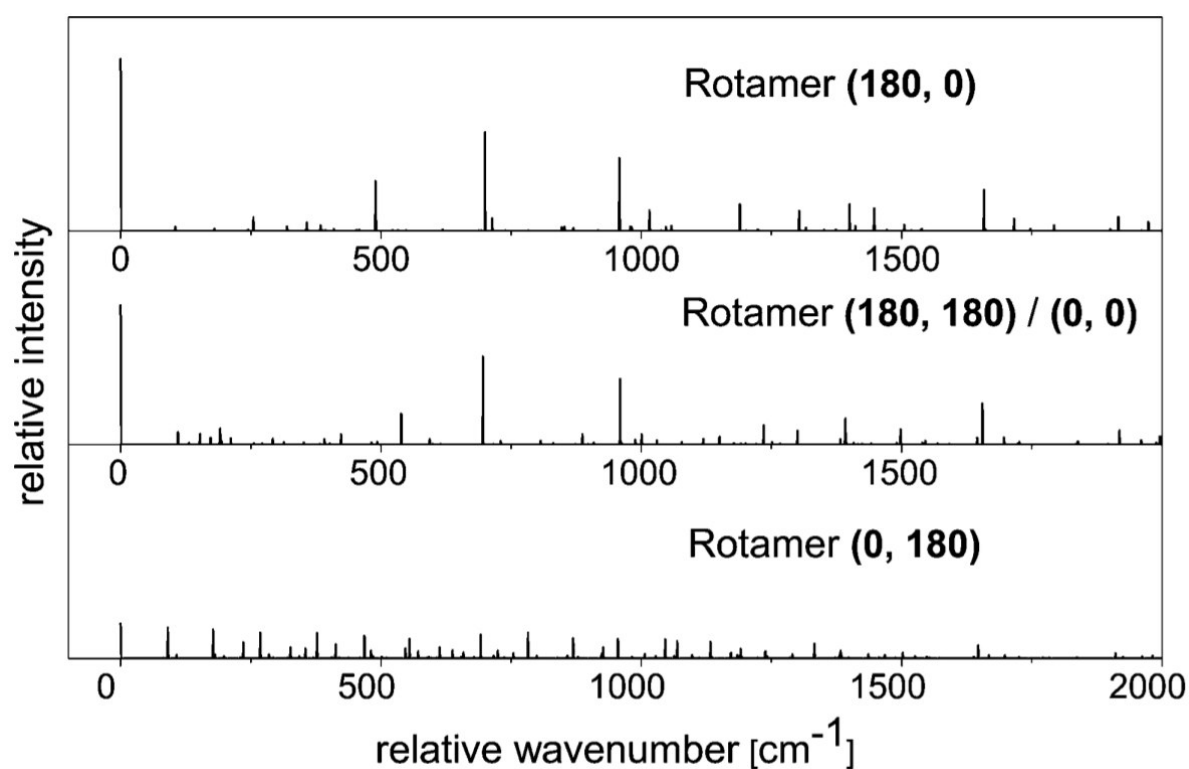


**Figure 5.7.:** Franck-Condon simulations of the excitation spectra of the possible rotamers of 1,3-dimethoxybenzene at CC2/cc-pVTZ level of theory. The individual spectra are normalized to the total area of all bands within this spectrum.

Condon factor for the origin excitation. [54] Looking at the calculated inertial defects of 1,3-dimethoxybenzene in Table 7.1 shows that the excited state value of the (0, 180) rotamer is higher by more than  $1 \text{ u\AA}^2$  compared to the other rotamers. This is caused by puckering of the hydrogen atom at C2 out of the aromatic plane by  $24^\circ$ . In order to evaluate this effect, Franck-Condon simulations of the excitation spectra of all possible conformers of 1,3-dimethoxybenzene have been calculated and are summarized in Figure 5.7. They have been obtained from the *ab initio* optimized ground and excited state structures of each rotamer and the respective Hessian using the program FCFit,[78, 79] which computes the excitation spectrum in the FC approximation in the basis of multidimensional harmonic oscillator wavefunctions. While the excitation spectra of the (180, 0) and (180, 180) / (0, 0) rotamers are quite similar, with only a few vibronic bands with significant intensities, most of the oscillator strength of the (0, 180) rotamer is distributed over higher vibronic levels. Consequently, the Franck-Condon factor for the origin excitation of the (0, 180) rotamer is dramatically smaller than for the other rotamers.

Table 7.4 summarizes the adiabatic and vertical excitation energies for all rotamers at CC2/cc-pVTZ level of theory. Inspection of the vertical excitation energies, calculated at the optimized ground state geometry, and comparing them to the one at the optimized excited state geometry, shows that the difference for rotamer (0, 180) is almost twice that of the other rotamers. This confirms that the geometry change upon excitation is considerably larger for this rotamer. Although rotamer (0, 180) is the most unstable in the ground state, its energy differs by less than  $250 \text{ cm}^{-1}$  compared to the most stable one. Thus, it is unlikely that one of the rotamers is not populated thermally prior to expansion. Additionally, the barrier heights from Figure 5.3 and the potential energy surface, given in Figure 5.4, rule out the possibility of a depopulation of one rotamer into another. Therefore, the small Franck-Condon factor seems to be the most plausible explanation for the absence of rotamer (0, 180) in our experiments.

A similar assumption based on intensities has already been made by Yang *et al.*[56] , where the origin peak of the most intense band (*A*) assigned to the (180, 180) / (0, 0) rotamer is observed to be more than ten times higher than the one of band *C*, which they assigned to the rotamer (0, 180). However, in both experiments from Breen [55] and Yang [56] the band, that they assign to the electronic origin of rotamer (0, 180) lies at the highest energy, while our CC2-calculations predict the lowest excitation energy compared to the other rotamers. The inertial parameters of the *C* band, which we obtained from the analysis of the rovibronic spectrum in the present study, clearly shows that the *C* band is a vibronic band belonging to the *A* origin. Thus, the origin of the (0, 180) still remains

**Table 5.4.:** Natural charges from a natural population analysis (NPA) for all possible rotamers of 1,3-dimethoxybenzene using the CC2/cc-pVTZ wave functions. For atomic labeling see Figure 5.1. The bold marked values designate the atomic positions where the natural charges (or differences of natural charges) are highest.

	(180, 180) / (0, 0)			(180, 0)			(0, 180)		
	$q_{S_0}$	$q_{S_1}$	$\Delta q$	$q_{S_0}$	$q_{S_1}$	$\Delta q$	$q_{S_0}$	$q_{S_1}$	$\Delta q$
C1	0.32	0.29	-0.03	0.31	0.28	-0.03	0.32	0.29	-0.03
C2	<b>-0.35</b>	<b>-0.42</b>	<b>-0.07</b>	-0.30	<b>-0.36</b>	<b>-0.07</b>	<b>-0.40</b>	<b>-0.48</b>	<b>-0.09</b>
C3	0.31	0.28	-0.04	0.31	0.28	-0.03	0.32	0.29	-0.03
C4	-0.27	-0.21	0.06	<b>-0.32</b>	-0.24	0.08	-0.27	-0.19	0.08
C5	-0.16	<b>-0.28</b>	<b>-0.11</b>	-0.16	<b>-0.27</b>	<b>-0.11</b>	-0.17	-0.29	<b>-0.12</b>
C6	<b>-0.33</b>	-0.23	0.10	<b>-0.32</b>	-0.24	0.08	-0.27	-0.19	0.08
O7	-0.47	-0.43	0.05	-0.47	-0.43	0.05	-0.47	-0.43	0.05
O8	-0.47	-0.43	0.05	-0.47	-0.43	0.05	-0.47	-0.43	0.05
C9	-0.21	-0.21	-0.01	-0.21	-0.21	-0.01	-0.21	-0.21	-0.01
C10	-0.21	-0.21	0.00	-0.21	-0.21	-0.01	-0.21	-0.21	-0.01
H2	0.22	0.22	0.00	0.22	0.22	0.00	0.21	0.20	-0.01
H4	0.21	0.20	-0.01	0.21	0.20	-0.01	0.21	0.20	-0.01
H5	0.20	0.20	0.00	0.20	0.20	0.00	0.20	0.20	0.00
H6	0.21	0.20	-0.01	0.21	0.20	-0.01	0.21	0.20	-0.01
H9.1	0.18	0.18	0.00	0.18	0.18	0.00	0.18	0.18	0.00
H9.2	0.16	0.17	0.01	0.16	0.16	0.01	0.16	0.17	0.01
H9.3	0.16	0.17	0.01	0.16	0.16	0.01	0.16	0.17	0.01
H10.1	0.18	0.18	0.00	0.18	0.18	0.00	0.18	0.18	0.00
H10.2	0.16	0.17	0.01	0.16	0.16	0.01	0.16	0.17	0.01
H10.3	0.16	0.17	0.01	0.16	0.16	0.01	0.16	0.17	0.01

undetected.

In order to explain this observation, a natural bond orbital (NBO) analysis has been performed. In general, the methoxy group is a mesomeric donating substituent which increases the electron density inside the chromophore. As was already observed for 5-hydroxyindole [80] and various conformers of serotonin [81], there exists a conformation-dependent shift of electron density from the substituent to the chromophore depending on the orientation of the oxygen lone-pair with respect to the chromophore. The negative charge is highest at the atom opposite to the lone pair. This is confirmed by the results of the NBO analysis in the ground state of the different 1,3-dimethoxybenzene rotamers, summarized in Table 5.4. Thus, inside the chromophore the electron density at C2 and C6 for rotamer (180, 180) / (0, 0), at C4 and C6 for rotamer (180, 0), and at C2 for rotamer (0, 180) has the highest value. In the electronically excited state the situation changes. For all rotamers, a shift of around 0.11 elementary charges from the substituents into the chromophore upon excitation was calculated. However, this mainly affects C2 and C5 where the natural charges become significantly negative compared to the respective ground state values. Since for rotamer (0, 180), C2 exhibits already an extremely negative charge in the electronic ground state, it becomes the most negative atom in the whole molecule in the excited state. As a consequence of this, the charges are no longer perfectly delocalized as is typical for most aromatic compounds. Thus, the chromophore of rotamer (0, 180) loses its planarity in the excited state. In the online supporting material, the dihedral angles inside the chromophore of the different rotamers of 1,3-dimethoxybenzene are given which confirm the planar structure for rotamer (180, 180) / (0, 0) and (180, 0) and the non-planar structure for rotamer (0, 180).

## 5.6. Conclusion

Two rotamers of 1,3-dimethoxybenzene were studied using rotationally resolved electronic spectroscopy and assigned to the (180, 180) / (0, 0) (*A* band) and (180, 0) structure (*B* band) based on their rotational constants. Computational results of the conformational landscape reveal a planar structure for both rotamers which is confirmed by the experimental inertial defects. However, for the third possible rotamer (0, 180), theory predicts a non-planar geometry in the lowest electronically excited state. The strong geometry change upon excitation results in a remarkably small FC-factor for the respective origin compared to that of the other rotamers and was not observed in our experiments. The band, which was assigned before by Breen and Yang [55, 56] to this "missing" rotamer

has clearly been shown to be due to a vibronic band of the (180, 180) / (0, 0) rotamer.

For closely related systems with two adjacent substituents (1,2-dimethoxybenzene, 1,2-dihydroxybenzene and 1-hydroxy-2-methoxybenzene), rotamer (0, 180) is not a stable structure due to steric hindrance.[56, 82–84] Nevertheless, this cannot be used as an argument for the respective meta-substituted systems because both methyl groups are around 500 pm away from each other. Thus, electronic effects have to be responsible for the absence of this rotamer. This has been proven for 1,3-dimethoxybenzene by NBO calculations, which show that the electron density at the C(2) ring carbon atom, located between the two methoxy groups, is considerably increased upon electronic excitation. This partial charge localization leads to a decrease in aromaticity and an out-of-plane puckering of the C(2) atom. Since the electronic ground state is planar, the FC factor for the origin is much smaller than for the other rotamers. Similar results have been observed for 1-hydroxy-3-methoxybenzene[54] and can be expected for 1,3-dihydroxybenzene. Also for these systems, rotamer (0, 180) has not been observed experimentally in molecular beam studies although the energetic differences are small enough in the ground state to allow for thermal population, while the barriers between the rotamers are sufficiently high to avoid collisional relaxation into the lowest minimum at the PES.

The present study nicely shows the importance of molecular structural parameters in the determination of different rotamer or conformer structures. While the differences of inertial parameters (rotational constants) are large, different ionization potentials, different ion spectra and/or different vibrational spectra are not sufficiently sensitive to give a straightforward answer in these cases.

## 5.7. Acknowledgements

Financial support of the Deutsche Forschungsgemeinschaft via grant SCHM1043 12-3 is gratefully acknowledged. Computational support and infrastructure was provided by the "Center for Information and Media Technology" (ZIM) at the Heinrich-Heine-University Düsseldorf (Germany). We furthermore thank the Regional Computing Center of the University of Cologne (RRZK) for providing computing time on the DFG-funded High Performance Computing (HPC) system CHEOPS as well as support. Financial support provided by the Dirección de Apoyo a la Investigación y al Posgrado (DAIP)-Universidad de Guanajuato, under the grant CIFOREA 76/2016 is greatly appreciated. LAV acknowledges Dr. David Y. G. Delepine for his continue support for the establishment of the Molecular Spectroscopy High Resolution Laboratory in León, México JTY acknowledges

financial support via grant NSF RIA-1505311.

## 5.8. Publication

Chapter 5 was published under the heading *Rotationally Resolved Electronic Spectroscopy of the Rotamers of 1,3-Dimethoxybenzene* in *Physical Chemistry Chemical Physics*, **19**, 21364-21372, 2017. DOI: 10.1039/C7CP04401A.

The gasphase measurements, except the C-Band spectrum which was measured by John T. Yi, were performed by Marie-Luise Hebestreit, Martin Wilke and myself. The *ab initio* calculations and spectra evaluations were made by myself and Martin Wilke as well. Franck Condon simulations were performed by Christian Henrichs. My total share of this publication is about: 60%.

# 6 | Publication on Dipole Moments of Rotamers of Dimethoxybenzenes

## Excited state dipole moments and transition dipole orientations of different rotamers of 1,2-, 1,3- and 1,4-dimethoxybenzene

Michael Schneider,<sup>a</sup> Martin Wilke,<sup>a</sup> Marie-Luise Hebestreit,<sup>a</sup> Christian Henrichs,<sup>a</sup> W. Leo Meerts,<sup>b</sup> and Michael Schmitt<sup>a</sup> <sup>1</sup>

<sup>a)</sup> *Heinrich-Heine-Universität, Institut für Physikalische Chemie I, D-40225 Düsseldorf, Germany.*

<sup>b)</sup> *Radboud University, Institute for Molecules and Materials Felix Laboratory, Nijmegen, 6525 ED, The Netherlands*

### 6.1. Abstract

Rotationally resolved electronic Stark spectra of different rotamers of 1,2-, 1,3-, and 1,4-dimethoxybenzene have been recorded and analyzed using evolutionary strategies. The experimentally determined dipole moments as well as the transition dipole moments are compared to the results of *ab initio* calculations. For the electronic ground states of the experimentally observed dimethoxybenzenes, the permanent dipole moments can be obtained from vectorial addition of the monomethoxybenzene dipole moment. However, this is not the case for the electronically excited states. This behavior can be traced back to a state mixing of the lowest electronically excited singlet states.

---

<sup>1</sup>E-mail: mschmitt@uni-duesseldorf.de

## 6.2. Introduction

The knowledge of excited state dipole moments and of transition dipole moments are important prerequisites for the understanding of resonance energy transfer processes like Förster Resonant Energy Transfer (FRET)[85, 86] and for molecular excitonic interactions.[87] While experimental dipole moment measurements in the electronic ground state are straightforward, their exact values in electronically excited states can only be determined reliably using gas phase spectroscopic methods. Despite numerous attempts to improve the original Lippert-Mataga theory,[88–94] for a determination of excited state dipole moments (or at least their changes from the ground state values), the results are not very encouraging.[95–97] On the other hand, theoretical approaches frequently fail, when the excited states involve considerable charge transfer character.[98] Very subtle changes of the electron densities can change both magnitude and direction of the excited state dipole moments considerably.

Ligands, which show mesomeric (+M for electron releasing or –M for electron-withdrawing groups) effects cause large electron density changes upon electronic excitation of the chromophore. The hydroxy or methoxy groups e.g. shift electrons into an aromatic chromophore via their +M effect. This effect is substantially larger in the lowest excited singlet states of methoxy- and hydroxy-substituted benzenes,[77, 99] leading to quinoidal structures upon excitation, especially in the *ortho* and *para* disubstituted conformers.[100] However, also inductive (+I or –I) effects and even through-space effects influence the electron distribution between the ligand and the chromophore. For the hydroxy and methoxy substituents, it has been found, that the adjacent C-atom to which the lone pairs of the O-atom points, has the lower electron density.[54, 81, 101] Thus, it is interesting to investigate the dipole moments of different rotamers of disubstituted benzenes, which either can talk to each other electronically (*ortho* and *para*), or communicate only via inductive effects (*meta*).

Structural changes upon electronic excitation have been addressed by rotationally resolved electronic spectra of (mono)methoxy substituted benzene (anisole) in the groups of Becucci[99] and Pratt,[76] and of (mono)hydroxybenzene (phenol) in the groups of Meerts[77] and Schmitt.[102] For anisole, no spectral splitting due to the hindered three-fold internal rotation of the methoxy group has been observed, probably due to the high barriers for this motion.

Molecular beam R2PI spectra of 1,2-, 1,3- and 1,4-dihydroxybenzene have been reported by Dunn *et al.*, from which they concluded the existence of two rotamers

for 1,4-dihydroxybenzene and of three rotamers for 1,2- and 1,3-dihydroxybenzene, respectively.[47] Bürgi and Leutwyler studied 1,2-dihydroxybenzene (catechol), using hole-burning spectroscopy.[83] They found, that all bands in the vibronic spectrum belong to a single rotamer. Myszkiewicz *et al.* presented a study on 1,3-dihydroxybenzene (resorcinol), using rotationally resolved laser induced fluorescence spectroscopy.[53] Only two rotamers could be identified in the molecular beam spectra of 1,3-dihydroxybenzene. Two 1,4-dihydroxybenzene (benzoquinone) rotamers have been studied at rotational resolution in the group of Pratt and the two origins were assigned to the *cis* and *trans* rotamers on the basis of their different nuclear spin statistical weights and the different rotational constants.[100]

Huang *et al.*[103] measured the vibrational spectrum of 1,2-dimethoxybenzene (1,2-DMB) in the  $S_1$  and in the  $D_0$  states and found only one conformer in the resonant two-color ionization spectrum. A high resolution study of 1,2-DMB and its water cluster has been performed in the Pratt group.[82] They could show, that all bands in the vibronic spectrum have the same rotational constants in the ground state and belong therefore to the same rotamer, which was identified from a comparison to quantum chemical calculations as the *trans*-1,2-DMB rotamer. Three bands, labelled by *A*, *B*, and *C* at 36101.5, 36163.9, and 36 256.9  $\text{cm}^{-1}$  in the R2PI molecular beam spectrum of 1,3-dimethoxybenzene (1,3-DMB) have been assigned to the origins of three different rotamers by Breen *et al.*[55] Yang *et al.*[56] performed two-color resonant two-photon mass-analyzed threshold ionization spectroscopy to investigate selected rotamers of 1,2-DMB and 1,3-DMB in their ionic states. They found three different ionization potentials for the bands *A* to *C* in the R2PI spectrum of the 1,3-conformer from ref.[55] and also concluded the existence of three different rotamers. However, Schneider *et al.*[104] could show, that the *C*-band is in fact not due to another rotamer, but is a vibronic transition that is build on the electronic *A* band origin. Oikawa *et al.*[105] and Tzeng *et al.*[106] investigated structures and vibrations of 1,4-dimethoxybenzene (1,4-DMB) conformers in their  $S_0$  and  $S_1$  states. They found two planar rotamers, which they named *cis* and *trans*. Yamamoto *et al.*[107] recorded the fluorescence emission spectra of both rotamers of 1,4-DMB. They found that the *cis* rotamer of 1,4-DMB selectively forms complexes with polar solvent molecules, while both the *cis* and the *trans* rotamer form complexes with unpolar solvent molecules. In the following we will present a thorough study of the permanent dipole moments of several rotamers of the three isomeric DMBs in the ground and the first electronically excited singlet state and of the transition dipole moments for the transition connecting these two states.

## 6.3. Computational Methods

### 6.3.1. Quantum chemical calculations

Structure optimizations were performed employing Dunning’s correlation consistent polarized valence triple zeta (cc-pVTZ) basis set from the TURBOMOLE library. [59, 60] The equilibrium geometries of the electronic ground and the lowest excited singlet states were optimized using the approximate coupled cluster singles and doubles model (CC2) employing the resolution-of-the-identity approximation (RI).[61–63] Anharmonic normal mode analyses have been performed to compute vibrational averaging effect on the inertial defects of the molecules under consideration. Such an anharmonic analysis is implemented in the Gaussian program package. [108] The procedure for the calculation of cubic and of some of the quartic force constants utilizes numerical derivatives of the analytically determined Hessian with respect to the normal coordinates. We performed the analysis at the MP2 level with the 6-311G(d,p) basis set.

### 6.3.2. Fits of the rovibronic spectra using evolutionary algorithms

Evolutionary algorithms have proven to be perfect tools for the automated fit of rotationally resolved spectra, even for large molecules and dense spectra. [68–71] Beside a correct Hamiltonian to describe the spectrum and reliable intensities inside the spectrum, an appropriate search method is needed. Evolutionary strategies are powerful tools to handle complex multi-parameter optimizations and find the global optimum. For the analysis of the presented high-resolution spectra we used the covariance matrix adaptation evolution strategy (CMA-ES), which is described in detail elsewhere. [72, 73] In this variant of global optimizers mutations are adapted via a covariance matrix adaptation (CMA) mechanism to find the global minimum even on rugged search landscapes that are additionally complicated due to noise, local minima and/or sharp bends. The analysis of the rotationally resolved electronic Stark spectra is described in detail in ref. [109]

## 6.4. Experimental Methods

1,2-Dimethoxybenzene ( $\geq 99\%$ ), 1,3-Dimethoxybenzene (98%) and 1,4-Dimethoxybenzene ( $\geq 98\%$ ) were purchased from Sigma-Aldrich and used without further purification. The samples were heated to 60°C (for 1,2- and 1,3-Dimethoxybenzene) and 100°C (for 1,4-Dimethoxybenzene) and co-expanded with 200 - 300 mbar of argon into the vacuum

through a 200  $\mu\text{m}$  nozzle. After the expansion a molecular beam was formed using two skimmers (1 mm and 3 mm, 330 mm apart) linearly aligned inside a differentially pumped vacuum system consisting of three vacuum chambers. The molecular beam was crossed at right angles with the laser beam 360 mm downstream of the nozzle. To create the excitation beam, 10 W of the 532 nm line of a diode pumped solid state laser (Spectra-Physics Millennia eV) pumped a single frequency ring dye laser (Sirah Matisse DS) operated with Rhodamine 110. The light of the dye laser was frequency doubled in an external folded ring cavity (Spectra Physics Wavetrain) with a resulting power of about 25 mW (1,2-Dimethoxybenzene) and about 80 mW (1,3- and 1,4-Dimethoxybenzene) during the experiments. The fluorescence of the samples was collected perpendicular to the plane defined by laser and molecular beam using an imaging optics setup consisting of a concave mirror and two plano-convex lenses onto the photocathode of a UV enhanced photomultiplier tube (Thorn EMI 9863QB). The signal output was then discriminated and digitized by a photon counter and transmitted to a PC for data recording and processing. The relative frequency was determined with a *quasi* confocal Fabry-Perot interferometer. The absolute frequency was obtained by comparing the recorded spectrum to the tabulated lines in the iodine absorption spectrum.[31] A detailed description of the experimental setup for the rotationally resolved laser induced fluorescence spectroscopy has been given previously. [57, 58]

To record rotationally resolved electronic Stark spectra, a parallel pair of electro-formed nickel wire grids (18 mesh per mm, 50 mm diameter) with a transmission of 95% in the UV was placed inside the detection volume, one above and one below the molecular beam - laser beam crossing with an effective distance of  $23.49 \pm 0.05$  mm. [109] In this setup the electric field is parallel to the polarization of the laser radiation. With an achromatic  $\lambda/2$  plate (Bernhard Halle, 240-380nm), mounted on a linear motion vacuum feedthrough, the polarization of the incoming laser beam can be rotated by  $90^\circ$  inside the vacuum.

## 6.5. Results

### 6.5.1. Computational Results

The nomenclature for the rotamers of the three isomeric dimethoxybenzenes we adopt here, refers to the dihedral angles of the methoxy groups with respect to the aromatic plane. The numbering starts at the lowest number in the benzene ring, at the position adjacent to the first substituent. For the first rotamer of 1,2-DMB in Figure 6.1 the first dihedral angle formed by C(2)C(1)O(7)C(9) is  $180^\circ$ , the second by C(3)C(2)O(8)C(10) is

0°. Thus, the labeling for this rotamer is (180/0). The second rotamer has a dihedral angle C(2)C(1)O(7)C(9) of 0° and C(3)C(2)O(8)C(10) of 0°, therefore named (0/0).

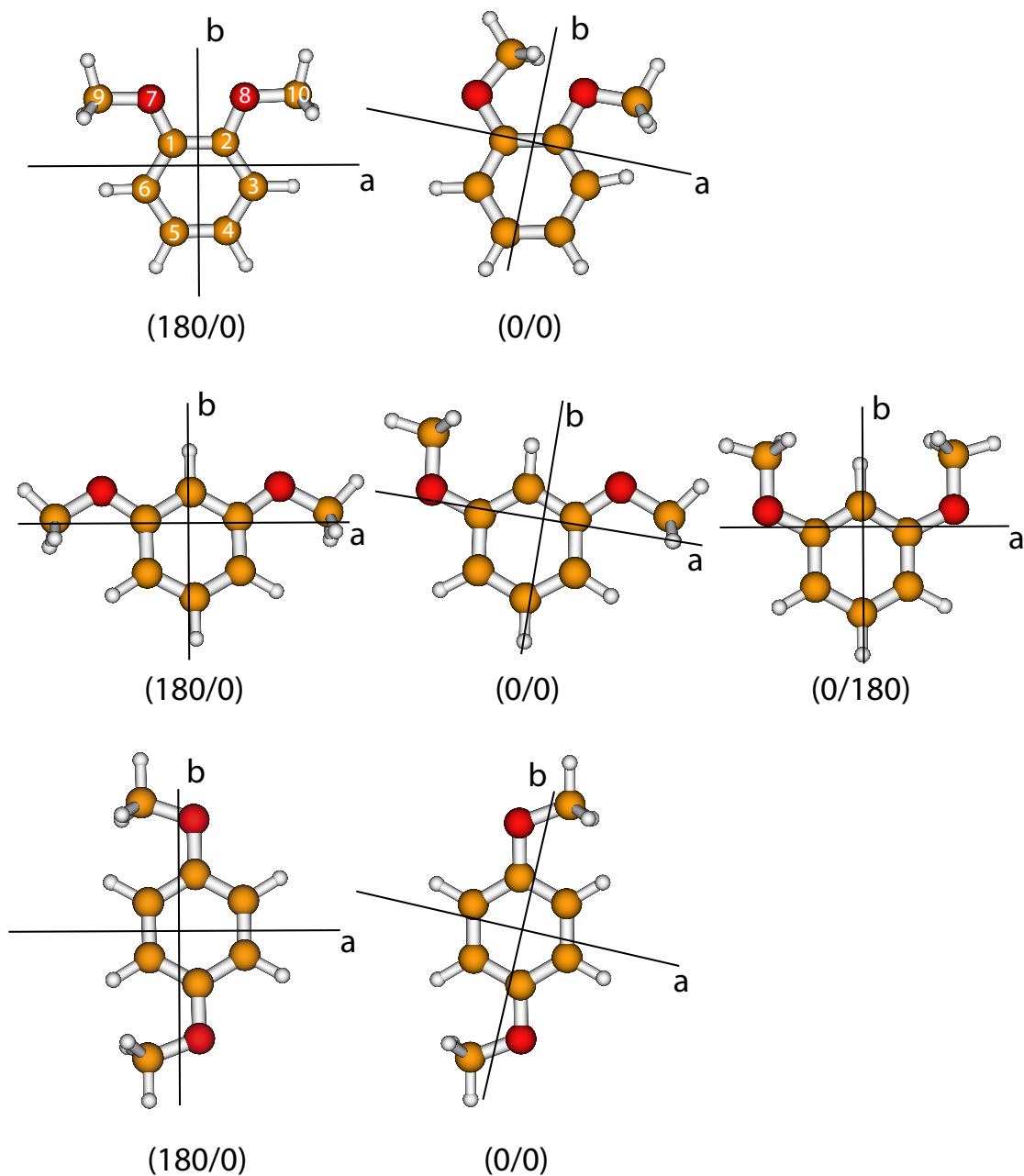


**Figure 6.1.:** Structures of the rotamers of 1,2-dimethoxybenzene, 1,3-dimethoxybenzene, and 1,4-dimethoxybenzene with their principal inertial axes. The (180/180) rotamers of all three conformers are equivalent to the (0/0) rotamer. For 1,4-dimethoxybenzene (0/180) and (180/0) are also equivalent structures. The (0/180) rotamer of 1,2-dimethoxybenzene is no stable minimum due to steric hindrance of the neighboring methoxy groups.

The (180/0) rotamer of 1,2-DMB was optimized at the CC2//cc-pVTZ level of theory in the  $S_0$  and the lowest excited singlet state  $S_1$  and found to be the most stable conformer of 1,2-DMB. The Cartesian coordinates of all stable structures are given in the online supporting material. Starting the optimization at the (0/0) geometry, the structure converges to a gauche rotamer with one methoxy group tilted out of the aromatic plane, while the other methoxy group stays in-plane. The energy of this rotamer is 6.2 kJ/mol higher than the lowest energy rotamer (180/0), cf. Table 6.1. Under molecular beam conditions, this conformer is probably not populated. Furthermore, the experimentally determined inertial defects (cf. section Experimental Results) prove heavy-atom planarity for all observed rotamers. Therefore, this rotamer is omitted from the further discussion. Confining the optimization of the (0/0) rotamer to a planar heavy atom arrangement, leads to a first order transition state. For the (0/180) rotamer the methyl groups overlap within their van der Waals radii. A structure optimization starting from this geometry converges to the most stable (180/0) rotamer.

Three 1,3-DMB rotamers, shown in the second line of Figure 6.1 have been found to be energetically compatible with cooling conditions in a molecular beam. The lowest energy rotamer is (0/0), followed by (180/0), which is 2.2 kJ/mol higher in energy and (0/180), which is 2.7 kJ/mol higher. All three rotamers are planar in the electronic ground state. The (0/0) and (180/0) structures are also planar in the electronically excited state, while the six-ring of the (0/180) rotamer is tilted considerably out-of-plane in the excited  $S_1$ -state. This non-planarity upon electronic excitation has already been reported by Wilke *et al.* [104].

The smallest energetic difference between the two stable rotamers is found for 1,4-DMB. The (180/0) rotamer is more stable by 1.1 kJ/mol than the (0/0) rotamer. Also for 1,4-DMB, both rotamers have planar heavy atom structures in both electronic states.

Additionally, we calculated the dipole moments of anisole (monomethoxybenzene) at the CC2//cc-pVTZ level of theory for both electronic states. These quantities will be utilized in the following for construction of the dipole moments of the dimethoxybenzenes from vector addition arguments. They are given in Table 6.2.

The dipole moments in ground and lowest excited singlet states of anisole and of the most stable rotamers of 1,2-DMB, 1,3-DMB, and 1,4-DMB are compiled in Tables 6.2, 6.3, 6.4, and 6.5. The rotamers, with the methoxy groups symmetric to the  $b$ -axis, have for symmetry reasons no component of the dipole moment in  $a$  direction.

**Table 6.1.:** Absolute energies, zero-point vibrational energies and relative energies including zero-point energy (ZPE) corrections of different rotamers of 1,2-, 1,3- and 1,4-dimethoxybenzene in the electronic ground state at CC2//cc-pVTZ level of theory. The relative energies are given with respect of the most stable rotamer of each isomer.

Rotamer	1,2-DMB			1,3-DMB			1,4-DMB		
	(180, 0)	(0, 0)	(180, 0)	(180, 0)	(0, 0)	(0, 180)	(180, 0)	(180, 0)	(0, 0)
$E_{abs}$ /a.u.	-460.4062926	-460.4036199	-460.4107042	-460.4115791	-460.4105434	-460.4085741	-460.408131	-460.408131	-460.408131
ZPE/a.u.	0.1659015	0.1655773	0.1660763	0.1660966	0.1660894	0.1658473	0.165837	0.165837	0.165837
$E_{rel}$ /kJ/mol	0.000	6.166	2.244	0.000	2.700	0.000	0.000	0.000	1.137

## 6.5.2. Experimental Results

### Permanent dipole moments and transition dipole moment of anisole

The rotationally resolved electronic spectrum of anisole (monomethoxybenzene) has been presented and analyzed before.[76, 99] However, no Stark measurements have been performed until now, and the dipole moment in the excited singlet state is not known experimentally. For anisole in solution an excited state dipole moment from solvatochromic shifts has been reported.[110] However, agreement with gas phase Stark data are usually bad, and the components in the inertial frame of the molecule were not given. Since the orientation of the dipole moments in the excited state are needed in the discussion of the DMBs, we measured and analyzed the Stark spectrum of anisole. The dipole moments have been obtained from a combined fit to the Stark spectra in parallel as well as in perpendicular arrangement of laser polarization and electric field.[109] The fit using the CMA-ES algorithm yielded the parameters given in Table 6.2. The dipole components, which have been obtained by Desyatnyk *et al.* [75] using microwave Stark spectroscopy, have been kept fixed in our fit, due to the inherently larger accuracy of the MW values. Experimental rotational constants and dipole moments of both electronic states are in good agreement with the results for the CC2//cc-pVTZ optimized structure. From the ratio of intensities of the *a* and the *b* lines of anisole, the angle of the TDM with the inertial *a* axis can be determined to be  $72^\circ$  in close agreement to the theoretical value.

### Permanent dipole moments and transition dipole moment of 1,2-DMB

Fig.6.2 shows the rotationally resolved electronic spectrum of the origin band of 1,2-DMB at zero field and at a field strength of 400.24V/cm with parallel orientation of electromagnetic and electric field ( $\Delta M = 0$ ). The zero-field spectrum of 1,2-DMB has been measured before in the group of David Pratt and its inertial parameters are reported in Ref. [82]. The zero-field spectrum was fit using a rigid rotor Hamiltonian,[111] while the spectrum with electric field was fit using a Stark rigid rotor Hamiltonian with  $\Delta M = 0$  selection rules.[109, 112, 113]

The experimental rotational constants and the permanent dipole moments in both electronic states, which are derived from the fit of the Stark spectrum are given in Table 6.3 and compared to the calculated dipole moments of both rotamers of 1,2-DMB. Both, the inertial parameters and the dipole moments point to the (180/0) rotamer to be responsible for the origin band of 1,2-DMB. The small dipole moment of 0.17 D in the ground state and 0.78 D in the electronically excited state makes an angle  $\theta_D$  of  $90^\circ$  with the

**Table 6.2.:** Calculated rotational constants, permanent electric dipole moments  $\mu$  and their components  $\mu_i$  along the main inertial axes  $i=a, b, c$  of anisole compared to the respective experimental values. Doubly primed parameters belong to the electronic ground and single primed to the excited state.  $\theta_D$  is the angle of the dipole moment vector with the main inertial  $a$ -axis. A positive sign of this angle means a clockwise rotation of the dipole moment vector onto the main inertial  $a$ -axis.  $\theta$  is the angle of the transition dipole moment with the main inertial  $a$ -axis. A positive sign of this angle means a clockwise rotation of the dipole moment vector onto the main inertial  $a$ -axis.

	theory	experiment
$A''$ / MHz	5019	5028.84414(19) <sup>1</sup>
$B''$ / MHz	1578	1569.364308(68) <sup>1</sup>
$C''$ / MHz	1210	1205.825614(41) <sup>1</sup>
$\Delta I''$ / amu Å <sup>2</sup>	-3.29	-3.409
$\mu_a''$ / D	0.58	0.69 <sup>1</sup>
$\mu_b''$ / D	1.20	1.05 <sup>1</sup>
$\mu_c''$ / D	1.33	1.26 <sup>1</sup>
$\theta_D''$ / °	64	56.7
$A'$ / MHz	4773	4795.17(13)
$B'$ / MHz	1566	1555.68(4)
$C'$ / MHz	1188	1184.45(3)
$\Delta I'$ / amu Å <sup>2</sup>	-3.20	-3.58
$\mu_a'$ / D	1.55	1.59(3)
$\mu_b'$ / D	1.70	1.50(3)
$\mu_c'$ / D	2.30	2.19(4)
$\theta_D'$ / °	+48	±43.4
$\theta$ / °	73	69.70(1)
$\nu_0$ / cm <sup>-1</sup>	37179 <sup>2</sup>	36384.07

inertial  $a$ -axis in both states, which means that it is oriented along the inertial  $b$ -axis of the molecule. Also the transition dipole moment is purely  $b$ -axis polarized with an angle  $\theta$  of  $90^\circ$ . This value has already been reported by the Pratt group.[82] They presented a fit of the zero-field spectrum of 1,2-DMB with pure  $b$ -type selection rules. Thus, for 1,2-DMB, the dipole moments in both electronic states, as well as the transition dipole moment are collinear.

The CC2/cc-pVTZ calculated rotational constants of the (180/0) rotamer are in very good agreement with the experimentally determined parameters. This holds for the ground state rotational constants, as well as for the excited state. The changes of the rotational constants upon electronic excitation are all negative and similarly small ( $\Delta A = -21.5$  MHz,  $\Delta B = -20.7$  MHz,  $\Delta C = -9.9$  MHz).

**Table 6.3.:** Calculated rotational constants, permanent electric dipole moments  $\mu$  and their components  $\mu_i$  along the main inertial axes  $i=a, b, c$  of the (180/0) and the (0/0) conformers of 1,2-dimethoxybenzene compared to the respective experimental values. Doubly primed parameters belong to the electronic ground and single primed to the excited state.  $\theta_D$  is the angle of the dipole moment vector with the main inertial  $a$ -axis. A positive sign of this angle means a clockwise rotation of the dipole moment vector onto the main inertial  $a$ -axis.

	theory		experiment
	(180/0)	(0/0) <sup>2</sup>	A band
$A''$ / MHz	1679	1751	1663.1(1)
$B''$ / MHz	1348	1375	1349.8(1)
$C''$ / MHz	755	778	752.6(1)
$\Delta I''$ / amu $\text{\AA}^2$	-6.40	-6.58	-6.80
$\mu_a''$ / D	0.00	1.87	0.00
$\mu_b''$ / D	0.05	1.42	0.17(22)
$\mu_c''$ / D	0.05	2.35	0.17(22)
$\theta_D''$ / $^\circ$	90	37	90(1)
$A'$ / MHz	1658	1734	1641.6(1)
$B'$ / MHz	1322	1369	1329.1(1)
$C'$ / MHz	742	773	742.7(1)
$\Delta I'$ / amu $\text{\AA}^2$	-6.42	-6.82	-7.68
$\Delta A$ / MHz	-21	-17	-21.5
$\Delta B$ / MHz	-26	-6	-20.7
$\Delta C$ / MHz	-13	-23	-9.9
$\mu_a'$ / D	0.00	3.48	0.00
$\mu_b'$ / D	0.97	0.92	0.78(4)
$\mu_c'$ / D	0.97	3.59	0.78(4)
$\theta_D'$ / $^\circ$	90	14	90(1)
$\theta$ / $^\circ$	90	40	90
$\nu_0$ / $\text{cm}^{-1}$	37884	35586 <sup>2</sup>	35751

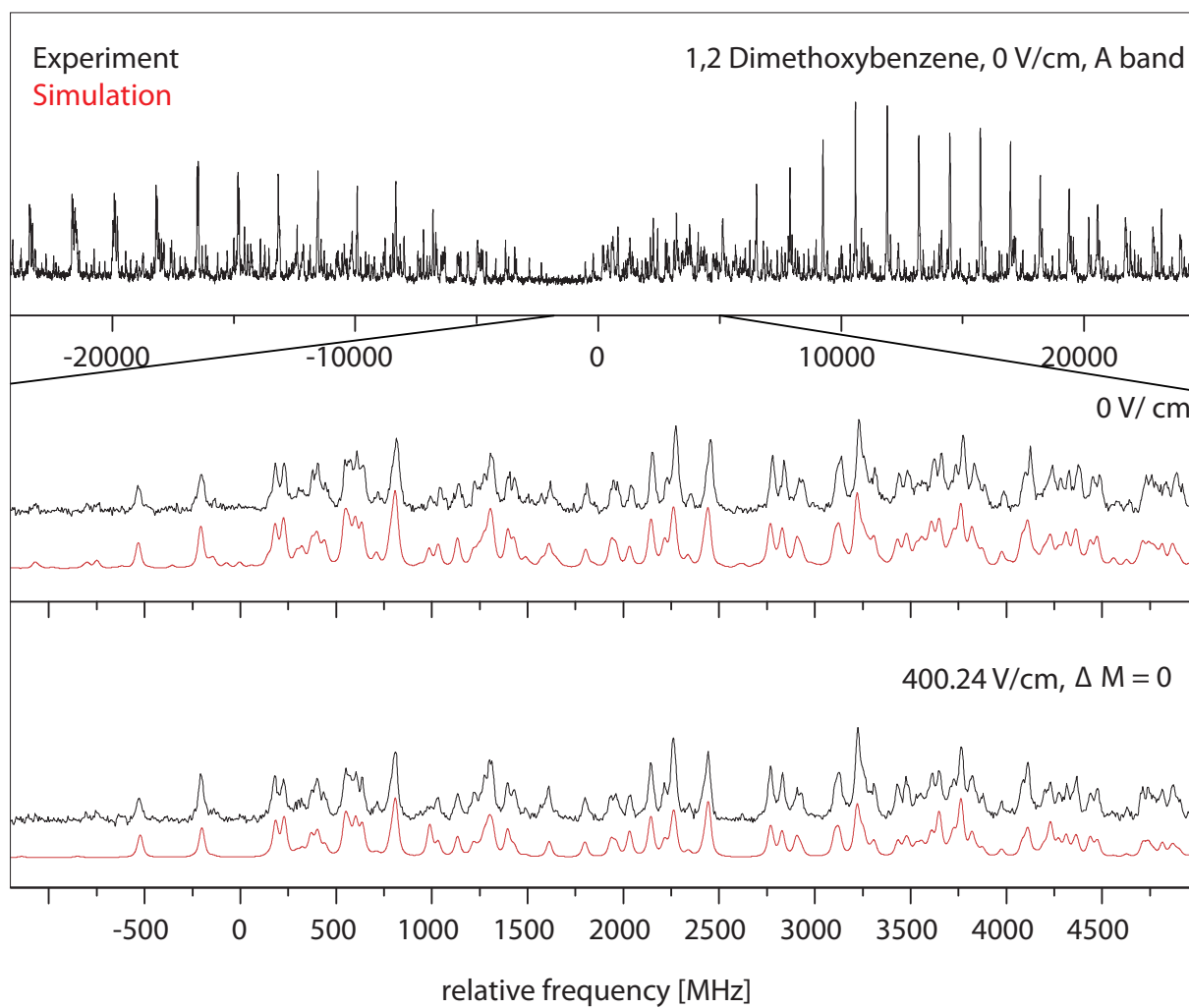


**Figure 6.2.:** Rotationally resolved electronic spectrum of the electronic origin of the A band of 1,2-DMB at zero field and at 400.24 V/cm  $\Delta M=0$  selection rules, along with a simulation with the best CMA-ES fit parameters.

### Permanent dipole moments and transition dipole moment of 1,3-DMB

Three origin bands of different rotamers of 1,3-DMB have been observed by Tzeng *et al.*[55] and Breen *et al.*[55] using resonant two-photon ionization spectroscopy and labelled *A*, *B* and *C*. The zero-field spectra of these three bands of 1,3-DMB have been presented previously by Schneider *et al.*[104]. They showed, that the *C* band is not due to a third rotamer, but instead a vibronic band build on the *A* band origin. The rotational constants for the fit of *A* and the *B* band in the two electronic states have been set fixed to the values from this publication and only the dipole moment components in both states have been fit. Fig. 6.3 shows the rotationally resolved electronic spectrum of the *A* band of 1,3-DMB at zero field and at 400.24V/cm. The zero-field and Stark spectra of the *B* band are shown in the online supporting material, see Figure A.5.

The experimental rotational constants and the permanent dipole moments from CMA-ES fits of both bands are given in Table 6.4 and compared to the calculated molecular parameters of the three most stable rotamers of 1,3-DMB. From the comparison of the rotational constants it is clear, that the *A* band belongs to the (0/0) rotamer and the *B* band to the (180/0) rotamer. Although the (0/180) rotamer is only by 2.7 kJ/mol less stable than the most stable (0/180) rotamer, it has not been observed in molecular beam experiments. This finding has been explained in a previous publication by the non-planarity of the (0/180) rotamer in the electronically excited states, which causes a small Franck-Condon factor in the excitation spectrum.[104]

It should be mentioned, that not only the ground state rotational constants of the *A* and the *B* band of 1,3-DMB allow for a straightforward assignment of the origin bands to the (0/0) and (180/0) rotamers, but also the changes of the rotational constants upon electronic excitation show very good agreement for both rotamers. Interestingly, the changes of the *A* rotational constants are quite different:  $\Delta A$  for the (0/0) rotamer decreases by 55.79 MHz, while  $\Delta A$  for the (180/0) rotamer decreases by 123.68 MHz.  $\Delta B$  and  $\Delta C$  are both small and negative.

The permanent dipole moment of the *A* band, which is assigned to the (0/0) rotamer, has components along both the *a* and the *b* inertial axes, which result in an absolute dipole moment of 1.19 D in the ground state and of 1.42 D in the excited state. The dipole moments make angles  $\theta_D$  with the *a* axis of 15° in the electronic ground state and of 29° in the excited state. The transition dipole makes an angle  $\theta$  with the *a* axis of 14.5°. Thus, dipole moment and transition dipole moment have roughly the same orientation in the molecular frame.

The permanent dipole moment of the *B* band, which is assigned to the (180/0) rotamer,

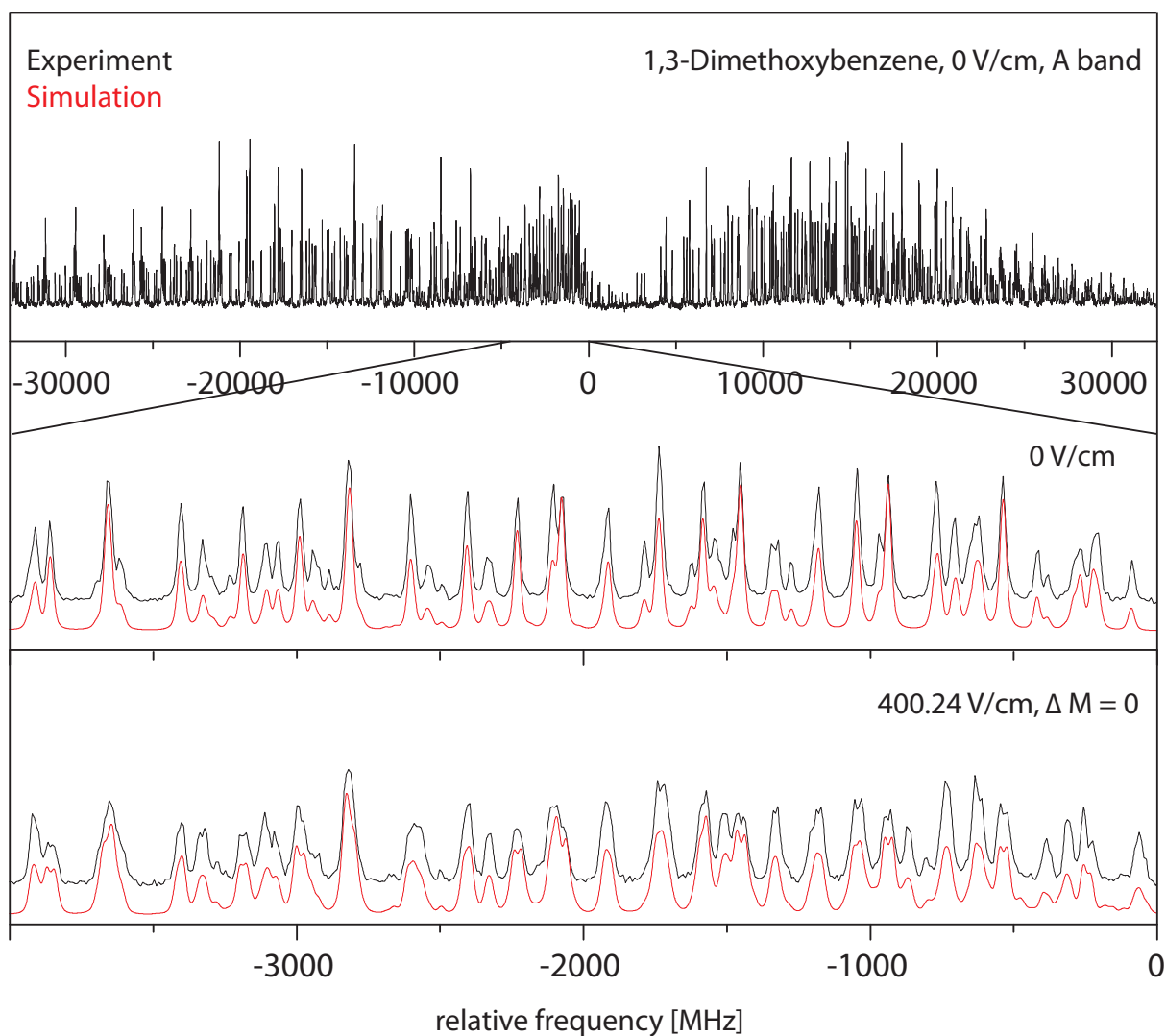


**Figure 6.3.:** Rotationally resolved electronic spectrum of the electronic origin of the A band of 1,3-DMB at zero field and at  $400.24 \text{ V/cm}^{-1}$  with 80% transitions of  $\Delta M=0$ , along with a simulation with the best CMA-ES fit parameters.

**Table 6.4.:** Summary of the calculated and experimental permanent electric dipole moments  $\mu$  and their components  $\mu_i$  along the main inertial axes  $i=a,b,c$  of the rotamers of 1,3-dimethoxybenzene. Double primed parameters belong to the electronic ground and single primed to the excited state. Additionally the angle  $\theta_D$  of the dipole moment vector with the main inertial  $a$ -axis is given.

	theory			experiment	
	(0/0)	(180/0)	(0/180)	A band	B band
$A''$ / MHz	2539	3486	1892	2533.44(45)	3461.98(36)
$B''$ / MHz	893	771	1108	887.52(2)	768.20(4)
$C''$ / MHz	666	636	705	663.11(2)	634.01(4)
$\Delta I''$ / amu $\text{\AA}^2$	-6.40	-6.40	-6.41	-6.78	-6.74
$\mu''_a$ / D	1.04	0.00	0.00	1.15(4)	0.00
$\mu''_b$ / D	0.79	1.52	2.62	0.31(5)	1.66(1)
$\mu''$ / D	1.30	1.52	2.62	1.19(5)	1.66(1)
$\theta''_D$ / $^\circ$	37	90	90	15(3)	90(1)
$A'$ / MHz	2482	3358	1863	2477.65(45)	3338.30(36)
$B'$ / MHz	880	763	1091	875.60(3)	760.63(4)
$C'$ / MHz	655	626	695	652.93(3)	624.86(4)
$\Delta I'$ / amu $\text{\AA}^2$	-6.42	-6.42	-7.44	-7.14	-7.03
$\Delta A$ / MHz	-57	-128	-29	-55.79	-123.68
$\Delta B$ / MHz	-13	-8	-17	-11.92	-7.57
$\Delta C$ / MHz	-11	-10	-10	-10.18	-9.15
$\mu'_a$ / D	1.71	0.00	0.00	1.25(4)	0.00
$\mu'_b$ / D	0.16	1.28	3.01	0.68(10)	1.36(1)
$\mu'$ / D	1.72	1.28	3.01	1.42(8)	1.36(1)
$\theta'_D$ / $^\circ$	6	90	90	29(5)	90(1)
$\theta$ / $^\circ$	6	0	0	$\pm 14.5(1)$	0.0 <sup>1</sup>
$\nu_0$ / $\text{cm}^{-1}$	36809 <sup>2</sup>	36986 <sup>2</sup>	36455 <sup>2</sup>	36117.61(2)	36185.72(1)

is oriented along the inertial  $b$  axis, with a slightly smaller absolute value in the excited state (1.36 D) compared to the ground state (1.66 D). However, the transition dipole is oriented along the  $a$  axis and thus rotated by  $90^\circ$  with respect to the individual permanent dipole moments of both states. This surprising behavior will be explained later.

### Permanent dipole moments and transition dipole of 1,4-DMB

1,4-DMB exists in two different stable rotamers, named  $A$  and  $B$  by Oikawa *et al.*[105], equivalent to the *cis* and *trans* 1,4-dihydroxybenzene (hydroquinone) rotamers, which are according to the above nomenclature the (180/0) and the (0,0) rotamer, respectively. Since the (0/0) rotamer has a center of symmetry, the resulting dipole moment should be exactly zero by symmetry arguments. The rotationally resolved zero-field electronic spectra of both rotamers have not been presented before and are used in the following to determine the inertial parameters of the two rotamers.

In a first step, the zero-field spectra of the  $A$  (cf Figure 6.4) and the  $B$  (Figure A.6 of the online supporting material) bands were fit using CMA-ES algorithm, yielding the inertial parameters in both electronic states. These are presented in Table 6.5, along with the results of the CC2/cc-pVTZ calculations. The comparison of the experimental and calculated rotational constants clearly shows, that the  $A$  band can be assigned to the (0/0) rotamer, while the  $B$  band is due to the (180/0) rotamer. As for 1,2-DMB and 1,3-DMB also the changes of the rotational constants upon electronic excitation are very well reproduced by the CC2 calculations. For both rotamers of 1,4-DMB large negative changes of  $\Delta A$  and very small changes for  $\Delta B$  and  $\Delta C$  are found

Subsequently the Stark spectra were recorded at field strengths of 400.24 V/cm and were fit using the CMA-ES algorithm. The spectrum of the  $A$  band does not show line splittings or shifts, and for the permanent dipole moment in both states we determine an upper limit of 0.1 D for the individual components and 0.14 D for the absolute value in both states. The  $B$  band, which is due to the (180/0) rotamer has a dipole moment along the inertial  $b$  axis of 2.76 D.

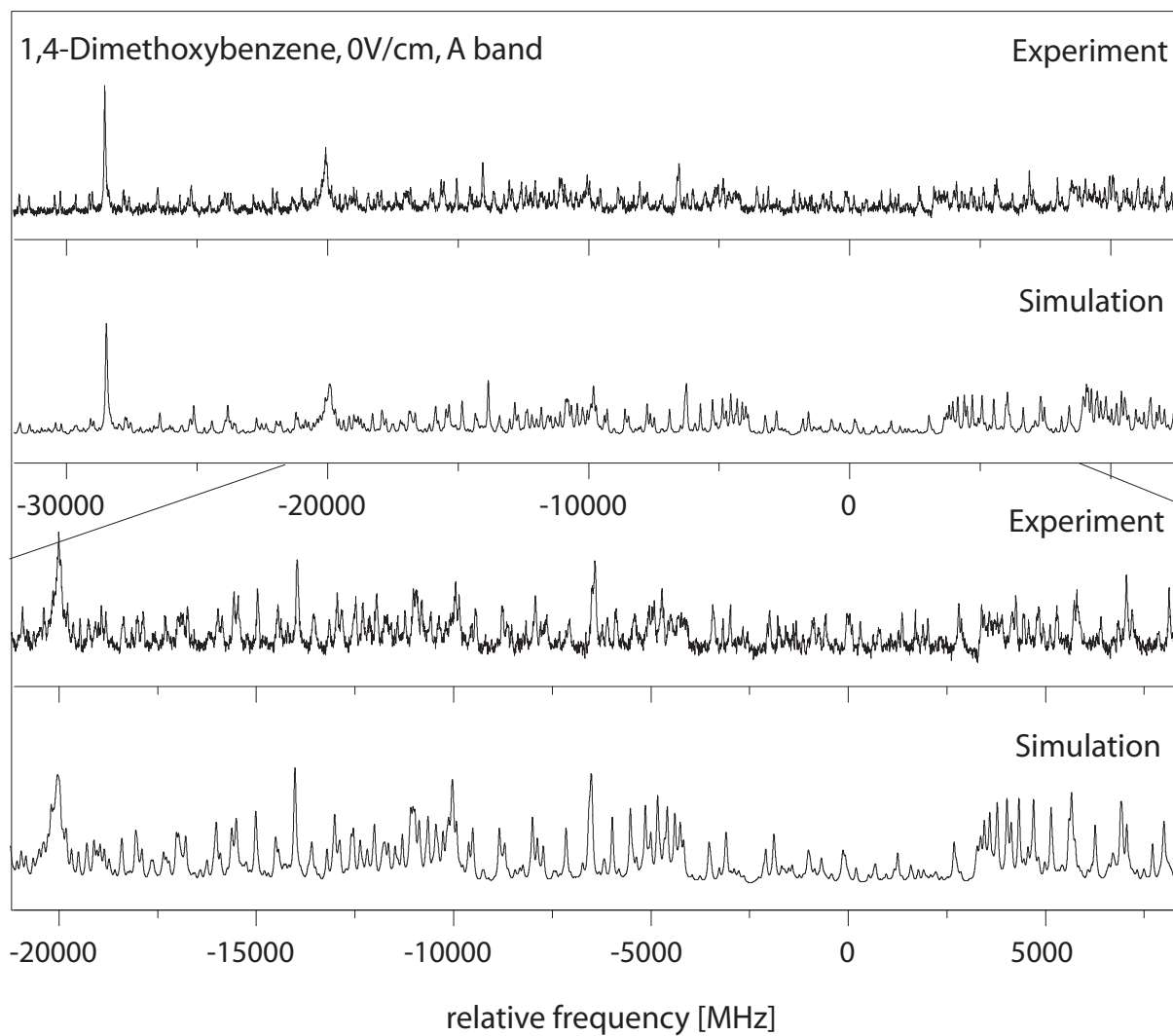


**Figure 6.4.:** Rotationally resolved spectrum of the electronic origin of the A band of 1,4-dimethoxybenzene, along with a simulation using the best CMA-ES fit parameters.

**Table 6.5.:** Molecular parameters of the two rotamers of 1,4-dimethoxybenzene from a CMA-ES fit of the electronic zero-field spectra. The angle of the transition dipole moment with the main inertial  $a$ -axis is given by  $\theta$  and the adiabatic excitation energy by  $\nu_0$ .

	theory		experiment	
	(0/0)	(180/0)	$A$ band	$B$ band
$A''$ / MHz	4477	3963	4494.55(20)	3995.84(8)
$B''$ / MHz	699	721	693.99(4)	714.52(2)
$C''$ / MHz	609	615	606.26(4)	611.23(2)
$\Delta I''$ / amu $\text{\AA}^2$	-6.40	-6.39	-7.07	-6.96
$\mu''_a$ / D	0.00	0.00	0.00(10)	0.00 <sup>1</sup>
$\mu''_b$ / D	0.00	2.24	0.00(10)	2.23(1)
$\mu''$ / D	0.00	2.24	0.00(14)	2.23(1)
$\theta''_D$ / $^\circ$	-	90	-	90(1)
$A'$ / MHz	4294	3794	4319.35(36)	3835.76(11)
$B'$ / MHz	701	724	695.47(5)	716.68(3)
$C'$ / MHz	607	613	604.18(5)	609.05(3)
$\Delta I'$ / amu $\text{\AA}^2$	-6.42	-6.43	-7.21	-7.14
$\Delta A$ / MHz	-183	-169	-175.2	-160.08
$\Delta B$ / MHz	+2	+3	+1.48	+2.16
$\Delta C$ / MHz	-2	-2	-2.08	-2.18
$\mu'_a$ / D	0.00	0.00	0.00	0.00 <sup>1</sup>
$\mu'_b$ / D	0.00	2.92	0.00	2.76(1)
$\mu'$ / D	0.00	2.92	0.00	2.76(1)
$\theta'_D$ / $^\circ$	-	90	-	90(1)
$\theta$ / $^\circ$	81	90	71.91(1)	90.00
$\tau$ / ns	-	-	2.58(1)	2.64(1)
$\nu_0$ / $\text{cm}^{-1}$	33674 <sup>2</sup>	33945 <sup>2</sup>	33629.66(21)	33849.63(11)

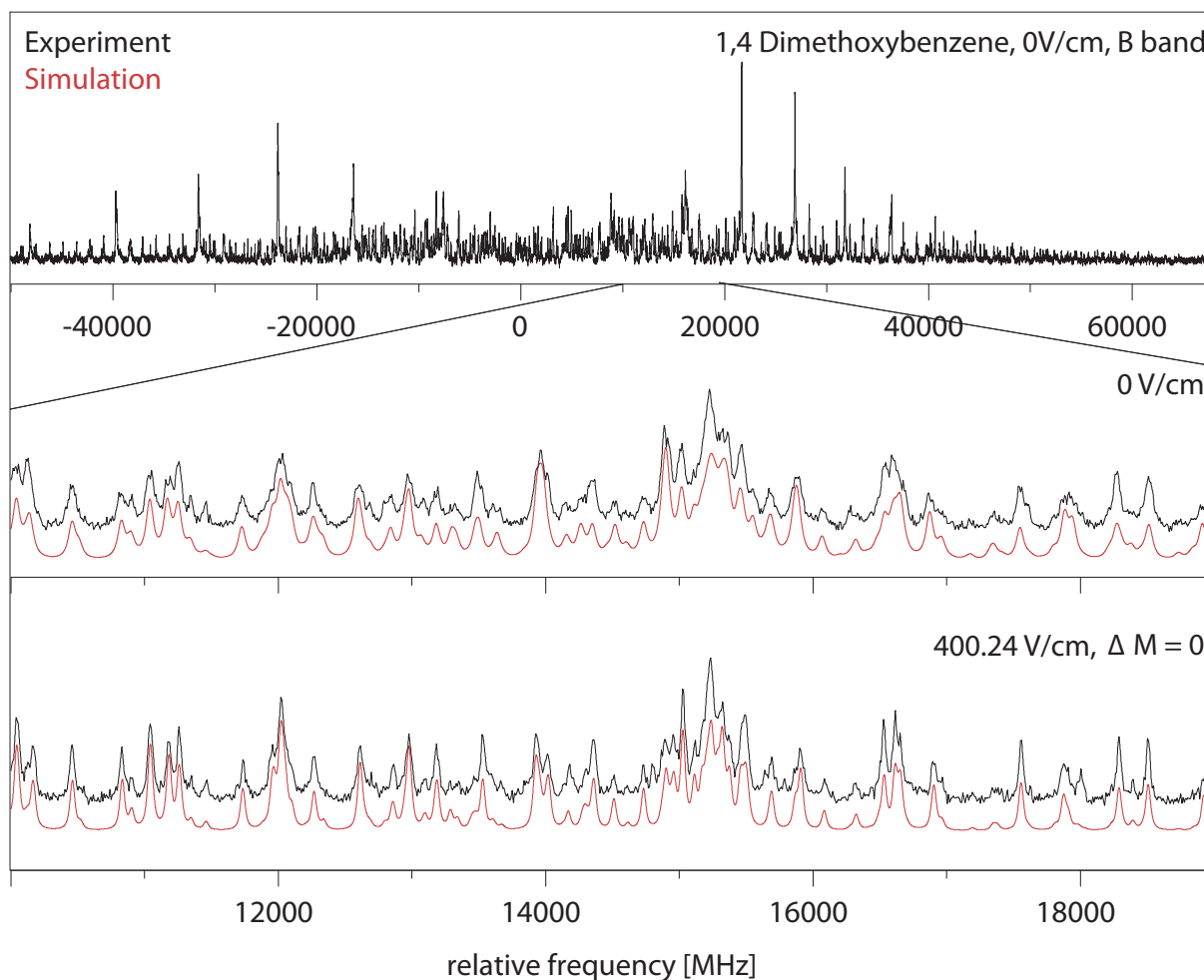


**Figure 6.5.:** Rotationally resolved electronic spectrum of the electronic origin of the B band of 1,4-DMB at zero field and at  $400.24\text{V}/\text{cm}^{-1}$  with 80% transitions of  $\Delta M=0$ , along with a simulation with the best CMA-ES fit parameters.

---

## 6.6. Discussion

### 6.6.1. Permanent Dipole Moments

#### Ground State

The molecular dipole moments of the three isomeric DMBs in their electronic ground states can be derived from simple vector addition models. Each of the DMB dipole moments can be thought as a sum of two individual anisole dipole moments whose orientations are given by the mutual orientation and the position of the two methoxy groups in the aromatic ring.

Using microwave Stark spectroscopy, the dipole moment components of anisole in the electronic ground state has been determined by Desyatnyk *et al.* [75] to be  $\mu_a = 0.6937(12)$  D,  $\mu_b = 1.0547(8)$  D from which a value of  $|\mu| = 1.2623(14)$  D results for the absolute dipole moment. The dipole moment makes an angle of  $56.7^\circ$  with the inertial  $a$  axis of anisole (cf. Figure 6.6a).

Figure 6.6 shows the results of a vectorial addition of the dipole moments derived from anisole for the 1,2-, 1,3-, and 1,4-DMB rotamers in this study. The dipole vectors have been shifted from the anisole center of mass (COM) to the COM of the respective DMB for sake of clarity. Figure 6.6a shows the dipole moment of anisole in its inertial axis frame.

For the only rotamer, which was observed for 1,2-DMB (180/0), the vector addition shown in Figure 6.6b results in a cancelation of the  $a$ -components of the dipole moment in the ground state. Since the angle between the two anisole dipole moment vectors is small, the resulting dipole moment is oriented along the  $b$ -axis of the molecule and close to zero, as determined experimentally. The exact analysis yields an angle of  $170^\circ$  between the two vectors with a length of 1.26 D, resulting in a sum dipole moment of 0.2 D, close to the experimental value of 0.17 D.

Two rotamers were observed for 1,3-DMB. For the (180/0) rotamer, the two anisole dipole moments lie symmetrically about the  $b$ -axis and form an angle of  $50^\circ$  with the  $b$ -axis (Figure 6.6c). The resulting dipole moment in  $b$  direction is 1.62 D, again in good agreement with the experimental value for  $\mu_b$  of 1.66 D. For the (0/0) rotamer, vector addition of the two anisole dipole vectors results in a vector with both  $a$  and  $b$  components (Figure 6.6d). Assuming an angle between the anisole fragment dipoles of  $104^\circ$  (as in the (180/0) rotamer), numerical values of 1.20 D and 0.45 D for the dipole moment components are obtained, in fair agreement with the experimental values of 1.15 D for  $\mu_a$  and of 0.31 D for  $b$ .

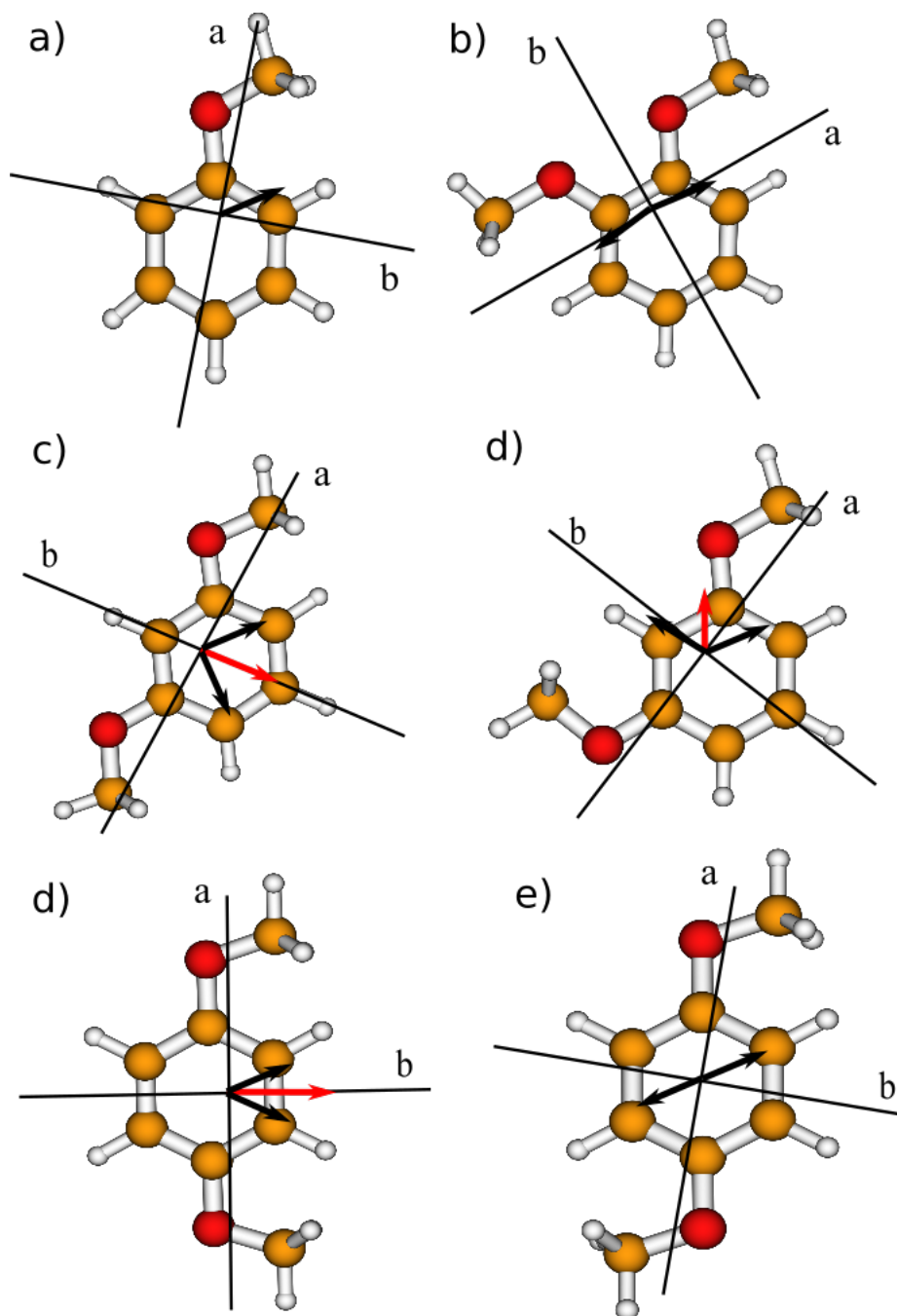


**Figure 6.6.:** a) Inertial axes and ground state dipole moment of anisole (from Ref. [75]). b) Vector addition of the experimental anisole ground state dipole moment for (180/0)-1,2-DMB. c) Vector addition of the experimental anisole dipole moment for (180/0)-1,3-DMB. The resulting dipole moment (in red) is oriented along the *b*-axis. d) Vector addition of the experimental anisole dipole moment for (0/0)-1,3-DMB. The resulting dipole moment (in red) has components both on the *a*- and the *b*-axis. e) Vector addition of the experimental anisole dipole moment for (180/0)-1,4-DMB. The resulting dipole moment (in red) is oriented along the *b*-axis. f) Vector addition of the experimental anisole dipole moment for (0/0)-1,4-DMB. The individual dipoles cancel each other out.

Also, for 1,4-DMB two rotamers have been found experimentally. While for the (0,0) rotamer no dipole moment results, due to its inversion symmetry (Figure 6.6f), the (180/0) rotamer shows a dipole moment in  $b$  direction, which has the largest value of all components for the rotamers of the three DMB conformers, due to the small angle of  $63^\circ$  between the anisole fragment dipoles. From this angle, we calculate a resulting dipole moment of 2.24 D in good agreement with the experimental value of 2.22 D.

Thus, for the electronic ground state, the dipole moments of all rotamers can nicely be calculated from the anisole fragment dipole moments. For rotamers, in which the dipole moment is oriented along one of the inertial axes, the agreement is very good, for the (0/0) rotamer of 1,3-DMB, which shows an  $ab$  hybrid dipole, the agreement is fair. This ground state additivity of bond dipole moments has already been shown for different conformers of aminophenol by Reese *et al.* [114] and for aminobenzonitrile by Borst *et al.* [115].

### Excited State

In the following section, we will apply the same vector addition of bond dipole moments of anisole to the excited states of the DMBs. The resulting dipole moment components in the excited state have been determined to be  $\mu_a = 1.59(3)$  D and  $\mu_b = 1.50(3)$  D from which a value of  $|\mu| = 2.19(4)$  D results for the absolute dipole moment, cf. Table 6.2. Thus, the absolute dipole moment of anisole increases by 0.93 D, and the angle between the dipole moment vector and the inertial  $a$  axis changes from  $56.7^\circ$  to  $43.4^\circ$  upon electronic excitation. The orientation and absolute value of the excited state anisole dipole is shown in Figure 6.7a.

For 1,2-DMB we found that the dipole moment in  $b$  direction greatly increases from 0.17 D to 0.78 D. However, this increase is not found in the vectorial addition of the anisole bond dipole moments. Figure 6.7b shows the result of the vector addition with the anisole bond dipole moment added for each of the methoxy groups in 1,2-DMB. Although the excited state dipole vector of anisole is larger by a factor of 4.6, the angle between the inertial  $a$  axis and the dipole moment changes only by  $10^\circ$ . Thus, both bond dipoles are still nearly antiparallel and cancel each other nearly out.

Also for the (180/0) rotamer of 1,3-DMB vectorial addition completely fails for the excited state dipole moment. For the ground state, a permanent dipole of 1.66 D in  $b$  direction was determined experimentally, which decreases to 1.36 D upon electronic excitation. Vector addition of the anisole dipoles, which include an angle of  $100^\circ$  should lead to a value of 1.92 D (Figure 6.7c), i.e. an increase of 16% in spite of the experimentally determined decrease of 8%.

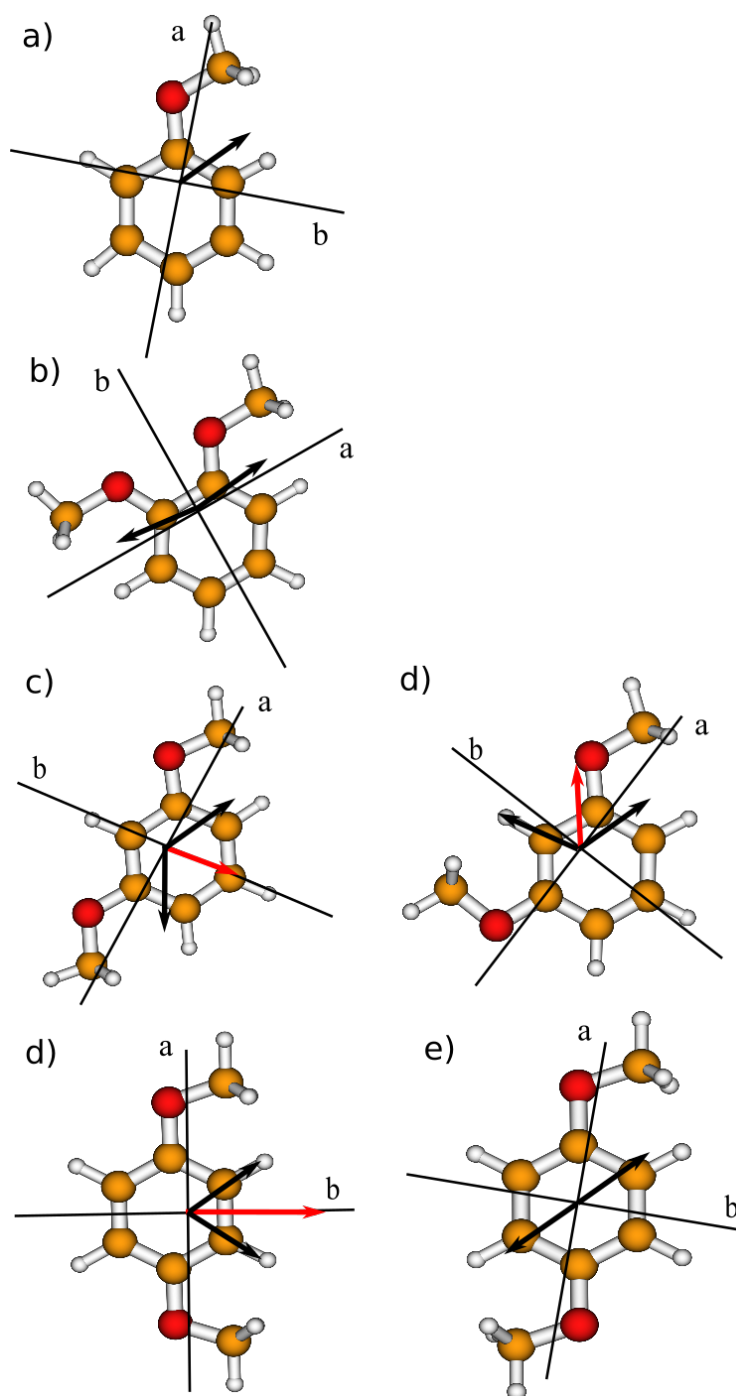


**Figure 6.7.:** a) Inertial axes and excited state dipole moment of anisole. b) Vector addition of the experimental anisole excited state dipole moment for (180/0)-1,2-DMB. c) Vector addition of the experimental anisole dipole moment for (180/0)-1,3-DMB. The resulting dipole moment (in red) is oriented along the *b*-axis. d) Vector addition of the experimental anisole dipole moment for (0/0)-1,3-DMB. The resulting dipole moment (in red) has components both on the *a*- and the *b*-axis. e) Vector addition of the experimental anisole dipole moment for (180/0)-1,4-DMB. The resulting dipole moment (in red) is oriented along the *b*-axis. f) Vector addition of the experimental anisole dipole moment for (0/0)-1,4-DMB. The individual dipoles cancel each other out.

Finally the same analysis for the (180/0) rotamer of 1,4-DMB leads to an excited state dipole moment from vector addition of 3.35 D in  $b$  direction, much higher than the experimentally observed value of 2.76 D, cf. Figure 6.7d.

### 6.6.2. Transition Dipole Moments

We start the discussion with the cases, in which dipole moments and transition dipole moment (TDM) are oriented along one of the inertial axes. The  $S_1 \leftarrow S_0$  TDMs of the (180/0) rotamers of 1,2-DMB and 1,4-DMB are oriented along the inertial  $b$ -axis, as the permanent dipole moments in the ground and excited states. For the (180/0) rotamer of 1,3-DMB the TDM is oriented along the inertial  $a$ -axis, while both ground and excited state dipole moments are oriented along the  $b$ -axis. So we have the special case in (180/0) rotamer of 1,3-DMB, that the permanent dipole moments in both states and the transition dipole moment are perfectly perpendicular to each other. We recall the fact that the expectation value of the permanent dipole moment is defined as  $\langle \Psi'' | \hat{\mu} | \Psi'' \rangle$  for the ground state, as  $\langle \Psi' | \hat{\mu} | \Psi' \rangle$  for the excited state dipole moments, and as  $\langle \Psi' | \hat{\mu} | \Psi'' \rangle$  for the transition dipole moment. Here, the  $\Psi''$  and  $\Psi'$  are the wave functions of the ground and excited state, respectively and  $\hat{\mu}$  is the dipole operator. In other words, the transition dipoles are the off-diagonal matrix elements of the three-dimensional position operator, multiplied with the elementary charge and the permanent dipoles are the diagonal elements. For dipole moments along one axis, the question arises, if a non-zero expectation value of the dipole moment with respect to this axis defines also a non-zero expectation value of the transition dipole moment with respect to the same axis. Obviously, this is not the case for the (180/0) rotamer of 1,3-DMB. The molecular frontier orbitals and the excitations, which contribute to the  $S_1 \leftarrow S_0$  transitions of the observed rotamers of the three dimethoxybenzenes are given in the ESI (Figures S3 - S5). For the discussion here, the relative phases of the leading contributions to the transition are sufficient. Figure 6.8 shows, how the orientation of the TDM in the inertial axes frames can be derived from the relative phases of the MOs. The upper row of the figure shows the phases of the HOMOs of the respective conformer, the second row those of the LUMOs and the third row gives the product, from which the TDM orientation results.

The angles, which the TDMs make with the inertial axes in the (0/0) rotamers of 1,3-DMB and of 1,4-DMB are determined only by the rotation of the inertial axis system, due to the internal rotation of one of the methoxy groups. For both the 1,3-DMB and 1,4-DMB (0/0) rotamers the inertial axis systems are rotated by  $15^\circ$  with respect to the (180/0) rotamers. The experimental TDM orientation of (0/0) 1,3-DMB makes an angle

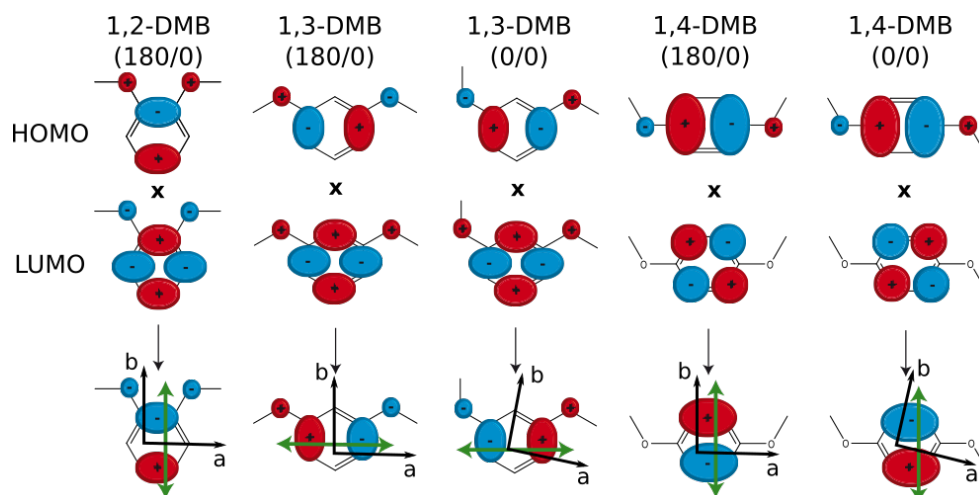


**Figure 6.8.:** TDM orientations of the experimentally observed rotamers of 1,2-DMB, 1,3-DMB, and 1,4-DMB. The lowest row shows the direct product of the phases of the HOMO and the LUMO wavefunctions, the resulting TDM (in green) and the inertial axes systems.

of  $14.5^\circ$  with the  $a$ -axis, in excellent agreement with the former consideration. For (0/0) 1,4-DMB the angle of the TDM with the  $a$ -axis is  $72^\circ$ , close to the value expected from a pure geometric axis rotation of  $90^\circ - 15^\circ = 75^\circ$ .

The electronic character of the excited state can be described by the nodal planes of the molecular orbitals involved in the transition. According to the particle-on-a-ring model for cata-condensed hydrocarbons of Platt [116], nodes of the MOs, which bisect the bonds of benzene lead to an  $L_a$  state, while nodes of the MOs, which go through the atoms of benzene lead to a  $L_b$  state. Heilbronner and Murrell have extended the original Platt classification of excited states for substituted benzenes, which have a  $C_2$  symmetry axis. Here, the labels  $a$  and  $b$  distinguish the symmetry with respect to that symmetry axis.<sup>3</sup> States, which give transitions that are parallel to the twofold axis have the label  $a$ , while those transitions that are perpendicular to this axis are labelled as  $b$ . [117]

We start the discussion with the three rotamers, that have a twofold symmetry axis. For the (180/0) rotamer of 1,2-DMB, the symmetry axis is the  $b$  axis, and the TDM is parallel to this axis (Figure 6.8). Hence, the  $S_1 \leftarrow S_0$  transition of 1,2-DMB is labelled as  $L_a$  state, in agreement with the fact, that the leading contribution to the  $S_1 \leftarrow S_0$  transition of 1,2-DMB is LUMO  $\leftarrow$  HOMO (Figure A.7). For the (180/0) rotamer of 1,3-DMB, the symmetry axis is still the inertial  $b$  axis, but now the TDM is oriented perpendicular to

<sup>3</sup>"For both the odd and even-atom systems, if the molecule has a two-fold symmetry axis passing through an atom, then transitions to a states are polarized parallel to that axis, transitions to b states at right angles to this." [117]

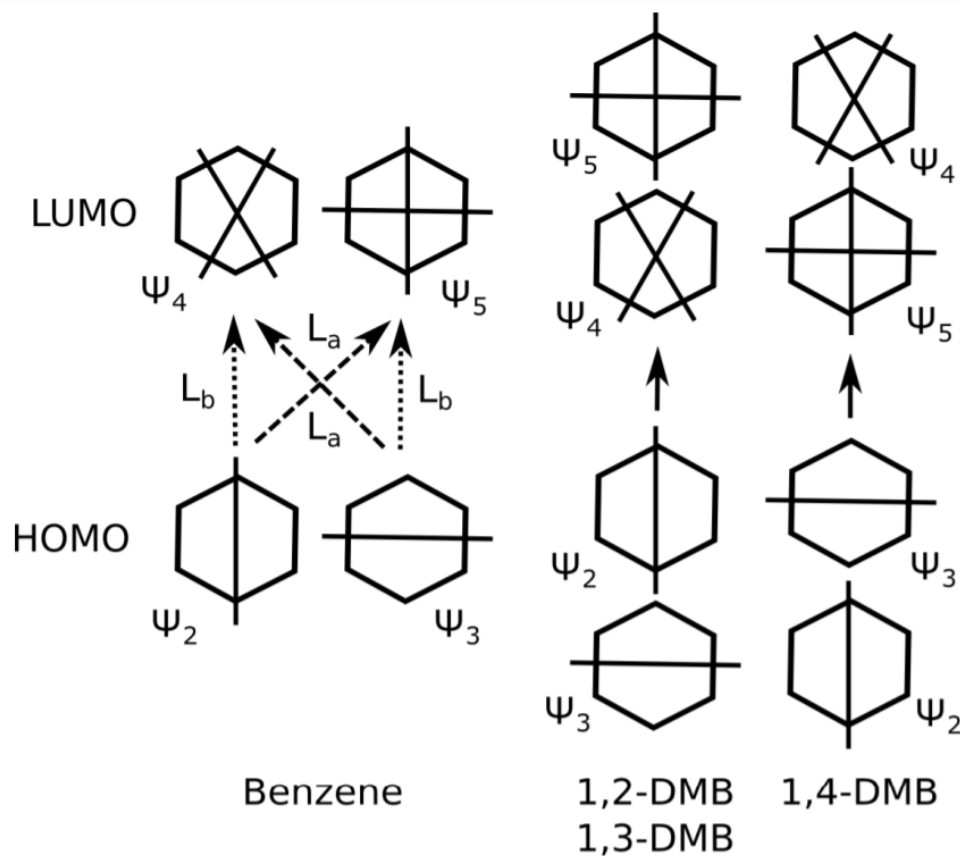


**Figure 6.9.:** Nodes of the four frontier MOs for benzene and for the three symmetric DMBs. The two (degenerate) LUMO  $\leftarrow$  HOMO transitions in benzene ( $L_a$  dashed lines,  $L_b$  dotted) are forbidden by symmetry. The degeneracy is lifted by the substituents in the DMBs.

that axis. Hence the resulting excited state is an  $L_b$  state for this isomer. Finally, for the (180/0) rotamer of 1,4-DMB, the symmetry axis is the inertial  $b$  axis, which bisects the bonds of the aromatic ring in this case. The TDM parallel to this axis leading to an  $L_b$  state.

**Table 6.6.:** Changes of the rotational constants upon electronic excitation. The rotamers with  $C_2$  symmetry axis are (180/0), those without are (0/0) rotamers.

	$C_2$ axis			no $C_2$ axis	
	1,2-DMB	1,3-DMB	1,4-DMB	1,3-DMB	1,4-DMB
$\Delta A$ / MHz	-21.5	-123.7	-160.1	-55.8	-175.2
$\Delta B$ / MHz	-20.7	-7.6	+2.2	-11.9	+1.5
$\Delta C$ / MHz	-9.9	-9.15	-2.2	-10.2	-2.1
state	$L_a$	$L_b$	$L_b$	mixed $L_a/L_b$	

These assignments are further supported by the experimentally observed changes of the rotational constants upon electronic excitation. While excitation to an  $L_a$  state leads to a benzenoid distortion of the ring, excitation to the  $L_b$  state results in a quinone-like distortion. The first case will have the decrease of the rotational constants distributed evenly, while the  $L_b$  excitation will show a large  $\Delta A$  and much smaller  $\Delta B$  and  $\Delta C$ . Table 6.6 shows exactly this behavior.

The electronically excited states of the unsymmetric (0/0) rotamer of 1,3-DMB are mixed, what can be deduced from the intermediate changes of the rotational constants (Table 6.6) and from the coefficients of the MOs for the excitation to the lowest singlet state (Figure A.8). While all other (symmetric) rotamers have components of the excitation from HOMO to LUMO and from HOMO-1 to LUMO+1, there is some amount of HOMO-1 to LUMO excitation in this rotamer. There is surprisingly little mixing of the excited states in the unsymmetric (0/0) rotamer of 1,4-DMB. Therefore, the orientation of the TDM in the molecular frame is determined by the amount, the inertial axes are rotated away from the positions of the symmetric molecules.

## 6.7. Conclusions

For several rotamers of the three isomeric dimethoxybenzenes, the orientation and magnitudes of the permanent dipole moments in the ground ( $S_0$ ) and lowest excited singlet ( $S_1$ ) states, and the orientation of the transition dipole moment for the  $S_1 \leftarrow S_0$  transition have been determined from rotationally resolved electronic Stark spectroscopy. The orientation of the permanent dipole moments and of the transition dipole moment for excitation of

the same electronically excited state of the DMB rotamers is not necessarily the same. For 1,2-DMB the permanent dipole moments in both states and the transition dipole moment for the transition to the  $S_1$ -state are all oriented along the inertial  $b$  axis. For 1,3-DMB the permanent dipole moments lies along the  $b$  axis, while the TDM for the  $S_1 \leftarrow S_0$  transition is  $a$ -polarized. 1,4-DMB shows the same behavior as 1,2-DMB. All dipoles and the TDM are oriented along the inertial  $b$  axis. For the (0/0) rotamers, which do not have the TDMs oriented along one of the inertial axes, the angle of TDM with the inertial  $a$  axis is directly obtained from the rotation of the inertial axis system upon internal rotation of one of the methoxy groups by  $180^\circ$ , i.e. the effect of the orientation of the oxygen lone pairs with respect to the chromophore is small.

For all isomers and rotamers studied here, the ground state dipole moments of the dimethoxybenzenes can be deduced from the dipole moment of anisole by bond dipole moment vector addition. However, this is not true for the electronically excited singlet state. Such a non-additivity of bond dipole moments has been found before by Reese *et al.* [114] for *cis* and *trans* m-aminophenol. They assumed that the off-axis substitution in these isomers is responsible for a state mixing of  $S_1$  and  $S_2$  zero-order states<sup>4</sup>. We therefore calculated the contributions to the excitation to the  $S_1$  and  $S_2$  states, respectively. They are summarized in Table 6.7. For the symmetric (180/0) rotamers, the contributions to the excitations to the  $S_1$  state are either HOMO-1  $\rightarrow$  LUMO and HOMO  $\rightarrow$  LUMO+1 with different relative phases, or nearly pure HOMO  $\rightarrow$  LUMO excitations, i.e. can be described in a pure  $L_a$  or  $L_b$  scheme. The respective  $S_2$  states have strong contributions of mixed excitations. Thus, for the  $S_1$  state, there is no strong state mixing, which might be responsible for the non-additivity of the excited state dipole moments.

---

<sup>4</sup>The  ${}^1L_b$  and  ${}^1L_a$  states in the notation of Platt [116].

## 6.8. Acknowledgements

Financial support of the Deutsche Forschungsgemeinschaft via grant SCHM1043 12-3 is gratefully acknowledged. Computational support and infrastructure was provided by the "Center for Information and Media Technology" (ZIM) at the Heinrich-Heine-University Düsseldorf. We furthermore thank the Regional Computing Center of the University of Cologne (RRZK) for providing computing time on the DFG-funded High Performance Computing (HPC) system CHEOPS as well as support.

## 6.9. Publication

Chapter 6 was published under the heading *Excited state dipole moments and transition dipole orientations of different rotamers of 1,2-, 1,3, and 1,4-dimethoxybenzene* in *ChemPhysChem*, **19**, 307-318, 2018. DOI: 10.1002/cphc.201701095.

The gas phase measurements were performed by Marie-Luise Hebestreit, Martin Wilke and myself. The *ab initio* calculations and spectra evaluations were made by myself and Martin Wilke. My total share of this publication is about: 70%.

**Table 6.7.:** CC2/cc-pVTZ calculated vertical excitation energies and coefficients of the contributions to the excitation to the  $S_1$  and  $S_2$  states.

$\nu_{vert}$	1,2-DMB						1,3-DMB						1,4-DMB											
	(0/0)		(180/0)		(0/0)		(180/0)		(0/0)		(180/0)		(0/0)		(180/0)									
	$S_1$	$S_2$	$S_1$	$S_2$	$S_1$	$S_2$	$S_1$	$S_2$	$S_1$	$S_2$	$S_1$	$S_2$	$S_1$	$S_2$	$S_1$	$S_2$								
HOMO $\rightarrow$ LUMO	33580	33597	34805	35173	30245	30651	37503	42581	32594	33376	32992	33091	0.91	-0.61	-	0.85	-	0.91	-	0.60	0.74	0.95	-	
HOMO-1 $\rightarrow$ LUMO	-	0.44	0.50	-0.21	0.87	0.21	0.85	-	0.34	-0.20	-	0.41	-	0.44	-	-	-	-	-	-	-	-	-	0.41
HOMO-2 $\rightarrow$ LUMO	0.22	-	-	0.18	-	-0.22	-	0.31	-	-	-	-	-	0.22	-	-	-	-	-	-	-	-	-	-
HOMO $\rightarrow$ LUMO+1	-	0.51	-0.69	0.31	-0.31	-	-0.49	-	-0.66	0.57	-	-0.86	-	0.51	-	-	-	-	-	-	-	-	-	-0.86
HOMO $\rightarrow$ LUMO+2	-	-	-	-	-	-0.14	-	-	-	-	0.16	-	-	-	-	-	-	-	-	-	-	-	-	-



# 7 | Publication on 3-Cyanoindole and its Water Complex

## Rotationally Resolved Electronic Spectroscopy of 3-Cyanoindole and the 3-Cyanoindole-water complex

Michael Schneider,<sup>a</sup> Marie-Luise Hebestreit,<sup>a</sup> Mirko Matthias Lindic,<sup>a</sup> Hilda Parsian,<sup>a</sup> América Torres-Boy,<sup>b</sup> Leonardo Álvarez-Valtierra,<sup>b</sup> W. Leo Meerts,<sup>c</sup> Ralf Kühnemuth,<sup>d</sup> and Michael Schmitt<sup>a</sup>

<sup>a)</sup> *Heinrich-Heine-Universität, Institut für Physikalische Chemie I, D-40225 Düsseldorf, Germany.*

<sup>b)</sup> *Universidad de Guanajuato-Campus León, División de Ciencias e Ingenierías, León, Guanajuato 37150, México.*

<sup>c)</sup> *Radboud University, Institute for Molecules and Materials Felix Laboratory, Nijmegen, 6525 ED, The Netherlands.*

<sup>d)</sup> *Heinrich-Heine-Universität, Lehrstuhl für Molekulare Physikalische Chemie, D-40225 Düsseldorf, Germany.*

### 7.1. Abstract

The rotationally resolved electronic spectra of the origin bands of 3-cyanoindole, 3-cyanoindole(d<sub>1</sub>), and the 3-cyanoindole-(H<sub>2</sub>O)<sub>1</sub> cluster have been measured and analyzed using evolutionary algorithms. For the monomer, permanent dipole moments of 5.90 D for the ground state, and of 5.35 D for the lowest excited singlet state have been obtained from electronic Stark spectroscopy. The orientation of the transition dipole moment is that of an <sup>1</sup>L<sub>b</sub> state for the monomer. The water moiety in the water cluster could be

determined to be *trans*-linearly bound to the NH group of 3-cyanoindole, with an NH...O hydrogen bond length of 201.9 pm in the electronic ground state. Like the 3-cyanoindole monomer, the 3-cyanoindole-water cluster also shows an  $^1L_b$ -like excited singlet state. The excited state lifetime of isolate 3-cyanoindole in the gas phase has been determined to be 9.8 ns, that of 3-cyanoindole( $d_1$ ) has found to be 14.8 ns, while that of the 1:1 water cluster is considerably shorter (3.6 ns). The excited state lifetime of 3-cyanoindole( $d_1$ ) in D<sub>2</sub>O solution has found to be smaller than 20 ps.

## 7.2. Introduction

Understanding solvent reorganization processes at a molecular level is a key to the determination of dipole moments of electronically excited molecules in solution. Beforehand, the driving forces, which determine the solvent orientation in both electronic states have to be investigated on a molecular level. Indole derivatives are especially interesting in this respect, since they have two energetically close-lying excited singlet states, which have considerably different dipole moments. Dipole-dipole interactions with polar solvent molecules lead to different stabilization of the electronically excited states. Depending on the dipole moments, even the energetic order of the lowest excited singlet states might switch upon cluster formation or solvation in polar solvents. These states are called  $^1L_a$  and  $^1L_b$  in the nomenclature of Platt [116], adapted to indole by Weber [118]. The  $^1L_b$  state has a small dipole moment and is lower in energy in apolar surroundings, while the  $^1L_a$  state on the other hand has a comparatively large dipole moment, leading to an inversion of the electronic state ordering in polar solvents. Some molecular systems change the energetic order of the excited states already upon addition of the first water molecules to the chromophore like azaindole. [119]

Indole, as chromophore of the aromatic amino acid tryptophane is extensively studied, mainly regarding the location of the higher electronically excited  $^1L_a$  state relative to the lowest  $^1L_b$  state, both experimentally [120–128] as well as theoretically. [129–134]

Exchange of one hydrogen atom in the chromophore by the highly polar cyano group, changes the fluorescence properties of the indole chromophore considerably.[135, 136] 5-cyanotryptophane is used as fluorescence probe of protein hydration.[137] Its chromophore, 5-cyanoindole has been studied using rotationally resolved electronic spectroscopy and fluorescence emission spectroscopy in our group. [138–140] For 5-cyanoindole, we found that the lowest electronically excited singlet state is of  $^1L_a$  character. The question arises, if for other substitution positions, the cyano group has the same stabilizing effect to the

${}^1L_a$  state. Therefore, we varied the position from the 5-position, which is located in the benzene ring of the chromophore, to the 3-position within the pyrrolic ring, in the present study. The 3-cyanoindole system is of general interest, since differently cyano-substituted indole derivatives find increasing interest as small fluorescence reporters in fluorescent proteins.[135, 136]

Considerably less work has been performed on hydrogen bonded clusters of indole or indole derivatives. Korter *et al.*[141] could show that the binary indole-water complex undergoes considerable solvent reorientation upon excitation to the lowest excited singlet state. The lowest excited singlet states of both the monomer and the water cluster, in which the water is bound linearly to the pyrrolic NH group, have shown to be of  ${}^1L_b$  character. Dipole moment of the indole-water complex was determined by Kang and Pratt using rotationally resolved electronic Stark spectroscopy.[125] They found that the dipole of the water molecule induces a dipole moment in the indole moiety, which amounts a substantial fraction of 30-40% to the total dipole moment of the cluster. Azaindole-water clusters have been examined using high resolution laser induced fluorescence (HRLIF) spectroscopy. It could be shown that the lowest excited singlet state has  ${}^1L_b$  character, while the excitation in the n=1 and n=2 water clusters is to the  ${}^1L_a$  state.[119]

Ahn *et al.* [142] investigated 3-cyanoindole and several 3-cyanoindole-water cluster, using mass-selected resonant two-photon ionization (R2PI) and UV-UV hole-burning (UVHB) spectroscopy. Assignments of the different cluster structures were made on the basis of a Franck-Condon analysis of the vibronic spectra. From the comparison of experiment and FC simulation they concluded, that only the most stable conformer is present in the molecular beam. According to *ab initio* calculations, this is the linearly N-H $\cdots$ O hydrogen bound complex.

In the present study, we investigate the electronic nature of the lowest excited state of 3-cyanoindole, its dipole moments in both ground and excited singlet states and the geometry and electronic nature of the binary 3-cyanoindole-water cluster using a combination of rotationally resolved fluorescence spectroscopy, rotationally resolved electronic Stark spectroscopy, time-correlated single photon counting, and *ab initio* quantum chemical calculations for a deeper understanding of the photophysics of electronically excited 3-cyanoindole.

## 7.3. Experimental section

### 7.3.1. Experimental procedures

#### Rotationally resolved electronic (Stark) spectroscopy

3-Cyanoindole (> 95%) was purchased from Oxchem and used without further purification. To record rotationally resolved electronic spectra, the sample was heated to 200°C and co-expanded with 300 mbar of argon into the vacuum through a 200  $\mu\text{m}$  nozzle. After the expansion, a molecular beam was formed using two skimmers (1 mm and 3 mm) linearly aligned inside a differentially pumped vacuum system consisting of three vacuum chambers. The molecular beam was crossed at right angles with the laser beam 360 mm downstream of the nozzle. To create the excitation beam, 10 W of the 532 nm line of a diode pumped solid state laser (Spectra-Physics Millennia eV) pumped a single frequency ring dye laser (Sirah Matisse DS) operated with Rhodamine 110. The fluorescence light of the dye laser was frequency doubled in an external folded ring cavity (Spectra Physics Wavetrain) with a resulting power of about 10 - 15 mW during the experiments. The fluorescence light of the samples was collected perpendicular to the plane defined by laser and molecular beam by an imaging optics setup consisting of a concave mirror and two planoconvex lenses onto the photocathode of a UV enhanced photomultiplier tube (Thorn EMI 9863QB). The signal output was then discriminated and digitized by a photon counter and transmitted to a PC for data recording and processing. The relative frequency was determined using a *quasi* confocal Fabry-Perot interferometer. The absolute frequency was obtained by comparing the recorded spectrum to the tabulated lines in the iodine absorption spectrum.[31] A detailed description of the experimental setup for rotationally resolved laser induced fluorescence spectroscopy has been given previously. [57, 58] The Stark plates consist of a parallel pair of electroformed nickel wire grids (18 mesh per mm, 50 mm diameter) with a transmission of 95% in the UV. Their effective distance is  $23.49 \pm 0.05$  mm, symmetrically aligned with respect to the laser beam. This distance was calibrated using the accurately known dipole moment of benzonitrile.[109, 143]. The polarization plane of the incoming laser beam can be rotated by 90° inside the vacuum chamber by means of an achromatic  $\lambda/2$  plate (Bernhard Halle 240 - 380 nm). The  $\lambda/2$  plate can be pushed in or pulled out of the laser beam using a linear motion vacuum feedthrough.

### Time-correlated single photon counting

Time-correlated-single-photon-counting (TCSPC) was performed with a DeltaFlex Ultima spectrometer (HORIBA Jobin Yvon), equipped with a supercontinuum light source SuperK Extreme EXR-20 and frequency doubler SuperK Extend-UV/DUV (both NKT Photonics). The signal was recorded under magic angle conditions, a pulse repetition rate of 19.2 MHz and a sample temperature of 20°. The instrument response function (IRF, FWHM approximately 60 ps) was recorded, using a scattering solution (Ludox) for each excitation wavelength and used in the fits applying an iterative reconvolution algorithm to minimize  $\chi^2$ .

#### 7.3.2. Quantum chemical calculations

Structure optimizations were performed employing Dunning’s correlation-consistent polarized valence triple zeta (cc-pVTZ) basis set from the TURBOMOLE library. [59, 60] The equilibrium geometries of the electronic ground and the lowest excited singlet states were optimized using the approximate coupled cluster singles and doubles model (CC2) employing the resolution-of-the-identity approximation (RI).[61–63] For the structure optimizations spin-component scaling (SCS) modifications to CC2 were taken into account.[144] Vibrational frequencies and zero-point corrections to the adiabatic excitation energies were obtained from numerical second derivatives using the NumForce script. [64] For the cluster stabilization energies, the basis set superposition errors (BSSE) have been accounted for, using the counterpoise corrections described by Boys and Bernardi [145] and implemented in the JOBBSSE jobscript of turbomole. Additionally, the equilibrium geometries of the lowest electronically excited singlet states were geometry optimized by means of a time-dependent density functional theory (TD-DFT) gradient [146, 147] using the Becke, three-parameter, Lee-Yang-Parr (B3-LYP) density functional. [148]

#### 7.3.3. Fits of the rovibronic spectra using evolutionary algorithms

Evolutionary algorithms allow us to make a quick and successful automatic assignment of the rotationally resolved spectra, even for large molecules and dense spectra. [68–71] Beside a correct Hamiltonian to describe the spectrum and reliable intensities inside the spectrum, an appropriate search method is needed. Evolutionary strategies are a powerful tool to handle complex multi-parameter optimizations and find the global optimum. For the analysis of the presented high-resolution spectra, we used the covariance matrix adaptation evolution strategy (CMA-ES), which is described in detail elsewhere. [73, 149]

In this variant of global optimizers mutations are adapted via a CMA mechanism to find the global minimum, even on rugged search landscapes that are additionally complicated due to noise, local minima and/or sharp bends.

## 7.4. Results

### 7.4.1. Computational Results

#### 3-cyanoindole

The optimization of 3-cyanoindole in the ground and lowest excited singlet state yields a planar structure in both states both with genuine CC2 as well as with SCS-CC2. Contrary to 5-cyanoindole, CC2 and the spin component scaled variant SCS-CC2 obtain the same state as lowest excited singlet state. [138] The molecular parameters (rotational constants  $A$ ,  $B$ , and  $C$  in both electronic states, the inertial defects  $\Delta I$ , the angle  $\theta$  of the transition dipole moment with the inertial  $a$  axis, and the zero-point corrected origin frequency  $\nu_0$ ) are compiled in Table 7.1 and are compared to the experimental results, which are described in section 7.5.1.

The inertial defects of 3-cyanoindole in both states are exactly zero for the equilibrium structures what immediately shows the planarity of the molecule.

The calculated angle of the transition dipole moment with the inertial  $a$ -axis is  $+4^\circ$ , cf. Figure 7.1. To compare this value better with the transition dipole moment vector of bare indole, the transition dipole moment (TDM) is rotated into the inertial axis frame of indole. This yields an angle of  $+52^\circ$  with the inertial  $a$ -axis of indole. The respective values in indole ( $L_b$ ) and 5-cyanoindole ( $L_a$ ) are  $+38^\circ$  and  $-12^\circ$ , respectively. Thus, the orientation of the TDM in 3-cyanoindole, is clearly that of an  ${}^1L_b$  state. The main contributions to the excitation to the lowest excited singlet state are  $0.81(\text{LUMO} \leftarrow \text{HOMO}-1)+0.43(\text{LUMO}+1 \leftarrow \text{HOMO})+0.24(\text{LUMO}+2 \leftarrow \text{HOMO})$ , cf. Figure 7.3, which are also representative for a transition to a  ${}^1L_b$  state. The zero-point corrected adiabatic excitation energy amounts to  $36156 \text{ cm}^{-1}$  ( $36045 \text{ cm}^{-1}$ ) at the CC2 (SCS-CC2) level of theory. The permanent dipole moment in the ground state amounts to 5.95 D and to 5.51 D in the electronically excited  ${}^1L_b$  state.

An explicit *caveat* has to be given for the  ${}^1L_a$ -state optimization. This state is vertically the second excited singlet state at SCS-CC2 level of theory. Optimization of this state leads, independently of the starting geometry, into a conical intersection with the lowest excited state. However, it is well-known, that the order of  ${}^1L_a$  and  ${}^1L_b$  states is reversed

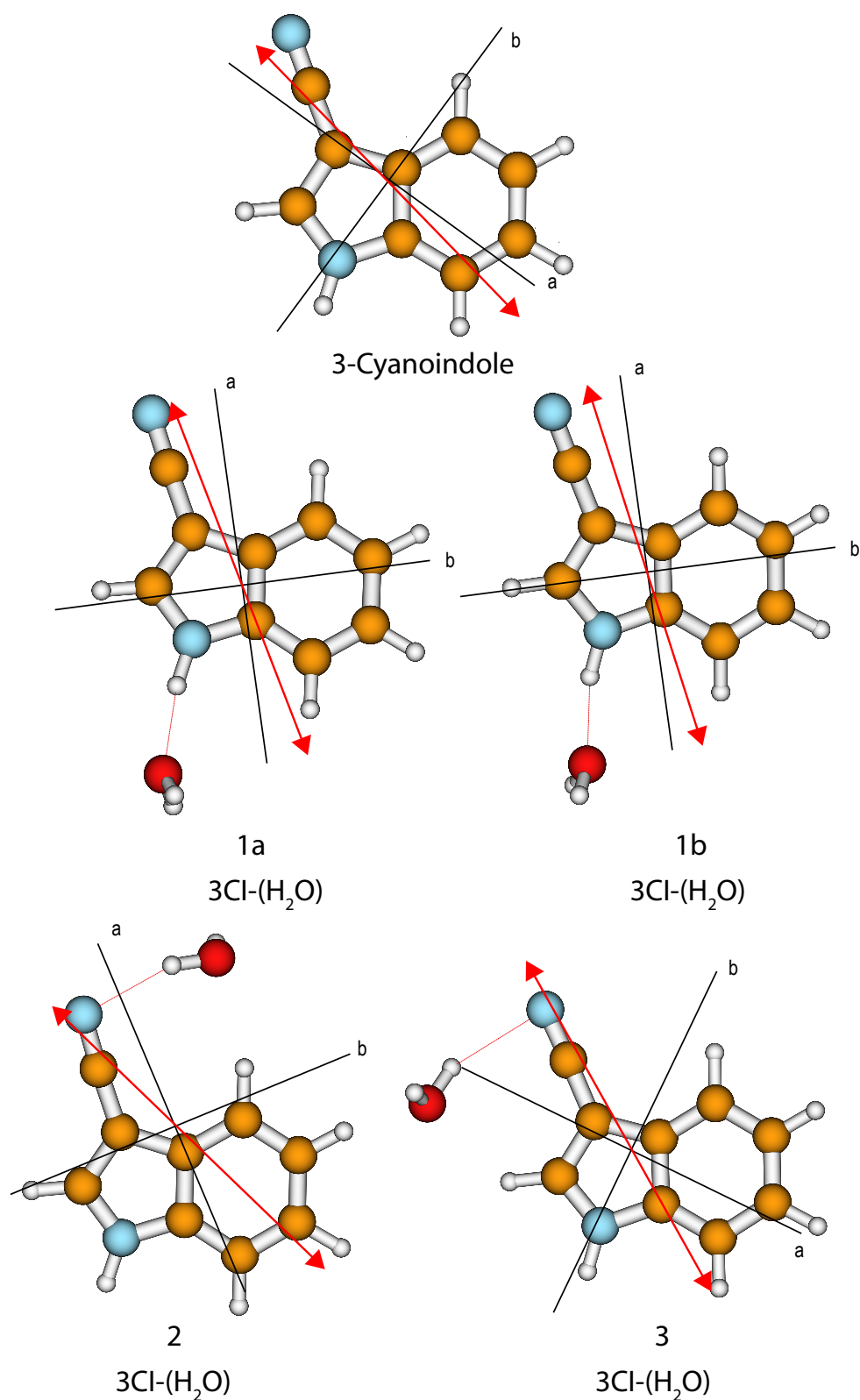


**Figure 7.1.:** Calculated structures, inertial axes and transition dipole moments of 3-cyanoindole and the 3-cyanoindole water cluster

for time-dependent density functional theory (TD-DFT).[150–153] Therefore, we changed the level of theory to TD-DFT using the B3-LYP functional and the cc-pVTZ basis set. As expected, at TD-DFT level, the vertically lowest state is the  ${}^1L_a$  state, well below the  ${}^1L_b$ . Geometry optimization led to the lowest excited state, which remained the  ${}^1L_a$  state. Thus, the  ${}^1L_a$  is also adiabatically the lowest excited singlet state at TD-DFT level. The fact that TD-DFT, employing the B3-LYP functional reverses the order of  ${}^1L_a$  and  ${}^1L_b$  states has been observed before in tryptamine.[153]

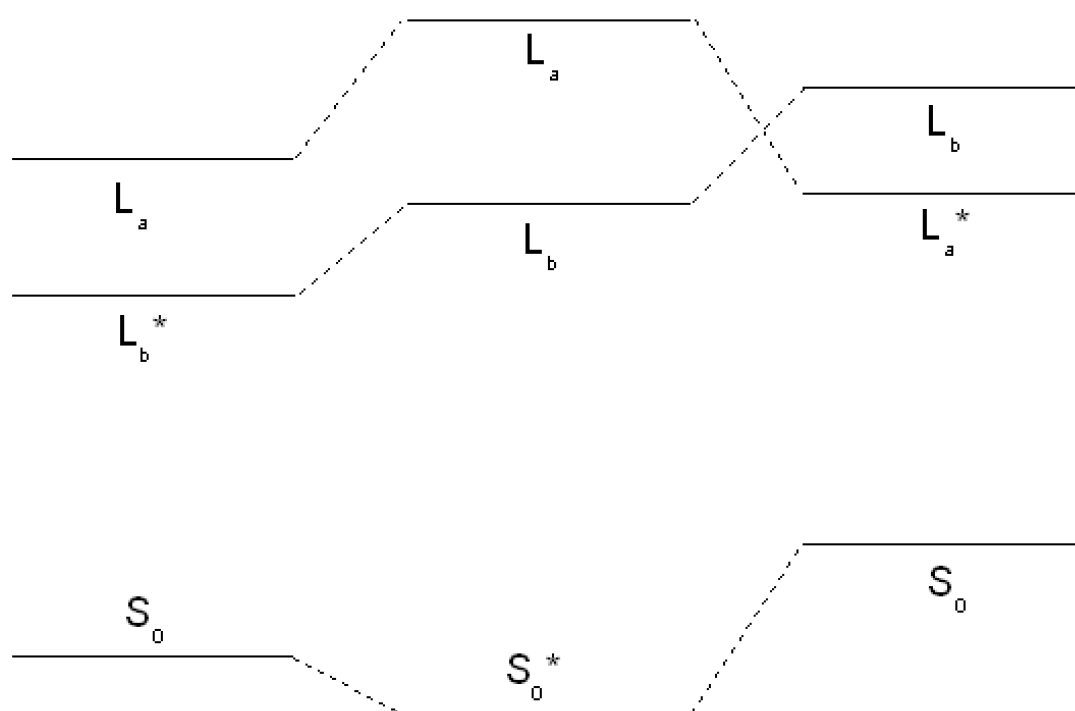


**Figure 7.2.:** Energies of the ground and excited  ${}^1L_a$  and  ${}^1L_b$  states of 3-cyanoindole from SCS-CC2/cc-pVTZ calculations at the TD-B3-LYP/cc-pVTZ optimized geometries. The optimized state is marked by an asterisk. In the left part of the figure, the  ${}^1L_b$  is the geometry optimized state, in the middle the ground state, and in the right part, the  ${}^1L_a$  state.

For tryptamine, the correct energetic order of the excited states could be obtained using density functional multi-reference configuration interaction (DFT-MRCI), which correctly takes dynamic and static electron correlation into account, at the TD-DFT optimized geometries. For 3-cyanoindole, the SCS-CC2 energy of the  ${}^1L_a$  state, which constitutes the second electronically excited singlet state was calculated at the geometry of the  ${}^1L_b$  state at TD-DFT level, where it is the lowest electronically excited singlet state. In this geometry, the  ${}^1L_a$  is adiabatically also at SCS-CC2 level the lowest excited singlet state. These findings are resumed in Figure 7.2. However, further optimization starting from

this geometry again led to the conical intersection with the  ${}^1L_b$  state.

Using the SCS-CC2 energy at the TD-B3-LYP optimized structure for the  ${}^1L_a$  state an angle of the TDM with the inertial  $a$  axis of  $-80^\circ$  is calculated. The leading contributions to the excitation are:  $0.87(\text{LUMO} \leftarrow \text{HOMO}) + 0.39(\text{LUMO-1} \leftarrow \text{HOMO+1})$ . The zero-point corrected adiabatic excitation energy amounts to  $39392 \text{ cm}^{-1}$  and the permanent dipole moment to  $5.18 \text{ D}$  in the electronically excited  ${}^1L_a$  state, with an angle of  $+31^\circ$  to the inertial  $a$ -axis.

**Table 7.1.:** SCS-CC2/cc-pVTZ computed and experimental molecular parameters of 3-cyanoindole (3-CI) and the N-deuterated isotopologue ( $(d_1)$ ). Doubly primed parameters belong to the electronic ground and single primed to the excited state.  $\theta_D$  is the angle of the permanent dipole moment vector with the main inertial  $a$ -axis. A negative sign of this angle means an anticlockwise rotation of the main inertial  $a$ -axis onto the dipole moment vector, shown in Figure 7.1.  $\theta$  is the angle of the transition dipole moment vector with the main inertial  $a$ -axis. The same convention for its sign is used as for  $\theta_D$ . For details see text.

	theory SCS-CC2		experiment	
	3-CI	3-CI( $d_1$ )	3-CI	3-CI( $d_1$ )
$A'' / \text{MHz}$	2255	2171	2258.53(48)	2180.09(17)
$B'' / \text{MHz}$	943	942	947.38(3)	950.80(2)
$C'' / \text{MHz}$	665	657	667.44(3)	660.88(1)
$\Delta I'' / \text{amu}\text{\AA}^2$	0	0	-0.02	-0.02
$\mu''_a / \text{D}$	+3.94	+3.96	$\pm 4.15(1)$	-
$\mu''_b / \text{D}$	-4.38	-4.34	$\pm 4.20(1)$	-
$\mu'' / \text{D}$	5.89	5.89	5.90(1)	-
$\theta''_D / ^\circ$	+48.0	+47.53	$\pm 45.3$	-
$A' / \text{MHz}$	2221	2140	2227.15(49)	2150.84(18)
$B' / \text{MHz}$	931	931	937.46(4)	938.81(3)
$C' / \text{MHz}$	656	649	659.83(4)	653.59(2)
$\Delta I' / \text{amu}\text{\AA}^2$	0	0	-0.08	-0.06
$\mu'_a / \text{D}$	+3.71	+3.75	$\pm 4.14(1)$	-
$\mu'_b / \text{D}$	-3.91	-3.87	$\pm 3.39(1)$	-
$\mu' / \text{D}$	5.39	5.39	5.35(1)	-
$\theta'_D / ^\circ$	+46.5	+45.92	$\pm 39.3$	-
$\Delta A / \text{MHz}$	-34	-31	-31.38(1)	-27.90(1)
$\Delta B / \text{MHz}$	-12	-12	-9.93(1)	-9.64(1)
$\Delta C / \text{MHz}$	-9	-9	-7.61(1)	-7.71(1)
$\Delta\nu_{\text{Lorentz}} / \text{MHz}$	-	-	16.31(1)	10.72(1)
$\tau / \text{ns}$	-	-	9.8(1)	14.8(1)
$\theta / ^\circ$	+4	+4	$\pm 15.3(1)$	$\pm 3.16(73)$
$\theta_T / ^\circ$	-0.45	-0.45	$\mp 0.52(5)$	-
$\nu_0 / \text{cm}^{-1}$	36045	36156	35299.36(12)	35306.58(15)

Apart from the two lowest excited  $\pi\pi^*$  states, the photophysics of indoles is governed

by the repulsive  $\pi\sigma^*$  state. We calculated the vertical excitation to all three states at SCS-CC2/cc-pVTZ level of theory. While the two lowest  $\pi\pi^*$  states are relatively close at the ground state geometry, there is a larger gap to the  $\pi\sigma^*$  state, cf. Table 7.3. The coefficients for this transition are shown in Figure 7.3. The  $\sigma^*$  orbital at the hydrogen atom of the NH is diffuse and collapses into the hydrogen 1s orbital upon distortion along the NH coordinate, as has been shown by Sobolewski and Domcke.[133, 154–156] For 3-cyanoindole, the  $\pi\sigma^* - \pi\pi^*$  difference is by more than  $1000 \text{ cm}^{-1}$  smaller compared to indole. The dipole moment of the  $\pi\sigma^*$  state in indole is more than 5 D higher than in the ground state, while for 3-cyanoindole only an increase of 2 D is found. The oscillator strengths of the respective states of indole and 3-cyanoindole are of comparable size, with the  ${}^1L_a$  oscillator strength between 2 and 3 times larger than for the  ${}^1L_b$  state.

**Table 7.2.:** SCS-CC2/cc-pVTZ computed vertical excitation energies, relative to the energy of the lowest excitation in  $\text{cm}^{-1}$ , excited state dipole moment  $\mu$  and oscillator strength  $f$  of indole and 3-cyanoindole.

	indole			3-cyanoindole		
	$E (\text{cm}^{-1})$	$\mu (\text{D})$	$f$	$E (\text{cm}^{-1})$	$\mu (\text{D})$	$f$
$\pi\pi^* (L_b)$	0	2.2	0.04	0	5.4	0.05
$\pi\pi^* (L_a)$	3534	5.0	0.09	1828	6.3	0.12
$\pi\sigma^*$	13727	7.3	0.00	12552	7.6	0.00

### 3-cyanoindole-water

Several starting geometries for the optimization of the 3-cyanoindole-water cluster have been employed. Three fundamentally different binding motifs can be distinguished: NH $\cdots$ O-hydrogen bound structures (1a and 1b in Figure 7.1), CN $\cdots$ H-hydrogen bound structures (2 and 3 in Figure 7.1), and  $\pi$ -bound van der Waals structures. No stable van der Waals bound minimum structure at the CC2-cc-pVTZ level of theory has been found. All structures have been optimized both using genuine CC2, as well as SCS-CC2. Similar resulting structures have been found with both methods, with the exception, that at SCS-CC2 level no stable structure 1b in the  $S_1$  state has been found.

The stabilization energies, including zero-point energy (ZPE) corrections and considering the BSSE are given in Table 7.4. Both NH $\cdots$ O-hydrogen bound structures are by about 7 and 6 kJ/mole more stable than the CN $\cdots$ H-hydrogen bound structures. The stabilization energies of 1a and 1b are too close to make a definite statement, which of the two cluster structures is the more stable one. Both cluster structures show a slightly larger stabilization in the excited state and slight red shifts of their adiabatic excitation

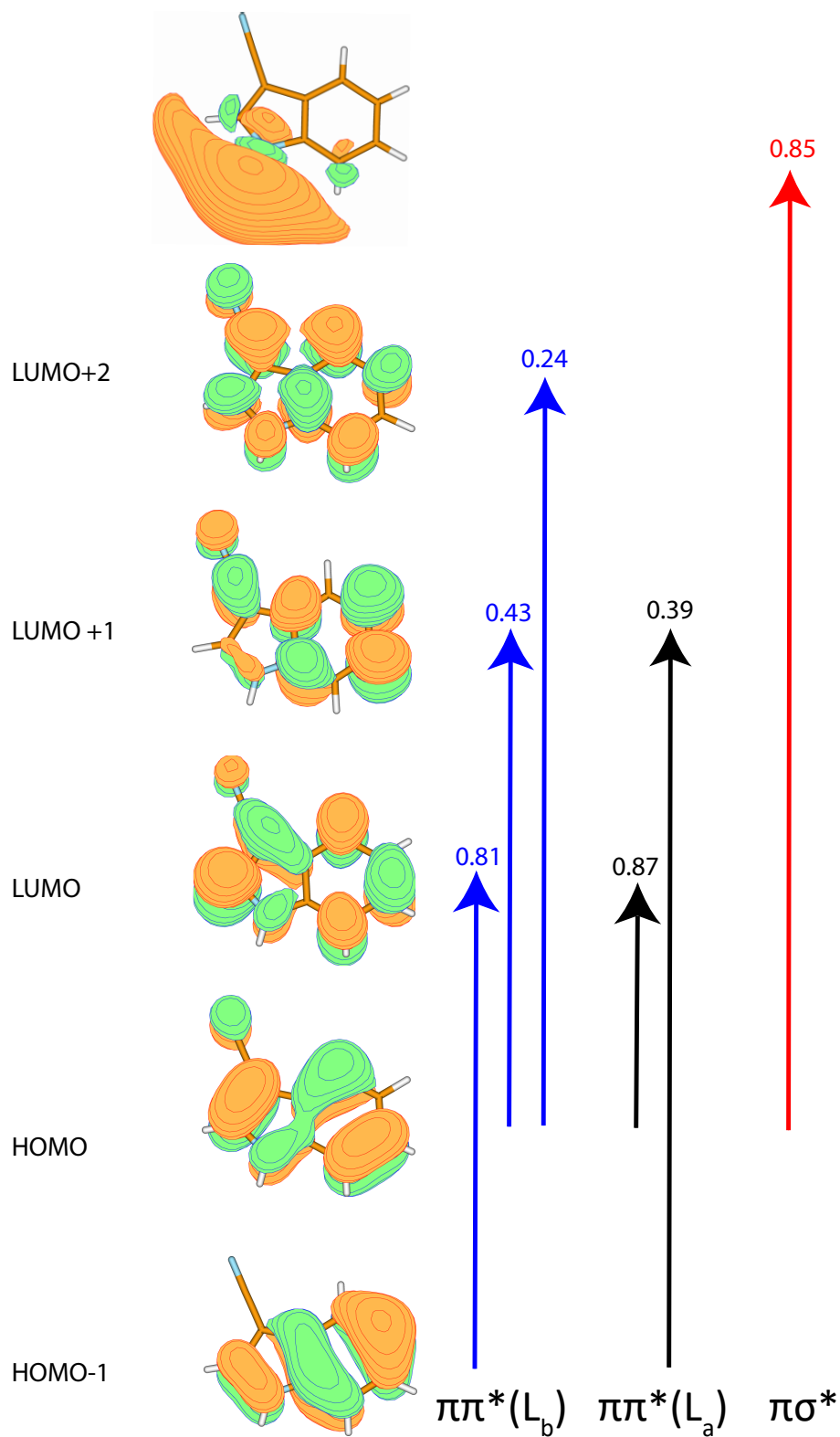


**Figure 7.3.:** Molecular orbitals of 3-cyanoindole with the coefficients of the  $\pi\pi^*$  ( $L_b$ ) (blue),  $\pi\pi^*$  ( $L_a$ ) (black) and  $\pi\sigma^*$  (red) excitations according to SCS-CC2/cc-pVTZ calculations.

energies relative to that of the monomer. The origin of conformer 1a is red-shifted by 16  $\text{cm}^{-1}$ , 1b shows a red-shift of 21  $\text{cm}^{-1}$ . The experimental value is 51  $\text{cm}^{-1}$ , cf. section 7.5.1.

The orientation of the transition dipole moment (Figure 7.1), as well as the main contributions to the excitation to the lowest excited singlet state of  $0.81(\text{LUMO} \leftarrow \text{HOMO}-1)+0.41(\text{LUMO}+1 \leftarrow \text{HOMO})-0.27(\text{LUMO}+2 \leftarrow \text{HOMO})$ , cf. Figure A.10 of the online supporting material are indicative for a transition to the  ${}^1L_b$  state also for the 1:1 water cluster.

## 7.4.2. Experimental results

### 3-cyanoindole

Figure 7.4 shows the rotationally resolved electronic spectrum of the origin of 3-cyanoindole at 35299.36  $\text{cm}^{-1}$  (0 on the scale of the figure) along with the best fit at zero field (trace b) and at a field strength of 851.11 V/cm trace c)). The electric field in the chosen set-up is parallel to the polarization of the plane of the exciting light, thus  $\Delta M = 0$  selection rules for the Stark spectrum hold. The spectrum was fit using a CMA-ES; the molecular parameters from the fit are summarized in Table 7.1 and are compared to the results of the SCS-CC2/cc-pVTZ calculations.

The origin band is an *ab*-hybrid with predominant *a*-type character. The exact analysis yields an angle of  $\pm 15.3^\circ$ . The indeterminacy of the TDM orientation can be resolved by comparison to the *ab initio* computed value of  $+4^\circ$ . Thus, the orientation, as shown in Figure 7.1 seems to be the experimentally observed one. A more reliable determination can be performed on the basis of the TDM angle in the deuterated isotopologue of 3-cyanoindole, and on the relative orientation of transition moment and axis reorientation angle, which will be presented in section 7.5.1.

A Lorentzian linewidth of 16.31 MHz corresponds to an excited state lifetime of 9.8 ns.

### N-deuterated 3-cyanoindole

The knowledge of the position of the pyrrolic amino hydrogen in the inertial frame of 3-cyanoindole is crucial for the determination of the hydrogen bond length in the 3-cyanoindole-water cluster. Therefore, we measured the spectrum of the N-D isotopologue, which allows for the determination of the hydrogen coordinates through application of Kraitchman's equations. Figure 7.5 shows the rotationally resolved electronic spectrum of the origin of 3-cyanoindole-(d<sub>1</sub>) at 35306.58  $\text{cm}^{-1}$  (0 on the scale of the figure). The

**Table 7.3.:** SCS-CC2/cc-pVTZ computed and experimental molecular parameters of different 1:1 3-cyanoindole-water complexes. For details see text.

	SCS CC2/cc-pVTZ				experiment		
	1a	1b	2	3	$\sigma = 1$	$\sigma = 0$	$\Delta\sigma$
$A''$ / MHz	1083	1093	1292	2015	1104.10	1100.04	-4.06
$B''$ / MHz	745	743	739	559	728.29	728.01	-0.28
$C''$ / MHz	442	443	471	439	439.07	438.99	-0.08
$\Delta I''$ / amuÅ <sup>2</sup>	-2.33	-2.33	-1.92	-2.06	-0.6380	-2.3774	
$A'$ / MHz	1091	1092	1279	1979	1099.63	1096.97	-2.66
$B'$ / MHz	734	734	731	554	724.63	724.33	-0.30
$C'$ / MHz	440	440	466	434	437.28	437.20	0.00
$\Delta I'$ / amuÅ <sup>2</sup>	-2.56	-3.25	-1.90	-2.46	-1.2938	-2.0979	
$\Delta A$ / MHz	8.10	-2.33	-12.85	-36.19	-4.47	-3.07	
$\Delta B$ / MHz	-10.95	-8.79	-7.70	-5.44	-3.65	-3.68	
$\Delta C$ / MHz	-2.56	-3.25	-4.84	-4.92	-1.79	-1.79	
$\Delta\nu_{Lor.}$ / MHz	-	-	-	-	43.51	43.51	
$\tau$ / ns	-	-	-	-	3.66	3.66	
$\theta$ / °	-39	-39	-26	+13	$\pm 48.26$	$\pm 48.26$	
$\nu_0$ / cm <sup>-1</sup>	36029	36024	35980	36140	35262.2	35261.9	
$\Delta\nu_0$ / MHz	-	-	-	-	-8977.46		

**Table 7.4.:** Summary of stabilization energies (including ZPE and BSSE corrections) and adiabatic excitation (including ZPE) and vertical excitation and emission energies of four most stable isomers of the 3-cyanoindole-water cluster at SCS CC2/cc-pVTZ level of theory.

	1a	1b	2	3
$\Delta E_{stab.}(S_0)$ / kJ mol <sup>-1</sup>	-28.46	-28.35	-20.41	-21.86
$\Delta E_{stab.}(S_0)$ / cm <sup>-1</sup>	-2378.7	-2370.2	-1706.4	-2122.01
$\Delta E_{stab.}(S_1)$ / kJ mol <sup>-1</sup>	-28.64	-28.61	-21.18	-20.71
$\Delta E_{stab.}(S_1)$ / cm <sup>-1</sup>	-2379.9	-2391.3	-1770.7	-1731.2
$\Delta E_{adiabatic}$ / cm <sup>-1</sup>	36029	36024	35980	36140
$\Delta E_{vertical}$ @ opt. S <sub>0</sub>	38832	38870	38884	38940
$\Delta E_{vertical}$ @ opt. S <sub>1</sub>	35843	35842	35735	36009

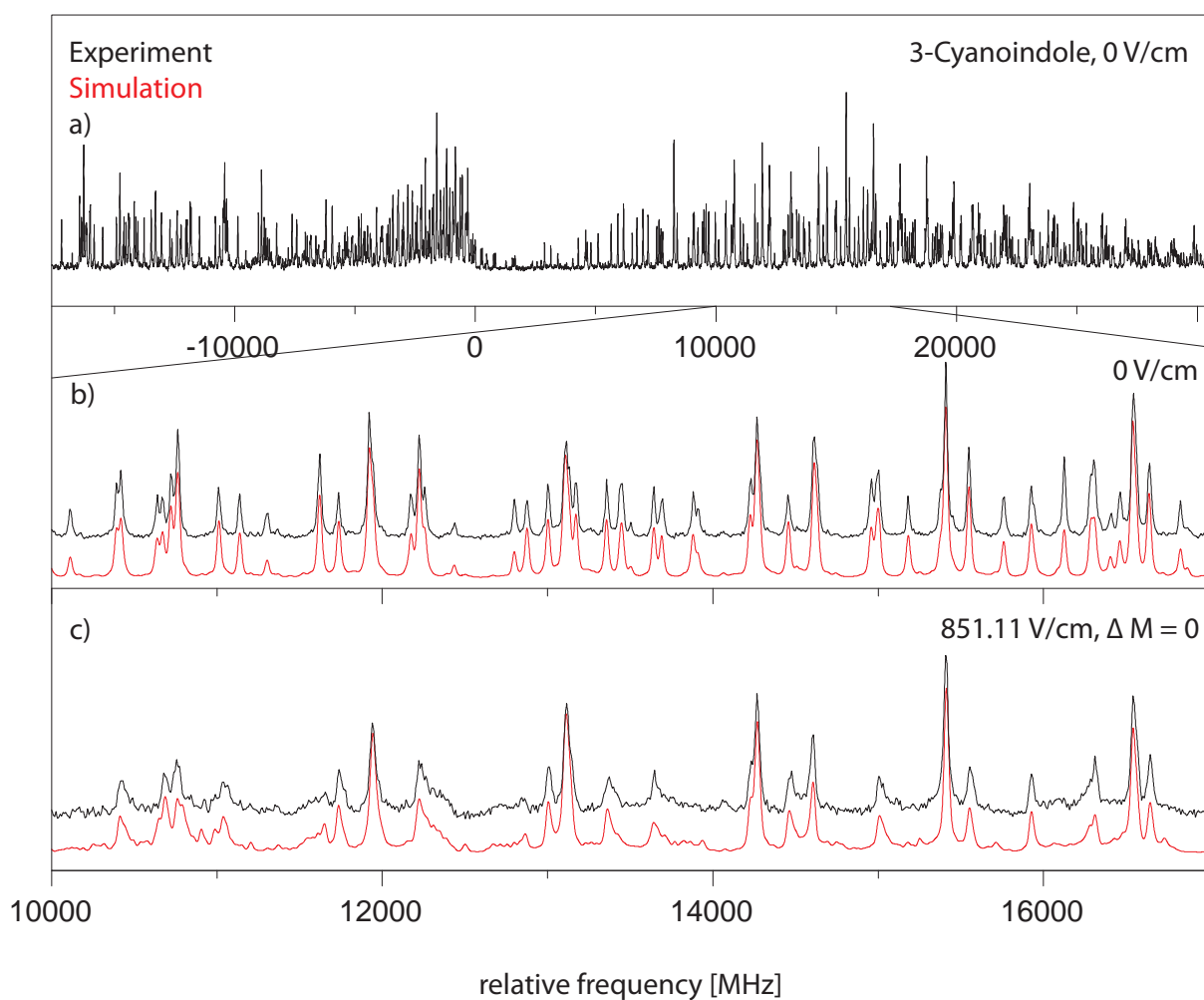


**Figure 7.4.:** Rotationally resolved electronic spectrum of the electronic origin of 3-cyanoindole at zero field and at 851.11 V/cm  $\Delta M=0$  selection rules, along with a simulation with the best CMA-ES fit parameters.

spectrum is composed mainly of *a*-type bands similar to the undeuterated species. The results of the CMA-ES fit of the spectrum are summarized in Table 7.1, where they are compared to the results of the SCS-CC2/cc-pVTZ calculations. The excited state lifetime of 14.8 ns is considerably longer than that of undeuterated 3-cyanoindole.

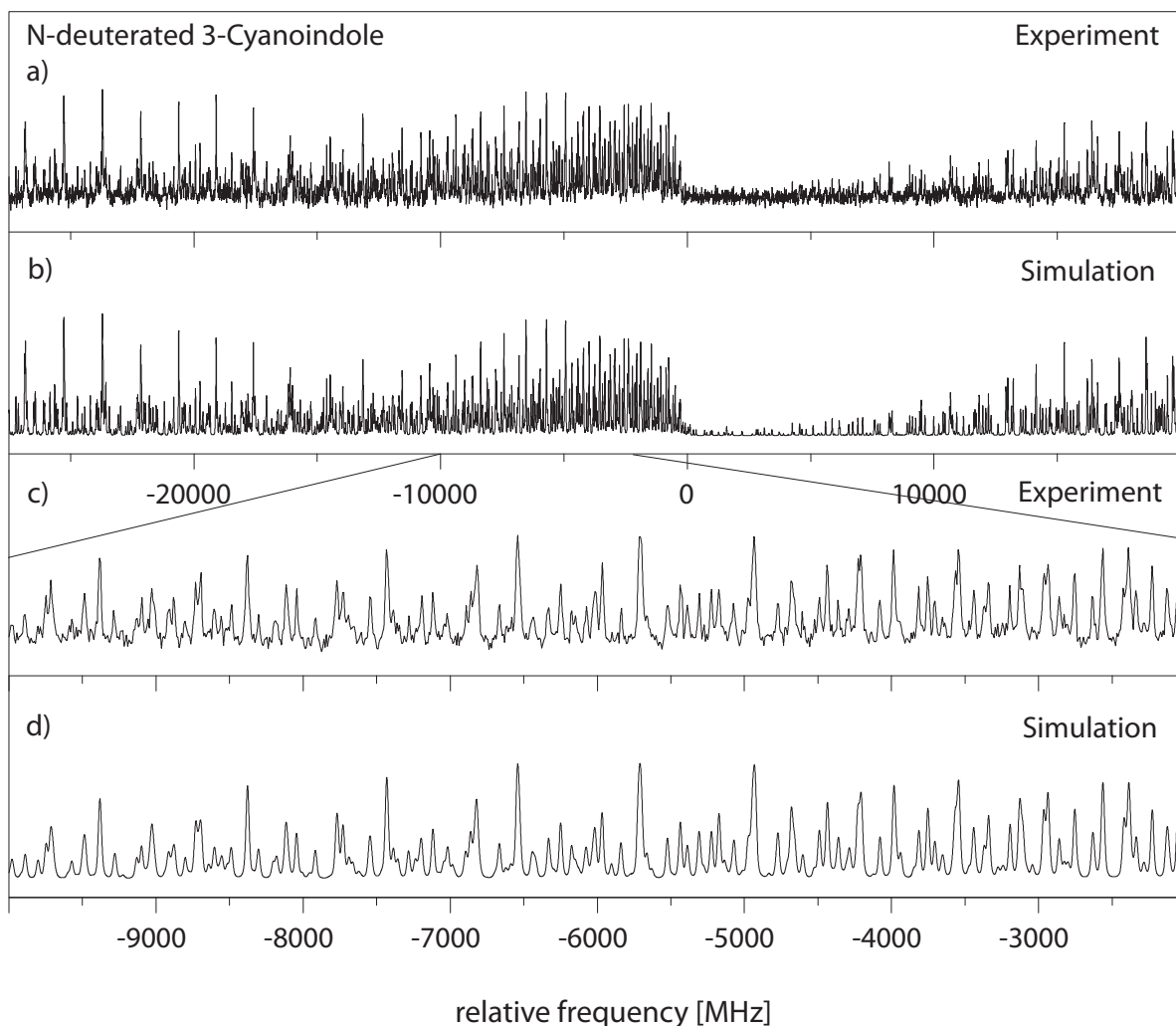


**Figure 7.5.:** Rotationally resolved electronic spectrum of the electronic origin of N-deuterated 3-cyanoindole, along with a simulation with the best CMA-ES fit parameters.

### 3-cyanoindole-water

Figure A.3 presents the rotationally resolved electronic spectrum of the origin of the binary 3-cyanoindole-water cluster at  $35262.2 \text{ cm}^{-1}$ . This origin band is redshifted by  $51 \text{ cm}^{-1}$  relative to the origin of 3-cyanoindole at  $35299.36 \text{ cm}^{-1}$ . The spectrum is split into two subbands due to the large amplitude internal motion of the water moiety. The molecular

symmetry group which takes this motion into account is  $G_4$ , isomorphic with the point group  $C_{2v}$ . The lowest torsional state (with  $\sigma = 0$ ) is of  $A_1$  symmetry, the energetically following (with  $\sigma = 1$ ) of  $B_2$  symmetry. Both subbands are fit using rigid asymmetric rotor selection rules, with the difference of the vibronic origins as additional parameter. Trace a) of Figure A.3 shows the experimental spectrum, trace b) the simulation using the best fit parameters from Table 7.3. The following traces c) and d) give the individual simulations for the two torsional subbands, due to the internal rotation of the water moiety. The resulting molecular parameters are given in Table 7.3. The spectrum is an  $ab$ -hybrid band with 56 %  $b$ -type and 44 %  $a$ -type character, and is split into two subbands by the internal rotation of the water moiety. The splitting between the origins of the two subbands amounts to 8977 MHz. The Lorentzian linewidth was determined to be 43 MHz, leading to an excited state lifetime of 3.6 ns.

### Excited state lifetimes

Since the question of excited state lifetimes is crucial for the discussion of the photophysical properties of 3-cyanoindole we performed lifetime measurements of 3-cyanoindole and of 5-cyanoindole and indole in different solvents using time correlated single photon counting. Figure 7.7 presents the decay curves for indole, 3-cyanoindole, and 5-cyanoindole in ethyl acetate. The excited state lifetimes of isolated indole, 5-cyanoindole, 3-cyanoindole, and 3-cyanoindole( $d_1$ ) in ethyl acetate (EA) and of 3-cyanoindole( $d_1$ ) in  $D_2O$  are summarized in Table 7.5.

## 7.5. Discussion

### 7.5.1. 3-Cyanoindole

#### Geometric and electronic structure of the excited state

The small negative inertial defects of 3-cyanoindole in the electronic ground state ( $-0.02$  amu  $\text{\AA}^2$ ) and in the lowest electronically excited state ( $-0.08$  amu  $\text{\AA}^2$ ) show its planarity in both electronic states. In contrast to indole and 5-cyanoindole, the inertial defect decreases slightly upon excitation to the  $S_1$  state.

The angle of the TDM with the inertial  $a$ -axis was determined experimentally to be  $\pm 15.3^\circ$ . In the following we will show two independent determinations of the sign of the TDM angle, which do rely on the comparison to the calculated TDM orientation.

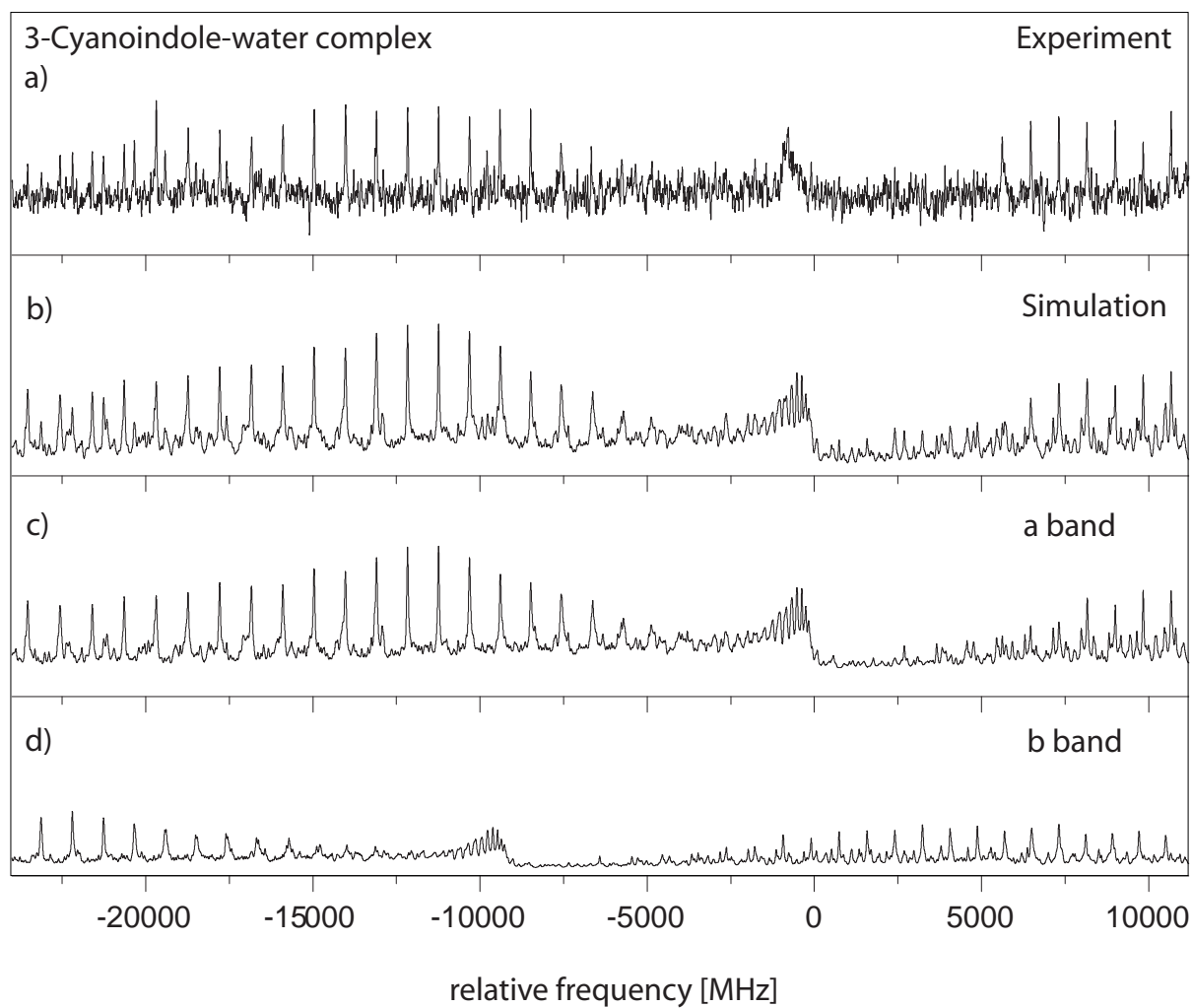


**Figure 7.6.:** Rotationally resolved spectrum of the electronic origin of the 3-cyanoindole-water cluster, along with a simulation using the best CMA-ES fit parameters.

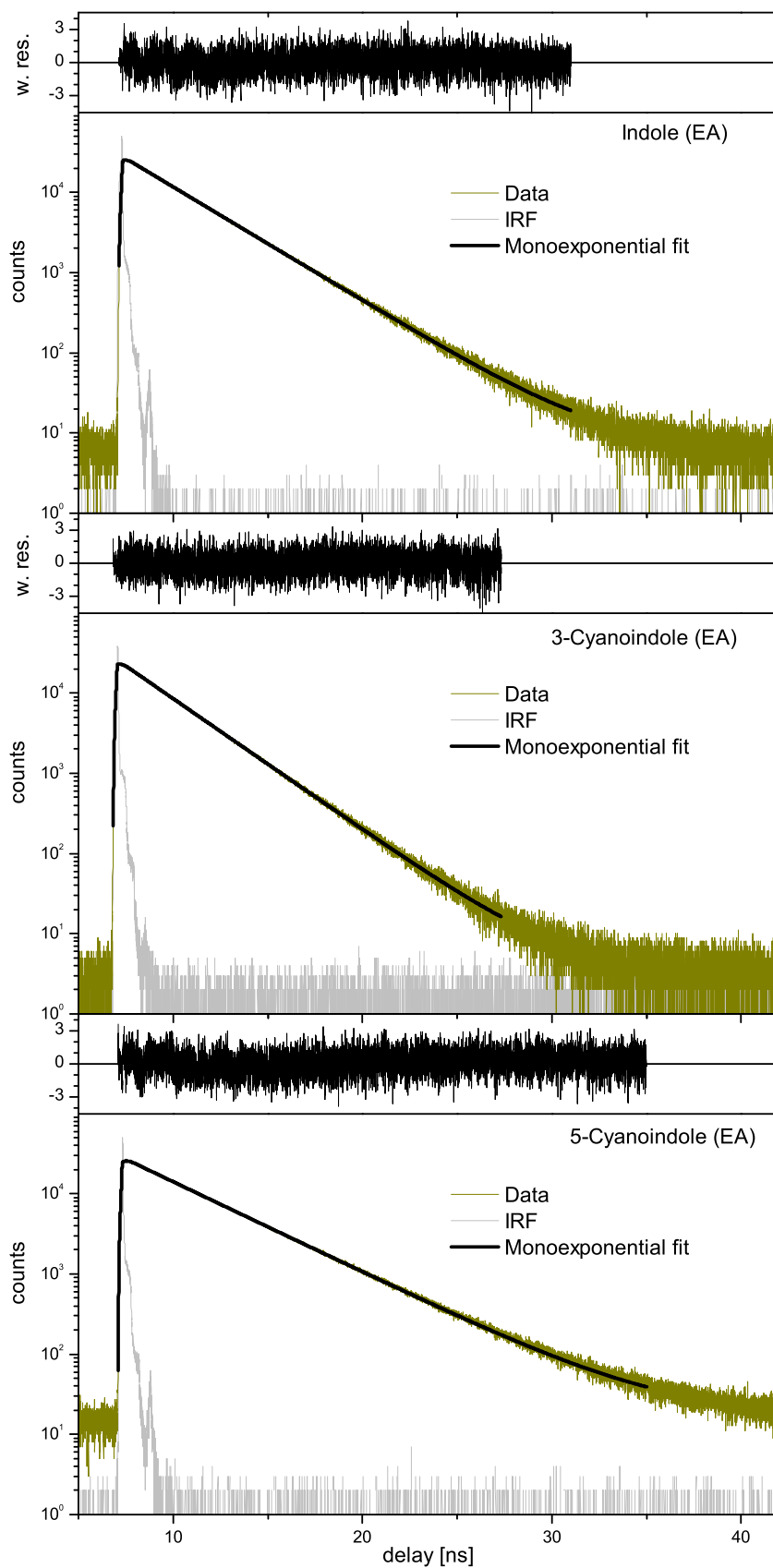


**Figure 7.7.:** TCSPC of Indole, 3-Cyanoindole, and 5-Cyanoindole in ethyl acetate (EA) with monoexponential fits and weighted residuals (w. res.). The instrument response function (IRF) at the respective excitation wavelength is shown in light gray.

The geometry change upon electronic excitation causes a reorientation of the inertial axes of a molecule if its symmetry is sufficiently low. [157] The molecule fixed coordinate system, which rotates with the molecule, and the space fixed coordinate system can be interconverted by the Euler rotation matrix. In case of different geometries of the two states, which are connected by the spectroscopic transition, two moving axis systems, and consequently two sets of Eulerian angles  $\theta$ ,  $\phi$ , and  $\chi$  are needed, one for each state. In this way, the rotational selection rules, which are valid only for unchanged geometries, have to be modified. Hougen and Watson's approach to this problem is the diagonalization of the rotational Hamiltonian for each state separately, and a rotation of the eigenvectors through a rotation matrix containing the axis reorientation angles  $\theta_T$ ,  $\phi_T$ , and  $\chi_T$ . Pratt and coworkers introduced a different procedure. [158] In spite of rotating the wave functions, they express the Hamiltonian of the excited state in the coordinates of the ground state. Thus, the rotation of the eigenvectors is replaced by a rotation of the Hamiltonian about the axis reorientation angles  $\theta_T$ ,  $\phi_T$ , and  $\chi_T$ . This approach has the big advantage that the similarity transformation has to be applied only once, while in the Hougen-Watson approach, each  $J$  block has to be rotated by means of a  $(2J+1) \times (2J+1)$  rotation matrix. When rotated, the excited state Hamiltonian has no longer the four group symmetry of the ground state. Thus, the effect of axis reorientation is a change of the intensities of several rovibronic lines. The line positions however are not altered, since the rotated and unrotated eigenfunctions are related through a similarity transformation. Thus, the eigenvalues of the rotated and unrotated Hamiltonian are the same. [158]

Pratt and coworkers have shown, how the relative orientation of the transition dipole moment  $\theta$  and the axis reorientation  $\theta_T$  can be used to remove the indeterminacy of the sign of  $\theta$ . The combination of  $+\theta/+ \theta_T$  and  $-\theta/- \theta_T$  have the same intensity pattern, which in turn is different for the  $+\theta/- \theta_T$  and  $-\theta/+ \theta_T$  combinations. From a fit of the rovibronic intensities to the signed value of the axis reorientation angle, it can be deduced if TDM and axis reorientation have the same or opposite signs.

From the SCS-CC2 optimized structures, the axis reorientation angle of the inertial axis system upon electronic excitation  $\theta_T$  can be determined using the relation for planar molecules given by Hougen and Watson [157]:

$$\tan(\theta_T) = \frac{\sum_i m_i (a'_i b''_i - b'_i a''_i)}{\sum_i m_i (a'_i a''_i + b'_i b''_i)} \quad (7.1)$$

Here, the doubly primed coordinates refer to the principal axis system in the electronic ground state and the singly primed quantities to the respective excited state inertial system

and the  $m_i$  are the atomic masses. Using the SCS-CC2 optimized structures for the  ${}^1L_b$  state, we obtain an axis reorientation angle  $\theta_T$  of  $-0.45^\circ$  for the  ${}^1L_b$  state. Since the optimization of the  ${}^1L_a$  state ran into a conical intersection at SCS-CC2 level of theory (*vide supra*), the TD-DFT optimized geometry was used and an angle of  $0.99^\circ$  was obtained for the  ${}^1L_a$  state. The calculated value for the  ${}^1L_b$  state is in good agreement with the value from the fit of the spectrum using the axis reorientation Hamiltonian of  $0.52^\circ$ .

Since axis reorientation has no effect on the eigenvalues, i.e. the energies of the rovibrational levels, the only quantity to be fit is the axis reorientation angle  $\theta_T$ , leaving all other parameters at their before determined values. However, only few lines are considerably affected by axis reorientation. Improvement of the cost function in the course of the optimization might therefore be concealed by the majority of lines whose intensities do change. In order to circumvent this problem, we included only sections of the spectrum in the fit, which show, guided by a preliminary simulation, strong intensity variations. Two kind of solutions were obtained. The combination of  $\theta$  positive and  $\theta_T$  negative, as well as  $\theta$  negative and  $\theta_T$  positive had a better cost function than the combination of both angles positive or both angles negative. Therefore, we know,  $\theta_T$  and  $\theta$  must have different signs. Using the fact that  $\theta_T$  is negative from the above considerations,  $\theta$  must be positive.

To facilitate the comparison to other indoles, we transform the angle of the TDM to refer to the *pseudo*  $C_2$ -axis of indole. The results are shown in Table 7.5. Clearly, the orientation of the TDM is the same as in indole, and the lowest excited singlet state of 3-cyanoindole can be assigned to an  ${}^1L_b$  like state, in contrast to 5-cyanoindole in which the opposite sign of the TDM points to an  ${}^1L_a$  state.

**Table 7.5.:** Angles  $\theta$  of the orientation of the transition dipole moment and excited state lifetimes (molecular beam and solution) of 3-cyanoindole (3-CI), 5-cyanoindole (5-CI) and the 3-cyanoindole-water cluster. In contrast to the  $\theta$  values shown in Table 7.1, those given here are given with respect to the *pseudo*  $C_2$ -axis of indole.

<sup>a</sup> Excitation of 3-cyanoindole and 3-cyanoindole( $d_1$ ) in ethyl acetate (EA) at 283 nm.

<sup>b</sup> 3-CI( $d_1$ ) has been measured in  $D_2O$  with excitation at 283 nm.

<sup>c</sup> Excitation of indole in EA at 284 nm.

<sup>d</sup> Excitation of 5-cyanoindole in EA at 295 nm.

	Indole	3-CI	3-CI( $d_1$ )	5-CI	3-CI- $H_2O$
$\theta /^\circ$	+38 [128]	+35	+36	-12[138]	+51
$\tau /ns$	17.6 [128]	9.8	14.8	12[138]	3.9
$\tau(EA)^{solv.}/ns$	3.1 <sup>c</sup>	2.6 <sup>a</sup>	2.7 <sup>a</sup>	3.6 <sup>d</sup>	-
$\tau(H_2O)^{solv.}/ns$	4.5[135]	<0.05[135]	<0.02 <sup>b</sup>	0.3[135]	-

The fact that no stable minimum at SCS-CC2 level could be located for the  ${}^1L_a$  state,

might arise from two different reasons. (i) The  ${}^1L_a$  minimum might be so far outside the Franck-Condon region, that our searches just missed the minimum structure and followed instead the falling  ${}^1L_a$  potential right into the conical intersection (CI) with the  ${}^1L_b$ . Although we tried a plethora of starting geometries, which were constructed from the known  ${}^1L_a$  geometries of indole and 5-cyanoindole, we cannot completely exclude this reason. (ii) A much more probable explanation for this finding is a very shallow  ${}^1L_a$  minimum in the coordinate, which connects the  ${}^1L_a$  and the  ${}^1L_b$  through the CI. Such a case was found for tryptamine.[159] Slightest deviations from the correct  ${}^1L_a$  geometry at the chosen level of theory will then cause the optimization to run into the CI.

### Excited state lifetimes

The  $S_1$  state lifetime of the isolated 3-cyanoindole was determined to be 9.8 ns, which is shorter than the respective lifetimes of indole (17 ns) [128] and 5-cyanoindole (12 ns). [138] In different solvents a similar trend for the lifetimes indole and of the cyanoindoles was found. Independent of the solvent, the fluorescence lifetime of 3-cyanoindole was always shorter than that of 5-cyanoindole and of indole. [135] For the isolated 1:1 water complex the shortest lifetime of 3.6 ns has been measured, cf. Table 7.5. Interestingly, also the lifetime of 3-cyanoindole in water solution is the shortest ( $<0.05$  ns[135]), followed by the aqueous solution of 5-cyanoindole (0.3 ns[135]) and indole (4.5 ns[135]). The lifetime of deuterated 3-cyanoindole in the gas phase is longer than that of the undeuterated isotopologue (14.8 vs. 9.8 ns). A similar trend has been found for phenol (13.3 ns vs. 2.4 ns). Sobolewski and Domcke have shown, that along with the lowest two excited singlet  ${}^1L_a$  and  ${}^1L_b$  states, which are of  $\pi\pi^*$  character, a third state of  $\pi\sigma^*$  character plays a crucial role in the photophysics of these chromophores. [133, 154–156] This  $\pi\sigma^*$  state is repulsive along the OH coordinate for phenol and along the NH coordinate for indole and forms conical intersections with the directly excited state and subsequently with the electronic ground state. For excitations above the threshold, a rapid decay channel is open, which connects the primarily excited  $\pi\pi^*$  state through a conical intersection (CI) with the  $\pi\sigma^*$  state, and subsequently through a second CI, with the ground state. The  $\pi\pi^* - \pi\sigma^*$  CI induces a barrier on the  $S_1$  potential energy surfaces, through which a wave packet, prepared at the zero-point level of the primarily excited state can tunnel. This causes the  $S_1$  state lifetime of phenol to be as short as 2.4 ns, while the lifetime of deuterated phenol is considerably longer (13.3 ns) due to the lower zero-point energy. The same behavior is found for 3-cyanoindole and its ND-deuterated isotopologue (Figure 7.8a). The isotope effect on the excited state lifetime of indole is negligible (17.6 ns vs. 17.2 ns

for the deuterated isotopologue[160]), a consequence of the larger barrier formed by the  $\pi\pi^* - \pi\sigma^*$  CI in indole. We therefore claim a lower barrier, formed on the  $S_1$  potential energy surface, to be responsible for the shorter lifetime of 3-cyanoindole compared to indole and 5-cyanoindole. The calculation of the vertically excited  $\pi\pi^*$  and  $\pi\sigma^*$  states in section 7.4.1 strongly support this suggestion.

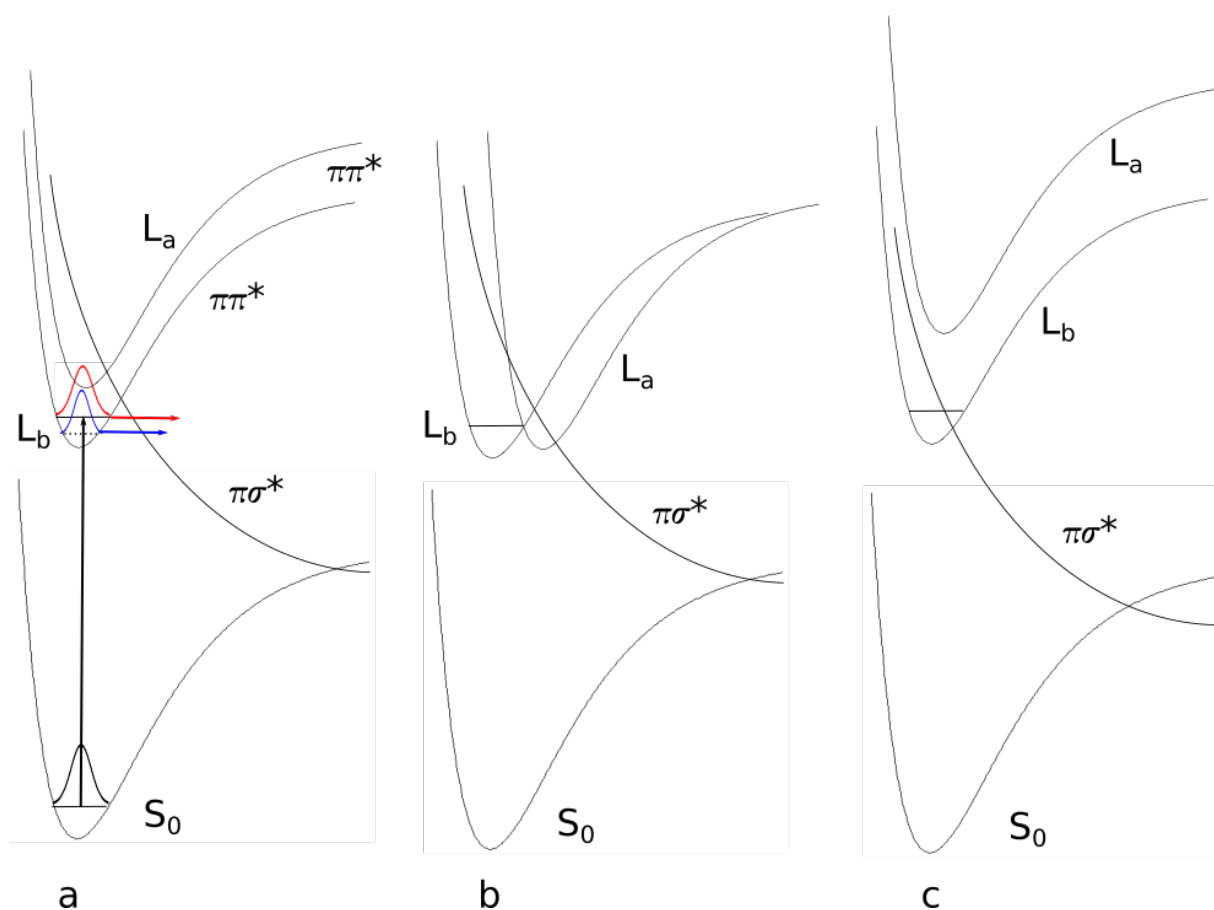


**Figure 7.8.:** Schematic potential energy profiles along the NH stretch coordinate.  
a) Conical intersection between  $\pi\pi^*$  and  $\pi\sigma^*$  above the zero-point energy level of the excited state. The dashed line represents the zero-point energy level of the N-deuterated isotopologue. The wave packet prepared at zero-point level (in red for the NH isotopologue, in blue for the ND isotopologue) tunnels through the barrier, formed by the  $\pi\pi^* - \pi\sigma^*$  conical intersection  
b) Same situation as in a) but the minimum of the second  $\pi\pi^*$  is shifted and forms a new CI with the lower  $\pi\pi^*$  state.  
c) The  $\pi\sigma^*$  state is further stabilized with respect to the  $\pi\pi^*$  state. The zero point energy level is above the conical intersection.

For the water clusters in the gas phase, only lifetimes for indole- $H_2O$  and 3-cyanoindole- $H_2O$  (3.6 ns) are known experimentally. Indole- $H_2O$  however, is hard to compare, because two very different values are reported. Korter *et al.* determined a value of 5 ns from the

Lorentz component to the full linewidth in a rotationally resolved electronic spectrum of the origin band. [141] Arnold and Sulkes found a value of 21 ns using time-correlated single photon counting after excitation of the electronic origin. [161] What is then the reason for the short lifetime in the 1:1 cluster and the ultrashort lifetime in aqueous solution of 3-cyanoindole? The answer to this problem is further complicated by the fact, that depending on the relative stabilization of the different excited states, conical intersections not only between the  $\pi\pi^*$  and the  $\pi\sigma^*$  states develop, but also between the lowest  $\pi\pi^*$   ${}^1L_a$  and  ${}^1L_b$  states [159] (cf. Figure 7.8b). Regarding the fact that the  $\pi\pi^* - \pi\sigma^*$  barrier of 3-cyanoindole is lower, than that of indole (*vide supra*), it seems plausible, that the  $\pi\sigma^*$  potential is lowered even further through stabilization via the water dipole (Figure 7.8c). The short lifetime would then originate from the increase of the nonradiative decay rate. A conclusive answer, however can only be given, if the oscillator strengths to the fully adiabatically optimized excited states along the dissociative NH coordinate are known. These calculations are currently under way.

### Dipole moments

The ground state dipole moment of 5.90 D decreases to 5.35 D in the excited singlet state. The angle of the dipole moment with the inertial  $a$ -axis slightly decreases from 45 to 39 ° upon excitation. For bare indole, values of 1.963 D ( $S_0$ ) and 1.856 D ( $S_1$ ) with angles to the  $a$ -axis of 45 and 33 °, respectively have been reported. [125] However, one has to keep in mind, that the heavy cyano group rotates the inertial  $a$ -axis by 36 ° in the molecular frame as shown in Figure 7.9.

For 5-cyanoindole we found a good additivity of the dipole moments of indole and of the cyano fragment in the electronic ground state. [162] In this molecule, the indole dipole and the dipole of the cyano fragment which is attached to the benzenoid ring, are nearly aligned. For 3-cyanoindole, the individual dipoles form a large angle, and the cyano fragment is attached to the pyrrolic ring. Figure 7.9b shows the experimental dipole moment vector of 3-cyanoindole (red, straight vector) and of indole (black, straight vector). Subtracting the experimentally determined dipole moment vector of 3-cyanoindole from that of indole [125] should lead to the dipole moment vector of the substituent ( $\vec{\mu}_{\text{CN}} = \vec{\mu}_{\text{3CN-indole}} - \vec{\mu}_{\text{indole}}$ ). If the dipole moment of indole and the cyano fragment is additive like in 5-cyanoindole, the difference vector will point into the direction of the fragment dipole with the respective length of the fragment dipole, cf. Figure 7.9b and c. The most appropriate dipole moments to mimic the fragment dipole of the cyano group, attached to the pyrrole ring, are those of methyl cyanide  $\text{CH}_3\text{CN}$ , isopropyl cyanide  $(\text{CH}_3)_2\text{CHCN}$  and benzonitrile  $\text{C}_6\text{H}_5\text{CN}$ . The

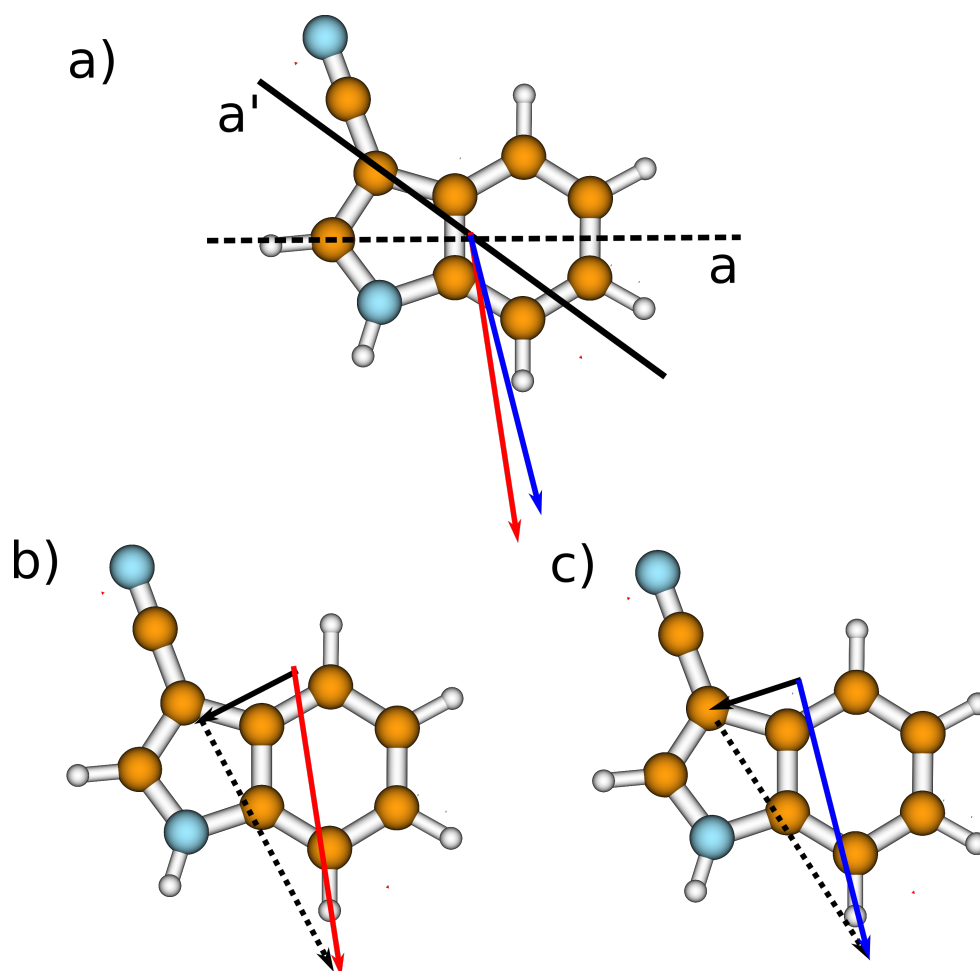


**Figure 7.9.:** a) Inertial  $a$ -axis of indole (dashed line) and 3-cyanoindole (straight line). The ground state dipole moment of 3-cyanoindole is shown as red vector with direction from  $-$  to  $+$ , that of the excited state as blue vector.  
 b) Ground state dipole moments of 3-cyanoindole (red, straight), indole (black, straight) and the difference vector (black, dotted).  
 c) Excited state dipole moments of 3-cyanoindole (blue, straight), indole (black, straight) and the difference vector (black, dotted). In all cases the dipole vectors are shifted from their position in the original molecule for sake of clarity.

ground state dipole moment of methyl cyanide was determined by Steiner and Gordy to be 3.913 D,[163] the dipole moment of isopropyl cyanide has been determined to 4.07 D by Müller *et al.*[164] The most exact value of the benzonitrile dipole moment was reported by Wohlfahrt *et al.* to be 4.5152 D.[143] Thus, a value of around 4 D for the cyano fragment, colinear with the CN bond can be expected. Inspection of Figure 7.9b shows that the fragment dipole indeed points in the same direction as the cyano fragment dipole. From the vectorial difference of the ground state dipoles a fragment dipole moment of 5.5 D is predicted, which is more than 1 D larger than expected from a simple additivity model. Using the excited state dipole moments of indole and 3-cyanoindole, a value of 5.6 D results in agreement with the fragment dipole determined from the ground state values. Inspection of the direction of the fragment dipole in Figure 7.9c however shows that in the excited state, even the direction of the dipole moment deviates from that of the fragment.

### 7.5.2. 3-Cyanoindole-water

#### Barrier to water torsion

The origin spectrum of the 3-cyanoindole-water cluster is split into two subbands, due to an internal motion of the water moiety in the cluster. The basic theory for this motion of the water moiety has been worked out in detail for phenol-water[77] and indole-water.[141] Therefore, we keep the theoretical description short, all necessary equations and their derivation can be found in Ref. [165] The motion of the water can be described as motion in a periodic two-fold potential. The rotational levels split into two subtorsional components,  $\sigma = 0$  and  $\sigma = 1$ . This  $\sigma$  is chosen such that it represents the symmetry of the torsional wavefunctions and therefore the torsional problem is diagonal in  $\sigma$ . The  $\sigma = 0$  levels have *A* symmetry and a spin statistical weight of 1, while the  $\sigma = 1$  levels are of *B* symmetry with a spin statistical weight of 3 in the G4 molecular symmetry group.[77]  $\Delta\sigma = 0$  selection rules hold for the transitions from the electronic ground to the excited state. Since for the vibrational ground state (and for all even  $v$  states) the  $\sigma = 0$  state is below the  $\sigma = 1$  state, the fact that the strong subtorsional band ( $\sigma = 1 \leftrightarrow \sigma = 1$ ) is blue to the weak band ( $\sigma = 0 \leftrightarrow \sigma = 0$ ) immediately shows that the barrier in the electronically excited state must be smaller than in the ground state. The energy difference of 8977.46 MHz between these subtorsional bands is given by difference in the subtorsional splittings in the two electronic states  $E_{\sigma=0} - E_{\sigma=1}$ .

Further information is contained in the difference of the rotational constants between the  $\sigma = 0$  and  $\sigma = 1$  bands. Table 7.3 shows that in the electronic ground state mainly *A*

changes, while  $B$  and  $C$  are nearly the same for the subtorsional levels. Thus, the torsional axis is mostly parallel to the  $a$  inertial axis in the cluster. The difference of the rotational constants between  $\sigma = 0$  and  $\sigma = 1$  bands ( $\Delta B_g = B_g^{\sigma=0} - B_g^{\sigma=1}$ ) contains the second order perturbation terms, which can be used for an independent determination of the torsional barrier. A Levenberg-Marquart fit of the subtorsional splitting and the differences of the rotational constants yield barriers of  $148 \text{ cm}^{-1}$  for the  $S_0$  and of  $125 \text{ cm}^{-1}$  for the  $S_1$  state, respectively for a torsional constant of  $15.2 \text{ cm}^{-1}$ .

### Structure of the water cluster

The inertial defects  $\Delta I$  of both torsional sub-bands of the 3-cyanoindole-water cluster in the ground and electronically excited state are small and negative ( $\Delta I'' = -0.6380 \text{ amu } \text{\AA}^2$  of the of  $\sigma = 1$  subband and  $-2.3774 \text{ amu } \text{\AA}^2$  of  $\sigma = 0$ ) They are in the range of what is expected for a structure in which all heavy atoms are in-plane. For indole-water and phenol-water trans-linear hydrogen bond structures are found with inertial defects of  $-1.412 \text{ amu } \text{\AA}^2$  (indole-water) and  $-2.086 \text{ amu } \text{\AA}^2$  (phenol-water). Thus, we conclude that also 3-cyanoindole-water cluster forms a structure, in which only the hydrogen atoms of the water moiety are located outside the plane of the chromophore in agreement with the structures of the computed most stable complexes (a and b in Figure 7.1). Torsional excitation of the water averages the position of the water hydrogen atoms with respect to the plane. This explains, why the inertial defect of the  $\sigma = 1$  component is smaller than that of the  $\sigma = 0$  component.

The position of the water molecule in the 3-cyanoindole-water cluster can be determined from the rotational constants of the water cluster and the monomer, without further knowledge of the monomer structure using a Kraitchman [166] analysis. The only assumption, which is made therein, is that the structure of the monomer moiety does not change upon cluster formation. While the original intention in using the Kraitchman equations is the determination of the Cartesian coordinates of an isotopically substituted atom in a molecule, it is also applicable in determining the center-of-mass (COM) distance of the two constituents of binary clusters. This procedure has first been applied to noble gas clusters of organic molecules,[167] which directly yields the position of the noble gas atom in the inertial frame of the uncomplexed monomer. Later, it was extended to molecular clusters of hydrogen donors with water, in which the distance of the water COM from the COM of the organic molecule was determined. From the known structure of the water moiety, and the position of the oxygen (phenol) or nitrogen (indole) in the inertial frame of the monomer, also the heavy atom distance in hydrogen bonded clusters like  $\text{N-H} \cdots \text{O}$

or O-H...O could be determined.

Using this method, we determined the distance between the COMs of the 3-cyanoindole monomer and of the water moiety in the ground state to be 494.1 pm and in the electronically excited state to 492.1 pm. The Kraitchman analysis for the amino hydrogen position in both the ground and excited states of 3-cyanoindole has been performed using the rotational constants of 3-cyanoindole and of the N-deuterated 3-cyanoindole isotopologue from Table 7.1. The  $r_0$  coordinates of the H-atom along with the  $r_0$  coordinates of the water COM in the same reference frame are shown in Table 7.6.

**Table 7.6.:** Kraitchman  $r_0$  coordinates of the pyrrolic amino hydrogen atom and of the water center of mass (COM) in pm.

State	S <sub>0</sub>		S <sub>1</sub>	
	NH	water	NH	water
<i>a</i>	7.4	155.3	7.6	157.2
<i>b</i>	285.3	469.1	283.9	466.3
<i>R</i>	285.4	494.1	284.0	492.1
NH...O(exp.)	201.9		201.7	
NH...O(theo.)	192.6		192.3	

From the so determined distance of the water COM from the amino hydrogen and the known distance of the COM of the water moiety from the water oxygen atom, the NH...O distance can be determined to be 201.9 pm in the ground state and 201.7 in the excited state. This is the lower limit under the assumption, that amino hydrogen, water COM and oxygen atom are located on a straight line. If there is an angle  $\alpha$  between the HOH plane and the hydrogen bond, the resulting bond length would be smaller by a factor of  $\cos(\alpha)$ . For both conformers 1a and 1b this angle is smaller than 10 °, equivalent to a reduction of less than 3 pm. The obvious difference between the experimental and the *ab initio* value for the hydrogen bond length results from zero-point vibrational averaging of the hydrogen bond along its very shallow stretching coordinate.

### Electronic structure of the excited state

Table 7.5 shows that the orientation of the TDM vector of 3-cyanoindole-water, if transformed into the principal axis system of indole, is the same as in indole and in the 3-cyanoindole monomer, but opposite to that of 5-cyanoindole. The lowest excited state is therefore an  $^1L_b$  like state as for the monomer. The reason for this deviant behavior can be found in the fact, that for 3-cyanoindole the dipole moment in the  $^1L_a$  state is smaller than in the  $^1L_b$  state. All other indoles have a larger  $^1L_a$  dipole moment and thus a stabilization

of the  ${}^1L_a$  state with respect to the  ${}^1L_b$  state.

## 7.6. Conclusions

The dipole moment of 3-cyanoindole and its orientation in ground and lowest electronically excited state could be determined to be very similar. The excited state lifetime of 3-cyanoindole is considerably shorter than that of indole and 5-cyanoindole with the 1:1 water cluster of 3-cyanoindole being especially short-lived. The electronic nature of the lowest excited state is a locally excited (LE) state with strong  ${}^1L_b$  character. The adiabatically higher lying  ${}^1L_a$  state has, in contrast to indole and 5-cyanoindole (and many other indole derivatives), a smaller permanent dipole moment. Therefore, the  ${}^1L_b$  state is stabilized stronger upon attachment of the polar water molecule than the  ${}^1L_a$  state. This causes the 1:1 water cluster to be also of  ${}^1L_b$  character. Although, we can confirm the above statement only for the binary water cluster, one might speculate that the exceptionally short lifetime of 3-cyanoindole in water solution might be due to the fact, that the emitting state is the  ${}^1L_b$  which is different from the other cyanoindoles and indole in which  ${}^1L_a$  emission is observed.[130]

The characterization of the emitting state could be performed using high resolution (Stark) spectroscopy for the first time. Permanent dipole moments, transition dipoles, fluorescence lifetimes and structures of the isolated molecule, as well as of the 1:1 water cluster (with the exception of the permanent dipole moments) could be obtained for the first time. These investigations show, that already the first solvating water molecule opens the way to the unusually short life time of 3-cyanoindole in water solution. One might ask, why we omitted the measurement of the Stark spectrum for the water cluster. Certainly, this would have added extremely important information about the function of the water moiety in the photophysics of the monomer. Unfortunately, 3-cyanoindole behaves different than other cyanoindoles. Upon heating in the source chamber, 3-cyanoindole sublimates into an extremely fine powder, which clogs the orifice of the nozzle after a few minutes even at strongly elevated temperatures of the nozzle. Since the time for optimization of the cluster conditions was too short to get a better signal to noise ratio, we were unable to record the Stark spectrum. The current investigations show, that already the first solvating water molecule opens the way to the unusually short life time in water solution.

## Conflicts of interest

There are no conflicts to declare.

## 7.7. Acknowledgements

Financial support of the Deutsche Forschungsgemeinschaft via grant SCHM1043/12-3 is gratefully acknowledged. Computational support and infrastructure was provided by the "Center for Information and Media Technology" (ZIM) at the Heinrich-Heine-University Düsseldorf (Germany). We furthermore thank the Regional Computing Center of the University of Cologne (RRZK) for providing computing time on the DFG-funded High Performance Computing (HPC) system CHEOPS as well as support. Financial support provided by CONACYT under the grant 277871 is greatly appreciated.

## 7.8. Publication

Chapter 7 was published under the heading *Rotationally Resolved Electronic Spectroscopy of 3-Cyanoindole and the 3-Cyanoindole-water complex* in *Physical Chemistry Chemical Physics*, **20**, 23441-23452, 2018. DOI: 10.1039/C8CP04020F.

The gasphase measurements were performed by Marie-Luise Hebestreit and myself. The *ab initio* calculations and spectra evaluations were made by myself as well. The TCSPC measurements were made by Hilda Parsian. My total share of this publication is about: 65%.



## 8 | Summary

Via high resolution laser induced fluorescence spectroscopy a lot of molecular parameters were accessible to study several molecules. Namely, the three dimethoxybenzenes and 3-cyanoindole in this doctoral thesis. With the experimental results of this method, in combination with *ab initio* calculations, structures were assigned, the nature of excited states determined, fluorescence behavior compared and dipole moments investigated. The chapters 5, 6 and 7 are dealing with these studies.

In Chapter 5, published under the heading *Rotationally Resolved Electronic Spectroscopy of the Rotamers of 1,3-Dimethoxybenzene*, the conformational landscape of 3-dimethoxybenzene was explored. For this, the origin bands of the three planar rotamers of 1,3-dimethoxybenzene were recorded rotationally resolved. The origin bands of these rotamers were received from publications via resonant two-photon ionization and two-color resonant two-photon mass analyzed threshold ionization spectroscopy. Surprisingly, two of the three bands had nearly the same rotational constants in the ground state, but not in the first excited state. It was shown that one of these two bands is a vibrational band of one rotamer. Consequently, the origins of the (0,0) and of the (180,0) were found and assigned, while the origin of the (0,180) rotamer was assigned to a vibrational band of the (0,0) rotamer. The results of quantum chemical calculations have shown a non-planar geometry of this rotamer in the  $S_1$  state, which results in a small Franck-Condon factor. The non-observation of the (180,0) rotamer, in which the two groups are pointing at each other, occurs also for similar molecules as 1,3-dihydroxybenzene and 1,3-methophenol in molecular beam experiments.[1, 2] The investigations via rotationally resolved spectroscopy have shown that this method is an important tool for a final structural assignment of rotamers. Chapter 6 focuses on the excited state dipole moments and on transition dipole moments of the rotamers of 1,2-, 1,3- and 1,4-dimethoxybenzene. The results were released in the Journal *ChemPhysChem* with the title *Excited-State Dipole Moments and Transition Dipole Orientations of Rotamers of 1,2-, 1,3, and 1,4-Dimethoxybenzene*. In this study additionally Stark-experiments, by application of an electric field were performed. These

experiments open the possibility to determine the permanent dipole moments of the electronic ground and first excited state. The analysis showed that the permanent dipole moments in the electronic ground state can be derived by vectorial addition from the dipole moment of the monomethoxybenzene. In the lowest electronically excited state this worked only for asymmetric rotamers, but not for symmetrical. Reasons why this approach has failed are given by investigation of their electronic nature in this state and traced back on state-mixing in asymmetric rotamers.

Finally, investigations on 3-cyanoindole and its water cluster were performed and published under *Rotationally resolved electronic spectroscopy of 3-cyanoindole and the 3-cyanoindole-water complex* in the journal *PCCP*. Since the water moiety has several possible positions to attach to the chromophore, structural investigations showed that the trans-linearly NH-O hydrogen bond was observed. Its bond length was determined to 201 pm. Research on the electronic nature of the monomer and the water cluster showed  $^1L_b$  character of the first excited state for both systems. Further, the influence of solvents to fluorescence lifetime of 3-cyanoindole was revealed. The fluorescence lifetime from 3-cyanoindole decreases from 9.8 ns to 3.9 ns for its water cluster. In aqueous phase the lifetime was with 0.05 ns the shortest. The same trend was observed for indole and 5-cyanoindole. The N-deuterated 3-cyanoindole showed the longest fluorescence lifetime. This fluorescence behavior can be explained by the role of a  $\pi\sigma^*$  state forming a conical intersection from the excited state to the electronic ground state.

The studies on the above mentioned molecules via high resolution laser induced fluorescence spectroscopy showed that this technique, in combination with *ab initio* calculations, is a powerful tool for investigations of molecular properties. Structural assignments were made, the electronic nature of excited states were determined and fluorescence behavior explained.

## 9 | List of Publications and Conference Contributions

### Publications

- Marie-Luise Hebestreit, Christian Henrichs, Michael Schneider, Martin Wilke, W. Leo Meerts, Daniel Krügler and Michael Schmitt: Structural changes upon electronic excitation in 1,2-dimethoxybenzene from rotationally resolved electronic spectroscopy of various isotopologues, *J. Mol. Struct.*, **1184**, 139-145, 2019
- Michael Schneider, Marie-Luise Hebestreit, Mirko Matthias Lindic, Hilda Parsian, América Torres-Boy, Leonardo Álvarez-Valtierra, W. Leo Meerts, Ralf Kühnemuth, and Michael Schmitt: Rotationally Resolved Electronic Spectroscopy of 3-Cyanoindole and the 3-Cyanoindole-water Complex, *PCCP*, **20**, 23441-23452, 2018
- Mirko Matthias Lindic, Matthias Zajonz, Marie-Luise Hebestreit, Michael Schneider, W. Leo Meerts, Michael Schmitt: Excited state dipole moments of anisole in gas phase and solution, *J. Photochem. and Photobiol. A: Chem.*, **365**, 213-219, 2018
- Michael Schneider, Martin Wilke, Marie-Luise Hebestreit, Christian Henrichs, Leo W. Meerts, Michael Schmitt: Excited-State Dipole Moments and Transition Dipole Orientations of Rotamers of 1,2-, 1,3-, and 1,4-Dimethoxybenzene, *ChemPhysChem*, **19**, 1–13, 2018
- Michael Schneider, Martin Wilke, Marie-Luise Hebestreit, José Arturo Ruiz-Santoyo, Leonardo Álvarez-Valtierra, John T. Yi, W. Leo Meerts, David W. Pratt and Michael Schmitt: Rotationally Resolved Electronic Spectroscopy of Rotamers of 1,3-Dimethoxybenzene. *PCCP*, **19**, 21364-21372 , 2017
- Martin Wilke, Michael Schneider, Josefin Wilke, José Arturo Ruiz-Santoyo, Jorge J. Campos-Amador, M. Elena González-Medina, Leonardo Álvarez-Valtierra and Michael Schmitt: Rotationally Resolved Electronic Spectroscopy Study of the Conformational Space of 3-methoxyphenol. *J. Mol. Struct.*, **1140**, 59-66, 2017

### Conference Contributions

- **Poster:** Michael Schneider, Marie-Luise Hebestreit, Mirko Matthias Lindic, Hilda Parsian, América Torres-Boy, Leonardo Álvarez-Valtierra, W. Leo Meerts and Michael Schmitt. Rotationally Resolved Electronic Spectroscopy of 3-Cyanoindole and the 3-Cyanoindole-water Complex. 34th European Congress on Molecular Spectroscopy, Coimbra, Portugal 08/2018.
- **Talk:** Michael Schneider, Marie-Luise Hebestreit, Christian Henrichs and Michael Schmitt: Rotationally Resolved Electronic Stark Spectroscopy of 3-Cyanoindole and the 3-Cyanoindole-water complex. Frühjahrstagung der Deutschen Physikalischen Gesellschaft, Erlangen, Germany 03/2018.
- **Poster:** Michael Schneider, Martin Wilke, Marie-Luise Hebestreit, Leo Meerts and Michael Schmitt. Excited state dipole moments and transition dipoles of different rotamers of 1,2-, 1,3- and 1,4-dimethoxybenzene. Colloquium on High Resolution Molecular Spectroscopy, Helsinki, Finland 08/2017.
- **Talk:** Michael Schneider, Josefin Wilke, Martin Wilke, and Michael Schmitt, Observation of 3-methoxyphenol rotational isomers via high resolution laser induced fluorescence spectroscopy. Frühjahrstagung der Deutschen Physikalischen Gesellschaft, Hanover, Germany 03/2016.

# Bibliography

- [1] José Arturo Ruiz-Santoyo, Marcela Rodríguez-Matus, José Luis Cabellos, John T. Yi, David W. Pratt, Michael Schmitt, Gabriel Merino, and Leonardo Álvarez Valtierra. Intramolecular structure and dynamics of mequinol and guaiacol in the gas phase: Rotationally resolved electronic spectra of their s1 states. *The Journal of Chemical Physics*, 143(9):094301, 2015.
- [2] Martin Wilke, Christian Brand, Josefin Wilke, and Michael Schmitt. Influence of the position of the methoxy group on the stabilities of the syn and anti conformers of 4-, 5-, and 6-methoxyindole. *Journal of Molecular Spectroscopy*, 337:137–144, 2017.
- [3] PJ Breen, Elliot R Bernstein, Henry V Secor, and Jeffrey I Seeman. Spectroscopic observation and geometry assignment of the minimum energy conformations of methoxy-substituted benzenes. *Journal of the American Chemical Society*, 111(6):1958–1968, 1989.
- [4] David R. Borst, Timothy M. Korter, and David W. Pratt. On the additivity of bond dipole moments. stark effect studies of the rotationally resolved electronic spectra of aniline, benzonitrile, and aminobenzonitrile. *Chemical Physics Letters*, 350(5):485–490, 2001.
- [5] T. M. Korter, D. R. Borst, C. J. Butler, and D. W. Pratt. Stark effects in gas-phase electronic spectra. dipole moment of aniline in its excited s1 state. *Journal of the American Chemical Society*, 123(1):96–99, 2001.
- [6] Josefin Wilke, Martin Wilke, Christian Brand, W Leo Meerts, and Michael Schmitt. On the additivity of molecular fragment dipole moments of 5-substituted indole derivatives. *ChemPhysChem*, 17(17):2736–2743, 2016.
- [7] John R Platt. Classification of spectra of cata-condensed hydrocarbons. *The Journal of chemical physics*, 17(5):484–495, 1949.

- [8] Cheolhwa Kang, Timothy M Korter, and David W Pratt. Experimental measurement of the induced dipole moment of an isolated molecule in its ground and electronically excited states: Indole and indole-h 2 o. *The Journal of chemical physics*, 122(17):174301, 2005.
- [9] Timothy M. Korter, David W. Pratt, and Jochen Küpper. Indole-h2o in the gas phase. structures, barriers to internal motion, and s1  $\leftarrow$  s0 transition moment orientation. solvent reorganization in the electronically excited state. *The Journal of Physical Chemistry A*, 102(37):7211–7216, 1998.
- [10] Olivia Oeltermann, Christian Brand, Bernd Engels, Jörg Tatchen, and Michael Schmitt. The structure of 5-cyanoindole in the ground and the lowest electronically excited singlet states, deduced from rotationally resolved electronic spectroscopy and ab initio theory. *Physical Chemistry Chemical Physics*, 14(29):10266–10270, 2012.
- [11] Michael Schmitt. *Hochauflösende elektronische Spektroskopie an Molekülen und Clustern*. Habilitationsschrift, 2000.
- [12] W. Demtröder. *Molekülphysik: Theoretische Grundlagen und experimentelle Methoden*. De Gruyter, 2013.
- [13] Martin Wilke. *Einfluss unterschiedlicher Substituenten auf den Charakter elektronisch angeregter Zustände*. PhD thesis, 2017.
- [14] H.W. Kroto. *Molecular Rotation Spectra*. Dover Publications, 2003.
- [15] Josefin Wilke. *Rotationsaufgelöste elektronische Starspektroskopie*. PhD thesis, 2016.
- [16] Wolfgang Demtröder. *Laserspektroskopie: Grundlagen und Techniken*. Springer-Verlag, 2007.
- [17] S Golden and E Bright Wilson Jr. The stark effect for a rigid asymmetric rotor. *The Journal of Chemical Physics*, 16(7):669–685, 1948.
- [18] John R Lombardi. Stark effect in electronic spectra: The asymmetric rotor. *The Journal of Chemical Physics*, 48(1):348–353, 1968.
- [19] G Weber. Fluorescence-polarization spectrum and electronic-energy transfer in proteins. *Biochemical Journal*, 75(2):345, 1960.

- 
- [20] J.R. Lakowicz. *Principles of Fluorescence Spectroscopy*. Springer US, 2007.
- [21] Josefin Wilke, Martin Wilke, Christian Brand, J Dominik Spiegel, Christel M Marian, and Michael Schmitt. Modulation of the la/lb mixing in an indole derivative: A position-dependent study using 4-, 5-, and 6-fluoroindole. *The Journal of Physical Chemistry A*, 121(8):1597–1606, 2017.
- [22] E Heilbronner and JN Murrell. A theoretical study of the electronic spectra of the benzazulenes and benzologue-tropylium cations and a critical examination of the perimeter model. *Molecular Physics*, 6(1):1–18, 1963.
- [23] Michael Schneider, Martin Wilke, Marie-Luise Hebestreit, Christian Henrichs, W Leo Meerts, and Michael Schmitt. Excited-state dipole moments and transition dipole orientations of rotamers of 1, 2-, 1, 3-, and 1, 4-dimethoxybenzene. *ChemPhysChem*, 19(3):307–318, 2018.
- [24] Jan-Willem Pieterse, James D Kafka, Shinan S Sheng, and William L Nighan Jr. *US Patent 5,696,780, Frequency conversion system*. 1997.
- [25] Sirah Laser-und Plasmatechnik GmbH. *Matisse User's Guide Version 2.2*.
- [26] Christian Brand. *Shaping and Modelling Electronically Excited States of Indoles*. PhD thesis, 2013.
- [27] Sirah Laser-und Plasmatechnik GmbH. *Matisse User's Guide Version 1.12*.
- [28] Hans Joachim Eichler and Jürgen Eichler. *Laser: Bauformen, Strahlführung, Anwendungen*. Springer-Verlag, 2015.
- [29] Wolfgang Demtröder. *Experimentalphysik 2*. Springer, 2004.
- [30] Arnim Westphal. *Hochaufgelöste Laserfluoreszenzspektroskopie am Phenol (Methanol) 1-Cluster*. PhD thesis, 2003.
- [31] S. Gerstenkorn and P. Luc. *Atlas du spectre d'absorption de la molécule d'iode 14800–20000 cm<sup>-1</sup>*. CNRS, Paris, 1986.
- [32] Ingo Meusel, W Richter, and Hans-Joachim Freund. *Aufbau einer Molekularstrahlapparatur für oberflächenkinetische Untersuchungen—Setup of a molecular beam apparatus for surface kinetic studies*. PhD thesis, 2002.

- [33] Roger Campargue. *Atomic and Molecular beams: The state of the art 2000*. Springer Science and Business Media, 2012.
- [34] Thomas Dorfmueller, Manfred Faubel, Peter Fischer, Helmut Grubmueller, Hellmut Haberland, Gerd Hauck, Gerd Heppke, Siegfried Hess, Karl Kleinermanns, and Martin Kroeger. *Gase, Nanosysteme, Flüssigkeiten*. Walter de Gruyter, 2005.
- [35] LK Ono, T Majima, Y Hamamoto, K Norizawa, K Yoshida, and A Itoh. Preliminary study of gas cluster ion beam source. *Department of Nuclear Engineering, Kyoto University*.
- [36] Vitrek Corporation. *Operatin and Maintenance Manual Vitrek*. 2017.
- [37] W Leo Meerts and Michael Schmitt. Application of genetic algorithms in automated assignments of high-resolution spectra. *International Reviews in Physical Chemistry*, 25(3):353–406, 2006.
- [38] W Leo Meerts, Michael Schmitt, and Gerrit C Groenenboom. New applications of the genetic algorithm for the interpretation of high-resolution spectra. *Canadian journal of chemistry*, 82(6):804–819, 2004.
- [39] W. L. Meerts Schmitt and M. *Description and features of the programs ga and gamr: Automated assign and fit programs for high resolution spectra using evolutionary algorithm*. 2014.
- [40] G. Scoles, editor. *Atomic and Molecular Beam Methods*, volume 1. Oxford University Press, New York, Oxford, 1988.
- [41] G. Scoles, editor. *Atomic and Molecular Beam Methods*, volume 2. Oxford University Press, New York, Oxford, 1992.
- [42] Peter Felder and Hs. H. Günthard. Conformational interconversions in supersonic jets: matrix ir spectroscopy and model calculations. *Chem. Phys.*, 71:9–25, 1982.
- [43] R. S. Ruoff, T. D. Klots, T. Emilsson, and H. S. Gutowski. Relaxation of conformers and isomers in seeded supersonic jets of inert gases. *J. Chem. Phys.*, 93:3142–3150, 1990.
- [44] P. D. Godfrey, R. D. Brown, and Fiona M. Rogers. The missing conformers of glycine and alanine: relaxation in seeded supersonic jets. *J. Mol. Struct.*, 376:65–81, 1996.

- 
- [45] Tomas Baer and Alan R. Potts. Nonstatistical chemical reactions: the isomerization over low barriers in methyl and ethyl cyclohexane. *J. Phys. Chem. A*, 104:9397–9402, 2000.
- [46] Marcel Böhm, Robert Brause, Christoph Jacoby, and Michael Schmitt. Conformational relaxation paths in tryptamine. *J. Phys. Chem. A*, 113:448–455, 2009.
- [47] T. M. Dunn, R. Tembreull, and D. M. Lubman. Free-jet spectra and structure of o-, m-, and p-dihydroxybenzene. *Chem. Phys. Letters*, 121:453–457, 1985.
- [48] Claudio Puebla and Tae-Kyu Ha. A theoretical study of conformations and rotational barriers in dihydroxybenzenes. *Journal of Molecular Structure: THEOCHEM*, 204:337 – 351, 1990.
- [49] M Gerhards, W Perl, and K Kleineremanns. Rotamers and vibrations of resorcinol obtained by spectral hole burning. *Chemical physics letters*, 240(5-6):506–512, 1995.
- [50] Sonia Melandri, Gianni Maccaferri, Walther Caminati, and Paolo G Favero. Conformational equilibrium in resorcinol by means of the free-jet absorption millimeter wave spectrum. *Chemical physics letters*, 256(4-5):513–517, 1996.
- [51] Wolf D Geppert, Caroline EH Dessent, Susanne Ullrich, and Klaus Müller-Dethlefs. Observation of hydrogen-bonded rotational isomers of the resorcinol water complex. *The Journal of Physical Chemistry A*, 103(36):7186–7191, 1999.
- [52] Wolf D Geppert, Caroline EH Dessent, and Klaus Müller-Dethlefs. Zeke and hole-burning spectroscopy of the rotational isomers of resorcinol co. *The Journal of Physical Chemistry A*, 103(48):9687–9692, 1999.
- [53] Grzegorz Myszkiewicz, W. Leo Meerts, Christian Ratzler, and Michael Schmitt. Structure determination of resorcinol rotamers by high-resolution UV spectroscopy. *ChemPhysChem*, 6:2129–2136, 2005.
- [54] M. Wilke, M. Schneider, J. Wilke, J.A. Ruiz-Santoyo, J.J. Campos-Amador, M.E. Gonzléz-Medina, L. Álvarez-Valtierra, and M. Schmitt. Rotationally resolved electronic spectroscopy study of the conformational space of 3-methoxyphenol. *J. Mol. Struct.*, 1140:59–66, 2017.
- [55] P. J. Breen, E. R. Bernstein, H. V. Sector, and J. I. Seeman. Spectroscopic observation and geometry assignment of the minimum energy conformations of methoxy-substituted benzenes. *J. Am. Chem. Soc.*, 111:1958–1968, 1989.

- [56] Shih Chang Yang, Ssu Wei Huang, and Wen Bih Tzeng. Rotamers of o- and m-dimethoxybenzenes studied by mass-analyzed threshold ionization spectroscopy and theoretical calculations. *J. Phys. Chem. A*, 114:11144–11152, 2010.
- [57] Michael Schmitt. *Spektroskopische Untersuchungen an Wasserstoffbrückenbindungen*. Habilitation, Heinrich-Heine-Universität, Math. Nat. Fakultät, Düsseldorf, 2000.
- [58] Michael Schmitt, Jochen Küpper, Daniel Spangenberg, and Arnim Westphal. Determination of the structures and barriers to hindered internal rotation of the phenol-methanol cluster in the  $S_0$  and  $S_1$  state. *Chem. Phys.*, 254:349–361, 2000.
- [59] R. Ahlrichs, M. Bär, M. Häser, H. Horn, and C. Kölmel. Electronic structure calculations on workstation computers: The program system turbomole. *Chem. Phys. Letters*, 162:165–169, 1989.
- [60] Jr. T. H. Dunning. Gaussian basis sets for use in correlated molecular calculations. i. the atoms boron through neon and hydrogen. *J. Chem. Phys.*, 90:1007–1023, 1989.
- [61] C. Hättig and Florian Weigend. Cc2 excitation energy calculations on large molecules using the resolution of the identity approximation. *J. Chem. Phys.*, 113:5154–5161, 2000.
- [62] C. Hättig and Andreas Köhn. Transition moments and excited-state first-order properties in the coupled cluster model cc2 using the resolution-of-the-identity approximation. *J. Chem. Phys.*, 117:6939–6951, 2002.
- [63] C. Hättig. Geometry optimizations with the coupled-cluster model cc2 using the resolution-of-the-identity approximation. *J. Chem. Phys.*, 118:7751–7761, 2002.
- [64] P. Deglmann, F. Furche, and R. Ahlrichs. An efficient implementation of second analytical derivatives for density functional methods. *Chem. Phys. Letters*, 362:511–518, 2002.
- [65] A. E. Reed, R. B. Weinstock, and F. Weinhold. Natural population analysis. *J. Chem. Phys.*, 83:735–746, 1985.
- [66] TURBOMOLE V6.5 2013, a development of University of Karlsruhe and Forschungszentrum Karlsruhe GmbH, 1989-2007, TURBOMOLE GmbH, since 2007; available from <http://www.turbomole.com>.

- 
- [67] M. J. Frisch, G. W. Trucks, H. B. Schlegel, G. E. Scuseria, M. A. Robb, J. R. Cheeseman, G. Scalmani, V. Barone, B. Mennucci, G. A. Petersson, H. Nakatsuji, M. Caricato, X. Li, H. P. Hratchian, A. F. Izmaylov, J. Bloino, G. Zheng, J. L. Sonnenberg, M. Hada, M. Ehara, K. Toyota, R. Fukuda, J. Hasegawa, M. Ishida, T. Nakajima, Y. Honda, O. Kitao, H. Nakai, T. Vreven, J. A. Montgomery, Jr., J. E. Peralta, F. Ogliaro, M. Bearpark, J. J. Heyd, E. Brothers, K. N. Kudin, V. N. Staroverov, R. Kobayashi, J. Normand, K. Raghavachari, A. Rendell, J. C. Burant, S. S. Iyengar, J. Tomasi, M. Cossi, N. Rega, J. M. Millam, M. Klene, J. E. Knox, J. B. Cross, V. Bakken, C. Adamo, J. Jaramillo, R. Gomperts, R. E. Stratmann, O. Yazyev, A. J. Austin, R. Cammi, C. Pomelli, J. W. Ochterski, R. L. Martin, K. Morokuma, V. G. Zakrzewski, G. A. Voth, P. Salvador, J. J. Dannenberg, S. Dapprich, A. D. Daniels, Ö. Farkas, J. B. Foresman, J. V. Ortiz, J. Cioslowski, and D. J. Fox. Gaussian 09 Revision E.01. Gaussian Inc. Wallingford CT 2009.
- [68] W. Leo Meerts, M. Schmitt, and G. Groenenboom. New applications of the genetic algorithm for the interpretation of high resolution spectra. *Can. J. Chem.*, 82:804–819, 2004.
- [69] W. L. Meerts and M. Schmitt. A new automated assign and analyzing method for high resolution rotational resolved spectra using genetic algorithms. *Phys. Scripta*, 73:C47–C52, 2005.
- [70] W. L. Meerts and M. Schmitt. Application of genetic algorithms in automated assignments of high-resolution spectra. *Int. Rev. Phys. Chem.*, 25:353–406, 2006.
- [71] M. Schmitt and W. Leo Meerts. Rotationally resolved electronic spectroscopy and automatic assignment techniques using evolutionary algorithms. In Martin Quack and Frederic Merkt, editors, *Handbook of High Resolution Spectroscopy*. John Wiley and Sons, 2011. ISBN: 978-0-470-06653-9.
- [72] A. Ostermeier, A. Gawelcyk, and N. Hansen. Step-size adaptation based on non-local use of selection information. In Y. Davidor, H.-P. Schwefel, and R. Männer, editors, *Parallel Problem Solving from Nature, PPSN III*. Springer, Berlin/Heidelberg, 1994.
- [73] N. Hansen and A. Ostermeier. Completely derandomized self-adaptation in evolution strategies. *Evolutionary Computation*, 9(2):159–195, 2001.
- [74] O Desyatnyk, L Pszczółkowski, S Thorwirth, TM Krygowski, and Z Kisiel. The

- rotational spectra, electric dipole moments and molecular structures of anisole and benzaldehyde. *Physical Chemistry Chemical Physics*, 7(8):1708–1715, 2005.
- [75] O. Desyatnyk, L. Pszczolkowski, S. Thorwirth, T. M. Krygowski, and Z. Kisiel. The rotational spectra, electric dipole moments and molecular structures of anisole and benzaldehyde. *Phys. Chem. Chem. Phys.*, 7:1708–1715, 2005.
- [76] J. W. Ribblett, W. E. Sinclair, D. R. Borst, J. T. Yi, and D. W. Pratt. High resolution electronic spectra of anisole and anisole-water in the gas phase: Hydrogen bond switching in the  $s_1$  state. *J. Phys. Chem. A*, 110:1478–1483, 2006.
- [77] Giel Berden, W. Leo Meerts, Michael Schmitt, and Karl Kleinermanns. High resolution UV spectroscopy of phenol and the hydrogen bonded phenol-water cluster. *J. Chem. Phys.*, 104:972–982, 1996.
- [78] D. Spangenberg, P. Imhof, and K. Kleinermanns. The  $s_1$  state geometry of phenol determined by simultaneous franck-condon and rotational constants fits. *Phys. Chem. Chem. Phys.*, 5:2505–2514, 2003.
- [79] R. Brause, M. Schmitt, D. Spangenberg, and K. Kleinermanns. Determination of the excited state structure of 7-azaindole using a franck–condon analysis. *Mol. Phys.*, 102:1615–1623, 2004.
- [80] Olivia Oeltermann, Christian Brand, Martin Wilke, and Michael Schmitt. Ground and electronically excited singlet state structures of the syn and anti rotamers of 5-hydroxyindole. *J. Phys. Chem. A*, 116:7873–7879, 2012.
- [81] Martin Wilke, Christian Brand, Josefin Wilke, and Michael Schmitt. The conformational space of the neurotransmitter serotonin: how the rotation of a hydroxyl group changes all. *Phys. Chem. Chem. Phys.*, 18:13538, 2016.
- [82] J. T. Yi, J. W. Ribblett, and D. W. Pratt. Rotationally resolved electronic spectra of 1,2-dimethoxybenzene and the 1,2-dimethoxybenzene-water complex. *J. Phys. Chem. A*, 109:9456–9464, 2011.
- [83] T. Bürgi and S. Leutwyler. O-h torsional vibrations in the  $s_0$  and  $s_1$  states of catechol. *J. Chem. Phys.*, 101:8418–8429, 1994.
- [84] J. Arturo Ruiz-Santoyo, Marcela Rodríguez-Matus, Leonardo Alvarez-Valtierra, JosŽ-Luis Cabellos, Gabriel Merino, John Yi, David W. Pratt, and Michael Schmitt.

- Intramolecular structure and dynamics of mequinol and guaiacol in the gas phase. rotationally resolved electronic spectra of their  $s_1$  states. *J. Chem. Phys.*, 143:094301, 2015.
- [85] Th. Förster. Zwischenmolekulare energiewanderung und fluoreszenz. *Ann. Phys.*, 437:55–75, 1948.
- [86] J Lakowicz. *Principles of Fluorescence Spectroscopy*. Plenum, New York, USA, 2 edition, 1999.
- [87] Herbert van Amerongen, Leonas Valkunas, and Rienk van Grondelle. *Photosynthetic Excitons*. World Scientific Publishing, Singapore, 2000.
- [88] E. Lippert. Dipolmoment und elektronenstruktur von angeregten molekülen. *Z. Naturforsch.*, 10A:541, 1955.
- [89] N. Mataga, Y. Kaifu, and M. Koizumi. Solvent effects upon fluorescence spectra and the dipolemoments of excited molecules. *Bull. Chem. Soc. Jpn.*, 29:465, 1956.
- [90] Takehiro Abe. Estimation of angles between ground- and excited-state dipole moments from solvent spectral frequency shifts. *Bull Chem. Soc. Jpn.*, 64:3224–3228, 1991.
- [91] P. Suppan. Invited review solvatochromic shifts: The influence of the medium on the energy of electronic states. *J. Photochem. Photobiol. A*, 50:293, 1990.
- [92] L. Bilot and A. Kawski. Zur Theorie des Einflusses von Lösungsmitteln auf die Elektronenspektren der Moleküle. *Z. Naturforsch.*, 17A:621–627, 1962.
- [93] N.G. Bakhshiev. Universal intermolecular interactions and their effect on the position of the electronic spectra of molecules in two component solutions. *Opt. Spektrosk.*, 13:24–29, 1962.
- [94] E. M. Rae. Theory of solvent effects on molecular electronic spectra. Frequency shifts. *J. Phys. Chem.*, 61:562–572, 1957.
- [95] John R. Lombardi. Solvatochromic shifts: A reconsideration. *J. Phys. Chem. A*, 102:2817–2823, 1998.
- [96] John R. Lombardi. Solvatochromic shifts reconsidered: Field-induced mixing in the nonlinear region and application to indole. *J. Phys. Chem. A*, 103:6335–6338, 1999.

- [97] Ephrem G. Demissie, Ephriem T. Mengesha, and Girma W. Woyessa. Modified solvatochromic equations for better estimation of ground and excited state dipole moments of p-aminobenzoic acid (PABA): Accounting for real shape over hypothetical spherical solvent shell. *J. Photochem. and Photobiol. A*, 337:184–191, 2016.
- [98] Janus J. Eriksen, Stephan P.A. Sauer, Kurt V. Mikkelsen, Ove Christiansen, Hans Jorgen Aa. Jensen, and Jacob Kongsted. Failures of tddft in describing the lowest intramolecular charge-transfer excitation in para-nitroaniline. *Mol. Phys.*, 111:1235–1248, 2013.
- [99] C.G. Eisenhardt, G. Pietraperzia, and M. Becucci. The high resolution spectrum of the  $s_0 \leftarrow s_1$  transition of anisole. *Phys. Chem. Chem. Phys.*, 3:1407, 2001.
- [100] Susan J. Humphrey and David W. Pratt. High resolution  $s_1 \leftarrow s_0$  fluorescence excitation spectra of hydroquinone. distinguishing the cis and trans rotamers by their nuclear spin statistical weights. *J. Chem. Phys.*, 99:5078–5086, 1993.
- [101] Nicola Schiccheri, Massimiliano Pasquini, Giovanni Piani, Giangaetano Pietraperzia, Maurizio Becucci, Malgorzata Biczysko, Julien Bloino, and Vincenzo Barone. Integrated experimental and computational spectroscopy study on  $\pi$ -stacking interaction: the anisole dimer. *Phys. Chem. Chem. Phys.*, 12:13547–13554, 2010.
- [102] Ch. Ratzer, J. Küpper, D. Spangenberg, and Michael Schmitt. The structure of phenol in the  $S_1$ -state determined by high resolution UV-spectroscopy. *Chem. Phys.*, 283:153–169, 2002.
- [103] Jian-Han Huang, Wen-Bih Tzeng, and Ke-Long Huang. Vibrational spectrum of o-dimethoxybenzene in the  $s_1$  and  $d_0$  states. *Chinese J. Chem.*, 26:51–54, 2008.
- [104] Michael Schneider, Martin Wilke, Marie-Luise Hebestreit, José Arturo Ruiz-Santoyo, Leonardo Álvarez Valtierra, John T. Yi, W. Leo Meerts, David W. Pratt, and Michael Schmitt. Excited-state dipole moments and transition dipoleorientations of rotamers of 1,2-, 1,3-, and 1,4-dimethoxybenzene. *Phys. Chem. Chem. Phys.*, 19:21364–21372, 2017.
- [105] Akira Oikawa, Haruo Abe, Naohiko Mikami, and Mitsuo Ito. Electronic spectra and ionization potentials of rotational isomers of several disubstituted benzenes. *Chem. Phys. Letters*, 116:50–54, 1985.

- 
- [106] W. B. Tzeng, K. Narayanan, C.Y. Hsieh, and C. C. Tung. Structures and vibrations of p-dimethoxybenzene conformers in the  $s_0$  and  $s_1$  states studied by ab initio calculations and resonant two-photon ionization spectroscopy. *J. Mol. Struct.*, 448:91–100, 1998.
- [107] Naohiko Mikami, Seiji Yamamoto, Katsuhiko Okuyama and Mitsuo Ito. Selective complexation of rotational isomers of p-dimethoxybenzene as studied by electronic spectra in a supersonic jet. *Chem. Phys. Letters*, 125:1–4, 1986.
- [108] M. J. Frisch, G. W. Trucks, H. B. Schlegel, G. E. Scuseria, M. A. Robb, J. R. Cheeseman, J. A. Montgomery, Jr., T. Vreven, K. N. Kudin, J. C. Burant, J. M. Millam, S. S. Iyengar, J. Tomasi, V. Barone, B. Mennucci, M. Cossi, G. Scalmani, N. Rega, G. A. Petersson, H. Nakatsuji, M. Hada, M. Ehara, K. Toyota, R. Fukuda, J. Hasegawa, M. Ishida, T. Nakajima, Y. Honda, O. Kitao, H. Nakai, M. Klene, X. Li, J. E. Knox, H. P. Hratchian, J. B. Cross, C. Adamo, J. Jaramillo, R. Gomperts, R. E. Stratmann, O. Yazyev, A. J. Austin, R. Cammi, C. Pomelli, J. W. Ochterski, P. Y. Ayala, K. Morokuma, G. A. Voth, P. Salvador, J. J. Dannenberg, V. G. Zakrzewski, S. Dapprich, A. D. Daniels, M. C. Strain, O. Farkas, D. K. Malick, A. D. Rabuck, K. Raghavachari, J. B. Foresman, J. V. Ortiz, Q. Cui, A. G. Baboul, S. Clifford, J. Cioslowski, B. B. Stefanov, G. Liu, A. Liashenko, P. Piskorz, I. Komaromi, R. L. Martin, D. J. Fox, T. Keith, M. A. Al-Laham, C. Y. Peng, A. Nanayakkara, M. Challacombe, P. M. W. Gill, B. Johnson, W. Chen, M. W. Wong, C. Gonzalez, and J. A. Pople. Gaussian 03, revision a.1. Gaussian, Inc., Pittsburgh, PA, 2003.
- [109] Josefin Wilke, Martin Wilke, W. Leo Meerts, and Michael Schmitt. Determination of ground and excited state dipole moments via electronic Stark spectroscopy: 5-methoxyindole. *J. Chem. Phys.*, 144:044201–1–044201–10, 2016.
- [110] L. S. Prabhurashi, D. K. Narayanan Kutty, and Anajali S. Bhide. Excited state dipole moments of some monosubstituted benzenes from solvent effect on electronic absorption spectra. *Spectrochim. Acta*, 39A:663–668, 1983.
- [111] H. C. Allen and P. C. Cross. *Molecular Vib-Rotors*. Wiley, New York, 1963.
- [112] T. M. Korter, D. R. Borst, C. J. Butler, and D. W. Pratt. Stark effects in gas-phase electronic spectra. dipole moment of aniline in its excited  $s_1$  state. *J. Am. Chem. Soc.*, 123:96–99, 2001.

- [113] Dave R Borst. PhD thesis, University of Pittsburgh, Pittsburgh, 2001.
- [114] Jennifer A. Reese, Tri V. Nguyen, Timothy M. Korter, and David W. Pratt. Charge redistribution on electronic excitation. dipole moments of cis- and trans-3-aminophenol in their  $s_0$  and  $s_1$  electronic states. *J. Am. Chem. Soc.*, 126:11387–11392, 2004.
- [115] D. R. Borst, T. M. Korter, and D. W. Pratt. On the additivity of bond dipole moments. stark effect studies of the rotationally resolved electronic spectra of aniline, benzonitrile and aminibenzonitrile. *Chem. Phys. Letters*, 350:485–490, 2001.
- [116] J. R. Platt. Classification of spectra of cata-condensed hydrocarbons. *J. Chem. Phys.*, 17:484–495, 1949.
- [117] E. Heilbronner and J.N. Murrell. A theoretical study of the electronic spectra of the benzazulenes and benzologue-tropylium cations and a critical examination of the perimeter model. *Mol. Phys.*, 6:1–18, 1968.
- [118] G. Weber. Fluorescence-polarization spectrum and electronic-energy transfer in tyrosine, tryptophan and related compounds. *Biochem. J.*, 75:335–345, 1960.
- [119] Thi Bao Chau Vu, Ivo Kalkman, W. Leo Meerts, Yuriy N. Svartsov, Christoph Jacoby, and Michael Schmitt. Rotationally resolved electronic spectroscopy of water clusters of 7-azaindole. *J. Chem. Phys.*, 128:214311(1–8), 2008.
- [120] B. Albinsson and B. Nordén. Excited-state properties of the indole chromophore – electronic-transition moment directions from linear dichroism measurements – effect of methyl and methoxy substituents. *J. Phys. Chem.*, 96:6204, 1992.
- [121] D. M. Sammeth, S. Yan, L. H. Spangler, and P. R. Callis. Two-photon fluorescence excitation spectra of indole in vapor and jet: 1la states. *J. Phys. Chem.*, 94:7340, 1990.
- [122] T. L. O. Barstis, L. I. Grace, T. M. Dunn, and D. L. Lubman. *J. Phys. Chem.*, 97:5820, 1993.
- [123] Laura A. Philips and Donald H. Levy. The rotationally resolved electronic spectrum of indole in the gas phase. *J. Chem. Phys.*, 85:1327–1332, 1986.
- [124] G. Berden, W. Leo Meerts, and E. Jalviste. Rotationally resolved ultraviolet spectroscopy of indole, indazole and benzimidazole: Inertial axis reorientation in the  $S_1(^1L_b) \leftarrow s_0$  transition. *J. Chem. Phys.*, 103:9596–9606, 1995.

- 
- [125] Cheolhwa Kang, Timothy M. Korter, and David W. Pratt. Experimental measurement of the induced dipole moment of an isolated molecule in its ground and electronically excited states: Indole and indole-h<sub>2</sub>O. *J. Chem. Phys.*, 122:174301, 2005.
- [126] J Zuclich, J U von Schütz, and A H Maki. Phosphorescent state of indole - observations using optically detected magnetic-resonance. *J. Am. Chem. Soc.*, 96(3):710–714, 1974.
- [127] B. J. Fender, K. W. Short, D. K. Hahn, and P. R. Callis. Vibrational assignments for indole with the aid of ultrasharp phosphorescence spectra. *Int. J. Quantum Chem.*, 72:347–356, 1999.
- [128] Jochen Küpper, David W. Pratt, W. Leo Meerts, Christian Brand, Jörg Tatchen, and Michael Schmitt. Vibronic coupling in indole: II. investigation of the  $^1l_a$ - $^1l_b$  interaction using rotationally resolved electronic spectroscopy. *Phys. Chem. Chem. Phys.*, 12:4980–4988, 2010.
- [129] P. R. Callis, J. T. Vivian, and L. S. Slater. *Chem. Phys. Letters*, 244:53, 1995.
- [130] L. Serrano-Andrés and B. O. Roos. Theoretical study of the absorption and emission spectra of indole in the gas phase and in a solvent. *J. Am. Chem. Soc.*, 118:185–195, 1996.
- [131] A. C. Borin and L. Serrano-Andrés. A theoretical study of the absorption spectra of indole and its analogs: indene, benzimidazole, and 7-azaindole. *Chem. Phys.*, 262:253–265, 2000.
- [132] Luis Serrano-Andrés and Antonio Carlos Borin. A theoretical study of the emission spectra of indole and its analogs: indene, benzimidazole, and 7-azaindole. *Chem. Phys.*, 262:267–283, 2000.
- [133] A. L. Sobolewski and W. Domcke. Ab initio investigations on the photophysics of indole. *Chem. Phys. Letters*, 315:293–298, 1999.
- [134] Christian Brand, Jochen Küpper, David W. Pratt, W. Leo Meerts, Daniel Krügler, Jörg Tatchen, and Michael Schmitt. Vibronic coupling in indole: I. theoretical description of  $^1l_a$  and  $^1l_b$  interactions and the absorption spectrum. *Phys. Chem. Chem. Phys.*, 12:4968–4997, 2010.

- [135] Mary Rose Hilaire, Debopreeti Mukherjee, Thomas Troxler, and Feng Gai. Solvent dependence of cyanoindole fluorescence lifetime. *Chemical physics letters*, 685:133–138, 2017.
- [136] Mary Rose Hilaire, Ismail A Ahmed, Chun-Wei Lin, Hyunil Jo, William F De-Grado, and Feng Gai. Blue fluorescent amino acid for biological spectroscopy and microscopy. *Proceedings of the National Academy of Sciences*, 114(23):6005–6009, 2017.
- [137] Beatrice N. Markiewicz, Debopreeti Mukherjee, Thomas Troxler, and Feng Gai. Utility of 5-cyanotryptophan fluorescence as a sensitive probe of protein hydration. *J. Phys. Chem. B*, 210:936–944, 2016.
- [138] Olivia Oeltermann, Christian Brand, Bernd Engels, Jörg Tatchen, and Michael Schmitt. The structure of 5-cyanoindole in the ground and lowest electronically excited singlet state, deduced from rotationally resolved electronic spectroscopy and ab initio theory. *Phys. Chem. Chem. Phys.*, 14:10266–10270, 2012.
- [139] Christian Brand, Beatrice Happe, Olivia Oeltermann, Martin Wilke, and Michael Schmitt. High resolution spectroscopy of several rovibronically excited bands of 5-cyanoindole - the effect of vibrational averaging. *J. Mol. Struct.*, 1044:21–25, 2013.
- [140] Benjamin Stuhlmann, Anne Gräßle, and Michael Schmitt. Determination of the geometry change of 5-cyanoindole upon electronic excitation from a combined franck-condon/rotational constants fit. *Phys. Chem. Chem. Phys.*, 16:899–905, 2014.
- [141] Timothy M. Korter, David W. Pratt, and Jochen Küpper. Indole-H<sub>2</sub>O in the gas phase. structures, barriers to internal motion, and S<sub>1</sub> ← S<sub>0</sub> transition moment orientation. solvent reorganization in the electronically excited state. *J. Phys. Chem. A*, 102:7211–7216, 1998.
- [142] Ahreum Ahn, Ahreum Min, Cheol Joo Moon, Ji Hoon Lee, and Myong Yong Choi. Conformational structures of 3-cyanoindole-(h<sub>2</sub>o)<sub>n</sub>(n = 0,2):franck condon simulations. *Chem. Phys. Letters*, 616–617:55–60, 2014.
- [143] K. Wohlfart, M. Schnell, J. U. Grabow, and J. Küpper. Precise dipole moment and quadrupole coupling constants of benzonitrile. *J. Mol. Spec.*, 247:119–121, 2014.
- [144] A. Hellweg, S. Grün, and C. Hättig. Benchmarking the performance of spin-component scaled cc2 in ground and electronically excited states. *Phys. Chem. Chem. Phys.*, 10:1159–1169, 2008.

- 
- [145] S. F. Boys and F. Bernardi. The calculation of small molecular interactions by the differences of separate total energies. some procedures with reduced errors. *Mol. Phys.*, 19:553–566, 1970.
- [146] P. J. Stephens, F. J. Devlin, C. F. Chabalowski, and M. J. Frisch. Ab initio calculation of vibrational absorption and circular dichroism spectra using density functional force fields. *J. Phys. Chem.*, 98:11623–11627, 1994.
- [147] C. Lee, W. Yang, and R.G. Parr. Development of the colle-salvetti correlation-energy formula into a functional of the electron-density. *Phys. Rev. B*, 37:785–789, 1988.
- [148] F. Furche and R. Ahlrichs. Adiabatic time-dependent density functional methods for excited state properties. *J. Chem. Phys.*, 117:7433, 2003.
- [149] Andreas Ostermeier, Andreas Gawelczyk, and Nikolaus Hansen. Step-size adaptation based on non-local use of selection information. In *International Conference on Parallel Problem Solving from Nature*, pages 189–198. Springer, 1994.
- [150] Stefan Grimme and Maja Parac. Substantial errors from time-dependent density functional theory for the calculation of excited states of large  $\pi$  systems. *ChemPhysChem*, 4(3):292–295, 2003.
- [151] Maja Parac and Stefan Grimme. A tddft study of the lowest excitation energies of polycyclic aromatic hydrocarbons. *Chem. Phys.*, 292:11–21, 2003.
- [152] Xue-fang Yu, Shohei Yamazaki, and Tetsuya Taketsugu. Concerted or stepwise mechanism? caspt2 and lc-tddft study of the excited-state double proton transfer in the 7-azaindole dimer. *Journal of chemical theory and computation*, 7(4):1006–1015, 2011.
- [153] Michael Schmitt, Robert Brause, Christel Marian, Susanne Salzmann, and W. Leo Meerts. Electronically excited states of tryptamine and its microhydrated complex. *J. Chem. Phys.*, 125:124309(1–10), 2006.
- [154] A. L. Sobolewski and W. Domcke. Photoinduced electron and proton transfer in phenol and its clusters with water and ammonia. *J. Phys. Chem. A*, 105:9275–9283, 2001.
- [155] A. L. Sobolewski, W. Domcke, C.Dedonder-Lardeux, and C.Jouvet. Excited-state hydrogen detachment and hydrogen transfer driven by repulsive 1 pr \*states: A

- new paradigm for nonradiative decay in aromatic biomolecules. *Phys. Chem. Chem. Phys.*, 4:1093–1100, 2002.
- [156] Wolfgang Domcke and Andrzej L. Sobolewski. Unraveling the molecular mechanisms of photoacidity. *Science*, 302:1693–1694, 2003.
- [157] J. T. Hougen and J. K. G. Watson. Anomalous rotational line intensities in electronic transitions of polyatomic molecules: Axis-switching. *Can. J. Phys.*, 43:298–320, 1965.
- [158] A. Held, B. B. Champagne, and David W. Pratt. Inertial axis reorientation in the  $s_1 \leftarrow s_0$  electronic transition of 2-pyridone. a rotational duschinsky effect. structural and dynamical consequences. *J. Chem. Phys.*, 95:8732, 1991.
- [159] Marcel Böhm, Jörg Tatchen, Daniel Krügler, Karl Kleinermanns, Michael G. D. Nix, Tracy A. LeGreve, Timothy S. Zwier, and Michael Schmitt. High-resolution and dispersed fluorescence examination of vibronic bands of tryptamine: Spectroscopic signatures for  $I_a/I_b$  mixing near a conical intersection. *J. Phys. Chem. A*, 113:2456–2466, 2009.
- [160] G. A. Bickel, D. R. Demmer, E. A. Outhouse, and S. C. Wallace. *J. Chem. Phys.*, 91:6013, 1989.
- [161] S. Arnold and M. Sulkes. *J. Phys. Chem.*, 96:4768, 1992.
- [162] Josefin Wilke, Martin Wilke, Christian Brand, W. Leo Meerts, and Michael Schmitt. On the additivity of molecular fragment dipole moments of 5-substituted indole derivatives. *ChemPhysChem*, 17(17):2736–2743, 2016.
- [163] P Alston Steiner and Walter Gordy. Precision measurement of dipole moments and other spectral constants of normal and deuterated methyl fluoride and methyl cyanide. *Journal of Molecular Spectroscopy*, 21(1-4):291–301, 1966.
- [164] Holger SP Müller, Audrey Coutens, Adam Walters, Jens-Uwe Grabow, and Stephan Schlemmer. Rotational spectroscopy, dipole moment and  $^{14}\text{N}$  nuclear hyperfine structure of iso-propyl cyanide. *Journal of Molecular Spectroscopy*, 267(1-2):100–107, 2011.
- [165] Christoph Jacoby and M. Schmitt. Torsional barriers in aromatic molecular clusters as probe of the electronic properties of the chromophore. *Chem. Phys. Chem.*, 5:1686–1694, 2004.

- [166] J. Kraitchman. Determination of molecular structure from microwave spectroscopic data. *Am. J. Phys.*, 21:17, 1953.
- [167] W Leo Meerts, WA Majewski, and WM van Herpen. The structure of fluorene (c13h10) and the fluorine–argon van der waals complex from a high-resolution near ultraviolet spectrum. *Canadian journal of physics*, 62(12):1293–1299, 1984.



# A | Online Supporting Material

## A.1. Rotationally Resolved Electronic Spectroscopy of the Rotamers of 1,3-Dimethoxybenzene

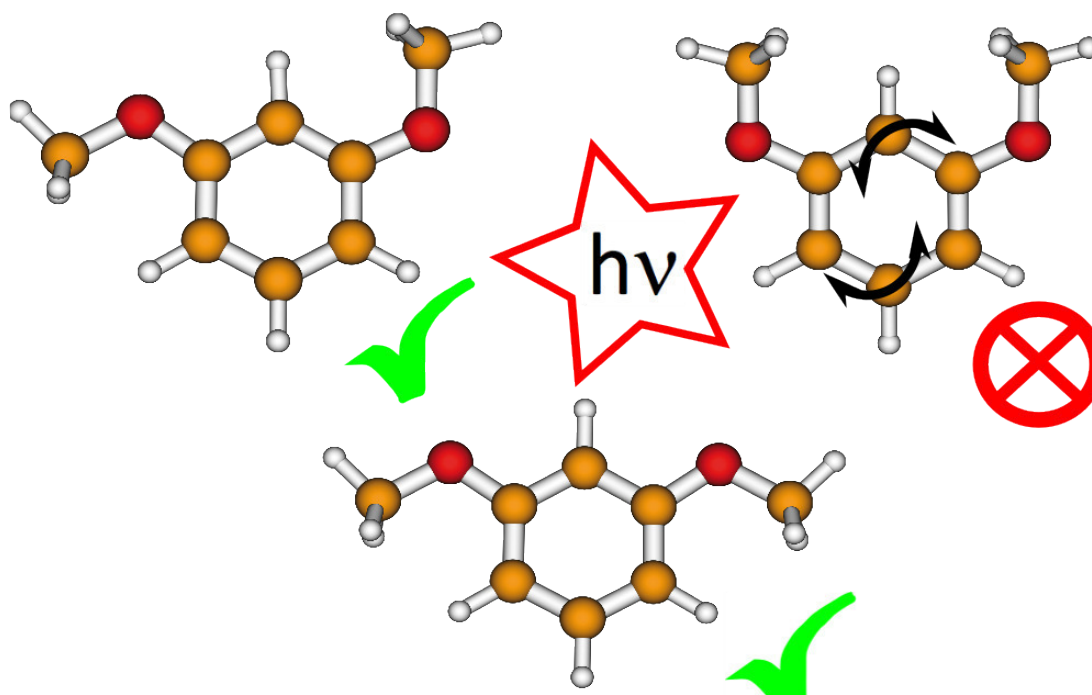


**Figure A.1.:** Graphical Abstract: Only two of three different rotamers of 1,3-dimethoxybenzene can be observed in molecular beam experiments. The missing rotamer adopts a non-planar ring structure upon electronic excitation and is absent due to small Franck-Condon factors. The different behavior of the three rotamers is a consequence of different electron densities in the aromatic ring, which partly lift the aromaticity.

## Electronic Supporting Material

The online supporting material contains the one figure with the rotationally resolved electronic spectrum of the *C*-band of 1,3-dimethoxybenzene (Figure A.2), modified versions of Figures 5 and 6 of the main paper with added residues of the fit, and tables with the Cartesian coordinates of the CC2/cc-pVTZ optimized structures of the (180, 180), (0, 180), and (180, 0) rotamers in their  $S_0$  and  $S_1$  states, respectively (Tables A.1 to A.6). Furthermore, the dihedral angles of the three rotamers are compared in Table A.7.

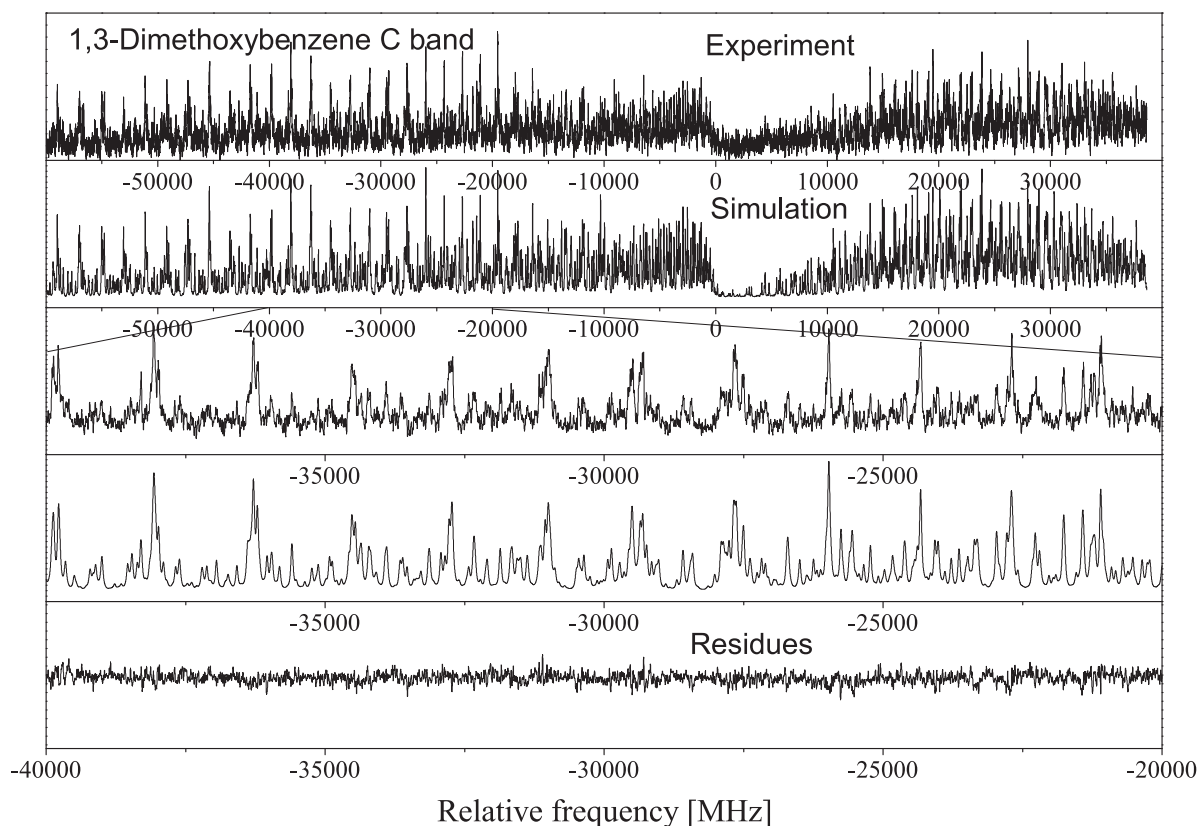


**Figure A.2.:** Rotationally resolved spectrum of the electronic origin of the *C* band of 1,3-dimethoxybenzene, along with a simulation using the best CMA-ES fit parameters, given in Table 2 of the main publication.

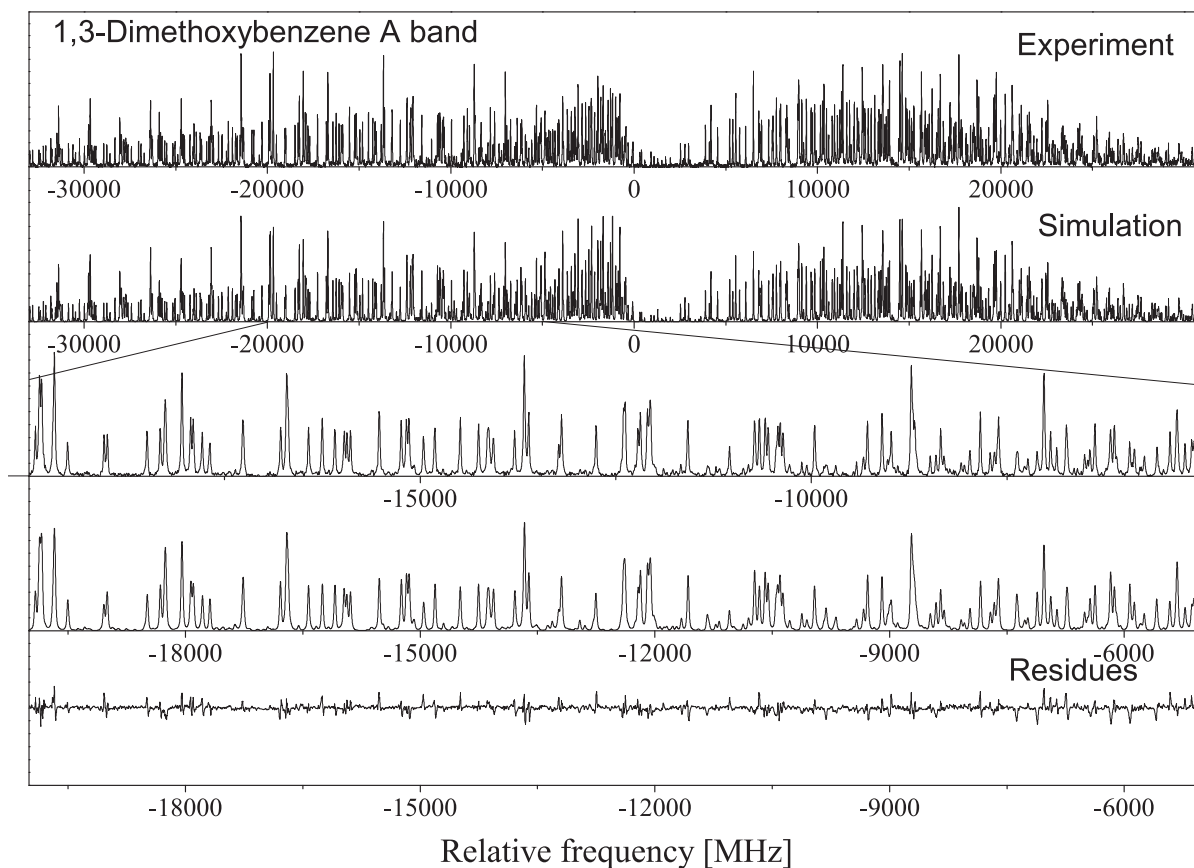


**Figure A.3.:** Modified version of Figure 5 of the main paper, along with the residues of the fit. Rotationally resolved spectrum of the electronic origin of the *A* band of 1,3-dimethoxybenzene, along with a simulation using the best CMA-ES fit parameters, given in Table 2 of the main publication.

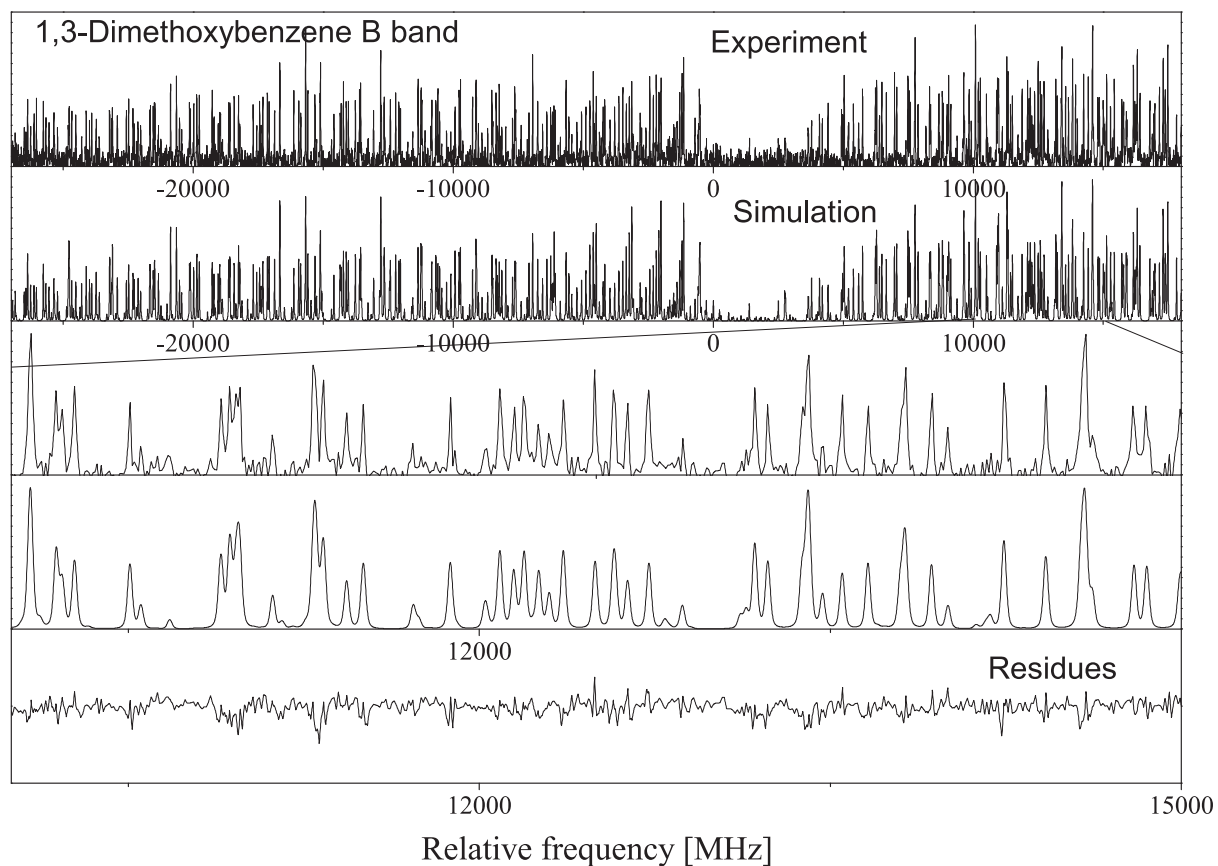


**Figure A.4.:** Modified version of Figure 6 of the main paper, along with the residues of the fit. Rotationally resolved spectrum of the electronic origin of the *B* band of 1,3-dimethoxybenzene, along with a simulation using the best CMA-ES fit parameters, given in Table 2 of the main publication.

**Table A.1.:** CC2/cc-pVTZ calculated optimized  $S_0$  cartesian coordinates of the (180, 180) rotamer 1,3-dimethoxybenzene (in bohr).

c	2.20820052	-0.00196223	-1.11432118
c	0.01128903	0.00059650	0.36998304
c	0.15869541	0.00139076	3.00129312
c	2.55392723	-0.00053052	4.13041856
c	4.74699941	-0.00305763	2.70082224
c	4.56482537	-0.00383312	0.05525691
o	-2.19340290	0.00220815	-0.97459382
c	-4.45317050	0.00459887	0.47803233
o	6.80769360	-0.00631611	-1.21756510
h	1.98347890	-0.00218489	-3.14130539
h	-1.51256164	0.00344158	4.16788246
h	2.68831484	-0.00005498	6.17087590
c	6.64133331	-0.00695732	-3.89897704
h	6.59715833	-0.00437499	3.56501998
h	-5.99055028	0.00540001	-0.87913151
h	-4.57743571	-1.67812605	1.66467168
h	-4.57465527	1.68835507	1.663494277
h	8.57567008	-0.00873511	-4.579508013
h	5.66357999	-1.68947649	-4.58359368
h	5.66631622	1.67676605	-4.58454606

**Table A.2.:** CC2/cc-pVTZ calculated optimized  $S_0$  cartesian coordinates of the (180, 0) rotamer 1,3-dimethoxybenzene (in bohr).

c	2.64031916	0.00089978	-1.12085448
c	0.36690703	0.00187427	0.21041212
c	0.37439989	0.00244476	2.84492847
c	2.66346284	0.00208508	4.17677518
c	4.91527321	0.00108816	2.80923839
c	4.95001041	0.00050171	0.17492832
o	-1.95545274	0.00341887	3.95567917
c	-1.98134028	0.00388183	6.64164168
o	2.41422554	0.00024840	-3.69202582
h	-1.40678759	0.00219042	-0.80289667
h	2.71698084	0.00265829	6.21432397
h	6.69104537	0.00082995	3.82390507
h	6.73248236	-0.00027412	-0.81363773
h	-3.96000823	0.00454144	7.18044126
h	-1.06003974	-1.67970828	7.39785754
h	-1.05907338	1.68719461	7.39729645
c	4.71498608	-0.00073046	-5.07821517
h	4.17439276	-0.00113500	-7.05639993
h	5.83472360	1.68254174	-4.66845409
h	5.83385514	-1.68435552	-4.66753230

**Table A.3.:** CC2/cc-pVTZ calculated optimized  $S_0$  cartesian coordinates of the (0, 180) rotamer 1,3-dimethoxybenzene (in bohr).

c	2.19021604	-0.00001405	-1.19930000
c	-0.05921458	-0.00034247	0.19786066
c	0.07374323	-0.00011837	2.84258796
c	2.40604415	0.00000421	4.07672490
c	4.61179385	0.00001592	2.64387875
c	4.53311243	0.00000436	0.01474538
o	-2.00686823	0.00028887	4.37287822
c	-4.39367424	0.00011179	3.14586764
o	2.26285887	0.00012765	-3.78107630
h	2.44501046	0.00019994	6.11826130
h	6.42306034	0.00000046	3.59237749
h	6.23325589	-0.00014366	-1.11612212
h	-1.86192050	-0.00104862	-0.74608010
c	-0.10525292	0.00021882	-5.04379786
h	-5.79290039	0.00034028	4.64514778
h	-4.63562879	1.68439509	1.97820545
h	-4.63559982	-1.68452649	1.97870332
h	0.33002230	0.00048761	-7.04787759
h	-1.20250338	-1.68432700	-4.57793826
h	-1.20258812	1.68459211	-4.57751006

**Table A.4.:** CC2/cc-pVTZ calculated optimized  $S_1$  cartesian coordinates of the (180, 180) rotamer 1,3-dimethoxybenzene (in bohr).

c	2.17208582	-0.00235493	-1.25040988
c	-0.00216500	0.00037515	0.33592625
c	0.15176911	0.00130885	3.02902142
c	2.55279608	-0.00061952	4.26229640
c	4.76343575	-0.00312148	2.69336637
c	4.55531760	-0.00394462	0.02614732
o	-2.23112087	0.00205487	-0.94019774
c	-4.50212129	0.00484336	0.51477679
o	6.80872991	-0.00620654	-1.21596842
h	1.94172559	-0.00350330	-3.27078087
h	-1.55399135	0.00352468	4.14746771
h	2.69271171	0.00004278	6.29424791
c	6.70297172	-0.00675969	-3.91283189
h	6.64269937	-0.00435881	3.49522693
h	-6.02995857	0.00579617	-0.85198499
h	-4.61847944	-1.68087101	1.69390661
h	-4.61518019	1.69171589	1.69257094
h	8.65430158	-0.00830255	-4.54169037
h	5.73889609	-1.69110101	-4.60305598
h	5.74128232	1.67862926	-4.60382582

**Table A.5.:** CC2/cc-pVTZ calculated optimized  $S_1$  cartesian coordinates of the (180, 0) rotamer 1,3-dimethoxybenzene (in bohr).

c	2.62838065	0.00093485	-1.13907145
c	0.26919017	0.00197621	0.15479900
c	0.35293341	0.00250077	2.84420287
c	2.67712071	0.00208551	4.20773738
c	5.03185532	0.00116064	2.87548764
c	4.98343294	0.00053646	0.17043459
o	-1.95032777	0.00340072	3.98189840
c	-2.00041808	0.00386621	6.67741242
o	2.43852395	0.00032560	-3.70097291
h	-1.49943777	0.00226413	-0.85549183
h	2.67956700	0.00246482	6.24706412
h	6.80130586	0.00094738	3.88629606
h	6.74136352	-0.00022937	-0.86327053
h	-3.98497232	0.00454490	7.19125821
h	-1.08367947	-1.68240699	7.42747010
h	-1.08267303	1.68984135	7.42690849
c	4.73501625	-0.00079272	-5.11321221
h	4.16966543	-0.00122503	-7.08371286
h	5.84726202	1.68512547	-4.70442893
h	5.84625350	-1.68712500	-4.70339713

**Table A.6.:** CC2/cc-pVTZ calculated optimized  $S_1$  cartesian coordinates of the (0, 180) rotamer 1,3-dimethoxybenzene (in bohr).

c	2.41674795	0.10180528	-1.14182430
c	-0.24927471	-0.02400580	-1.59447058
c	-1.71401179	-0.09387413	0.68106410
c	-0.65341084	-0.11917591	3.14035866
c	2.01660166	-0.23576342	3.51736697
c	3.52062125	0.07838551	1.29837347
o	-4.28730389	-0.03260409	0.66278141
c	-5.48185557	0.10690265	-1.75655131
o	4.12469718	0.36606914	-3.04943372
h	-1.95473150	0.00672643	4.71324175
h	2.83805131	-0.22318557	5.38019356
h	5.54346598	0.36146470	1.40430108
h	-0.99706295	-0.71849157	-3.36363207
c	3.13105682	0.51586745	-5.55739271
h	-7.47305481	0.40904434	-1.37239600
h	-4.71340333	1.67185923	-2.85186166
h	-5.23515424	-1.65731934	-2.79187411
h	4.72617794	0.98823308	-6.75580938
h	2.34175506	-1.29724041	-6.13607869
h	1.68404825	1.97591978	-5.67451458

**Table A.7.:** Dihedral angles of the different rotamers of 1,3-dimethoxybenzene according to the optimized CC2/cc-pVTZ structures. The atomic labeling is given in the full text article. All angles are given in degree.

	(180, 180) / (0, 0)		(180, 0)		(0, 180)	
	$S_0$	$S_1$	$S_0$	$S_1$	$S_0$	$S_1$
C1C2C3C4	0.0	0.0	0.0	0.0	0.0	1.9
C2C3C4C5	0.0	0.0	0.0	0.0	0.0	4.0
C3C4C5C6	0.0	0.0	0.0	0.0	0.0	-9.5
C4C5C6C7	0.0	0.0	0.0	0.0	0.0	9.5
C5C6C1C2	0.0	0.0	0.0	0.0	0.0	-4.0
C6C1C2C3	0.0	0.0	0.0	0.0	0.0	-1.9
H2C2C3C4	180.0	180.0	180.0	180.0	180.0	155.9
H4C4C5C6	180.0	180.0	180.0	180.0	180.0	168.8
H5C5C6C1	180.0	180.0	180.0	180.0	180.0	178.9
H6C6C1C2	180.0	180.0	180.0	180.0	180.0	174.4

## A.2. Excited state dipole moments and transition dipole orientations of different rotamers of 1,2-, 1,3, and 1,4-dimethoxybenzene

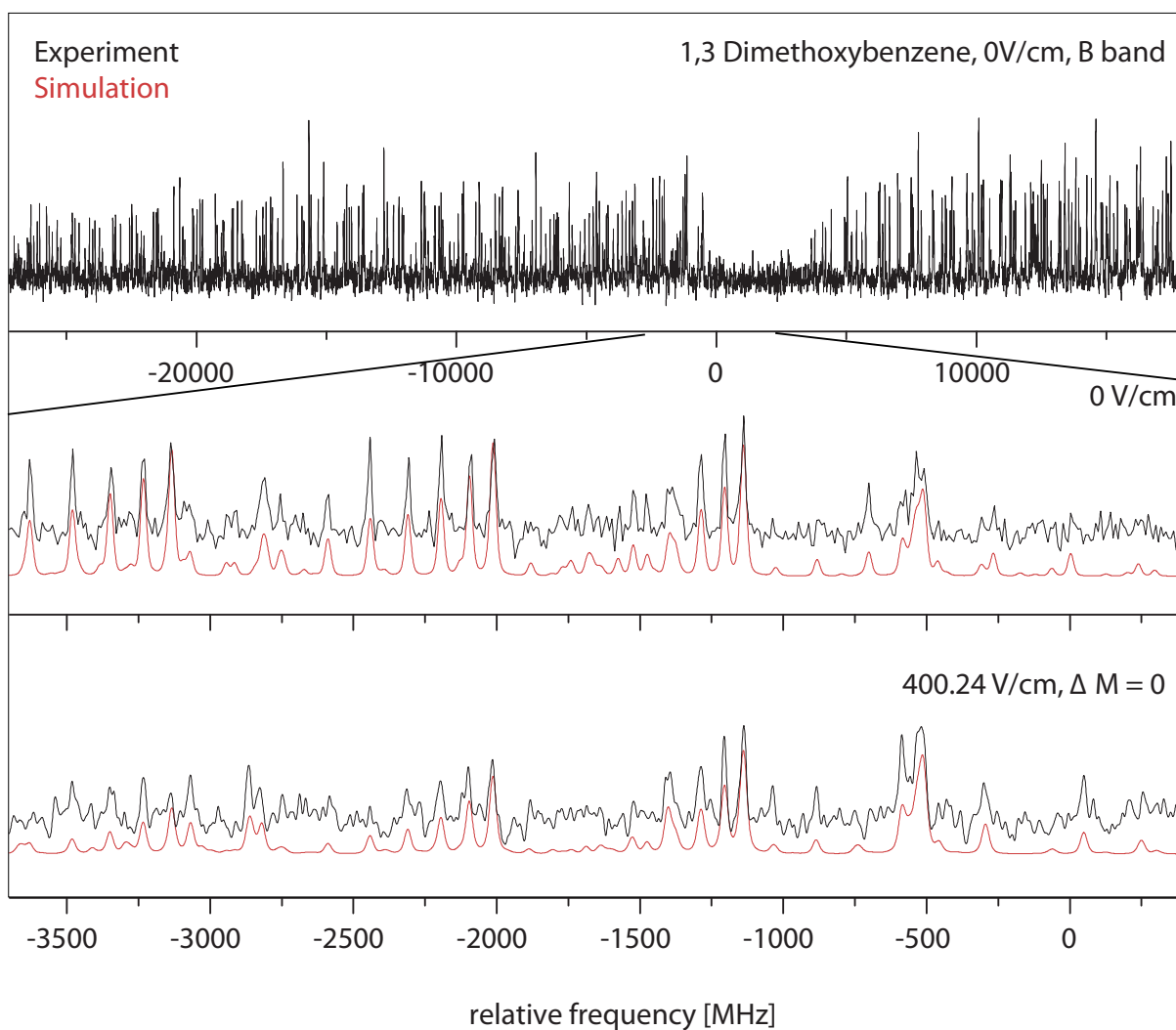


**Figure A.5.:** Rotationally resolved electronic spectrum of the electronic origin of the B band of 1,3-DMB at zero field and at  $400.24\text{V}/\text{cm}^{-1}$  with 80% transitions of  $\Delta M=0$ , along with a simulation with the best CMA-ES fit parameters.

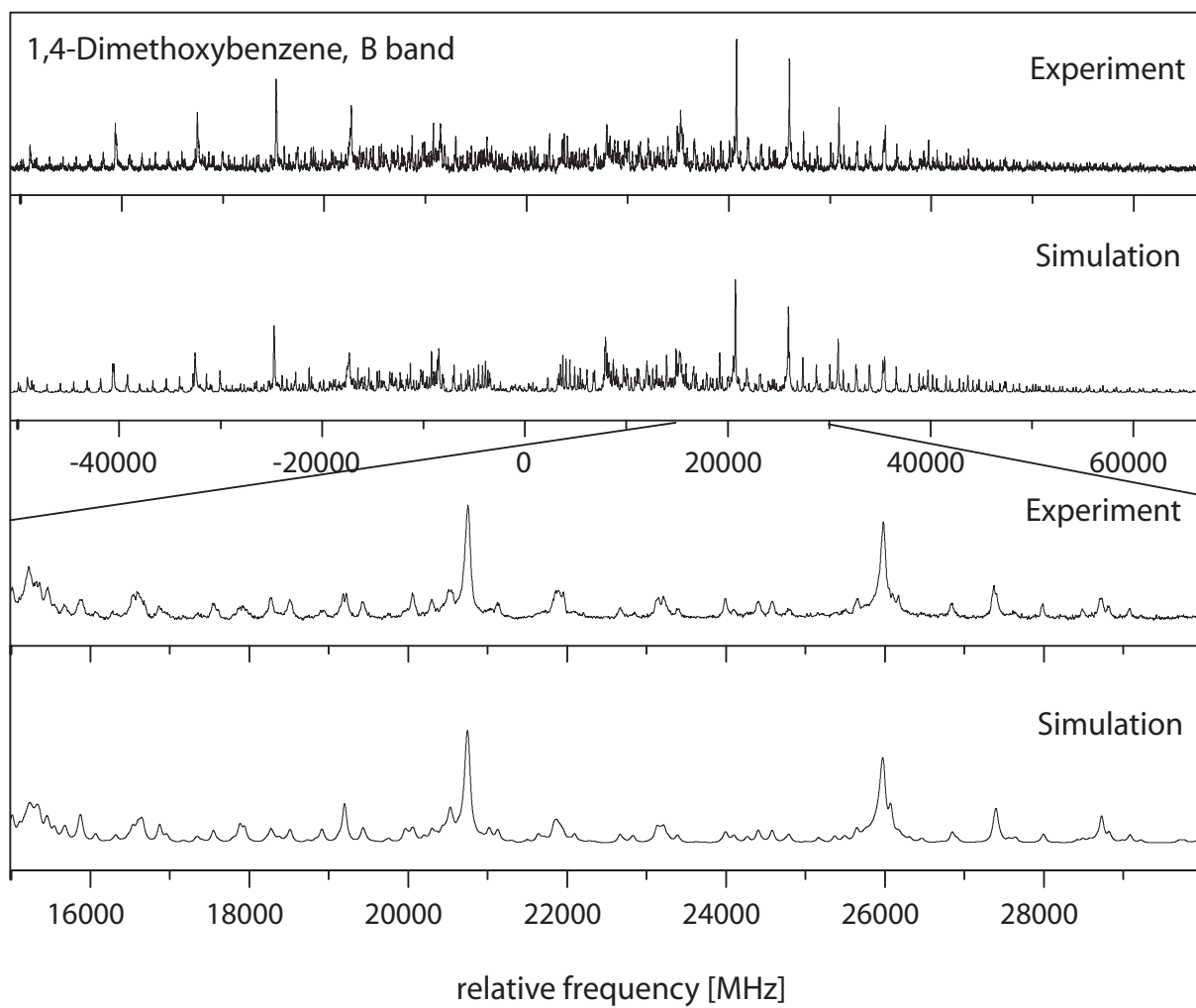


**Figure A.6.:** Rotationally resolved spectrum of the electronic origin of the *B* band of 1,4-dimethoxybenzene, along with a simulation using the best CMA-ES fit parameters.

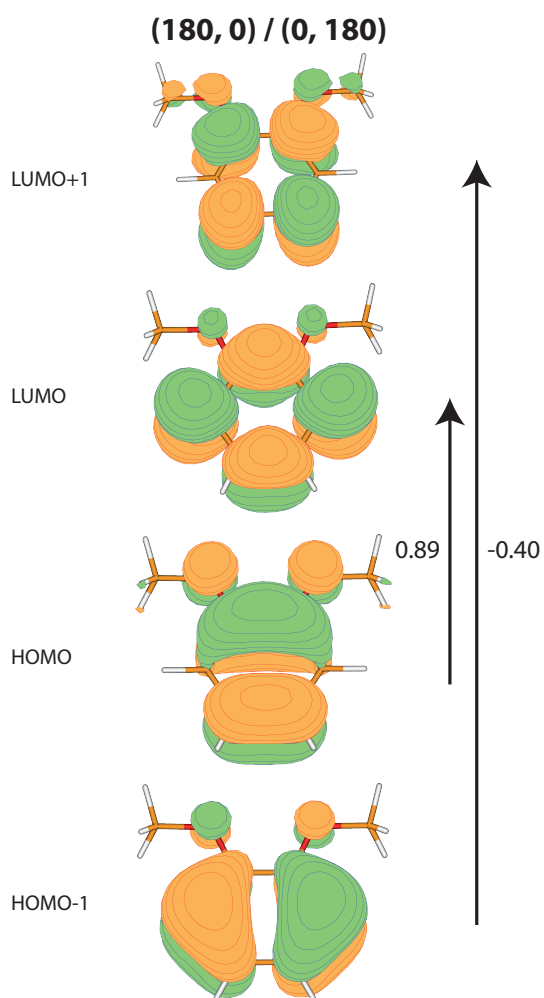


**Figure A.7.:** Molecular orbitals of 1,2-dimethoxybenzene

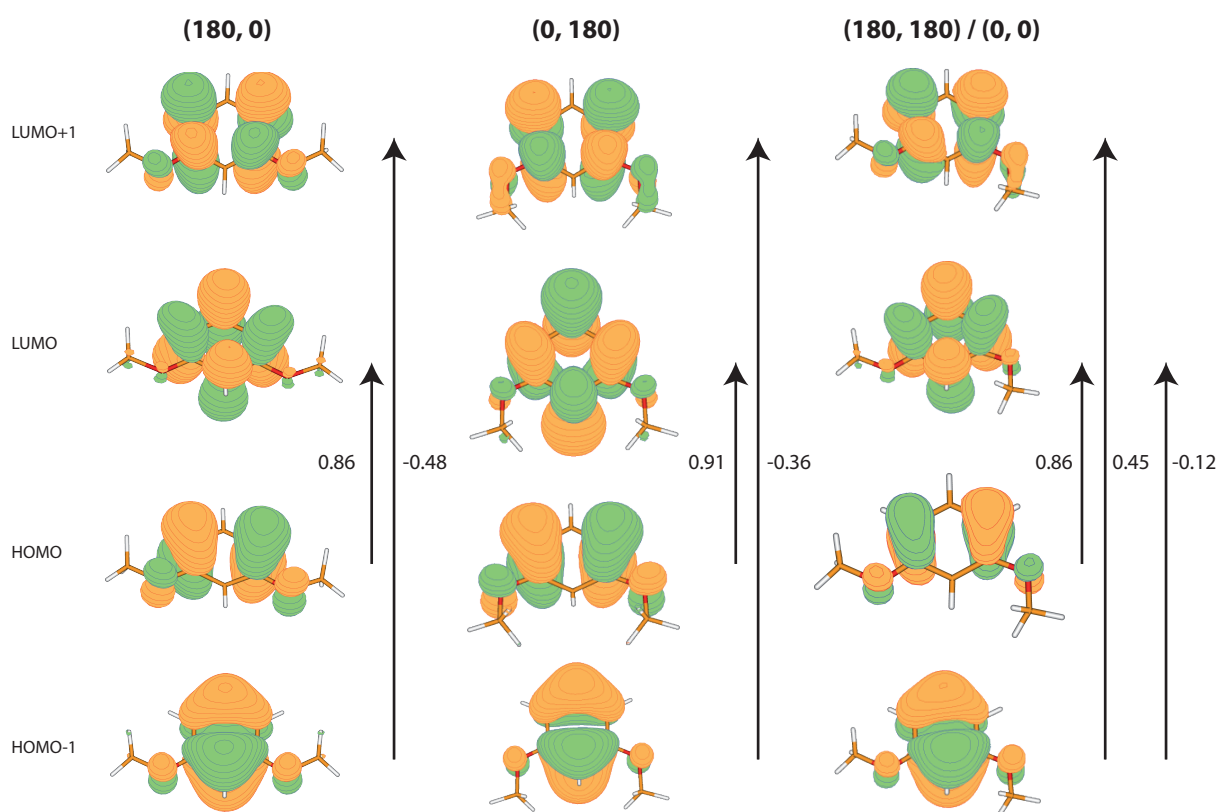


Figure A.8.: Molecular orbitals of 1,3-dimethoxybenzene

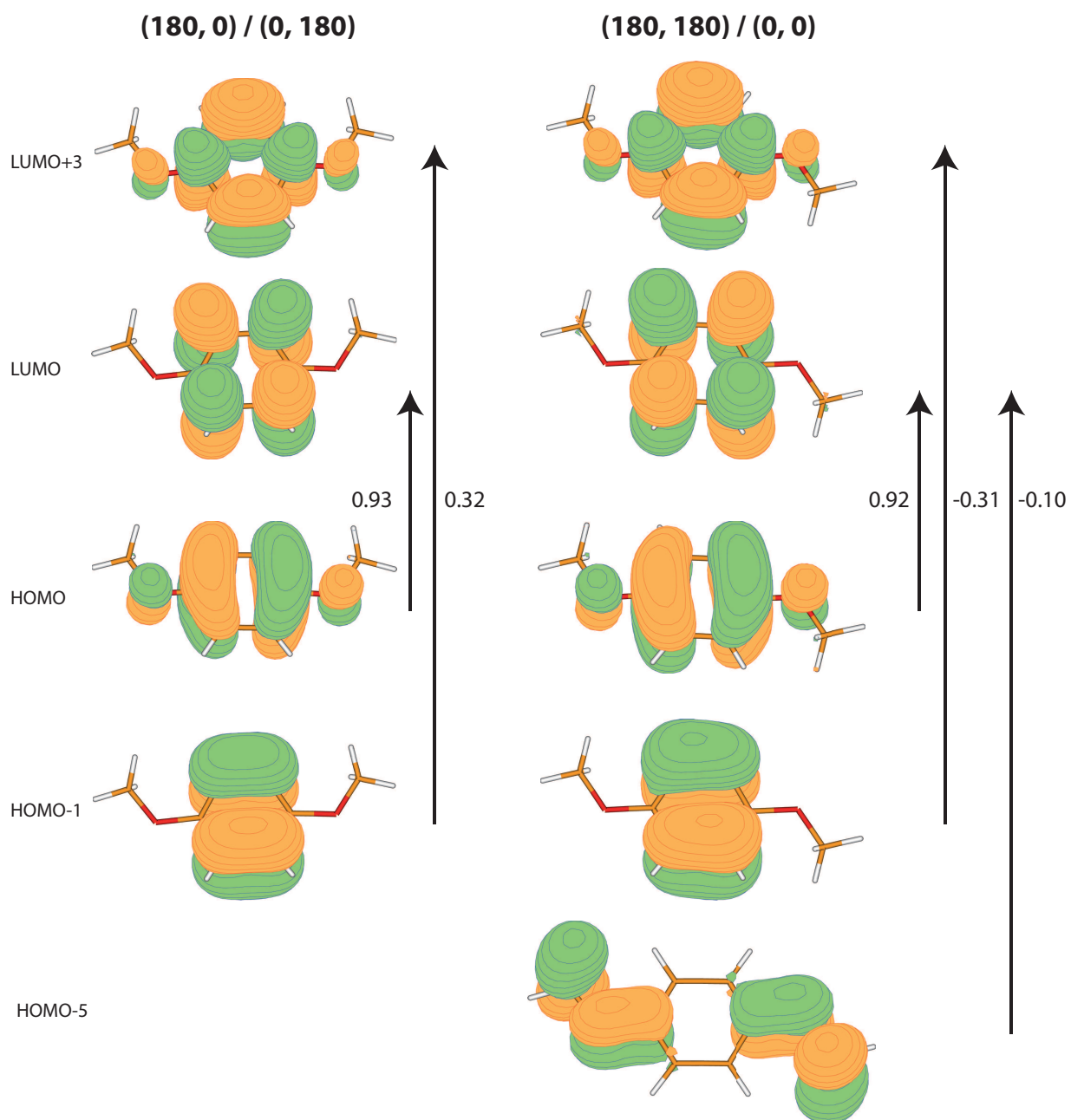


Figure A.9.: Molecular orbitals of 1,4-dimethoxybenzene

### A.3. Rotationally Resolved Electronic Spectroscopy of 3-Cyanoindole and the 3-Cyanoindole-water complex

The supporting online material contains:

- A figure with the molecular orbitals of the 3-cyanoindole-water cluster.
- A table with the CC2/cc-pVTZ computed and experimental molecular parameters of different 1:1 3-cyanoindole-water complexes.
- A table with the CC2/cc-pVTZ computed stabilization energies of the different 1:1 3-cyanoindole-water complexes.
- Tables with the Cartesian coordinates of the CC2/cc-pVTZ and SCS-CC2/cc-pVTZ optimized structures of 3-cyanoindole (Table A.10 - A.13) and the 3-cyanoindole water complexes (Table A.14-A.29) 1a, 1b, 2, 3 in their  $S_0$  and  $S_1$  states, respectively.

**Table A.8.:** CC2/cc-pVTZ computed and experimental molecular parameters of different 1:1 3-cyanoindole-water complexes. For details see text.

	CC2/cc-pVTZ				experiment		
	1a	1b	2	3	$\sigma = 1$	$\sigma = 0$	$\Delta\sigma$
$A''$ / MHz	1100	1113	1305	2025	1104.10	1100.04	-4.06
$B''$ / MHz	750	747	750	567	728.29	728.01	-0.28
$C''$ / MHz	447	448	477	444	439.07	438.99	-0.08
$\Delta I''$ / $\text{u}\text{\AA}^2$	-2.34	-2.34	-1.91	-2.12	-0.6380	-2.3774	
$A'$ / MHz	1121	1119	1279	2009	1099.63	1096.97	-2.66
$B'$ / MHz	739	740	731	560	724.63	724.33	-0.30
$C'$ / MHz	446	447	466	439	437.28	437.20	0.00
$\Delta I'$ / $\text{u}\text{\AA}^2$	-2.33	-3.31	-1.88	-3.75	-1.2938	-2.0979	
$\Delta A$ / MHz	21.01	6.01	-26.06	-16.33	-4.47	-3.07	
$\Delta B$ / MHz	-10.97	-6.57	-28.29	-6.91	-3.65	-3.68	
$\Delta C$ / MHz	-0.55	-1.03	-10.91	-4.40	-1.79	-1.79	
$\Delta\nu_{Lor.}$ / MHz	-	-	-	-	43.51	43.51	
$\tau$ / ns	-	-	-	-	3.66	3.66	
$\theta$ / $^\circ$	-20	-16	-25	+34	$\pm 48.26$	$\pm 48.26$	
$\nu_0$ / $\text{cm}^{-1}$	36335	36280	36093	36501	35262.2	35261.9	
$\Delta\nu_0$ / MHz	-	-	-	-	-8977.46		

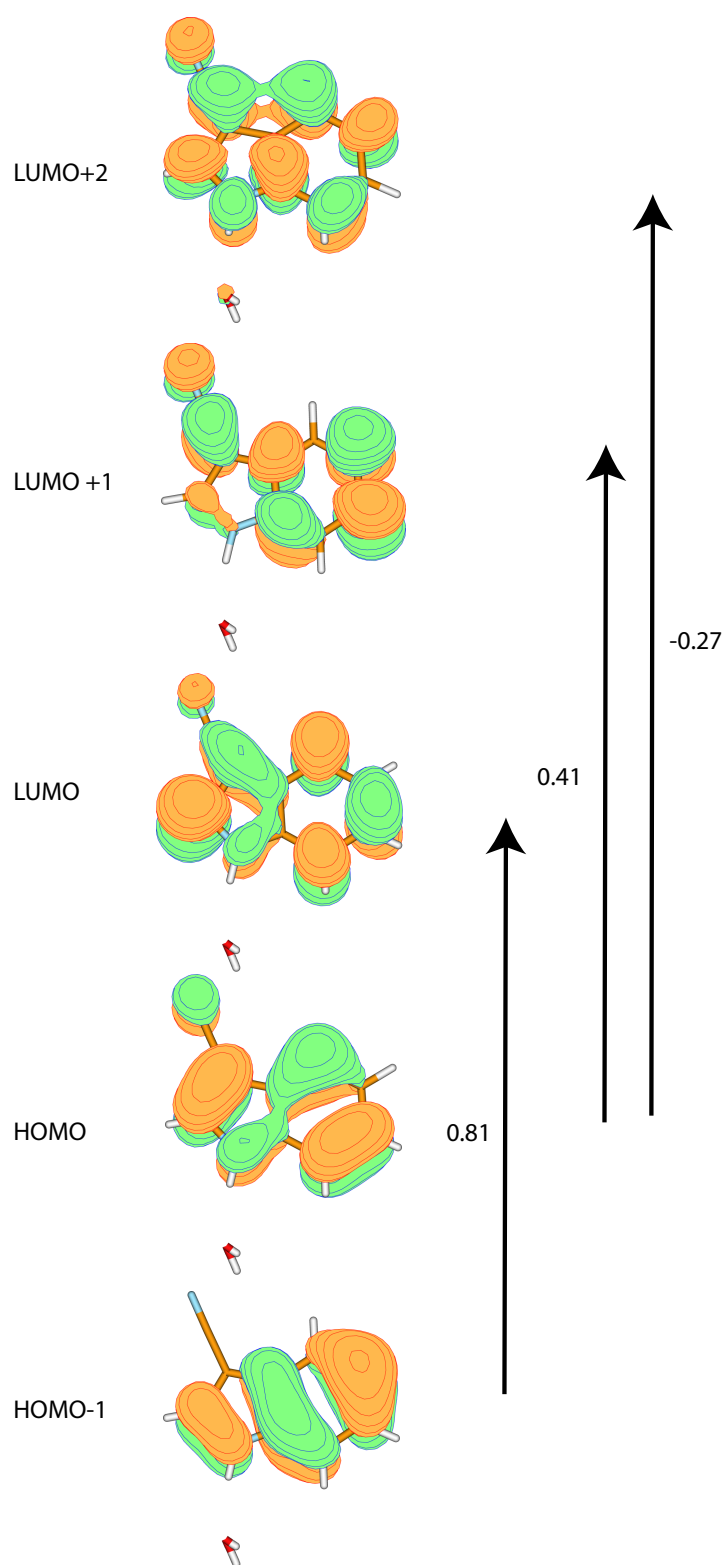


**Figure A.10.:** Molecular orbitals of 3-cyanoindole water cluster (1a) with the coefficients of the respective excitations according to SCS-CC2/cc-pVTZ calculations. Only  $\pi$ -orbitals were considered.

**Table A.9.:** Summary of stabilization energies (including ZPE and BSSE corrections) and adiabatic excitation (including ZPE) and vertical excitation and emission energies of four most stable isomers of the 3-cyanoindole-water cluster at CC2/cc-pVTZ level of theory.

	1a	1b	2	3
$\Delta E_{stab.}(S_0)$ /kJ mol <sup>-1</sup>	-32.08	-32.06	-24.20	-25.38
$\Delta E_{stab.}(S_0)$ /cm <sup>-1</sup>	-2681.70	-2679.89	-2023.1	-2122.01
$\Delta E_{stab.}(S_1)$ /kJ mol <sup>-1</sup>	-29.94	-30.57	-24.96	-21.26
$\Delta E_{stab.}(S_1)$ /cm <sup>-1</sup>	-2502.6	-2555.6	-2086.3	-1777.0
$\Delta E_{adiabatic}$ /cm <sup>-1</sup>	36335	36280	36093	36501
$\Delta E_{vertical}$ @ opt. S <sub>0</sub>	39299	39357	39322	39503
$\Delta E_{vertical}$ @ opt. S <sub>1</sub>	36002	33724	32614	34073

**Table A.10.:** CC2/cc-pVTZ calculated optimized S<sub>0</sub> cartesian coordinates of 3-Cyanoindole (in bohr).

c	-2.31860350	-4.71208238	-0.00237471
c	0.34505222	-4.71876513	-0.00206834
c	1.72123137	-2.48274302	-0.00176550
c	0.34710443	-0.22946807	-0.00165995
n	1.16269474	2.24767183	-0.00132971
c	-0.87176619	3.84603113	-0.00129166
c	-3.06707244	2.42460399	-0.00158323
c	-2.33217045	-0.18705951	-0.00182482
c	-3.67829789	-2.46885021	-0.00226125
h	-3.31687886	-6.49569444	-0.00274291
h	1.34135663	-6.50360103	-0.00201287
h	3.76654136	-2.49512894	-0.00159832
h	-0.63823912	5.86825568	-0.00106641
c	-5.56529264	3.37276034	-0.00158999
h	-5.72373272	-2.46842242	-0.00254132
h	2.98035993	2.80824638	-0.00113812
n	-7.67456788	4.11051580	-0.00157987

**Table A.11.:** CC2/cc-pVTZ calculated optimized  $S_1$  cartesian coordinates of 3-Cyanoindole (in bohr).

c	-0.38812082	-3.83487540	0.07146021
c	2.24004126	-3.38839598	0.00288695
c	3.17310639	-0.86722703	0.04338136
c	1.37256577	1.08308504	0.15215508
n	1.67347712	3.62885202	0.21556824
c	-0.67867807	4.94852297	0.32807896
c	-2.54939811	3.06977902	0.32895680
c	-1.34402699	0.64277833	0.22315865
c	-2.22844909	-1.84134292	0.18255211
h	-1.06325777	-5.76575037	0.03981881
h	3.53418536	-4.96348344	-0.08016863
h	5.17607565	-0.46207249	-0.00721536
h	-0.77182565	6.97566037	0.37016868
c	-5.18127510	3.44123174	0.41813629
h	-4.22697939	-2.26530633	0.23265957
h	3.36919202	4.50248639	0.19263515
n	-7.40694457	3.68306709	0.49123914

**Table A.12.:** SCS CC2/cc-pVTZ calculated optimized  $S_0$  cartesian coordinates of 3-Cyanoindole (in bohr).

c	-2.31879816	-4.72113457	-0.00223036
c	0.35084906	-4.72497653	-0.00204012
c	1.72285892	-2.48740682	-0.00185721
c	0.34295897	-0.22964943	-0.00191268
n	1.16487242	2.25154597	-0.00133592
c	-0.87606086	3.84890934	-0.00120510
c	-3.06839866	2.43030251	-0.00161916
c	-2.33063849	-0.18983957	-0.00209655
c	-3.67806966	-2.47828788	-0.00239326
h	-3.31566816	-6.50613706	-0.00222625
h	1.34852910	-6.50978426	-0.00207969
h	3.76838477	-2.49588137	-0.00159686
h	-0.64279591	5.87132784	-0.00085618
c	-5.57583118	3.39006973	-0.00154992
h	-5.72349295	-2.48080295	-0.00289781
h	2.98007428	2.81184887	-0.00104787
n	-7.67105447	4.13616617	-0.00148406

**Table A.13.:** SCS CC2/cc-pVTZ calculated optimized  $S_1$  cartesian coordinates of 3-Cyanoindole (in bohr).

c	-2.31314536	-4.74038251	-0.00233793
c	0.38627504	-4.78743558	-0.00205848
c	1.80161090	-2.49354956	-0.00169251
c	0.39305489	-0.22927146	-0.00169440
n	1.16962481	2.22845791	-0.00141271
c	-0.89351095	3.91681323	-0.00117351
c	-3.08481895	2.45938963	-0.00160334
c	-2.37889064	-0.15462168	-0.00203060
c	-3.74520547	-2.43441622	-0.00234170
h	-3.32359336	-6.51822115	-0.00254925
h	1.35257002	-6.58558124	-0.00215590
h	3.84429582	-2.48901068	-0.00142463
h	-0.62582255	5.93100026	-0.00072382
c	-5.60068821	3.38749672	-0.00161580
h	-5.78725044	-2.46090772	-0.00253656
h	2.99036628	2.78121524	-0.00143713
n	-7.70715283	4.10529481	-0.00164073

**Table A.14.:** CC2/cc-pVTZ calculated optimized  $S_0$  cartesian coordinates of 3-Cyanoindole water 1a (in bohr).

c	-0.47709694	-3.87415680	0.07362869
c	2.14308746	-3.39487669	0.00581837
c	3.08664693	-0.94506230	0.04400719
c	1.32829895	1.02217280	0.15255500
n	1.69971084	3.59846111	0.21201183
c	-0.58443551	4.79573634	0.31551514
c	-2.50052786	3.00853752	0.32562212
c	-1.31435759	0.57208874	0.22194654
c	-2.22160471	-1.91714301	0.18144851
h	-1.13476242	-5.80949670	0.04065728
h	3.44576512	-4.96844720	-0.07775805
h	5.09678815	-0.57182061	-0.00784941
h	-0.71728792	6.82670652	0.37547158
c	-5.12452540	3.49863411	0.42016400
h	-4.23181739	-2.29308781	0.23321821
h	3.42100321	4.45045330	0.18188580
n	-7.32991749	3.85344698	0.49800662
o	6.81743382	5.48895961	0.09797955
h	7.94861904	5.19472297	1.49056459
h	7.84950172	5.26590611	-1.38207855

**Table A.15.:** CC2/cc-pVTZ calculated optimized  $S_1$  cartesian coordinates of 3-Cyanoindole water 1a (in bohr).

c	-0.38105345	-3.83893075	0.07104077
c	2.23569351	-3.38570202	0.00336583
c	3.16355004	-0.85564384	0.04465052
c	1.35596294	1.08631767	0.15327724
n	1.66868498	3.62903100	0.21518646
c	-0.67651928	4.94764299	0.32548900
c	-2.55322145	3.07127666	0.32836306
c	-1.34698477	0.63452648	0.22340654
c	-2.22961258	-1.85074071	0.18249469
h	-1.05120922	-5.77198341	0.03841591
h	3.53469908	-4.95765835	-0.07957431
h	5.16234083	-0.43306498	-0.00437962
h	-0.76963448	6.97457317	0.37563546
c	-5.18266883	3.44816550	0.41781414
h	-4.22694121	-2.28093242	0.23260354
h	3.40444914	4.47083358	0.18623731
n	-7.40784925	3.69929659	0.49144544
o	6.81898056	5.36715589	0.09607916
h	7.89057050	4.89104121	1.48663756
h	7.79128496	4.95653074	-1.38537371

**Table A.16.:** CC2/cc-pVTZ calculated optimized  $S_0$  cartesian coordinates of 3-Cyanoindole water 1b (in bohr).

c	14.01062475	-3.02670173	2.32387528
c	16.35968064	-4.27112174	2.13769368
c	18.45811401	-3.08710787	1.09481879
c	18.13699180	-0.60954591	0.23926933
n	19.84927211	1.01399071	-0.86275675
c	18.69043472	3.25821062	-1.39327318
c	16.18309502	3.13847019	-0.64165215
c	15.78740553	0.67087326	0.41189409
c	13.69687053	-0.56490369	1.47226207
h	12.42363855	-4.01694839	3.14870986
h	16.53081291	-6.19006173	2.82217356
h	20.26474338	-4.03379350	0.94755928
h	19.69953830	4.79712735	-2.26497305
c	14.36682978	5.08313456	-0.87274371
h	11.89037178	0.38384441	1.61859348
h	21.68617777	0.58077377	-1.21395540
n	12.81079422	6.67861017	-1.04382922
o	24.87580944	-0.95216566	-1.51606613
h	26.30957139	-0.58045430	-0.46235115
h	25.59524736	-1.56900952	-3.06720467

**Table A.17.:** CC2/cc-pVTZ calculated optimized  $S_1$  cartesian coordinates of 3-Cyanoindole water 1b (in bohr).

c	14.04829139	-3.07604036	2.29115137
c	16.36687216	-4.30373337	2.23705212
c	18.52563161	-3.03732767	1.23623811
c	18.19152211	-0.57244521	0.34596300
n	19.86977778	1.01991601	-0.75772613
c	18.72950249	3.34039392	-1.61148123
c	16.18204293	3.16814479	-0.72891891
c	15.79052063	0.72167956	0.39300839
c	13.70886291	-0.53793050	1.35318907
h	12.41603207	-4.04211340	3.05864661
h	16.53995039	-6.20772237	2.95244732
h	20.36409198	-3.93123774	1.16781678
h	19.88406395	5.02385296	-1.74552548
c	14.31367591	5.03121955	-0.93555793
h	11.86275005	0.34182902	1.40041567
h	21.69639660	0.51836717	-1.12472716
n	12.69088375	6.57886350	-1.06790683
o	24.79929644	-1.09732172	-1.57051895
h	26.35331439	-0.56466837	-0.79108352
h	25.29254446	-1.67050475	-3.22443831

**Table A.18.:** CC2/cc-pVTZ calculated optimized  $S_0$  cartesian coordinates of 3-Cyanoindole water 2 (in bohr).

c	-0.84541036	-4.05462108	-0.35397617
c	1.78917761	-4.11797589	0.03520499
c	3.19216254	-1.91364697	0.29571365
c	1.86921612	0.36547366	0.15344416
n	2.71811115	2.82789755	0.33317146
c	0.73731690	4.46820079	0.07532844
c	-1.45653751	3.08741648	-0.27862750
c	-0.77896997	0.45743610	-0.23520503
c	-2.16254454	-1.78905516	-0.49415684
h	-1.86139052	-5.81750383	-0.55051332
h	2.74371388	-5.92318022	0.13218439
h	5.21505408	-1.96856043	0.59269460
h	1.00398758	6.48467620	0.15680589
c	-3.91606049	4.05812062	-0.62329953
h	-4.18871000	-1.73949508	-0.79324121
h	4.52629472	3.35109982	0.60850050
n	-6.01821145	4.75698423	-0.92285527
o	-8.49505060	-0.42383422	-1.27327369
h	-9.21293345	-0.42583235	0.39645736
h	-8.10254071	1.34110780	-1.53595888

**Table A.19.:** CC2/cc-pVTZ calculated optimized  $S_1$  cartesian coordinates of 3-Cyanoindole water 2 (in bohr).

c	-0.85238860	-4.03429696	-0.27104076
c	1.74859696	-4.18103609	0.06637571
c	3.17728715	-1.92327143	0.28842820
c	1.88485906	0.38726382	0.14958286
n	2.76627081	2.78552086	0.22825943
c	0.80263155	4.67033001	-0.20965245
c	-1.46076161	3.19209420	-0.31895676
c	-0.81596857	0.55018545	-0.20455033
c	-2.18730674	-1.65386230	-0.42885748
h	-1.94771861	-5.75441708	-0.43619701
h	2.67980995	-5.99427114	0.16726094
h	5.20386399	-1.97576726	0.57006295
h	1.01889541	6.50329632	0.67969363
c	-3.94027466	4.05455677	-0.57407178
h	-4.21610082	-1.62222397	-0.73205982
h	4.62425277	3.22465122	0.24740370
n	-6.10208585	4.64387249	-0.78337105
o	-8.33207265	-0.52573725	-1.35650999
h	-9.33890264	-0.58121395	0.15576581
h	-7.95621189	1.25903429	-1.51916779

**Table A.20.:** CC2/cc-pVTZ calculated optimized  $S_0$  cartesian coordinates of 3-Cyanoindole water 3 (in bohr).

c	-0.69382954	-4.02381608	0.03258585
c	1.93148558	-3.57906734	0.07686186
c	2.90589648	-1.14350127	0.19504916
c	1.16943838	0.84205423	0.26807445
n	1.55376232	3.42020682	0.38776307
c	-0.71375070	4.65753136	0.42253177
c	-2.63518159	2.88123492	0.32332175
c	-1.47912773	0.42987777	0.22453607
c	-2.41549430	-2.04543367	0.10503377
h	-1.37463060	-5.94895124	-0.05932216
h	3.21711682	-5.16710559	0.01815495
h	4.92328095	-0.80809589	0.22951186
h	-0.87583594	6.68658895	0.51480693
c	-5.24063488	3.45515022	0.33768254
h	-4.43048304	-2.39575248	0.07152071
h	3.25108452	4.27709932	0.45186277
n	-7.41400679	3.98174636	0.36156347
o	-4.57804958	9.35764669	0.41149673
h	-5.84394736	8.12982252	0.88021074
h	-5.03829997	9.76476340	-1.29951927

**Table A.21.:** CC2/cc-pVTZ calculated optimized  $S_1$  cartesian coordinates of 3-Cyanoindole water 3 (in bohr).

c	-0.67572528	-4.00970142	0.10850208
c	1.93039793	-3.65753954	0.19671344
c	2.92963595	-1.16261155	0.26817577
c	1.21315870	0.85148859	0.24266643
n	1.61840115	3.37993848	0.22551951
c	-0.67799789	4.84621184	-0.00090087
c	-2.62158950	2.97834453	0.09710405
c	-1.49971657	0.50697311	0.15033260
c	-2.44036503	-1.93190668	0.06843265
h	-1.43117603	-5.91046612	0.06337441
h	3.18701810	-5.26511616	0.21776621
h	4.94593761	-0.82705998	0.35536141
h	-0.76425516	6.75665039	0.71613484
c	-5.21975375	3.46722924	0.13123072
h	-4.45120333	-2.29196107	-0.03229937
h	3.35665520	4.16909791	0.16069278
n	-7.42261326	3.91066335	0.18450785
o	-4.78863885	9.37038303	0.73448502
h	-6.01877638	8.08545390	1.13752922
h	-4.95060059	9.50592716	-1.07160176

**Table A.22.:** SCS CC2/cc-pVTZ calculated optimized  $S_0$  cartesian coordinates of 3-Cyanoindole water 1a (in bohr).

c	-0.50943508	-3.90443260	0.07320923
c	2.11849563	-3.43424635	0.00586308
c	3.07027473	-0.98860819	0.04461428
c	1.31509552	0.99040069	0.15317802
n	1.70251905	3.57009586	0.21286945
c	-0.58142877	4.77677615	0.31610840
c	-2.50309642	3.00164567	0.32567182
c	-1.32384398	0.55233671	0.22172815
c	-2.24356123	-1.93918462	0.18081130
h	-1.17503783	-5.83761571	0.03988463
h	3.41472599	-5.01395943	-0.07766346
h	5.08181446	-0.62214869	-0.00671240
h	-0.70437275	6.80847168	0.37609827
c	-5.13561258	3.51485475	0.42034122
h	-4.25518008	-2.30755291	0.23226457
h	3.41839590	4.41933230	0.18365533
n	-7.32670823	3.89190795	0.49772843
o	6.87863147	5.54238500	0.09530881
h	8.02878180	5.35704486	1.49019913
h	7.93006440	5.42423187	-1.38234324

**Table A.23.:** SCS CC2/cc-pVTZ calculated optimized  $S_1$  cartesian coordinates of 3-Cyanoindole water 1a (in bohr).

c	-0.45796106	-3.89295986	0.07624751
c	2.20165044	-3.43699398	0.00103662
c	3.16856639	-0.92003646	0.03568034
c	1.36419282	1.04382456	0.14642949
n	1.68734228	3.59423192	0.20239687
c	-0.64750612	4.86778804	0.31271328
c	-2.54048039	3.04093719	0.32672774
c	-1.36844775	0.59685976	0.22402020
c	-2.29267290	-1.89654728	0.18882912
h	-1.11993158	-5.82795253	0.04718166
h	3.48108436	-5.02609680	-0.08297634
h	5.17138894	-0.52554053	-0.01981592
h	-0.75309503	6.89647847	0.36981764
c	-5.18106380	3.49460249	0.42524408
h	-4.29334924	-2.30304254	0.24379359
h	3.40396714	4.45128104	0.16905854
n	-7.38176752	3.81664090	0.50591543
o	6.88094157	5.50691401	0.10350224
h	7.97739931	5.11265909	1.49906503
h	7.90026414	5.20868751	-1.37205212

**Table A.24.:** SCS CC2/cc-pVTZ calculated optimized  $S_0$  cartesian coordinates of 3-Cyanoindole water 1b (in bohr).

c	13.97494317	-3.03152503	2.33306627
c	16.32696199	-4.28401126	2.15294129
c	18.42876387	-3.10453451	1.11402893
c	18.11487672	-0.62068436	0.25319264
n	19.84051137	0.99821880	-0.84804944
c	18.68418591	3.24752250	-1.38295913
c	16.17856996	3.13606222	-0.63872660
c	15.77283631	0.66269304	0.41925873
c	13.67176818	-0.57033442	1.47818881
h	12.38332878	-4.01784286	3.15497854
h	16.49179270	-6.20330412	2.83984352
h	20.23368617	-4.05565580	0.97233750
h	19.70057740	4.78242017	-2.25353223
c	14.36547903	5.09983480	-0.88080912
h	11.86688357	0.38226970	1.61933238
h	21.67295292	0.56951335	-1.19750718
n	12.83062784	6.70003094	-1.06202630
o	24.98024636	-0.89708539	-1.56751792
h	26.42022204	-0.54930847	-0.51514425
h	25.68680970	-1.54105830	-3.11285244

**Table A.25.:** SCS CC2/cc-pVTZ calculated optimized  $S_1$  cartesian coordinates of 3-Cyanoindole water 1b (in bohr).

c	14.08777992	-3.05789027	2.33457602
c	16.46947179	-4.31405722	2.14541063
c	18.60080004	-3.06810047	1.06093088
c	18.20821441	-0.56971226	0.20730805
n	19.84043708	1.08459180	-0.89325833
c	18.65047525	3.39976636	-1.44982740
c	16.14663465	3.20580464	-0.66640587
c	15.77259678	0.73663851	0.39243065
c	13.68823946	-0.51777225	1.46683517
h	12.51429575	-4.06387999	3.16851119
h	16.64212833	-6.22798077	2.83561654
h	20.42206839	-3.97680454	0.89612163
h	19.65838463	4.93131495	-2.32644908
c	14.26923525	5.10917029	-0.86966686
h	11.86201344	0.38046405	1.63694665
h	21.68075925	0.68125391	-1.25776423
n	12.67439027	6.65472471	-1.01480411
o	25.03873553	-0.63928710	-1.69897144
h	26.06582575	-1.02218262	-0.24853123
h	25.33353805	-2.02284074	-2.84096487

**Table A.26.:** SCS CC2/cc-pVTZ calculated optimized  $S_0$  cartesian coordinates of 3-Cyanoindole water 2 (in bohr).

c	-0.82454230	-4.06523776	-0.35142410
c	1.81644522	-4.12520094	0.03610277
c	3.21476140	-1.91880762	0.29458516
c	1.88567929	0.36465736	0.15304890
n	2.74074952	2.83104445	0.33381389
c	0.75290801	4.46986096	0.07736585
c	-1.43850146	3.09205667	-0.27441561
c	-0.75744217	0.45443678	-0.23227542
c	-2.14071818	-1.79991012	-0.49001110
h	-1.83911941	-5.82958418	-0.54661934
h	2.77254978	-5.93030834	0.13234957
h	5.23822618	-1.96919329	0.58985604
h	1.01879978	6.48660595	0.15932707
c	-3.90609513	4.08043035	-0.61623422
h	-4.16591661	-1.75602545	-0.78796504
h	4.54672888	3.35422851	0.60659820
n	-5.99000458	4.80180461	-0.90900485
o	-8.62049107	-0.42886496	-1.28284493
h	-9.32442874	-0.41629308	0.39243870
h	-8.22291342	1.32900808	-1.56629355

**Table A.27.:** SCS CC2/cc-pVTZ calculated optimized  $S_1$  cartesian coordinates of 3-Cyanoindole water 2 (in bohr).

c	-0.82211776	-4.07223455	-0.34752152
c	1.84556001	-4.18733937	0.03845709
c	3.28750236	-1.92896104	0.30372312
c	1.94130768	0.36846504	0.16175154
n	2.75933413	2.80508758	0.33385206
c	0.75158465	4.55066774	0.07786400
c	-1.44476557	3.13410582	-0.27174068
c	-0.79979186	0.50359473	-0.23229323
c	-2.20103649	-1.73570916	-0.48751083
h	-1.85962494	-5.82325871	-0.54766482
h	2.76759645	-6.00648213	0.12557564
h	5.30921917	-1.97021823	0.59525743
h	1.06063339	6.55666592	0.16309449
c	-3.92312997	4.08171740	-0.61662459
h	-4.22514144	-1.71316897	-0.78070498
h	4.57317534	3.31333701	0.60279305
n	-6.02190751	4.76319006	-0.91401815
o	-8.63272107	-0.46771840	-1.28226071
h	-9.36961245	-0.43567081	0.37860957
h	-8.23938912	1.28863808	-1.58224049

**Table A.28.:** SCS CC2/cc-pVTZ calculated optimized  $S_0$  cartesian coordinates of 3-Cyanoindole water 3 (in bohr).

c	-0.68087267	-4.05140866	0.03714122
c	1.94923204	-3.59986200	0.08287741
c	2.91655941	-1.16210256	0.19771274
c	1.17144271	0.82488749	0.26617574
n	1.55768322	3.40873503	0.38184650
c	-0.71819819	4.64046989	0.41308312
c	-2.63513386	2.86558992	0.31570308
c	-1.47054895	0.40801691	0.22142618
c	-2.40434097	-2.07499680	0.10503928
h	-1.35763426	-5.97864895	-0.05217401
h	3.23784673	-5.18644095	0.02772779
h	4.93309441	-0.82047003	0.23313910
h	-0.87466506	6.66951374	0.50157219
c	-5.25457300	3.43769151	0.32618161
h	-4.41857602	-2.42987873	0.07045338
h	3.25118644	4.26772220	0.44594665
n	-7.41997551	3.95108338	0.34551774
o	-4.60259498	9.46197226	0.41531202
h	-5.87899949	8.25645895	0.90552799
h	-5.08213900	9.88366641	-1.28648273

**Table A.29.:** SCS CC2/cc-pVTZ calculated optimized  $S_1$  cartesian coordinates of 3-Cyanoindole water 3 (in bohr).

c	-0.68143478	-4.06540726	0.02006554
c	1.99000330	-3.65312386	0.06821297
c	3.00195346	-1.15817371	0.19848949
c	1.22985863	0.83534880	0.27439412
n	1.58151661	3.38884997	0.40076745
c	-0.72706349	4.70259448	0.43758414
c	-2.64071327	2.89919505	0.33028904
c	-1.51569456	0.43992376	0.22496380
c	-2.48165266	-2.03660361	0.09724981
h	-1.37290899	-5.98719592	-0.07833854
h	3.24555321	-5.26175500	0.00521494
h	5.01457465	-0.81291224	0.23823755
h	-0.84763253	6.72990725	0.54117168
c	-5.26399879	3.44599745	0.34140007
h	-4.48978637	-2.40563919	0.05982002
h	3.28211519	4.23954465	0.46851401
n	-7.43725664	3.92842559	0.36011666
o	-4.64880958	9.49948993	0.36831143
h	-5.91870386	8.34408117	0.97828434
h	-5.10112652	9.69945169	-1.38102153